National Institute of Materials Physics

ANNUAL REPORT 2017

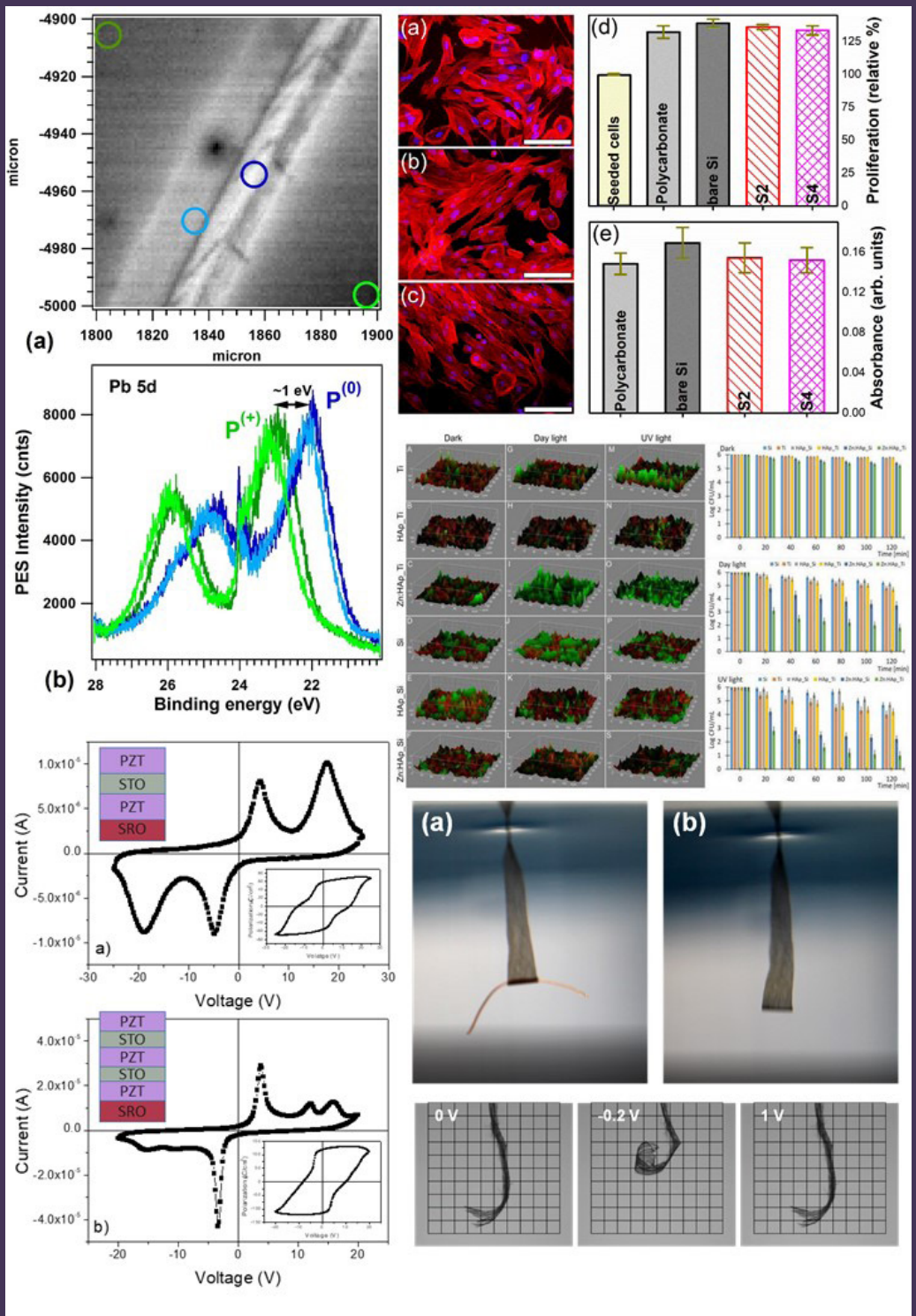

COVER IMAGE

Images selected for the cover are from following articles:

L. E. Abramiuc, L. C. Tănase, A. Barinov, N. G. Apostol, C. Chirilă, L. Trupină, L. Pintilie, C. M. Teodorescu, Nanoscale 9, 11055-11067 (2017).

G. A. Boni, L. D. Filip, C. Chirila, I. Pasuk, R. Negrea, I. Pintilie and L. Pintilie, Nanoscale 9, 19271–19278 (2017)

C. Besleaga, V. Dumitru, L. M. Trinca, A. C. Popa, C. C. Negrila, G. E. Stan, Ł. Kołodziejczyk, C. R. Luculescu, G. C. Ionescu, R. G. Ripeanu, A. Vladescu, Nanomaterials 7, 394 (2017).

S. L. Iconaru, A. M. Prodan, N. Buton, D. Predoi, Molecules, 22, 604 (2017).

M. Beregoi, A. Evanghelidis, V. C. Diculescu, H. Iovu, I. Enculescu, ACS Applied Materials & Interfaces 9, 38068-38075 (2017)

M. Beregoi, A. Evanghelidis, E. Matei, I. Enculescu, Sensors and Actuators B: Chemical 253, 576-583 (2017)

Directorate

General Director: **Dr. Ionuț Marius ENCULESCU**

Scientific Director: **Dr. Lucian PINTILIE**

Economic Director: **Ec. Gabriela IVĂNUȘ**

National Institute of Materials Physics
405A Atomistilor Street, PO BOX MG-7, Măgurele, Ilfov, România

Phone: + 4 021 369 01 85
Fax: + 4 021 369 01 77

Email

Dr. I. ENCULESCU: director@infim.ro
Dr. L. PINTILIE: pintilie@infim.ro

Website

www.infim.ro

Contents

FOREWORD

The 2017 year was marked by significant administrative and financial instability, produced by the change of Government following the elections at the end of 2016. This had a negative impact on socio-economic life, including research activities and institutions.

The main problem is the lack of predictability in funding, making difficult to maintain operational the researcher infrastructure and to preserve the human resource employed and trained in the last 5-6 years.

The Core Program 2016-2017 has ended on 31 of December 2017 and a new Core Program has been launched in late March 2018, with a delay of 2.5 months and only for the 2018 calendar year. Another problem was that only few major competitions were launched in 2016 in the frame of the National R&D program 2014-2020, some of them finalized end of 2016 or beginning 2017 (e.g. PED, Bridge Grant, PTE, PCE) some of them to be finalized in 2018 (e.g. PD, TE, PCCF). Only one major competition was launched in 2017, PCCDI, with contracts to be signed at the beginning of 2018.

NIMP has signed 9 PCE contracts in 2017 and will have in 2018 the following new contracts: 3 PCCDI projects as coordinator and other 7 as partners; 6 TE projects; 4 PD projects. Unfortunately, NIMP has no chance for a funded PCCF project, either as coordinator or as partner.

In 2018 has started a new H2020 project having NIMP as partners. The project title is “Energy efficient embedded non-volatile memory logic based on ferroelectric Hf(Zr)O2” and the consortium includes 8 partners, being led by CEA-France.

The funding insecurity is reflected in the number of published articles, which is on a slightly decreasing trend in the last years (see figure 1). This is because many researchers spend more time looking for various sources of funding than doing true research work disseminated through articles.

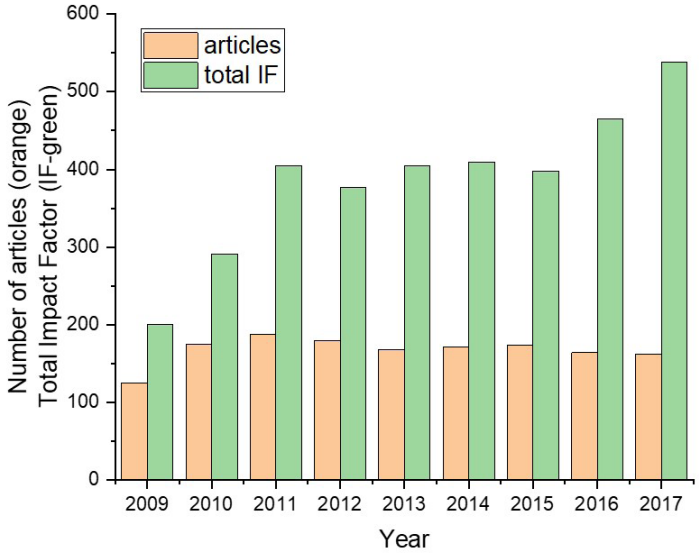

Fig. 1: The evolution of total number of articles and total IF in the last 9 years.

However, although the total number of articles in journals with Impact Factor (IF) has slightly decreased, the total impact factor has considerably increased in the last years, reaching a value of nearly 550 in 2017. This achievement implies that the number of articles published in journals with high Impact factor has significantly increased, as can be seen from figure 2.

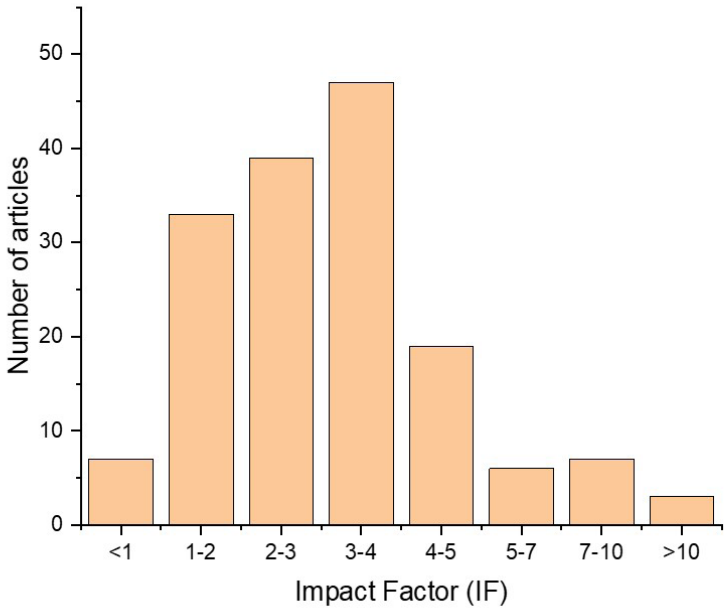

Fig. 2: Distribution of articles upon the IF of journal where they were published.

Another significant achievement in 2017 was the increase of the number for national patent request to 17.

Several scientific events were held in 2017, having NIMP as organizer od co-organizer: second edition of the International Workshop of materials Physics; 8th edition of the international conference on Amorphous and Nanostructured Chalcogenides (ANC-8); the joint conference of 9th edition of ROCAM and 2nd edition of ISyDMA (International Symposium on Dielectric Materials and Applications).

Although the amount of funding for the next years is largely unknown, NIMP maintained its attraction for young and experienced researchers. A record number of over 10 persons were employed in 2017 on positions standing from young research assistant to senior researcher rank 1 (equivalent university professor).

The NIMP's top management is making considerable efforts to identify new funding sources. In any case, without the Core Program and with project competitions organized very rarely and with small budgets it will be very difficult to secure the minimum funding for operation in 2019 and following years.

Dr. Ionuț Marius ENCULESCU
General Director

LABORATORIES

10. Laboratory of Multifunctional Materials and Structures

The laboratory is divided into two research groups:

- The group of functional nanostructures, which includes teams with research interests in the field of preparation and characterization of different nano-objects (nanoparticles, nanotubes, nanowires or nano-strips) with potential applications in micro- and nano-optoelectronics (field effect transistors, hybrid LED or photodiodes), advanced sensors (with a focus on bio- sensors), renewable energy and medicine (biocompatible and / or biofunctional materials).
- The group of complex heterostructures and perovskite oxides, which includes teams working with research interests in the preparation and characterization of oxide materials with dielectric, ferroelectric, multiferroic properties or semiconductors for applications in micro- and nano-electronics (non-volatile memories, transparent electronics), telecommunications and security (devices for emitting-receiving of microwaves), advanced sensors (pyroelectric sensing and photoconductor), solar cells (based on the photovoltaic effect in ferroelectrics or other perovskites), medicine (2D and 3D coatings with biocompatible / biofunctional oxides).

Teams working in the laboratory carry out both fundamental research related to identifying and explaining the physical and chemical phenomena that occur in the obtained materials and structures (in particular size effect, interfaces, doping/stoichiometry) , as well as development activities of various applications such as sensors, field effect transistors, photovoltaic cells, apparatus for processing materials. Research topics are generally multidisciplinary, requiring collaboration between physicists, chemists and engineers.

The human resources of the laboratory consist of 8 CS1, 4 CS2, 8 CS3, 4 CS, 14 ACS, two sub- engineers, five technicians and two workers. The laboratory infrastructure includes modern equipment for preparing and characterizing including: systems of pulsed laser deposition (PLD and MAPLE); sputter deposition systems in magnetron (RF and DC); scanning electron microscope (SEM); microfluorescence microscope; cryoprobes with vertical and horizontal magnetic fields and illumination facilities with UV radiation; vector analyzer for networks up to 325 GHz ; THz spectrometer (up to 7 THz); spectroscopic ellipsometer; FTIR spectrometers and UV-Vis; fluorescence spectrometer; magnetic circular dichroism spectrometer.

20. Laboratory of Magnetism and Superconductivity

The laboratory is devoted to research in the field of materials with magnetic or superconducting properties. The research process covers all stages from preparation (bulk materials, thin films and nanostructures) to structural and electronic characterization, completed by thorough analysis of magnetic and superconducting properties. The research is focused mainly on the study of nanostructures, especially nanoparticle systems and multilayer magnetic materials for colossal magnetoresistance (CMR), giant magnetoresistance (GMR) and tunneling magnetoresistance (TMR), soft and hard magnetic materials, magnetic diluted semiconductors, but also on materials working under extreme conditions. In the case of superconducting materials, superconductors of high critical temperatures are especially targeted, as thin films with nanometric inclusions for pinning, MgB2 (bulk and strip), superconductors in the class of Fe-based pnictides (FeSmAsFxO1-x), new superconducting materials, etc.

Among the most important research equipment, targeting both the infrastructure of preparation and characterization, we mention the following: spark plasma sintering equipment, microwave sintering installation, melt spinning installation, system for preparing nanoparticles by hydrothermal/solvothermal synthesis in autoclave and centrifugation for separation by size, laser ablation deposition (PLD) system, magnetic multilayer deposition system by RF and DC sputtering with 4 sources and vacuum based in the 10- 9 mbar domain, radiofrequency thermal transfer facility to determine SAR in magnetic nanoparticles systems, systems for thermo-gravimetric determination, Vibrating Sample Magnetometer systems (VSM) for up to 9 Tesla magnetic fields, Mossbauer systems with various accessories to carry out measurements at variable temperatures (4.5 K - 1000 K) also in applied fields by detection of radiation gamma / X-ray /conversion electrons, a complex system of measuring the physical properties (PPMS) with magnetic fields up to 14 Tesla, a SQUID type magnetometer system (Superconducting Quantum Interference Device) and a liquid He production unit (18 l / 24 h).

For the high temperatures field, the laboratory has a Laser Flash Analyzer system which enables the defining of thermal diffusivity, specific heat and thermal conductivity of the bulk or multi-layer (3-layer, including liquids) materials in the range of 25-1100 C, a dilatometer (Netzsch C 402, 2015) for determining the coefficients of thermal expansion (25-1600 C) and an equipment (Netzsch, Nemesis 2015) for determining electrical conductivity and the Seebeck coefficient (25-800 C).

Spark Plasma Sintering

30. Laboratory of Nanoscale Condensed Matter

The subjects of experimental investigation are directed towards the properties and the specific processes of the low dimensional systems, supplemented by modeling of the morphology, structure and composition, electric transport and phototransport, of the ferroic properties, chemical activity and surface/interface processes, as well as the phenomena of capture and storage of charge carriers for memory effects. Various types of nanostructured materials (e.g. nanostructures and nanocomposites, surfaces and interfaces with different features, especially magnetic, ferroelectric and catalytic properties) are prepared through advanced cleaning and deposition by physical methods (evaporation, sputtering).

An important part of the research that is done in the laboratory is aimed at applications in micro- and nanoelectronics, optoelectronics, spintronics, advanced sensors, photocatalysis and heterogeneous catalysis.

Theoretical investigations are largely motivated by recent results and aim at: the spectral properties of the Lieb optical networks and of the topological insulators, charge transport of the bidimensional materials (e.g. graphene, phosphorene), the dynamics of excitons in optically active quantum dots including magnetic impurities, artificial nanomagnets.

In the laboratory there are two "clusters" dedicated to the study of in-situ surfaces, which operate in ultra-vacuum (UHV 10^{-10} – 10^{-11} mbar). Each system is comprised of a preparation chamber by molecular beam epitaxy (MBE), a photoelectron spectroscopy characterization (XPS, UPS) chamber and a characterization by scanning tunneling microscopy (STM) chamber. In MBE systems there also the following in-situ characterization processes: fast and slow electron diffraction RHEED, LEED, thermal desorption by mass spectrometry studies, Auger electron spectroscopy. The XPS-UPS chambers permit spectroscopy measurements with angular resolution (photoelectron diffraction, dispersion laws in the valence band) and, in the case of one of the two clusters, also spin. Thus one can determine the atomic composition, the nature of chemical bonds, the structure at a nanoscopic scale, band structure.

Currently, one of the two clusters is located at Elettra synchrotron in Trieste. The LEEM-PEEM microscope (Low-Energy Electron Microscopy- Photoelectron Electron Microscopy) allows the investigation of samples with nanometer resolution using slow electrons (hence ideal for sensitive or insulating samples) as well as photoelectron spectroscopy studies with spatial resolution in the order of 20 nm. A third XPS automatic equipment allows investigation of several samples simultaneously and XPS analysis with spatial resolution in the order of 200 m, coupled with the possibility of in situ thermal treatment at high values of pressure (4 bar) and temperature (1000° C). The magnetron sputtering equipment (10-8 torr high vacuum) for deposition of thin films and multi-layer structures is equipped with in situ analysis techniques consisting of Auger electron surface spectroscopy and diffraction low-energy electron diffraction – LEED, as well as real time in situ ellipsometric monitoring. For thermal processing under controlled conditions, there is a rapid heat treatment equipment (RTA) in inert gas, oxidation - RTO and nitriding RTN.

Lab 30 carries out also complex experimental studies of the surfaces, interfaces (ferromagnetism, ferroelectrics, catalysis) of certain thin layers and multi- layer structures based on nanocrystals from the GeSiSn system (correlated with modeling studies), and studies of certain 2D semiconductor materials based on chalcogenides of (2D-TMD) transition metals.

For experimental studies, the laboratory is equipped with three chains for electrical and photoelectric, Hall effect and magnetoresistance measurements.

40. Laboratory of Optical Process in Nanostructured Materials

This laboratory is almost entirely dedicated to optical investigative methods applied to materials and focusing on nanostructures and nanocomposites. Other research topics are related to : the preparation and characterization of nanoscale semiconducting polymers with special properties, electrochemistry and production and characterization of chalcogenide glasses.

The main equipment used for optical characterization of investigated materials are: UV-Vis-NIR and FTIR absorption spectrophotometry, FTIR imaging microscope, FTRaman equipped with a YAG: Nd laser, confocal Raman spectrophotometer equipped with Ar and Kr lasers, SNOM (Scanning Near Field Optical Microscope) coupled with AFM (Atomic Force Microscope), systems for photoluminescence in VIS and NIR and thermoluminescence, and experimental setups for solar simulator and photoconductivity.

Other equipment used in the characterization and / or preparation of the studied materials are: broadband dielectric spectroscopy system, drop shape analysis for estimation of contact angle, equipment for deposition by vacuum evaporation of organic materials, Langmuir-Blodgett film deposition systems and potentiostats/galvanostats for the synthesis of composite materials and their testing as electrode materials in battery and supercapacitors.

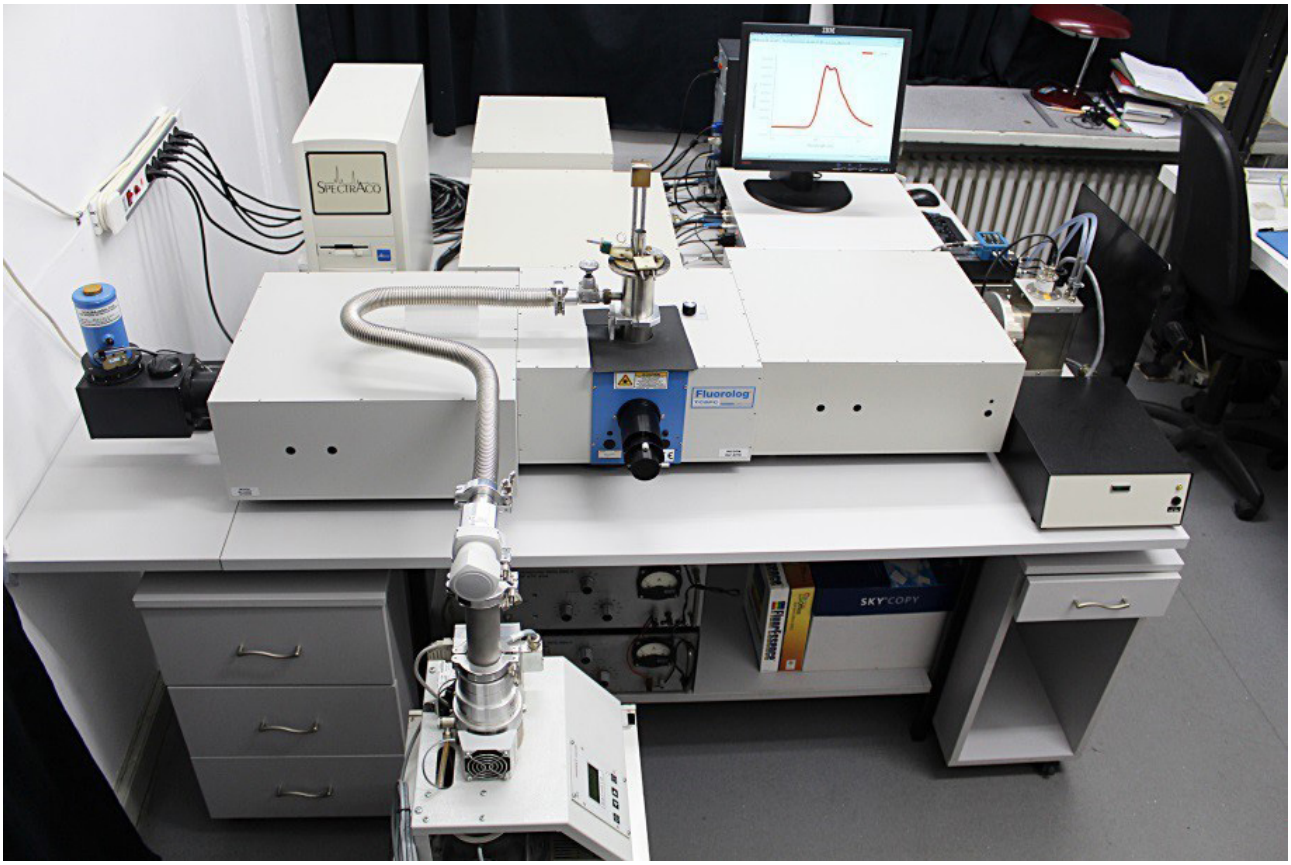

Fluorolog-3, model FL3-22, Horiba Jobin Yvon

50. Laboratory of Atomic Structures and Defects in Advanced Materials

This laboratory is mainly committed to structural investigations by advanced characterization methods such as analytical transmission electron microscopy (TEM) and scanning electron microscopy (SEM), electron paramagnetic resonance (EPR), Mössbauer spectroscopy, evaluation of physical properties in controlled environments (gas sensors, photocatalysis). The research activity includes, also, synthesis of nanostructured materials by the hydrothermal or co-precipitation methods. Among the important research equipment we mention: an aberration-corrected analytical HRTEM/STEM; a high-resolution analytical electron microscope for electron tomography and in-situ heating/cooling experiments; a conventional transmission electron microscopy; preparation equipment of TEM/SEM specimens; a SEM-FIB dual analytical system; five EPR spectrometers operating in several microwave bands and working modes in continuous wave or in pulsed regime, down to liquid He temperature; He liquefaction station; three Mössbauer spectrometers in the temperature range 4-1000 K; XRD diffractometers for powders and thin films; gas mixing station and associated electrical measurements equipments for materials testing under controlled atmosphere; specialized equipment for hydrothermal and co-precipitation synthesis.

The high resolution electron microscope is provided with probe Cs corrector of the spherical aberration and EDS and EELS microanalytical facilities, allowing a spatial resolution under 1 A and atomic elemental mapping. The SEM-FIB dual system is used for morphostructural and microanalytical investigations (SEM, EDS, EBSD) and for the processing of advanced materials at micro and nanometric scale by means of a Ga+ ion beam and nanomanipulators. The HRTEM and EPR spectroscopy facilities are included in the European network of research infrastructures C-ERIC (http://www.c-eric.eu/).

The research activity of the scientists working in this laboratory is focused on the physical properties of advanced materials (structure, optical), resulting either as size effects (nanostructures, thin films) or as structural defect engineering. The scientific concerns are mainly directed towards the discovery, investigation and manipulation of physical properties at nanometric and atomic scale for the development and characterization of functional materials to be used in various applications.

a. High resolution analytical transmission electron microscope (0.08 nm in mode STEM HAADF);

b. Analytical SEM-FIB dual system;

c. RES spectrometer in X band (9.7 GHz) in pulsed regime with accessories ENDOR;

d. Mossbauer spectrometer with cryostate for high magnetic fields (7 T) and cryogenic temperatures

e. Setup for electrical measurements in controlled atmosphere gas mixing station.

PERSONNEL

LIST OF PERSONNEL

Lab. 10 – Laboratory of Multifunctional Materials and Structures	
HEAD: Dr. Silviu POLOSAN	**E-mail:** silv@infim.ro **Phone:** (+4) 021.369.01.85 **Fax:** (+4) 021.369.01.77

#	NAME	POSITION
01	Dr. Marian Gabriel BANCIU	Senior Researcher I
02	Dr. Victor-Constantin DICULESCU	Senior Researcher I
03	Dr. Maria Monica ENCULESCU	Senior Researcher I
04	Dr. Aurelian Catalin GALCA	Senior Researcher I
05	Dr. Corneliu Florin MICLEA	Senior Researcher I
06	Dr. Ioana PINTILIE	Senior Researcher I
07	Dr. Nicoleta Roxana PREDA	Senior Researcher I
08	Dr. Daniela PREDOI	Senior Researcher I
09	Dr. George STAN	Senior Researcher I
10	Dr. Lucian-Dragos FILIP	Senior Researcher II
11	Dr. Lucia LEONAT	Senior Researcher II
12	Dr. Elena MATEI	Senior Researcher II
13	Dr. Liviu NEDELCU	Senior Researcher II
14	Dr. Luminita AMARANDE	Senior Researcher III
15	Dr. Cristina BESLEAGA STAN	Senior Researcher III
16	Dr. Andra-Georgia BONI	Senior Researcher III
17	Dr. Florentina Cristina CHIRILA	Senior Researcher III
18	Dr. Steluta Carmen CIOBANU	Senior Researcher III
19	Dr. Teodor-Adrian ENACHE	Senior Researcher III
20	Dr. Mihaela FLOREA	Senior Researcher III
21	Dr. Luminita Mirela HRIB	Senior Researcher III
22	Dr. Madalina-Maria IGNAT-BARSAN	Senior Researcher III
23	Dr. Alin IUGA	Senior Researcher III

#	NAME	POSITION
24	Dr. Iuliana PASUK	Senior Researcher III
25	Dr. Roxana RADU	Senior Researcher III
26	Dr. Viorica STANCU	Senior Researcher III
27	Dr. Lucian TRUPINA	Senior Researcher III
28	Dr. Ioana-Mihaela BOTEA	Senior Researcher
29	Dr. Marius CIOANGHER	Senior Researcher
30	Dr. Iulia Corina CIOBOTARU	Senior Researcher
31	Dr. Liliana Andreea COSTAS	Senior Researcher
32	Dr. Viorel DUMITRU	Senior Researcher
33	Dr. Camelia-Florina FLORICA	Senior Researcher
34	Anca ALDEA	Assistant Researcher
35	Liliana-Marinela BALESCU	Assistant Researcher
36	Mihaela BEREGOI	Assistant Researcher
37	Dr. Constantin Claudiu CIOBOTARU	Assistant Researcher
38	Daniela Emilia DOGARU	Assistant Researcher
39	Alexandru-Ionut EVANGHELIDIS	Assistant Researcher
40	Irina Sorina GHITA	Assistant Researcher
41	Simona-Liliana ICONARU	Assistant Researcher
42	Melania Loredana ONEA	Assistant Researcher
43	Dr. Adrian Claudiu POPA	Assistant Researcher
44	Dorin RUSU	Assistant Researcher
45	Andrei-Gabriel TOMULESCU	Assistant Researcher
46	Alexandru GAVRILA	Assistant Engineer
47	Constantin JELEA	Assistant Engineer
48	Vasilica TOMA	Assistant Engineer

Lab. 20 – Laboratory of Magnetism and Superconductivity	
HEAD: Dr. Victor Eugen KUNCSER	**E-mail:** kuncser@infim.ro **Phone:** (+4) 021.369.01.85 **Fax:** (+4) 021.369.01.77

#	NAME	POSITION
01	Dr. Gheorghe ALDICA	Senior Researcher I
02	Dr. Petre BADICA	Senior Researcher I
03	Dr. Ioan Adrian CRISAN	Senior Researcher I
04	Dr. Ovidiu Alexandru CRISAN	Senior Researcher I
05	Dr. George FILOTI	Senior Researcher I (associate collaborator)
06	Dr. Andrei GALATANU	Senior Researcher I
07	Dr. Lucica MIU	Senior Researcher I
08	Dr. Neculai PLUGARU	Senior Researcher I
09	Dr. Viorel Constantin SANDU	Senior Researcher I
10	Dr. Mihaela VALEANU	Senior Researcher I
11	Dr. Florin VASILIU	Senior Researcher I
12	Dr. Petru PALADE	Senior Researcher II
13	Dr. Gabriel-Alexandru SCHINTEIE	Senior Researcher II
14	Dr. Daniela-Alina CRISAN	Senior Researcher II
15	Dr. Cristina BARTHA	Senior Researcher III
16	Dr. Ancuta BIRSAN	Senior Researcher III
17	Dr. Valentina MIHALACHE	Senior Researcher III
18	Dr. Felicia TOLEA	Senior Researcher III
19	Dr. Simona-Gabriela GRECULEASA	Senior Researcher
20	Dr. Ion IVAN	Senior Researcher
21	Dr. Bogdan Vasilica POPESCU	Senior Researcher
22	Dr. Mihaela SOFRONIE	Senior Researcher
23	Mihail BURDUSEL	Assistant Researcher
24	Andrei CATRINA	Assistant Researcher
25	Dr. Cezar Catalin COMANESCU	Assistant Researcher
26	Magdalena GALATANU	Assistant Researcher

#	NAME	POSITION
27	**Mihai-Alexandru GRIGOROSCUTA**	Assistant Researcher
28	**Marinela Alina IONESCU**	Assistant Researcher
29	**Anda Elena STANCIU**	Assistant Researcher
30	**Dr. Carmen PLAPCIANU**	Chemist
31	**Nicusor IACOB**	Engineer
32	**Aurel LECA**	Engineer
33	**Dr. Marilena Tatiana TOMUT**[1]	Senior Researcher III

[1]GSI / KP2 Nuclear Structure and Nuclear Chemistry, Darmstadt.

Lab. 30 – Laboratory of Nanoscale Condensed Matter	
HEAD: Dr. Valeriu MOLDOVEANU	**E-mail:** valim@infim.ro **Phone:** (+4) 021.369.01.85 **Fax:** (+4) 021.369.01.77

#	NAME	POSITION
01	Dr. Lidia Magdalena CIUREA	Senior Researcher I
02	Dr. Sorina LAZANU	Senior Researcher I
03	Dr. Toma STOICA	Senior Researcher I
04	Dr. Cristian Mihail TEODORESCU	Senior Researcher I
05	Dr. Nicoleta Georgiana APOSTOL	Senior Researcher II
06	Dr. Rodica GHITA	Senior Researcher II
07	Dr. Marius Adrian HUSANU	Senior Researcher II
08	Dr. Mihail Florin LAZARESCU	Senior Researcher II
09	Dr. Ionel STAVARACHE	Senior Researcher II
10	Dr. Bogdana-Lenuta BORCA	Senior Researcher III
11	Dr. Maria-Ruxandra COSTESCU	Senior Researcher III
12	Dr. Ion Viorel DINU	Senior Researcher III
13	Dr. Ana Maria LEPADATU	Senior Researcher III
14	Dr. Constantin LOGOFATU	Senior Researcher III
15	Dr. George Adrian LUNGU	Senior Researcher III
16	Dr. Florentina NEATU	Senior Researcher III
17	Dr. Stefan NEATU	Senior Researcher III
18	Dr. Constantin Catalin NEGRILA	Senior Researcher III
19	Dr. Marian NITA	Senior Researcher III
20	Dr. Dana-Georgeta POPESCU	Senior Researcher III
21	Dr. Adrian SLAV	Senior Researcher III
22	Dr. Mugurel TOLEA	Senior Researcher III
23	Dr. Elena-Laura ABRAMIUC	Senior Researcher
24	Dr. Bogdan OSTAHIE	Senior Researcher
25	Dr. Catalin PALADE	Senior Researcher
26	Dr. Mihaela STEGARESCU	Senior Researcher

#	NAME	POSITION
27	Dr. Liviu Cristian TANASE	Senior Researcher
28	Amelia-Elena BOCIRNEA	Assistant Researcher
29	Dr. Costel COTIRLAN SIMIONIUC	Assistant Researcher
30	Ioana-Maria DASCALESCU	Assistant Researcher
31	Radu DRAGOMIR	Assistant Researcher
32	Stefan STANCIU	Assistant Researcher
33	Ioana Cristina BUCUR	Engineer
34	Cristian TACHE	Engineer
35	Dr. Nicolae BIRSAN[1]	Senior Researcher I
36	Dr. Andrei MANOLESCU[2]	Senior Researcher I
37	Dr. Gheorghe IORDACHE[3]	Senior Researcher II

[1]Institute of Physical and Theoretical Chemistry, University of Tübingen.
[2]School of Science and Engineering, Reykjavik, Iceland.
[3]King Abdullah University of Science and Technology, Saudi Arabia.

Lab. 40 – Laboratory of Optical Processes in Nanostructured Materials	
HEAD: Dr. Mihaela BAIBARAC	**E-mail:** barac@infim.ro **Phone:** (+4) 021.369.01.85 **Fax:** (+4) 021.369.01.77

#	NAME	POSITION
01	Dr. Mihail SECU	Senior Researcher I
02	Dr. Anca-Ioana STANCULESCU	Senior Researcher I
03	Dr. Adam LORINCZI	Senior Researcher II
04	Dr. Florinel SAVA	Senior Researcher II
05	Dr. Marian SIMA	Senior Researcher II
06	Dr. Alin VELEA	Senior Researcher II
07	Dr. Constantin Paul GANEA	Senior Researcher III
08	Dr. Oana RASOGA	Senior Researcher III
09	Dr. Elisabeta Corina SECU	Senior Researcher III
10	Dr. Mariana SIMA	Senior Researcher III
11	Dr. Marcela SOCOL	Senior Researcher III
12	Dr. Irina Ionela ZGURA	Senior Researcher III
13	Carmen Steliana BREAZU	Assistant Researcher
14	Monica Alexandra DAESCU	Assistant Researcher
15	Mirela ILIE	Assistant Researcher
16	Adelina MATEA	Assistant Researcher
17	Cristina MOZACEANU	Assistant Researcher
18	Andreea Alexandra NILA	Assistant Researcher
19	Dr. Iosif Daniel SIMANDAN	Assistant Researcher
20	Ion SMARANDA	Assistant Researcher
21	Dr. Malvina Simona STROE	Assistant Researcher

Lab. 50 – Laboratory of Atomic Structures and Defects in Advanced Materials	
HEAD: Dr. Corneliu GHICA	**E-mail:** cghica@infim.ro **Phone:** (+4) 021.369.01.85 **Fax:** (+4) 021.369.01.77

#	NAME	POSITION
01	Dr. Marin CERNEA	Senior Researcher I
02	Dr. Sergiu Vasile NISTOR	Senior Researcher I
03	Dr. Leona Cristina NISTOR	Senior Researcher I
04	Dr. Valentin Serban TEODORESCU	Senior Researcher I
05	Dr. Daniela GHICA	Senior Researcher II
06	Dr. Simona SOMANCESCU	Senior Researcher II
07	Dr. Adelina STANOIU	Senior Researcher II
08	Dr. Mariana STEFAN	Senior Researcher II
09	Dr. Alina BANUTA	Senior Researcher III
10	Dr. Adrian Valentin MARALOIU	Senior Researcher III
11	Dr. Traian POPESCU	Senior Researcher III
12	Dr. Cristian SIMION	Senior Researcher III
13	Dr. Aurel Mihai VLAICU	Senior Researcher III
14	Dr. Andrei Cristian KUNCSER	Senior Researcher
15	Dr. Ionel MERCIONIU	Senior Researcher
16	Dr. Raluca Florentina NEGREA	Senior Researcher
17	Dr. Ioana-Dorina VLAICU	Senior Researcher
18	Marian Cosmin ISTRATE	Assistant Researcher
19	Alexandra-Camelia JOITA	Assistant Researcher
20	Alexandra Maria PALICI	Assistant Researcher
21	Cristian RADU	Assistant Researcher
22	Dr. Manuela STIR	Assistant Researcher
23	Stefan BULAT	Engineer
24	Ovidiu Gabriel FLOREA	Engineer
25	Gheorghe STERIAN	Assistant Engineer

VISITING GUESTS

Dr. Dimitrie CULCER UNSW, Sydney Australia "Quantum transport of Dirac fermions in topological insulators"	**26.01.2017**
Dr. Arpad Mihai ROSTAS Freiburg University, Germany "Flavin mononucleotide radical and atomic Nitrogen characterization using EPR spectroscopy and sensitivity improvement approach"	**26.04.2017**
Dr. Catalin PICU Department of Mechanical, Aerospace and Nuclear Engineering, Rensselaer Polytechnic Institute, Troy, NY 12180, USA "Stability and Mechanical Behavior of Fibrous Materials"	**06.07.2017**
Prof. Masahiko TANI Research Center for Development of Far-Infrared Region, University of Fukui, Japan	**11-14.07.2017**
Dr. Hiroaki MINAMIDE RIKEN Center for Advanced Photonics, Sendai, Japan	**11-14.07.2017**
Prof. Tadao NAGATSUMA Graduate School of Engineering Science, Osaka University, Japan	**11-14.07.2017**
Prof. Nathan NEWMAN Arizona State University, Tempe, AZ, USA	**11-14.07.2017**
Prof. Corinne CHAMPEAUX University of Limoges, Limoges, France	**11-14.07.2017**

Dr. Martin KALTENBRUNNER Johannes Kepler University, Linz, Austria "Soft Electronics and Machines" "Solution-derived Perovskite Semiconductors for Next Generation Solar Cells and Light Emitting Diodes"	**02-03.08.2017**
Prof. Yoshiaki ITO Universitatea din Kyoto, Japonia "The investigation of natural line widths in the atoms with electron excitations and its application to the materials science using high resolution X-ray crystal spectroscopy"	**29.09.2017**
Prof. Arianna FILORAMO Commissariat à l'énergie atomique et aux énergies alternatives (CEA) Saclay, Franta "Polarization-sensitive single-wall carbon nanotubes all-in-one photo-detecting and emitting device working at 1.5 m"	**08.11.2017**
Dr. Simon VASANT Laboratoire d'Electronique et nanoPhotonique Organique, IRAMIS, CEA "Coupling and strong coupling of light emitters with plasmons"	**16.11.2017**
Dr. Mihai-Ionut Sturza Leibniz Institute for Solid State and Materials Research (IFW), Institute for Solid State Research (IFF), Germany "Synthesis and characterization of novel 2D chalcogenide compounds and Iron oxyfluorides with a perovskite-type structure"	**13.12.2017**
WORKING STAGES	
Dr. Marco GIORGETTI Università di Bologna - Dipartimento di Chimica Industriale "Toso Montanari", Italia High energy cathode material at work: structure and morphology checked by in situ XAS, in situ XRD and TEM Consortium C-ERIC, Lab. 50 electron microscopy group (invitation Dr. C. Ghica)	**13-15.11.2017**
Dr. Debora MEIRA ESRF - European Synchrotron Radiation Facility, Franta Cu-Pt bimetallic catalysts: understanding structure-function relationships under combustion of volatile organic compounds Consortium C-ERIC, Lab. 50 electron microscopy group (invitation Dr. C. Ghica)	**12-14.12.2017**

Dr. Barbara CAVALAZZI Università di Bologna, Italia Searching for biosignatures in ancient carbonaceous matter a as evidence of early life. Consortium C-ERIC, Lab. 50 electron microscopy group (invitation Dr. C. Ghica)	**23-26.05.2017**
Dr. Marko KARLUSIC Ruder Boskovic Institute, Croatia Comparison between swift heavy ion and highly charged ion impact sites on the surfaces of SiO2 and CaF2. Consortium C-ERIC, Lab. 50 electron microscopy group (invitation Dr. C. Ghica)	**05-08.06.2017**
Dr. Giovanni DE GIUDICI Università degli Studi di Cagliari - Dipartimento di Scienze della Terra, Italia Effects of X-rays irradiation on biofilm and induced biomineralization processes. Consortium C-ERIC, Lab. 50 electron microscopy group (invitation Dr. C. Ghica)	**03-07.04.2017**
Dr. Marwene OUMEZZINE Laboratoire de Physico-chimie des Matériaux, Département de Physique, Faculté des Sciences de Monastir, Université de Monastir, 5019, Tunisia Synthesis and characterization of new nanostructured compounds based on manganites. Work stage within Lab. 10 – Heterostructures Group (invitation Dr. A. C. Galca)	**23.06-20.08.2017**
Dr. Mihai Ionuț STURZA IFW Leibniz Institute for Solid State and Materials Research, Dresda, Germany Effects induced by chemical doping in two-dimensional calcogenes. Work stage within Lab. 10 – Heterostructures Group (invitation Dr. A. C. Galca)	**26.11 – 15.12.2017**
Mr. Mohamed Yassine ZAKI (doctorand) Ibn Tofail University, Kenitra, Maroc Characterization of Cu_2ZnSnS_4 films electrochemically deposited. Work stage within Lab. 10 – Heterostructures Group (invitation Dr. A. C. Galca)	**07.11 – 20.11.2017**

Ph. D. THESES

Liviu C. TĂNASE
The Surfaces and Interfaces Science applied in the Study of Ferroelectric Materials
November 2017

Carmen BREAZU
Heterostructures based on organic semiconductors for photovoltaic cells: structural, optical and electrical properties
September 2017

Andrei Cristian KUNCSER
The formation and control of magnetic domains and/or magnetic domain walls for various applications
October 2017

AWARDS

ROMANIAN ACADEMY AWARDS

"Radu Grigorovici" Prize for the year 2015 (awarded in 2017)

Raluca NEGREA, Cristina CHIRILA and Georgia BONI
The group of papers: "Structural properties in epitaxial oxide layers, nanostructures and nanocomposites"

Marius HUȘANU and Dana POPESCU
The group of papers: "Photoelectron Spectroscopy and ab-initio calculations in the study of surfaces and interfaces"

INTERNATIONAL AWARDS OBTAINED THROUGH SELECTION PROCESS

IEEE International Semiconductor Conference - CAS 2017 (Sinaia, 11–14.10.2017)

C. Palade, A. Slav, A. M. Lepadatu, S. Lazanu, M. L. Ciurea, T. Stoica
Light illumination effects on floating gate memory with Ge nanocrystals in HfO_2
BEST PAPER AWARD

AWARDS AT INTERNATIONAL FAIRS AND EXHIBITIONS

XV International Inventics Salon PRO INVENT, Cluj-Napoca

D. PREDOI, S. C. CIOBANU, R. GHITA, C. L. POPA, S. ICONARU
Method of obtaining Nano-hydroxyapatite in Silicon Matrix for environmental applications
GOLD MEDAL, DIPLOMA OF EXCELLENCE and DIPLOMA OF EXCELLENCE OF THE 'JUSTIN CAPRA' ASSOCIATION

D. PREDOI, S. C. CIOBANU, R. GHITA, C. L. POPA
Method of obtaining zinc doped Hydroxyapatite in collagen matrix with biomedical applications
GOLD MEDAL and DIPLOMA OF EXCELLENCE

M. L. CIUREA, I. STAVARACHE, V. S. TEODORESCU
Capacitor structure based on germanium nanocrystals embedded in silicon dioxide for nonvolatile memory and fabrication method
GOLD MEDAL and DIPLOMA OF EXCELLENCE

M. GALATANU, G. RUIU, M. ENCULESCU, A. GALATANU
Metallic Cu-based thermal barriers with insulator like thermal conductibility
GOLD MEDAL and DIPLOMA OF EXCELLENCE

European Exhibition of Creativity and Innovation EUROINVENT, IASI, MAI 2017
M. GALATANU, G. RUIU, M. ENCULESCU, A. GALATANU METALLIC Cu-based THERMAL BARRIERS WITH INSULATOR LOKE THERMAL CONDUCTIBILITY **GOLD MEDAL**
M. BURDUSEL, G. V. ALDICA, P. BADICA PROCESSING METHOD AND POWER-IN-A-METAL-SHEATH SUPERCONDUCTING MgB_2-BASED TAPE **GOLD MEDAL**
D. PREDOI, C. S. CIOBANU, R. GHITA, C. L. POPA METHOD OF OBTAINING ZINC DOPED HYDROXYAPATITE IN COLLAGEN MATRIX WITH BIOMEDICAL APPLICATIONS **GOLD MEDAL**
R. GHITA, F. FRUMOSU, C. LOGOFATU, D. PREDOI, C. C. NEGRILA, L. TRUPINA PASSIVATION PROCEDURE OF III-V SEMICONDUCTOR SURFACES AND THE OBTAINING OF A SENSITIVE STRUCTURE TYPE $GaCl_3$-Sb_2S_3/GasB **GOLD MEDAL**
M. ILIESCU, M. LAZAR, I. PINTILIE, L. VLADAREANU, T. NECSOIU, V. STANCU, A. G. TOMULESCU, C. BESLEAGASTAN, M. SIMA, L. LEONAT, E. M. STANCIU, B. COMANESCU, A. V. ENUICA PRINTER FOR SUCCESIVE DEPOSITION OF ULTRA-THIN FILMS WITH DIFFERENT PHYSICAL-CHEMICAL PROPERTIES **SILVER MEDAL and DIPLOMA OF EXCELLENCE CORNELIU GROUP**
D. PREDOI, C. S. CIOBANU, R. GHITA, C. L. POPA METHOD OF OBTAINING NANO-HYDROXYAPATITE IN SILICON MATRIX FOR ENVIRONMENTAL APPLICATIONS **SILVER MEDAL**
C. COTIRLAN-SIMIONUC, A. RIZEA, C. MARIN GOGGLES WITH PLASMONIC METASURFACES THAT OPERATES AS POLARIZATION STATE ANALYZER **SILVER MEDAL**
R. GHITA, C. LOGOFATU, C. C. NEGRILA, F. FRUMOSU, D. PREDOI OBTAINING OF OXIDE COMPOUNDS ON n-GaSb SURFACE **BRONZE MEDAL**
G. A. BONI, C. CHIRILA, L. HRIB, I. PINTILIE, L. PINTILIE FERROELECTRIC MEMORY STRUCTURE WITH MULTIPLE MEMORY STATES AND FABRICATION METHOD **BRONZE MEDAL and SILVER MEDAL of the 'STEFAN CEL MARE' UNIVERSITY, SUCEAVA**
M. BURDUSEL, G. V. ALDICA, P. BADICA PROCESSING METHOD AND POWER-IN-A-METAL-SHEATH SUPERCONDUCTING MgB_2-BASED TAPE **DIPLOMA OF EXCELLENCE CADET INOVA**

R. GHITA, C. LOGOFATU, C. C. NEGRILA, F. FRUMOSU, D. PREDOI
OBTAINING OF OXIDE COMPOUNDS ON n-GaSb SURFACE
DIPLOMA AND MEDAL HALLER PRO INVENTIO FOUNDATION

HONORARY MEMBERSHIP

NIMP is present in following databases:

- **ERRIS infrastructure database:**
  - www.erris.gov.ro: http://www.erris.gov.ro/XPS;
  - http://erris.gov.ro/CEUREMAVSU;
  - http://erris.gov.ro/CMATPHYS_ADVMAT; http://erris.gov.ro/RITECC
- **NIMP** is associate member of the **Agence universitaire de la Francophonie**: https://www.auf.org/) .
- **Magurele Science Park Member**: https://www.magurelesciencepark.ro/noutati/

Other websites:

- http://wikimapia.org/19116027/INCDFM-National-RD-Institute-of-Materials-Physics-NIMP
- http://cercetare.ccib.ro/intranetHTML/infoFILES/infoHTML/File/2012_03_22_prezentare INCDFM.pdf
- http://www.research.gov.ro/ro/articol/1320/sistemul-de-cercetare-incd-institute-nationale-de-cercetare-dezvoltare-institute-nationale-de-cercetare-dezvoltarehttp://www.infocercetare.ro/ro/Listeaza-Institutie/Ilfov-84_Localitate_Magurele- 86_Institutie_INCD-pentru-Fizica-Materialelor-INCDFM-253
- http://ro-ro.facebook.com/pages/INCDFM/122100527823931
- http://site.roinno.ro/data/pdf/ca/369.pdf
- http://www.mhtc.ro/parteneri_activi/institutul-national-pentru-fizica-materialelor-incdfm/
- https://www.e-nformation.ro/institution/incd-pentru-fizica-materialelor-incdfm-magurele
- http://nano-ecol.sanimed.ro/ro/incdfm/
- https://www.topfirme.com/afacere/institutul-na%C5%A3ional-de-cercetare-dezvoltare-pentru-fizica-materialelor-incdfm-bucure%C5%9Fti/1qh7kjrf53/
- http://www.jerome-robg.eu/contact.html
- http://www.demersys-robg.eu/contact.html
- http://primariamagurele.ro/orasul-magurele/institute-de-cercetare
- http://www.psychologies.ro/cunoaste-te/femeile-si-stiintele-exacte-2142052
- http://www.nanofutures.ro/files/misiune_web.pdf
- http://www.infocheck.ro/ro/c/centrul-international-pentru-pregatire-avansata-si-cercetare-in-fizica-filiala-a-incdfm-bucuresti-35920690/40629609
- https://www.emis.com/php/company-profile/RO/Institutul_Na%C8%9Bional_De_Cercetare-Dezvoltare_Pentru_Fizica_Materialelor_-_INCDFM_Bucure%C8%99ti_ro_2086925.html
- http://www.imt.ro/NANOPROSPECT/expozitie_Nanoprospect.htm
- https://indico.cern.ch/event/46144/sessions/177795/attachments/949761/1347571/NIMP.pdf

- http://www.eli-np.ro/2012-3_5-oct/Presentations/Wednesday/Teodorescu121003.pdf
- http://www.ceric-eric.eu/index.php?n=Location.Where
- http://studylib.net/doc/7897966/national-institute-for-materials-physics--nimp--bucharest...
- https://www.nanowerk.com/news/newsid=6723.php

NIMP is member of C-ERIC (Central European Research Infrastructure Consortium, http://www.ceric-eric.eu/). a distributed research facility, set up as an ERIC, by **Austria, Czech Republic, Italy, Romania, Croatia, Polonia, Slovenia, Serbia,** and **Hungary** and open to other interested countries.

The specific scope of this ERIC concerns the offer as an integrated service provided to external researchers who can thus accede to synchrotron light and other microscopic probes for analytical and processing techniques notably for materials preparation and characterization, structural investigations and imaging in Life Sciences, Nanoscience and Nanotechnology, Cultural Heritage, Enviroment and Materials Sciences and to their various technological and industrial outcomes ranging from energy to biomedical and of interest to most manufacturing industries.

CERIC's mission is to bring the integrated service to world-level quality thus contributing to the attractiveness of the European Research Area and stimulating a beneficial impact on the scientific and economic development of the entire region, also helping to introduce a strong interchange between scientists and technicians and attraction of scientists from other regions.

Membership in Other International Organizations, Evaluators and Members in Comissions of Trust

ALDICA GHEORGHE: MEMBER OF EUROPEAN APPLIED SUPERCONDUCTIVITY SOCIETY; EXPERT EVALUATOR UEFISCDI

APOSTOL NICOLETA: MEMBER OF THE ROMANIAN SOCIETY OF CATALYSIS

BADICA PETRE: MEMBER OF AMERICAN CHEMICAL SOCIETY, GERMAN PHYSICAL SOCIETY, EUROPEAN APPLIED SUPERCONDUCTIVITY SOCIETY; EXPERT EVALUATOR UEFISCDI; EXPERT EVALUATOR FOR ICC-IMR JAPAN AND FOR NATO SCIENCE FOR PEACE PROJECTS

BANCIU MARIAN GABRIEL: MEMBER OF IEEE: MICROWAVE THEORY AND TECHNIQUES SOCIETY, ANTENNAS AND PROPAGATION SOCIETY; FOUNDING MEMBER OF ROMANIAN SOCIETY FOR NON-IONIZING RADIATION SAFETY (SRPRNI); EXPERT EVALUATOR UEFISCDI

BARTHA CRISTINA: MEMBER OF ECERS; EXPERT EVALUATOR UEFISCDI

BAIBARAC MIHAELA: EXPERT EVALUATOR UEFISCDI

BURDUSEL MIHAI: MEMBER OF EUROPEAN APPLIED SUPERCONDUCTIVITY SOCIETY

CIUREA MAGDALENA LIDIA: MEMBER OF EUROPEAN PHYSICAL SOCIETY, EXPERT EVALUATOR UEFISCDI

COSTAS LILIANA ANDREEA: MEMBER OF EUROPEAN PHYSICAL SOCIETY; MEMBER OF EUROPEAN MICROSCOPY SOCIETY; MEMBER OF ROMANIAN SOCIETY OF ELECTRON MICROSCOPY

CRISAN OVIDIU: MEMBER OF INSTITUTE OF NANOTECHNOLOGY, UK; MEMBER OF MATERIALS RESEARCH SOCIETY; EXPERT EVALUATOR OF EC, PROGRAM H2020, CALLS H2020-ECSEL-2016-2-IA (INNOVATION ACTIONS) AND H2020-ECSEL-2016-1-RIA (RESEARCH AND INNOVATION ACTIONS); EXPERT EVALUATOR EC, EXECUTIVE AGENCY OF RESEARCH REA, PROGRAM H2020, FET OPEN, VICE-CHAIR, SUPERVISING EVALUATORS FOR CALLS H2020-FETOPEN-2015/2-RIA, H2020-FETOPEN-2016-RIA-1; MONITOR FOR EC OF THE PROJECT DENECOR OF ENIAC JU GRANT AGREEMENT NR. 324257; EXPERT EVALUATOR OF CFCA (CENTRAL FINANCE AND CONTRACTING AGENCY) LETONIA, FOR CALL INDUSTRY-DRIVEN RESEARCH OF THE OPERATIONAL PROGRAM GROWTH & DEVELOPMENT - EU STRUCTURAL AND COHESION FUND; EXPERT EVALUATOR PN III, CALLS EUREKA PN-III-P3-3.5-EUK-2016, ROMANIA-MOLDOVA PN-III-P3-3.1-PM-RO-MD-2016, BRIDGE GRANT PN-III-P2-2.1-BG-2016 AND TRANSFER TO ECONOMIC PARTNER PN-III-P2-2.1-PTE-2016; EXPERT EVALUATOR STRUCTURAL FUNDS POC AXE 1 RESEARCH CALL A P.4; EXPERT EVALUATOR UEFISCDI; MEMBER OF INSTITUTE OF NANOTECHNOLOGY, UK; MEMBER OF MATERIALS RESEARCH SOCIETY MRS;

CRISAN ADRIAN: EXPERT EVALUATOR UEFISCDI; MEMBRU AL EUROPEAN APPLIED SUPERCONDUCTIVITY SOCIETY, MEMBER OF EUROPEAN MATERIALS RESEARCH SOCIETY

DIAMANDESCU LUCIAN: MEMBER OF “AMERICAN NANO SCIENCE”; ROMANIAN REPRESENTATIVE IN INTERNATIONAL BOARD ON THE APPLICATIONS OF MÖSSBAUER EFFECT - IBAME (2011-2017); MEMBER IN EDITORIAL BOARD OF “ISRN NANOMATERIALS” (SUA); EXPERT EVALUATOR UEFISCDI

FRUNZA LIGIA: MEMBER OF AMERICAN CHEMICAL SOCIETY AND OF ROMANIAN SOCIETY OF CATALYSIS

FLOREA MIHAELA: EVALUATOR UEFISCDI; MEMBER OF THE ROMANIAN CHEMSITRY SOCIETY

GALCA AURELIAN CATALIN: EVALUATOR UEFISCDI

GALATANU ANDREI: EVALUATOR UEFISCDI

GHICA CORNELIU: MEMBER OF EUROPEAN MATERIALS RESEARCH SOCIETY; MEMBER OF EUROPEAN MICROSCOPY SOCIETY; VICEPRESIDENT OF ROMANIAN SOCIETY OF ELECTRON MICROSCOPY; EVALUATOR UEFISCDI

GHICA DANIELA: MEMBER OF EUROPEAN MATERIALS RESEARCH SOCIETY

KUNCSER ANDREI CRISTIAN: MEMBER OF EUROPEAN MICROSCOPY SOCIETY; MEMBER OF ROMANIAN SOCIETY OF ELECTRON MICROSCOPY

KUNCSER VICTOR: EXPERT EVALUATOR UEFISCDI; MEMBER IN COMMISSION FOR ASSOCIATE PROFESSOR POSITION AT THE DEPARTMENT OF THEORETICAL PHYSICS, FACULTY OF PHYSICS BUCHAREST

LEPADATU ANA MARIA: MEMBER OF EUROPEAN PHYSICAL SOCIETY

LAZANU SORINA: EXPERT EVALUATOR UEFISCDI

MARALOIU VALENTIN ADRIAN: MEMBER OF SOCIÉTÉ FRANÇAISE DES MICROSCOPIES; MEMBER OF ROMANIAN SOCIETY OF ELECTRON MICROSCOPY; MEMBER OF SOCIETE FRANCAIS DE MICROSCOPIE

MERCIONIU IONEL FLORINEL: MEMBER OF EUROPEAN MICROSCOPY SOCIETY; MEMBER OF ROMANIAN SOCIETY OF ELECTRON MICROSCOPY

NEATU FLORENTINA: MEMBER OF THE ROMANIAN CHEMSITRY SOCIETY

NEATU STEFAN: MEMBER OF THE ROMANIAN CHEMSITRY SOCIETY

NEGREA RALUCA FLORENTINA: MEMBER OF EUROPEAN MICROSCOPY SOCIETY; MEMBER OF ROMANIAN SOCIETY OF ELECTRON MICROSCOPY

NISTOR LEONA CRISTINA: MEMBER OF EUROPEAN MICROSCOPY SOCIETY; VICEPRESIDENT OF ROMANIAN SOCIETY OF ELECTRON MICROSCOPY

NISTOR SERGIU VASILE: MEMBER OF AMERICAN PHYSICAL SOCIETY

PALADE PETRU: MEMBER OF ROMANIAN ASSOCIATION FOR HYDROGEN ENERGY

PINTILIE LUCIAN: MEMBER OF EUROPEAN PHYSICAL SOCIETY; HONORARY MEMBER OF ROMANIAN SOCIETY OF ELECTRON MICROSCOPY; MEMBER IN TASK FORCE CHARACTERIZATION FOR RESEARCH DIRECTORATE OF EC; MEMBER OF THE BOARD FOR ROMANIAN PATRONATE IN RESEARCH; MEMBER CNATDCU; PRESIDENT OF COMISSION OF PHYSICS-CNATDCU; MEMBER OF CNCS; EXPERT EVALUATOR UEFISCDI

PINTILIE IOANA: MEMBER ROMANIAN SOCIETY OF PHYSICS AND EPS; PRESIDENT OF HUMBOLDT CLUB ROMANIA; EXPERT EVALUATOR UEFISCDI

PLUGARU NECULAI: MEMBER IN COMMISSION FOR ASSISTANT PROFESSOR POSITION AT THE DEPARTMENT OF ELECTRICITY, SOLID STATE PHYSICS AND BIOPHYSICS, FACULTY OF PHYSICS, BUCHAREST

POLOSAN SILVIU: EXPERT EVALUATOR UEFISCDI

POPESCU MIHAI: MEMBER OF NACNOG (NORTH ATLANTIC CONSORTIUM ON NON-OXIDE GLASSES, 19 COUNTRIES FROM EUROPE, CANADA ŞI SUA); MEMBER OF VIP (VIRTUAL INSTITUTE OF PHYSICS)

PREDOI DANIELA: MEMBER OF ROMANIAN SOCIETY OF CATALYSIS

SANDU VIOREL: MEMBER OF AMERICAN PHYSICAL SOCIETY AND MATERIAL RESEARCH SOCIETY SINGAPORE

SECU MIHAI: EXPERT EVALUATOR UEFISCDI: MEMBER OF “INTERNATIONAL SOL-GEL SOCIETY”

SOCOL MARCELA: MEMBER OF INTERNATIONAL ORGANIZATION ON CRYSTAL GROWTH

STANCULESCU ANCA: MEMBER OF INTERNATIONAL ORGANIZATION ON CRYSTAL GROWTH; MEMBER OF SPIE; EXPERT EVALUATOR H2020; EXPERT EVALUATOR UEFISCDI

TEODORESCU VALENTIN ŞERBAN: MEMBER OF EUROPEAN MICROSCOPY SOCIETY; GENERAL SECRETARY OF ROMANIAN SOCIETY OF ELECTRON MICROSCOPY

TEODORESCU CRISTIAN MIHAIL: EXPERT EVALUATOR UEFISCDI; EVALUATOR CZECH SCIENCE FOUNDATION; MEMBER OF THE ROMANIAN SOCIETY FOR CATALYSIS

VALEANU MIHAELA: EXPERT EVALUATOR UEFISCDI

VASILIU FLORIN: MEMBER OF EUROPEAN MICROSCOPY SOCIETY; MEMBER OF ROMANIAN SOCIETY OF ELECTRON MICROSCOPY

VLAICU AUREL MIHAI: MEMBER OF EUROPEAN MICROSCOPY SOCIETY; MEMBER OF ROMANIAN SOCIETY OF ELECTRON MICROSCOPY

VLAICU DORINA IOANA: MEMBER OF ROMANIAN SOCIETY OF CHEMISTRY; MEMBER OF ROYAL SOCIETY OF CHEMISTRY AND AMERICAN CHEMICAL SOCIETY

PUBLICATIONS AND PRESENTATIONS

BOOK CHAPTERS

R. V. Ghiță, C. Logofatu, C. C. Negrilă, L. Trupină and C. Cotîrlan-Simioniuc
Surface Modification of III-V Compounds Substrates for Processing Technology,
In: Nanotechnology and Nanomaterials, Chapter 5: "Nanoscaled Films and Layers", Edited by: Laszlo Nanai, ISBN 978-953-51-3143-4, InTech, London, U. K., DOI: 10.5772/65465, (2017).

P. Mele, **A. Crișan** and M. I. Adam
Pinning-Enginnered YBa_2Cu_3Ox Thin Films
In: Springer Series in Materials Science, Chapter: Vortices and Nanostructured Superconductors, pp 15-63, Edited by: Adrian Crisan, ISBN 978-3-319-59353-1, Springer, Cham, Berlin, Germany, (2017).

L. Miu, A. M. Ionescu, D. Miu**, I. Ivan and A. Crisan**
Behavior of the Second Magnetization Peak in Self-nanostructured La_{2-x} $SrxCuO_4$ Single Crystals
In: Springer Series in Materials Science, Chapter: Vortices and Nanostructured Superconductors, pp 159-184, Edited by: Adrian Crisan, ISBN 978-3-319-59353-1, Springer, Cham, Berlin, Germany, (2017).

P. Badica, G. Aldica, A.M. Ionescu, M. Burdusel, D. Batalu
The influence of different additives on MgB_2 superconductor obtained by ex-situ spark plasma sintering: pinning force aspects
In: Nanocomposites and Heterostructures, Chapter: Correlated Functional Oxides, pp 75-116, Edited by: Hiroaki Nishikawa, Nobuyuki Iwata, Tamio Endo, Yayoi Takamura, Gun-Hwan Lee, Paolo Mele, ISBN 978-3-319-43777-4, Springer, Cham, Berlin, Germany, (2017).

M. Popescu, R. Piticescu, E. Vasile, S. Burlacu, **V. Kuncser, G. Schinteie**, D. Appelhans, M. Meyer
High Pressure Hydrothermal Procedure: A Tool for Surface Modification of Superparamagnetic Nanostructured Materials for Medical Applications 695
In: Nanocomposites and Heterostructures, Chapter: Correlated Functional Oxides, pp 75-116, Edited by: Hiroaki Nishikawa, Nobuyuki Iwata, Tamio Endo, Yayoi Takamura, Gun-Hwan Lee, Paolo Mele, ISBN 978-3-319-43777-4, Springer, Cham, Berlin, Germany, (2017).

JOURNALS

Papers in ISI Ranked Journals (with Impact Factor and AIS)

01. **Borca, B**; Michnowicz, T; Petuya, R; Pristl, M; Schendel, V; Pentegov, I; Kraft, U; Klauk, H; Wahl, P; Gutzler, R; Arnau, A; Schlickum, U; Kern, K;
Electric-Field-Driven Direct Desulfurization
ACS NANO, (2017), **11**, pp.4703-4709, **13.942**, 3.995

02. Stange, D; den Driesch, NV; Rainko, D; Roesgaard, S; Povstugar, I; Hartmann, JM; **Stoica, T**; Ikonic, Z; Mantl, S; Grutzmacher, D; Buca, D;
Short-wave infrared LEDs from GeSn/SiGeSn multiple quantum wells
OPTICA, (2017), **4**, pp.185-188, **7.727**, **3.346**

03. Schutz, P; Di Sante, D; Dudy, L; Gabel, J; Stubinger, M; Kamp, M; Huang, Y; Capone, M; **Husanu, MA;** Strocov, VN; Sangiovanni, G; Sing, M; Claessen, R;
Dimensionality-Driven Metal-Insulator Transition in Spin-Orbit-Coupled $SrIrO_3$
PHYSICAL REVIEW LETTERS, (2017), **119**, 256404, **8.462**, **3.266**

04. Qiao, M; Tang, C; **Tanase, LC**; **Teodorescu, CM**; Chen, CM; Zhang, Q; Titirici, MM;
Oxygenophilic ionic liquids promote the oxygen reduction reaction in Pt-free carbon electrocatalysts
MATERIALS HORIZONS, (2017), **4**, pp.895-899, **10.706**, **3.043**

05. Opris, C; Cojocaru, B; **Gheorghe, NG**; Tudorache, M; Coman, SM; Parvulescu, VI; Duraki, B; Krumeich, F; van Bokhoven, JA;
Lignin Fragmentation onto Multifunctional Fe_3O_4@Nb_2O_5@Co@Re Catalysts:
The Role of the Composition and Deposition Route of Rhenium
ACS CATALYSIS, (2017), **7**, pp.3257-3267, **10.614**, **2.751**

06. **Boni, AG; Chirila, C; Pasuk, I; Negrea, RF; Pintilie, I; Pintilie, L;**
Steplike Switching in Symmetric $PbZr_{0.2}Ti_{0.8}O_3$/$CoFeO_4$/$PbZr_{0.2}Ti_{0.8}O_3$ Heterostructures for Multistate Ferroelectric Memory
PHYSICAL REVIEW APPLIED, (2017), **8**, 34035, **4.808**, **2.063**

07. Preuss, K; **Tanase, LC**; **Teodorescu, CM**; Abrahams, I; Titirici, MM;
Sustainable metal-free carbogels as oxygen reduction electrocatalysts
JOURNAL OF MATERIALS CHEMISTRY A, (2017), **5**, UNSP 16336, **8.867**, **1.781**

08. **Abramiuc, LE; Tanase, LC;** Barinov, A**; Apostol, NG; Chirila, C; Trupina, L; Pintilie, L; Teodorescu, CM;**
Polarization landscape effects in soft X-ray-induced surface chemical decomposition of lead zirco-titanate, evidenced by photoelectron spectromicroscopy
NANOSCALE, (2017), **9**, pp.11055-11067, **7.367**, **1.721**

09. Lin, F; Cojocaru, BE; Williams, LS; Cadigan, CA; Tian, CX; **Grecu, MN**; Xin, HL; Vyas, S; Parvulescu, VI; Richards, RM;
Intermediate selectivity in the oxidation of phenols using plasmonic Au/ZnO photocatalysts
NANOSCALE, (2017), **9**, pp.9359-9364, **7.367**, **1.721**

10. **Boni, AG; Filip, LD; Chirila, C; Pasuk, I; Negrea, RF; Pintilie, I; Pintilie, L;**
Multiple polarization states in symmetric ferroelectric heterostructures for multi-bit non-volatile memories
NANOSCALE, (2017), **9**, pp.19271-19278, **7.367**, **1.721**

11. Rizescu, C; Podolean, I; Albero, J; Parvulescu, VI; Coman, SM; **Bucur, IC**; Puche, M; Garcia, H;
N-Doped graphene as a metal-free catalyst for glucose oxidation to succinic acid
GREEN CHEMISTRY, (2017), **19**, pp.1999-2005, **9.125**, **1.697**

12. Karlusic, M; **Ghica, C**; **Negrea, RF**; Siketic, Z; Jaksic, M; Schleberger, M; Fazinic, S;
On the threshold for ion track formation in CaF_2
NEW JOURNAL OF PHYSICS, (2017), **19**, 23023, **3.786**, **1.637**

13. State, R; Papa, F; Tabakova, T; Atkinson, I; **Negrila, CC**; Balint, I;
Photocatalytic abatement of trichlorethylene over Au and Pd-Au supported on TiO_2 by combined photomineralization/hydrodechlorination reactions under simulated solar irradiation
JOURNAL OF CATALYSIS, (2017), **346**, pp.101-108, **6.844**, **1.622**

14. Candu, N; Dhakshinamoorthy, A; **Apostol, NG; Teodorescu, CM;** Corma, A; Garcia, H; Parvulescu, VI;
Oriented Au nanoplatelets on graphene promote Suzuki-Miyaura coupling with higher efficiency and different reactivity pattern than supported palladium
JOURNAL OF CATALYSIS, (2017), **352**, pp.59-66, **6.844**, **1.622**

15. Lazaridis, PA; Karakoulia, SA; **Teodorescu, CM; Apostol, NG; Macovei, D;** Panteli, A; Delimitis, A; Coman, SM; Parvulescu, VI; Triantafyllidis, KS;
High hexitols selectivity in cellulose hydrolytic hydrogenation over platinum (Pt) vs. ruthenium (Ru) catalysts supported on micro/mesoporous carbon
Applied Catalysis B: Environmental, (2017), **214**, pp.1-14, **9.446**, **1.589**

16. **Beregoi, M; Evanghelidis, A; Diculescu, VC;** Iovu, H; **Enculescu, I;**
Polypyrrole Actuator Based on Electrospun Microribbons
ACS APPLIED MATERIALS & INTERFACES, (2017), **9**, pp.38068-38075, **7.504**, **1.581**

17. **Popa, NC;**
Spherical harmonics analysis based on the Reuss model in elastic macro strain and stress determination by powder diffraction
JOURNAL OF APPLIED CRYSTALLOGRAPHY, (2017), **50**, pp.1735-1743, **2.614**, **1.528**

18. **Velea, A**; Opsomer, K; Devulder, W; Dumortier, J; Fan, J; Detavernier, C; Jurczak, M; Govoreanu, B;
Te-based chalcogenide materials for selector applications
SCIENTIFIC REPORTS, (2017), **7**, 8103, **4.259**, **1.484**

19. Diacon, A; Rusen, E; Mocanu, A; **Nistor, LC**;
Supported Cu-0 nanoparticles catalyst for controlled radical polymerization reaction and block-copolymer synthesis
SCIENTIFIC REPORTS, (2017), **7**, 10345, **4.259, 1.484**

20. **Hrib, LM; Pintilie, L;** Alexe, M;
Magnetocapacitance in $La_{0.7}Sr_{0.3}MnO_3$/$Pb(Zr_{0.2}Ti_{0.8})O^{-3}$/$La_{0.7}Sr_{0.3}MnO_3$ multiferroic heterostructures
SCIENTIFIC REPORTS, (2017), **7**, 6563, **4.259, 1.484**

21. Sitek, A; **Tolea, M; Nita, M**; Serra, L; Gudmundsson, V; Manolescu, A;
In-gap corner states in core-shell polygonal quantum rings
SCIENTIFIC REPORTS, (2017), **7**, 40197, **4.259, 1.484**

22. Mihailescu, IN; Bociaga, D; Popescu-Pelin, G; **Stan, GE**; Duta, L; Socol, G; Chifiriuc, MC; Bleotu, C; Lazar, V; **Husanu, MA; Zgura, I**; Miculescu, F; Negut, I; Hapenciuc, C;
Optimized silicon reinforcement of carbon coatings by pulsed laser technique for superior functional biomedical surfaces fabrication
BIOFABRICATION, (2017), **9**, 25029, **5.24, 1.342**

23. **Nita, M; Tolea, M**; Marinescu, DC; Manolescu, A;
Hund and anti-Hund rules in circular molecules
PHYSICAL REVIEW B, (2017), **96**, 235101, **3.836, 1.227**

24. Rogalev, VA; Rauch, T; Scholz, MR; Reis, F; Dudy, L; Fleszar, A; **Husanu, MA**; Strocov, VN; Henk, J; Mertig, I; Schafer, J; Claessen, R;
Double band inversion in alpha-Sn: Appearance of topological surface states and the role of orbital composition
PHYSICAL REVIEW B, (2017), **95**, 161117, **3.836, 1.227**

25. Krieger, JA; Chang, CZ; **Husanu, MA**; Sostina, D; Ernst, A; Otrokov, MM; Prokscha, T; Schmitt, T; Suter, A; Vergniory, MG; Chulkov, EV; Moodera, JS; Strocov, VN; Salman, Z;
Spectroscopic perspective on the interplay between electronic and magnetic properties of magnetically doped topological insulators
PHYSICAL REVIEW B, (2017), **96**, 184402, **3.836, 1.227**

26. **Teodorescu, CM; Pintilie, L; Apostol, NG; Costescu, RM; Lungu, GA; Hrib, LM; Trupina, L; Tanase, LC; Bucur, IC; Bocirnea, AE;**
Low-energy electron diffraction from ferroelectric surfaces: Dead layers and surface dipoles in clean $Pb(Zr, Ti)O^{-3}$(001)
PHYSICAL REVIEW B, (2017), **96**, 115438, **3.836, 1.227**

27. Miculescu, F; Maidaniuc, A; Voicu, SI; Thakur, VK; **Stan, GE**; Ciocan, LT;
Progress in Hydroxyapatite-Starch Based Sustainable Biomaterials for Biomedical Bone Substitution Applications
ACS SUSTAINABLE CHEMISTRY & ENGINEERING, (2017), **5**, pp.8491-8512, **5.951, 1.181**

28. **Stanoiu, A; Simion, CE;** Calderon-Moreno, JM; Osiceanu, P; **Florea, M; Teodorescu, VS**; Somacescu, S;
Sensors based on mesoporous SnO_2-$CuWO_4$ with high selective sensitivity to H_2S at low operating temperature
JOURNAL OF HAZARDOUS MATERIALS, (2017), **331**, pp.150-160, **6.065, 1.173**

29. Nemnes, GA; **Besleaga, C; Stancu, V; Dogaru, DE; Leonat, L; Pintilie, L**; Torfason, K; Ilkov, M; Manolescu, A; **Pintilie, I**;
Normal and Inverted Hysteresis in Perovskite Solar Cells
JOURNAL OF PHYSICAL CHEMISTRY C, (2017), **121**, pp.11207-11214, **4.536, 1.151**

30. **Plugaru, N**; Nemnes, GA; **Filip, LD; Pintilie, I; Pintilie, L**; Butler, KT; Manolescu, A;
Atomistic Simulations of Methylammonium Lead Halide Layers on $PbTiO_3$ (001) Surfaces
JOURNAL OF PHYSICAL CHEMISTRY C, (2017), **121**, pp.9096-9109, **4.536, 1.151**

31. **Kuncser, V; Schinteie, G; Kuncser, A; Leca, A**; Scarisoreanu, M; Morjan, I; **Filoti, G;**
Physical Mechanisms of Exchange Coupling Effects in Nanoparticulate Diluted Magnetic Oxides Obtained by Laser Pyrolysis
JOURNAL OF PHYSICAL CHEMISTRY C, (2017), **121**, pp.9063-9069, **4.536, 1.151**

32. Avram, D; Cojocaru, B; Tiseanu, I; **Florea, M**; Tiseanu, C;
Down-/Up-Conversion Emission Enhancement by Li Addition: Improved Crystallization or Local Structure Distortion?
JOURNAL OF PHYSICAL CHEMISTRY C, (2017), **121**, pp.14274-14284, **4.536, 1.151**

33. Nemnes, GA; **Besleaga, C; Tomulescu, AG; Pintilie, I; Pintilie, L**; Torfason, K; Manolescu, A;
Dynamic electrical behavior of halide perovskite based solar cells
SOLAR ENERGY MATERIALS AND SOLAR CELLS, (2017), **159**, pp.197-203, **4.784, 1.034**

34. Anastasescu, C; Zaharescu, M; Angelescu, D; Munteanu, C; Bratan, V; Spataru, T; **Negrila, CC**; Spataru, N; Balint, I;
Defect-related light absorption, photoluminiscence and photocatalytic activity of SiO_2 with tubular morphology
SOLAR ENERGY MATERIALS AND SOLAR CELLS, (2017), **159**, pp.325-335, **4.784, 1.034**

35. **Galca, AC**; Oumezzine, M; **Leca, A; Chirila, C; Kuncser, V; Kuncser, A; Ghica, C; Pasuk, I;** Oumezzine, M;
Structure, transition temperature, and magnetoresistance of titanium-doped lanthanum barium manganite epilayers onto STO 001 substrates
APPLIED PHYSICS LETTERS, (2017), **111**, 182409, **3.411, 0.969**

36. Woerle, J; Bisti, F; **Husanu, MA**; Strocov, VN; Schneider, CW; Sigg, H; Gobrecht, J; Grossner, U; Camarda, M;
Electronic band structure of the buried SiO_2/SiC interface investigated by soft x-ray ARPES
APPLIED PHYSICS LETTERS, (2017), **110**, 132101, **3.411, 0.969**

37. **Pintilie, I; Stancu, V; Tomulescu, AG; Radu, R; Besleaga, C; Trinca, LM; Pintilie, L;**
Properties of perovskite ferroelectrics deposited on F doped SnO_2 electrodes and the prospect of their integration into perovskite solar cells
MATERIALS & DESIGN, (2017), **135**, pp.112-121, **4.364, 0.956**

38. Galizia, P; **Cernea, M; Mihalache, V; Diamandescu, L**; Maizza, G; Galassi, C;
Easy batch-scale production of cobalt ferrite nanopowders by two-step milling: Structural and magnetic characterization
MATERIALS & DESIGN, (2017), **130**, pp.327-335, **4.364, 0.956**

39. **Popa, AC; Stan, GE; Husanu, MA; Mercioniu, I**; Santos, LF; Fernandes, HR; Ferreira, JMF;
Bioglass implant-coating interactions in synthetic physiological fluids with varying degrees of biomimicry
INTERNATIONAL JOURNAL OF NANOMEDICINE, (2017), **12**, pp.683-707, **4.3**, **0.938**

40. **Lepadatu, AM; Palade, C; Slav, A; Maraloiu, AV; Lazanu, S; Stoica, T; Logofatu, C; Teodorescu, VS; Ciurea, ML;**
Single layer of Ge quantum dots in HfO_2 for floating gate memory capacitors
NANOTECHNOLOGY, (2017), **28**, 175707, **3.44**, **0.913**

41. Gies, C; Gericke, F; **Gartner, P**; Holzinger, S; Hopfmann, C; Heindel, T; Wolters, J; Schneider, C; Florian, M; Jahnke, F; Hofling, S; Kamp, M; Reitzenstein, S;
Strong light-matter coupling in the presence of lasing
PHYSICAL REVIEW A, (2017), **96**, 23806, **2.925**, **0.879**

42. **Nila, AA; Baltog, I;** Dragoman, D; **Baibarac, M; Mercioniu, I;**
Influence of TiO_2 and Si on the exciton-phonon interaction in PbI_2 and CdS semiconductors evidenced by Raman spectroscopy
JOURNAL OF PHYSICS-CONDENSED MATTER, (2017), **29**, 365702, **2.678**, **0.870**

43. **Funza, L; Diamandescu, L; Zgura, I; Frunza, S; Ganea, CP; Negrila, CC; Enculescu, M**; Birzu, M;
Photocatalytic activity of wool fabrics deposited at low temperature with ZnO or TiO_2 nanoparticles: Methylene blue degradation as a test reaction
Catalysis Today, (2017), 251-259, **4.636**, **0.848**

44. Hrostea, L; Boclinca, M; **Socol, M**; Leontie, L; **Stanculescu, A**; Girtan, M;
Oxide/metal/oxide electrodes for solar cell applications
SOLAR ENERGY, (2017), **146**, pp.464-469, **4.018**, **0.830**

45. **Sima, M**; Vasile, E; Sima, A; **Logofatu, C**;
Anodic deposition of nanostructured hematite film using agarose gel as template. Application in water splitting
ELECTROCHIMICA ACTA, (2017), **258**, pp.1453-1462, **4.798**, **0.827**

46. Lazarescu, V; Enache, M; Anastasescu, M; Dobrescu, G; **Negrila, CC; Lazarescu, MF**;
Combined Electrochemical Impedance Spectroscopy, X-ray Photoelectron Spectroscopy, and Atomic Force Microscopy study of the distinct behavior of L-cysteine-thiolate formed at p- and n-GaAs(100) electrodes in Sodium Dodecyl Sulfate solution
ELECTROCHIMICA ACTA, (2017), **225**, pp.551-558, **4.798**, **0.827**

47. Nica, IC; Stan, MS; Popa, M; Chifiriuc, MC; Lazar, V; Pircalabioru, GG; Dumitrescu, I; Ignat, M; **Feder, M; Tanase, LC; Mercioniu, I; Diamandescu, L;** Dinischiotu, A;
Interaction of New-Developed TiO_2-Based Photocatalytic Nanoparticles with Pathogenic Microorganisms and Human Dermal and Pulmonary Fibroblasts
INTERNATIONAL JOURNAL OF MOLECULAR SCIENCES, (2017), **18**, 249, **3.226**, **0.806**

48. Turcu, I; Zarafu, I; Popa, M; Chifiriuc, MC; Bleotu, C; Culita, D; **Ghica, C**; Ionita, P;
Lipoic Acid Gold Nanoparticles Functionalized with Organic Compounds as Bioactive Materials
NANOMATERIALS, (2017), **7**, 43, **3.553**, **0.797**

49. Nica, IC; Stan, MS; Popa, M; Chifiriuc, MC; Pircalabioru, GG; Lazar, V; Dumitrescu, I; **Diamandescu, L; Feder, M; Baibarac, M; Cernea, M; Maraloiu, AV; Popescu, T;** Dinischiotu, A;
Development and Biocompatibility Evaluation of Photocatalytic TiO_2/Reduced Graphene Oxide-Based Nanoparticles Designed for Self-Cleaning Purposes
NANOMATERIALS, (2017), **7**, 279, **3.553**, **0.797**

50. **Besleaga, C; Dumitru, V; Trinca, LM; Popa, AC; Negrila, CC**; Kolodziejczyk, L; Luculescu, CR; Ionescu, GC; Ripeanu, RG; Vladescu, A; **Stan, GE**;
Mechanical, Corrosion and Biological Properties of Room-Temperature Sputtered Aluminum Nitride Films with Dissimilar Nanostructure
NANOMATERIALS, (2017), **7**, 394, **3.553**, **0.797**

51. **Beregoi, M; Evanghelidis, A; Matei, E; Enculescu, I;**
Polyaniline based microtubes as building-blocks for artificial muscle applications
SENSORS AND ACTUATORS B-CHEMICAL, (2017), **253**, pp.576-583, **5.401**, **0.786**

52. Grumezescu, V; Holban, AM; Sima, LE; Chiritoiu, MB; Chiritoiu, GN; Grumezescu, AM; Ivan, L; Safciuc, F; Antohe, F; **Florica, C**; Luculescu, CR; Chifiriuc, MC; Socol, G;
Laser deposition of poly(3-hydroxybutyric acid-co-3-hydroxyvaleric acid) - lysozyme microspheres based coatings with anti-microbial properties
INTERNATIONAL JOURNAL OF PHARMACEUTICS, (2017), **521**, pp.184-195, **3.649**, **0.766**

53. **Stanciu, AE; Kuncser, A; Schinteie, G; Palade, P; Leca, A; Greculeasa, SG; Catrina, A; Kuncser, V;**
Tuning magneto-transport properties of Fe-Au granular thin films by cluster organization
JOURNAL OF PHYSICS D-APPLIED PHYSICS, (2017), **50**, 275004, **2.588**, **0.761**

54. **Baibarac, M; Nila, AA; Baltog, I**; Lefrant, S; Mevellec, JY; Quillard, S; Humbert, B;
Influence of single-walled carbon nanotubes enriched in semiconducting and metallic tubes on the electropolymerization of tetrabromo ortho-xylene: Insights on the synthesis mechanism of poly(ortho-phenylenevinylene)
EUROPEAN POLYMER JOURNAL, (2017), **88**, pp.109-125, **3.531**, **0.759**

55. Carp, O; Tirsoaga, A; Ene, R; Ianculescu, A; **Negrea, RF**; Chesler, P; Ionita, G; Birjega, R;
Facile, high yield ultrasound mediated protocol for ZnO hierarchical structures synthesis: Formation mechanism, optical and photocatalytic properties
ULTRASONICS SONOCHEMISTRY, (2017), **36**, pp.326-335, **4.218**, **0.738**

56. Salem-Sugui, S; Mosqueira, J; Alvarenga, AD; Sonora, D; **Crisan, IA; Ionescu, AM;** Sundar, S; Hu, D; Li, SL; Luo, HQ;
Vortex-glass state in the isovalent optimally doped pnictide superconductor $BaFe_2(As_{0.68}P_{0.32})(_2)$
SUPERCONDUCTOR SCIENCE & TECHNOLOGY, (2017), **30**, 55003, **2.878**, **0.719**

57. **Crisan, IA**; Dang, VS; Mikheenko, P; **Ionescu, AM; Ivan, I; Miu, L**;
Synergetic pinning centres in $BaZrO_3$-doped $YBa_2Cu_3O_{7-x}$ films induced by $SrTiO_3$ nanolayers
SUPERCONDUCTOR SCIENCE & TECHNOLOGY, (2017), **30**, 45012, **2.878**, **0.719**

58. **Sandu, V; Greculeasa, SG; Kuncser, A;** Nicolescu, MS; **Kuncser, V;**
Effect of Cr_2O_3 on the magnetic properties of magnetite-based glass-ceramics obtained by controlled crystallization of Fe-containing aluminoborosilicate glass
JOURNAL OF THE EUROPEAN CERAMIC SOCIETY, (2017), **37**, pp.3089-3099, **3.454, 0.701**

59. **Predoi, D; Iconaru, SL**; Deniaud, A; Chevallet, M; Michaud-Soret, I; Buton, N; Prodan, AM;
Textural, Structural and Biological Evaluation of Hydroxyapatite Doped with Zinc at Low Concentrations
MATERIALS, (2017), **10**, 229, **2.654, 0.691**

60. **Predoi, D**; Predoi, MV; **Iconaru, SL**; El Kettani, MEC; Leduc, D; Prodan, AM;
Ultrasonic Measurements on Cyclodextrin/Hydroxyapatite Composites for Potential Water Depollution
MATERIALS, (2017), **10**, UNSP 681, **2.654, 0.691**

61. Tudose, M; Culita, DC; Musuc, AM; Somacescu, S; **Ghica, C**; Chifiriuc, MC; Bleotu, C;
Lipoic acid functionalized SiO2@Ag nanoparticles. Synthesis, characterization and evaluation of biological activity
MATERIALS SCIENCE & ENGINEERING C-MATERIALS FOR BIOLOGICAL APPLICATIONS, (2017), **79**, pp.499-506, **4.164, 0.681**

62. **Bartha, C; Secu, CE; Matei, E; Secu, M;**
Crystallization kinetics mechanism investigation of sol-gel-derived $NaYF_4$:(Yb,Er) up-converting phosphors
CRYSTENGCOMM, (2017), **19**, pp.4992-5000, **3.474, 0.654**

63. **Palade, P; Plapcianu, C; Mercioniu, I; Comanescu, C; Schinteie, G; Leca, A;** Vidu, R;
Structural, Magnetic, and Mossbauer Investigation of Ordered Iron Nitride with Martensitic Structure Obtained from Amorphous Hematite Synthesized via the Microwave Route
INDUSTRIAL & ENGINEERING CHEMISTRY RESEARCH, (2017), **56**, pp.2958-2966, **2.843, 0.630**

64. **Iconaru, SL;** Prodan, AM; Buton, N; **Predoi, D;**
Structural Characterization and Antifungal Studies of Zinc-Doped Hydroxyapatite Coatings
MOLECULES, (2017), **22**, 604, **2.861, 0.628**

65. **Stavarache, I; Maraloiu, AV; Negrila, CC**; Prepelita, P; Gruia, I; Iordache, G;
Photo-sensitive Ge nanocrystal based films controlled by substrate deposition temperature
SEMICONDUCTOR SCIENCE AND TECHNOLOGY, (2017), **32**, 105003, **2.305, 0.623**

66. **Neatu, F**; Trandafir, MM; Marcu, M; Preda, L; Calderon-Moreno, JM; **Neatu, S**; Somacescu, S; **Florea, M**;
Potential application of Ni and Co stabilized zirconia as oxygen reduction reaction catalyst
CATALYSIS COMMUNICATIONS, (2017), **93**, pp.37-42, **3.33, 0.614**

67. Vizireanu, S; Ionita, MD; Ionita, RE; Stoica, SD; **Teodorescu, CM; Husanu, MA; Apostol, NG; Baibarac, M;** Panaitescu, D; Dinescu, G;
Aging phenomena and wettability control of plasma deposited carbon nanowall layers
PLASMA PROCESSES AND POLYMERS, (2017), **14**, e1700023, **2.846, 0.614**

68. **Baibarac, M; Ilie, M; Baltog, I**; Lefrant, S; Humbert, B;
Infrared dichroism studies and anisotropic photoluminescence properties of poly(para-phenylene vinylene) functionalized reduced graphene oxide
RSC ADVANCES, (2017), **7**, pp.6931-6942, **3.108, 0.590**

69. Camps, I; Borlaf, M; Colomer, MT; Moreno, R; Duta, L; Nita, C; del Pino, AP; **Logofatu, C**; Serna, R; Gyorgy, E;
Structure-property relationships for Eu doped TiO_2 thin films grown by a laser assisted technique from colloidal sols
RSC ADVANCES, (2017), **7**, pp.37643-37653, **3.108**, **0.590**

70. **Rasoga, O**; Sima, L; Chiritoiu, M; Popescu-Pelin, G; Fufa, O; Grumezescu, V; **Socol, M; Stanculescu, A; Zgura, I**; Socol, G;
Biocomposite coatings based on Poly(3-hydroxybutyrate-co-3-hydroxyvalerate)/calcium phosphates obtained by MAPLE for bone tissue engineering
APPLIED SURFACE SCIENCE, (2017), **417**, pp.204-212, **3.387**, **0.589**

71. Duta, L; Mihailescu, N; Popescu, AC; Luculescu, CR; Mihailescu, IN; Cetin, G; Gunduz, O; Oktar, FN; **Popa, AC; Kuncser, A; Besleaga, C; Stan, GE;**
Comparative physical, chemical and biological assessment of simple and titanium-doped ovine dentine-derived hydroxyapatite coatings fabricated by pulsed laser deposition
APPLIED SURFACE SCIENCE, (2017), **413**, pp.129-139, **3.387**, **0.589**

72. **Socol, M; Preda, N; Stanculescu, A; Breazu, C; Florica, C**; Stanculescu, F; Iftimie, S; Girtan, M; Popescu-Pelin, G; Socol, G;
Organic heterostructures deposited by MAPLE on AZO substrate
APPLIED SURFACE SCIENCE, (2017), **417**, pp.196-203, **3.387**, **0.589**

73. **Bocirnea, AE; Costescu, RM; Pasuk, I; Lungu, GA; Teodorescu, CM;**
Structural and magnetic properties of Ni nanofilms on Ge(001) by molecular beam epitaxy
APPLIED SURFACE SCIENCE, (2017), **424**, pp.337-344, **3.387**, **0.589**

74. Antonova, K; Duta, L; Szekeres, A; **Stan, GE**; Mihailescu, IN; Anastasescu, M; Stroescu, H; Gartner, M;
Influence of laser pulse frequency on the microstructure of aluminum nitride thin films synthesized by pulsed laser deposition
APPLIED SURFACE SCIENCE, (2017), **394**, pp.197-204, **3.387**, **0.589**

75. Popescu-Pelin, G; Sima, F; Sima, LE; Mihailescu, CN; Luculescu, C; Iordache, I; **Socol, M**; Socol, G; Mihailescu, IN;
Hydroxyapatite thin films grown by pulsed laser deposition and matrix assisted pulsed laser evaporation: Comparative study
APPLIED SURFACE SCIENCE, (2017), **418**, pp.580-588, **3.387**, **0.589**

76. Boyadjiev, SI; Georgieva, V; Stefan, N; **Stan, GE**; Mihailescu, N; Visan, A; Mihailescu, IN; **Besleaga, C**; Szilagyi, IM;
Characterization of PLD grown WO3 thin films for gas sensing
APPLIED SURFACE SCIENCE, (2017), **417**, pp.218-223, **3.387**, **0.589**

77. **Stefan, M; Vlaicu, ID; Nistor, LC; Ghica, D; Nistor, SV;**
Origin and chemical composition of the amorphous material from the intergrain pores of self-assembled cubic ZnS:Mn nanocrystals
APPLIED SURFACE SCIENCE, (2017), **426**, pp.342-350, **3.387**, **0.589**

78. Prepelita, P; Filipescu, M; **Stavarache, I**; Garoi, F; Craciun, D;
Functionalization of carbon nanowalls by plasma jet in liquid treatment
APPLIED SURFACE SCIENCE, (2017), **424**, pp.368-373, **3.387**, **0.589**

79. Braic, M; Vladescu, A; Balaceanu, M; Luculescu, C; Padmanabhan, SC; Constantin, L; Morris, MA; Braic, V; Grigorescu, CEA; Ionescu, P; Dracea, MD; **Logofatu, C**;
A comparative study of the structural, mechanical and tribological characteristics of TiSiC-Cr coatings prepared in CH_4 and C_2H_2 reactive atmosphere by cathodic vacuum arc
APPLIED SURFACE SCIENCE, (2017), **400**, pp.318-328, **3.387**, **0.589**

80. Visan, A; Cristescu, R; Stefan, N; Miroiu, M; Nita, C; **Socol, M; Florica, C; Rasoga, O; Zgura, I**; Sima, LE; Chiritoiu, M; Chifiriuc, MC; Holban, AM; Mihailescu, IN; Socol, G;
Antimicrobial polycaprolactone/polyethylene glycol embedded lysozyme coatings of Ti implants for osteoblast functional properties in tissue engineering
APPLIED SURFACE SCIENCE, (2017), **417**, pp.234-243, **3.387**, **0.589**

81. Floroian, L; Craciun, D; Socol, G; Dorcioman, G; **Socol, M**; Badea, M; Craciun, V;
Titanium implants' surface functionalization by pulsed laser deposition of TiN, ZrC and ZrN hard films
APPLIED SURFACE SCIENCE, (2017), **417**, pp.175-182, **3.387**, **0.589**

82. **Greculeasa, SG; Palade, P; Schinteie, G; Kuncser, A; Stanciu, AE; Lungu, GA;** Porosnicu, C; Lungu, CP; **Kuncser, V**;
Significant change of local atomic configurations at surface of reduced activation Eurofer steels induced by hydrogenation treatments
APPLIED SURFACE SCIENCE, (2017), **402**, pp.114-119, **3.387**, **0.589**

83. Nemnes, GA; Iftimie, S; **Palici, AM**; Nicolaev, A; Mitran, TL; Radu, A; Antohe, S;
Optimization of the structural configuration of ICBA/P3HT photovoltaic cells
APPLIED SURFACE SCIENCE, (2017), **424**, pp.264-268, **3.387**, **0.589**

84. **Stanculescu, A; Rasoga, O; Socol, M**; Vacareanu, L; Grigoras, M; Socol, G; Stanculescu, F; **Breazu, C; Matei, E; Preda, N**; Girtan, M;
MAPLE prepared heterostructures with oligoazomethine: Fullerene derivative mixed layer for photovoltaic applications
APPLIED SURFACE SCIENCE, (2017), **417**, pp.183-195, **3.387**, **0.589**

85. **Stefan, M; Ghica, D; Nistor, SV; Maraloiu, AV**; Plugaru, R;
Mn2+ ions distribution in doped sol-gel deposited ZnO films
APPLIED SURFACE SCIENCE, (2017), **396**, pp.1880-1889, **3.387**, **0.589**

86. **Bocirnea, AE; Tanase, LC; Costescu, RM; Apostol, NG; Teodorescu, CM;**
Band bending at magnetic Ni/Ge(001) interface investigated by X-ray photoelectron spectroscopy
APPLIED SURFACE SCIENCE, (2017), **424**, pp.269-274, **3.387**, **0.589**

87. Prepelita, P; **Stavarache, I; Negrila, CC**; Garoi, F; Craciun, V;
Chalcogenide thin films deposited by rfMS technique using a single quaternary target
APPLIED SURFACE SCIENCE, (2017), **424**, pp.421-427, **3.387, 0.589**

88. Voicescu, M; Ionescu, S; Craciunescu, O; Tatia, R; Moldovan, L; **Teodorescu, VS; Nistor, LC**;
Synthesis, physicochemical characterization and cytotoxic properties of riboflavin loaded Myrj52-silver nanoparticles
NEW JOURNAL OF CHEMISTRY, (2017), **41**, pp.5533-5541, **3.269, 0.574**

89. Ilinca, TA; **Pasuk, I**; Circu, V;
Bis-imidazolium salts with alkyl sulfates as counterions: synthesis and liquid crystalline properties
NEW JOURNAL OF CHEMISTRY, (2017), **41**, pp.11113-11124, **3.269, 0.574**

90. Elisa, M; Iordanescu, CR; Vasiliu, IC; Feraru, ID; Epurescu, G; Filipescu, M; **Plapcianu, C; Bartha, C**; Trusca, R; Peretz, S
Synthesis and characterization of PLD glass phosphate films doped with CdS
JOURNAL OF MATERIALS SCIENCE, (2017), **52**, pp.2895-2901, **2.599, 0.561**

91. Le Febvrier, A; Deputier, S; Demange, V; Bouquet, V; **Galca, AC; Iuga, A; Pintilie, L**; Guilloux-Viry, M;
Effect of in-plane ordering on dielectric properties of highly {111}-oriented bismuth-zinc-niobate thin films
JOURNAL OF MATERIALS SCIENCE, (2017), **52**, pp.11306-11313, **2.599, 0.561**

92. **Boni, AG; Hrib, LM**; Porter, SB; Atcheson, G; **Pintilie, I**; Rode, K; **Pintilie, L**;
Electrical properties of $NiFe_2O_4$ epitaxial ultra-thin films
JOURNAL OF MATERIALS SCIENCE, (2017), **52**, pp.793-803, **2.599, 0.561**

93. **Tanase, LC; Lungu, GA; Abramiuc, LE; Bucur, IC; Apostol, NG; Costescu, RM; Tache, CA; Macovei, D;** Barinov, A**; Teodorescu, CM;**
Long-range magnetic interaction in Mn_xGe_{1-x}: structural, spectromicroscopic and magnetic investigations
JOURNAL OF MATERIALS SCIENCE, (2017), **52**, pp.3309-3320, **2.599, 0.561**

94. Zavoianu, R; Pavel, OD; Cruceanu, A; **Florea, M**; Birjega, R;
Functional layered double hydroxides and their catalytic activity for 1,4-addition of n-octanol to 2-propenonitrile
APPLIED CLAY SCIENCE, (2017), **146**, pp.411-422, **3.101, 0.560**

95. Queralto, A; del Pino, AP; **Logofatu, C**; Datcu, A; Amade, R; Alshaikh, I; Bertran, E; Urzica, I; Gyorgy, E;
MAPLE synthesis of reduced graphene oxide/silver nanocomposite electrodes: Influence of target composition and gas ambience
JOURNAL OF ALLOYS AND COMPOUNDS, (2017), **726**, pp.1003-1013, **3.133, 0.552**

96. Porosnicu, I; Avram, D; Cojocaru, B; **Florea, M**; Tiseanu, C;
Up-conversion luminescence of Er(Yb)-CeO_2: Status and new results
JOURNAL OF ALLOYS AND COMPOUNDS, (2017), **711**, pp.627-636, **3.133, 0.552**

97. Ozturk, K; Dancer, CEJ; Savaskan, B; Aksoy, C; Guner, B; **Badica, P; Aldica, G**; Celik, S;
The investigation on the regional nanoparticle Ag doping into $MgTi_{0.06}B_2$ bulk for improvement the magnetic levitation force and the bulk critical current
JOURNAL OF ALLOYS AND COMPOUNDS, (2017), **724**, pp.427-434, **3.133, 0.552**

98. **Birsan, A;**
Small interfacial distortions lead to significant changes of the half-metallic and magnetic properties in Heusler alloys: The case of the new CoFeZrSi compound
JOURNAL OF ALLOYS AND COMPOUNDS, (2017), **710**, pp.393-398, **3.133, 0.552**

99. Stanciu, CA; **Cernea, M; Secu, CE; Aldica, G; Ganea, P**; Trusca, R;
Lanthanum influence on the structure, dielectric properties and luminescence of $BaTiO_3$ ceramics processed by spark plasma sintering technique
JOURNAL OF ALLOYS AND COMPOUNDS, (2017), **706**, pp.538-545, **3.133, 0.552**

100. Monea, BF; Ionete, EI; Spiridon, SI; **Leca, A; Stanciu, AE**; Petre, E; Vaseashta, A;
Single Wall Carbon Nanotubes Based Cryogenic Temperature Sensor Platforms
SENSORS, (2017), **17**, 2071, **2.677, 0.546**

101. **Polosan, S; Ciobotaru, CC; Ciobotaru, IC**; Tsuboi, T;
Crystallization properties of IrQ(ppy)(2) organometallic complex films
JOURNAL OF MATERIALS RESEARCH, (2017), **32**, pp.1735-1740, **1.673, 0.541**

102. Khalakhan, I; Lavkova, J; Matolinova, I; Vorokhta, M; Potin, V; Kus, P; Vaclavu, M; **Maraloiu, AV; Kuncser, A**; Matolin, V;
Electrochemically shape-controlled transformation of magnetron sputtered platinum films into platinum nanostructures enclosed by high-index facets
SURFACE & COATINGS TECHNOLOGY, (2017), **309**, pp.6-11, **2.589, 0.523**

103. Micutz, M; **Pasuk, I**; Ilis, M;
Tuning the liquid crystalline properties of palladium(II) metallomesogens: A study of rod-like to disc-like transition in cyclopalladated complexes with N-benzoyl thiourea derivatives
JOURNAL OF MOLECULAR LIQUIDS, (2017), **243**, pp.151-156, **3.648, 0.490**

104. Ilis, M; Batalu, D; **Pasuk, I**; Circu, V;
Cyclometalated palladium(II) metallomesogens with Schiff bases and N-benzoyl thiourea derivatives as co-ligands
JOURNAL OF MOLECULAR LIQUIDS, (2017), **233**, pp.45-51, **3.648, 0.490**

105. **Iconaru, SL**; Chifiriuc, MC; Groza, A;
Structural and Antimicrobial Evaluation of Silver Doped Hydroxyapatite- Polydimethylsiloxane Thin Layers
JOURNAL OF NANOMATERIALS, (2017), 7492515, **1.871, 0.486**

106. Dragoman, D; **Breazu, C;**
Fault-tolerant bandstructure of two-dimensional square photonic crystals with different dielectric rod shapes
PHOTONICS AND NANOSTRUCTURES-FUNDAMENTALS AND APPLICATIONS, (2017), **24**, pp.12-17, **1.705, 0.475**

107. **Dinu, IV; Moldoveanu, V; Dragomir, R;** Tanatar, B;
Unpinning of heavy hole spin in magnetic quantum dots
PHYSICA STATUS SOLIDI B-BASIC SOLID STATE PHYSICS, (2017), **254**, 1600800, **1.674, 0.473**

108. **Nila, AA; Baibarac, M; Matea, A;** Mitran, R; **Baltog, I;**
Exciton-phonon interactions in the Cs3Bi2I9 crystal structure revealed by Raman spectroscopic studies
PHYSICA STATUS SOLIDI B-BASIC SOLID STATE PHYSICS, (2017), **254**, UNSP 1552805, **1.674, 0.473**

109. **Secu, CE; Secu, M; Cernea, M;**
Synthesis and up-conversion luminescence properties of BaFBr-Er^{3+} @SiO_2 core/shell heterostructures
JOURNAL OF LUMINESCENCE, (2017), **188**, pp.96-100, **2.686, 0.462**

110. Gheorghe, C; Hau, S; Gheorghe, L; Voicu, F; Greculeasa, M; Achim, A; **Enculescu, M;**
Optical properties of Sm^{3+} doped $Ca^{-3}(Nb,Ga)(5)O^{-12}$ and $Ca^{-3}(Li,Nb,Ga)(5)O^{-12}$ single crystals
JOURNAL OF LUMINESCENCE, (2017), **186**, pp.175-182, **2.686, 0.462**

111. **Nila, AA; Matea, A; Baibarac, M; Baltog, I;**
The exciton-phonon interaction as stimulated Raman scattering effect supported by the excitonic photoluminescence in BiI_3 layered crystal structure
JOURNAL OF LUMINESCENCE, (2017), **182**, pp.166-171, **2.686, 0.462**

112. Solodkyi, I; Bogomol, I; Loboda, P; Batalu, D; **Vlaicu, AM; Badica, P;**
Floating zone partial re-melting of B4C infiltrated with molten Si
CERAMICS INTERNATIONAL, (2017), **43**, pp.14718-14725, **2.986, 0.460**

113. Dippong, T; Cadar, O; Levei, EA; **Bibicu, I; Diamandescu, L**; Leostean, C; Lazar, M; Borodi, G; Tudoran, LB;
Structure and magnetic properties of $CoFe_2O_4/SiO_2$ nanocomposites obtained by sol-gel and post annealing pathways
CERAMICS INTERNATIONAL, (2017), **43**, pp.2113-2122, **2.986, 0.460**

114. **Amarande, L; Miclea, C; Cioangher, M; Pasuk, I; Iuga, A; Pintilie, I;**
Intrinsic and extrinsic effects near orthorhombic-tetragonal phase transition in barium titanate ceramics doped with small amounts of zirconium
CERAMICS INTERNATIONAL, (2017), **43**, pp.4919-4925, **2.986, 0.460**

115. **Sandu, V**; Cimpoiasu, E; **Greculeasa, SG; Kuncser, A**; Nicolescu, MS; **Kuncser, V**;
Magnetite-based glass-ceramics prepared by controlled crystallization of borosilicate glasses: Effect of nucleating agents on magnetic properties and relaxation
CERAMICS INTERNATIONAL, (2017), **43**, pp.3405-3413, **2.986, 0.460**

116. Mindru, I; Gingasu, D; Patron, L; Marinescu, G; Culita, DC; Calderon-Moreno, JM; Preda, S; **Secu, M;**
Structural and optical properties of un-doped and doped $Sr_3Al_2O_6$ obtained through the tartarate precursor method
CERAMICS INTERNATIONAL, (2017), **43**, pp.16668-16675, **2.986, 0.460**

117. **Kuncser, A;** Antohe, S; **Kuncser, V;**
A general perspective on the magnetization reversal in cylindrical soft magnetic nanowires with dominant shape anisotropy
JOURNAL OF MAGNETISM AND MAGNETIC MATERIALS, (2017), **423**, pp.34-38, **2.63, 0.456**

118. **Tolea, F; Tolea, M;**
Tuning the transmission phase by the dot size
PHYSICA E-LOW-DIMENSIONAL SYSTEMS & NANOSTRUCTURES, (2017), **85**, pp.169-173, **2.221, 0.446**

119. **Mihalache, V; Cernea, M; Pasuk, I;**
Relationship between ferromagnetism and, structure and morphology in un-doped ZnO and Fe-doped ZnO powders prepared by hydrothermal route
CURRENT APPLIED PHYSICS, (2017), **17**, pp.1127-1135, **1.971, 0.443**

120. **Polosan, S;**
Crystallisation of bismuth germanate glasses below their glass transition temperature
JOURNAL OF NON-CRYSTALLINE SOLIDS, (2017), **472**, pp.55-60, **2.124, 0.442**

121. Elisa, M; Iordanescu, R; Vasiliu, C; Sava, BA; Boroica, L; **Valeanu, M; Kuncser, V; Galca, AC**; Volceanov, A; Eftimie, M; Melinescu, A; Beldiceanu, A;
Structural and Biological Assessment of Zinc Doped Hydroxyapatite Nanoparticles
JOURNAL OF NON-CRYSTALLINE SOLIDS, (2017), **465**, pp.55-58, **2.124, 0.442**

122. **Baibarac, M; Smaranda, I; Baltog, I;** Lefrant, S; Mevellec, JY;
The influence of single-walled carbon nanotubes on optical properties of the poly[(2,5-bisoctyloy)-1, 4-phenylenevinylene] evidenced by infrared spectroscopy and anti-Stokes photoluminescence
OPTICAL MATERIALS, (2017), **67**, pp.52-58, **2.238, 0.437**

123. Acsente, T; **Negrea, RF; Nistor, LC; Matei, E**; Grisolia, C; Birjega, R; Dinescu, G;
Tungsten nanoparticles with controlled shape and crystallinity obtained by magnetron sputtering and gas aggregation
MATERIALS LETTERS, (2017), **200**, pp.121-124, **2.572, 0.437**

124. **Ilie, M; Baibarac, M;**
The spectrochemical behavior of composites based on poly (para-phenylenevinylene), reduced graphene oxide and pyrene
OPTICAL MATERIALS, (2017), **72**, pp.140-146, **2.238, 0.437**

125. **Tolea, F; Tolea, M; Valeanu, M;**
Thermal memory fading by heating to a lower temperature: Experimental data on polycrystalline NiFeGa ribbons and 2D statistical model predictions
SOLID STATE COMMUNICATIONS, (2017), **257**, pp.36-41, **1.554, 0.433**

126. Ilis, M; Micutz, M; **Pasuk, I**; Staicu, T; Circu, V;
Synthesis and liquid crystalline properties of novel fluorinated N-benzoyl thiourea compounds. Effect of perfluoroalkyl chains on the thermal behavior and smectic phases stability
JOURNAL OF FLUORINE CHEMISTRY, (2017), **204**, pp.84-89, **2.101, 0.432**

127. Barsan, V; **Kuncser, V;**
Exact and approximate analytical solutions of Weiss equation of ferromagnetism and their experimental relevance
PHILOSOPHICAL MAGAZINE LETTERS, (2017), **97**, pp.359-371, **0.941, 0.430**

128. Mindru, I; Gingasu, D; Patron, L; Marinescu, G; Calderon-Moreno, JM; **Diamandescu, L; Secu, M**; Oprea, O;
Tb^{3+}-doped alkaline-earth aluminates: Synthesis, characterization and optical properties
MATERIALS RESEARCH BULLETIN, (2017), **85**, pp.240-248, **2.446, 0.420**

129. Balas, M; **Ciobanu, CS**; Burtea, C; Stan, MS; Bezirtzoglou, E; **Predoi, D**; Dinischiotu, A;
Synthesis, Characterization, and Toxicity Evaluation of Dextran-Coated Iron Oxide Nanoparticles
METALS, (2017), **7**, 63, **1.984, 0.420**

130. **Pintilie, I; Trinca, LM; Trupina, L; Pasuk, I; Pintilie, L;**
Relation between domain structure and pyroelectric response in as-grown epitaxial Pb(Zr0.2Ti0.8)O-3 thin films on substrates with different resistivity
MATERIALS RESEARCH BULLETIN, (2017), **93**, pp.201-207, **2.446, 0.420**

131. **Sima, M;** Vasile, E**; Sima, Ma;**
Lead acetate film as precursor for two-step deposition of CH3NH3PbI3
MATERIALS RESEARCH BULLETIN, (2017), **89**, pp.89-96, **2.446, 0.420**

132. Dafinei, I; Nagorny, S; Pirro, S; Cardani, L; Clemenza, M; Ferroni, F; Laubenstein, M; Nisi, S; Pattavina, L; Schaeffner, K; Di Vacri, ML; Boyarintsev, A; Breslavskii, I; Galkin, S; Lalayants, A; Rybalka, I; Zvereva, V; **Enculescu, M**;
Production of Se-82 enriched Zinc Selenide (ZnSe) crystals for the study of neutrinoless double beta decay
JOURNAL OF CRYSTAL GROWTH, (2017), **475**, pp.158-170, **1.751, 0.402**

133. Palade, S; Pantazi, A; Vulpe, S; Berbecaru, C; Tucureanu, V; Oprea, O; **Negrea, RF**; Dragoman, D;
Tunable dielectric properties in polyacrylonitrile/multiwall carbon nanotube composites
POLYMER COMPOSITES, (2017), **38**, pp.1741-1748, **2.324, 0.401**

134. **Ciobotaru, CC; Ciobotaru, IC; Schinteie, G; Negrea, RF; Polosan, S;**
Enhancement of the electroluminescence of organic light emitting devices based on Ir(ppy)(3) by doping with metallic and magnetic nanoparticles
MATERIALS SCIENCE IN SEMICONDUCTOR PROCESSING, (2017), **72**, pp.78-84, **2.359, 0.398**

135. **Secu, CE; Secu, M**; Stokker-Cheregi, F; Ion, V; Brajnicov, S; Dinescu, M;
Laser processing of Yb^{3+}/Er^{3+} co-doped $LiYF_4$ thin films with up-conversion properties
THIN SOLID FILMS, (2017), **625**, pp.6-10, **1.879, 0.384**

136. Filip, V; **Filip, LD**; Wong, H;
Review on peculiar issues of field emission in vacuum nanoelectronic devices
SOLID-STATE ELECTRONICS, (2017), **138**, pp.3-15, **1.58, 0.377**

137. **Cernea, M; Mihalache, V; Secu, CE;** Trusca, R; Bercu, V; **Diamandescu, L;**
Structural, morphological, ferromagnetic and photoluminescence properties of Fe-doped ZnO, prepared by hydrothermal route
SUPERLATTICES AND MICROSTRUCTURES, (2017), **104**, pp.362-373, **2.123, 0.361**

138. **Tolea, F; Tolea, M; Sofronie, M; Popescu, B; Crisan, AD; Leca, A; Valeanu, M;**
Specific Changes in the Magnetoresistance of Ni-Fe-Ga Heusler Alloys Induced by Cu, Co, and Al Substitutions
IEEE TRANSACTIONS ON MAGNETICS, (2017), **53**, 4400307, **1.243, 0.348**

139. **Sandu, V**; Cimpoiasu, E; **Kuncser, A**; Nicolescu, MS;
Magnetic properties of glass-ceramics obtained by crystallization of iron-rich borosilicate glasses
JOURNAL OF ADVANCED CERAMICS, (2017), **6**, pp.251-261, **1.198, 0.336**

140. **Socol, M; Preda, N; Stanculescu, A; Breazu, C; Florica, C; Rasoga, O**; Stanculescu, F; Socol, G;
IZO deposited by PLD on flexible substrate for organic heterostructures
APPLIED PHYSICS A-MATERIALS SCIENCE & PROCESSING, (2017), **123**, 371, **1.455**, **0.325**

141. **Aldica, G; Ciurea, ML**; Chipara, DM; **Lepadatu, AM**; Lozano, K; **Stavarache, I; Popa, S**; Chipara, M;
Isotactic polypropylene-vapor grown carbon nanofibers composites: Electrical properties
JOURNAL OF APPLIED POLYMER SCIENCE, (2017), **134**, 45297, **1.86**, **0.320**

142. **Galatanu, M; Enculescu, M; Ruiu, G; Popescu, B; Galatanu, A;**
Cu-based composites as thermal barrier materials in DEMO divertor components
FUSION ENGINEERING AND DESIGN, (2017), **124**, pp.1131-1134, **1.319**, **0.316**

143. Carro, G; Munoz, A; Monge, MA; Savoini, B; **Galatanu, A; Galatanu, M**; Pareja, R;
Thermal conductivity and diffusivity of Cu-Y alloys produced by different powder metallurgy routes
FUSION ENGINEERING AND DESIGN, (2017), **124**, pp.1156-1160, **1.319**, **0.316**

144. **Crisan, IA**; Dang, VS; Mikheenko, P;
Nano-engineered pinning centres in YBCO superconducting films
PHYSICA C-SUPERCONDUCTIVITY AND ITS APPLICATIONS, (2017), **533**, pp.118-132, **1.404**, **0.316**

145. Von Muller, A; Ewert, D; **Galatanu, A**; Milwich, M; Neu, R; Pastor, JY; Siefken, U; Tejado, E; You, JH;
Melt infiltrated tungsten-copper composites as advanced heat sink materials for plasma facing components of future nuclear fusion devices
FUSION ENGINEERING AND DESIGN, (2017), **124**, pp.455-459, **1.319**, **0.316**

146. **Predoi, D; Popa, CL**; Predoi, MV;
Ultrasound studies on magnetic fluids based on maghemite nanoparticles
POLYMER ENGINEERING AND SCIENCE, (2017), **57**, pp.485-490, **1.449**, **0.305**

147. **Predoi, D; Iconaru, SL**; Albu, M; Petre, CC; Jiga, G;
Physicochemical and antimicrobial properties of silver-doped hydroxyapatite collagen biocomposite
POLYMER ENGINEERING AND SCIENCE, (2017), **57**, pp.537-545, **1.449**, **0.305**

148. Sava, BAC; Elisa, M; Boroica, L; **Kuncser, V; Valeanu, M**; Vasiliu, IC; Feraru, I; Iordanescu, R;
Sol-gel preparation and structural investigations of silico-phosphate glasses doped with Fe ions
JOURNAL OF SOL-GEL SCIENCE AND TECHNOLOGY, (2017), **81**, pp.294-302, **1.575**, **0.292**

149. **Matea, A; Baibarac, M; Baltog, I;**
Optical properties of single-walled carbon nanotubes highly separated in semiconducting and metallic tubes functionalized with poly(vinylidene fluoride)
JOURNAL OF MOLECULAR STRUCTURE, (2017), **1130**, pp.38-45, **1.753**, **0.268**

150. **Aldica, G;** Matei, C; Paun, A; Batalu, D; Ferbinteanu, M; **Badica, P;**
Thermal analysis on $C_6H_{10}Ge_2O_7$-doped MgB_2
JOURNAL OF THERMAL ANALYSIS AND CALORIMETRY, (2017), **127**, pp.173-179, **1.953**, **0.267**

151. Badea, M; Bucur, C; Chifiriuc, MC; Bleotu, C; **Grecu, MN**; Lazar, V; Marinescu, D; Olar, R;
Insight on thermal behaviour of new complexes of Ni(II), Cu(II) and Zn(II) with a bismacrocyclic ligand developed as biologically active species
JOURNAL OF THERMAL ANALYSIS AND CALORIMETRY, (2017), **127**, pp.487-497, **1.953**, **0.267**

152. Olar, R; **Vlaicu, ID**; Chifiriuc, MC; Bleotu, C; Stanica, N; Scaeteanu, GV; Silvestro, L; Dulea, C; Badea, M;
Thermal behavior of new nickel(II) complexes with unsaturated carboxylates and heterocyclic N-donor ligands
JOURNAL OF THERMAL ANALYSIS AND CALORIMETRY, (2017), **127,** pp.731-741, **1.953, 0.267**

153. **Baibarac, M; Baltog, I; Daescu, MA;**
Electrochemical characterization of the Poly(2, 2 '-Bithiophene-co-Pyrene) Functionalized Single-Walled Carbon Nanotubes Films and Their Applications in Supercapacitors Field
INTERNATIONAL JOURNAL OF ELECTROCHEMICAL SCIENCE, (2017), **12**, pp.2013-2025, **1.469, 0.265**

154. **Iconaru, SL;** Stanciu, GA; Hristu, R; **Ghita, RV;**
PROPERTIES OF SAMARIUM DOPED HYDROXYAPATITE THIN FILMS DEPOSITED BY EVAPORATION
ROMANIAN REPORTS IN PHYSICS, (2017), **69**, 508, **1.467, 0.242**

155. **Trinca, LM; Besleaga, C; Stancu, V; Radu, R; Iuga, A; Boni, AG; Galca, AC; Pintilie, L;**
TEMPERATURE INFLUENCE ON THE CAPACITANCE-VOLTAGE HYSTERESIS OF TRANSPARENT a-IGZO/PZT/FTO MFS-HETEROSTRUCTURE
ROMANIAN REPORTS IN PHYSICS, (2017), **69**, 506, **1.467, 0.242**

156. Stanculescu, F; **Socol, M; Matei, E; Stanculescu, A;**
Effect of heavy ions irradiation on the properties of benzil crystals
CRYSTAL RESEARCH AND TECHNOLOGY, (2017), **52**, 1700047, **1.000, 0.227**

157. Aukstuolis, A; Girtan, M; Mousdis, GA; Mallet, R; **Socol, M**; Rasheed, M; **Stanculescu, A**;
MEASUREMENT OF CHARGE CARRIER MOBILITY IN PEROVSKITE NANOWIRE FILMS BY PHOTO-CELIV METHOD
PROCEEDINGS OF THE ROMANIAN ACADEMY SERIES A-MATHEMATICS PHYSICS TECHNICAL SCIENCES INFORMATION SCIENCE, (2017), **18**, pp.34-41, **1.623, 0.216**

158. **Ionescu, AM; Ivan, I; Enculescu, M; Grigoroscuta, MA;** Miu, D; **Valeanu, M; Badica, P; Miu, L;**
From an Anomalous Peak Effect to a Second Magnetization Peak in Nb-rich Nb-Ti Alloys
JOURNAL OF SUPERCONDUCTIVITY AND NOVEL MAGNETISM, (2017), **30**, pp.1103-1108, **1.18, 0.179**

159. **Badica, P; Burdusel, M; Popa, S**; Hayasaka, Y; **Ionescu, AM; Aldica, G**;
Addition of Sb_2O_5 into MgB_2 Superconductor Obtained by Spark Plasma Sintering
JOURNAL OF SUPERCONDUCTIVITY AND NOVEL MAGNETISM, (2017), **30**, pp.2073-2080, **1.18, 0.179**

160. **Crisan, O; Crisan, AD;**
Elastic properties and crystallization of thermal barrier coatings of Cr_2AlC
Digest Journal of Nanomaterials and Biostructures, (2017), **12**, pp.1165-1174, **0.836, 0.150**

161. Birzu, M; **Frunza, L; Zgura, I; Cotorobai, VF; Ganea, CP; Preda, N; Enculescu, M;**
WETTABILITY BY WATER CONTACT ANGLE UPON THE SURFACE OF WOOL FABRICS COVERED WITH OXIDE NANOPARTICLES
Digest Journal of Nanomaterials and Biostructures, (2017), **12**, pp.921-931, **0.836, 0.150**

162. Fufa, O; **Socol, M; Preda, N**; Grigorescu, S; Croitoru, S; Socol, G;
MAPLE DEPOSITION OF PLGA MICROSPHERES FOR MEDICAL APPLICATIONS
DIGEST JOURNAL OF NANOMATERIALS AND BIOSTRUCTURES, (2017), **12**, pp.73-80, **0.836, 0.150**

163. **Secu, M;**
UPCONVERSION AVALANCHE IN THE Yb^{3+}/Ho^{3+} DOPED SiO_2-$LiYF_4$ NANO-GLASS CERAMIC
DIGEST JOURNAL OF NANOMATERIALS AND BIOSTRUCTURES, (2017), **12**, pp.1075-1080, **0.836, 0.150**

164. **Sima, M;** Vasile, E; **Sima, Ma;**
PHOTOACTIVITY OF HEMATITE ELECTRODE PREPARED VIA ANODIC ELECTRODEPOSITION ON FTO AND FTO/TiO_2 SUBSTRATES
DIGEST JOURNAL OF NANOMATERIALS AND BIOSTRUCTURES, (2017), **12**, pp.751-758, **0.836, 0.150**

165. Busuioc, AD; Ciovica, I; Stoleriu, S; **Enculescu, M; Evanghelidis, A**; Visan, T;
MORPHOLOGICAL AND OPTICAL PROPERTIES OF ELECTROSPUN SnO FIBERS
Digest Journal of Nanomaterials and Biostructures, (2017), **12**, pp.1097-1105, **0.836, 0.150**

166. **Simion, CE; Florea, OG; Stanoiu, A;**
Gas sensing mechanism involved in H2S detection with NiO loaded SnO_2 gas sensors
ROMANIAN JOURNAL OF INFORMATION SCIENCE AND TECHNOLOGY, (2017), **20**, pp.415-425, **0.365, 0.109**

167. Prilepov, V; Gashin, P; **Popescu, M**; Zalamai, V; Spoiala, D; Ketrush, P; Nasedchina, N;
Studies of vanadium and vanadium oxide based nanocomposite structures
JOURNAL OF OPTOELECTRONICS AND ADVANCED MATERIALS, (2017), **19**, pp.400-405, **0.449, 0.079**

168. Stanciulescu, M; Abrudeanu, M; **Galatanu, A**; Carlan, P; Mihalache, M;
Dissolution Behaviour of Alloying Elements Into Vanadium Matrix During Mechanical Milling
REVISTA DE CHIMIE, (2017), **68**, pp.1109-1113, **1.232, 0.057**

169. Iordanescu, CR; Elisa, M; Epurescu, G; Filipescu, M; Enculescu, M; Monteiro, RCC; Constantin, L;
CHARACTERIZATION OF CdS-DOPED GLASS FILMS OBTAINED BY PULSED LASER DEPOSITION
REVISTA ROMANA DE MATERIALE-ROMANIAN JOURNAL OF MATERIALS, (2017), **47**, pp.60-65, **0.56, 0.054**

170. **Diamandescu, L; Feder, M; Vasiliu, F; Tanase, LC;** Sobetkii, A; Dumitrescu, I; **Teodorescu, CM; Popescu, T;**
Hydrothermal route to (FE, N) codoped titania photocatalysts with increased visible light activity
INDUSTRIA TEXTILA, (2017), **68**, pp.303-308, **0.387, 0.035**

Articles in non-ISI Journals or Conference Proceedings

01. **Palade, C; Dascalescu, I; Slav, A; Lepadatu, AM; Lazanu, S; Stoica, T; Teodorescu, VS; Ciurea, ML**; Comanescu, F; Muller, R; Dinescu, A; Enuica, A
Photosensitive GeSi/TiO_2 multilayers in VIS-NIR
2017 INTERNATIONAL SEMICONDUCTOR CONFERENCE (CAS), 40TH EDITION, 67-70; 2017

2. **Banciu, M. G.**; Militaru, N.; Martian, A.; Nicolaescu, I.; Tuta, L.; **Geambasu, D. C.; Nedelcu, L.; Trupina, L.**; Ramer, R.
Microwave antenna array using new dielectric resonator antenna elements
2017 INTERNATIONAL SEMICONDUCTOR CONFERENCE (CAS), 40TH EDITION, 129-132; 2017

3. **Stanoiu, A.**; Somacescu, S.; **Simion, C. E.**; Calderon-Moreno, Jose Maria; **Florea, O. G.**
Gas sensing properties of NiO/mesoporous SnO_2
2017 INTERNATIONAL SEMICONDUCTOR CONFERENCE (CAS), 40TH EDITION, 93-96; 2017

4. **Slav, A; Palade, C; Stavarache, I; Teodorescu, VS; Ciurea, ML**; Muller, R; Dinescu, A; Sultan, MT; Manolescu, A; Gudmundsson, JT; Svavarsson, HG
Influence of preparation conditions on structure and photosensing properties of GeSi/TiO_2 multilayers
2017 INTERNATIONAL SEMICONDUCTOR CONFERENCE (CAS), 40TH EDITION, 63-66; 2017

5. **Palade, C; Slav, A; Lepadatu, AM; Lazanu, S; Ciurea, ML; Stoica, T**
Light illumination effects on floating gate memory with Ge nanocrystals in HfO_2
2017 INTERNATIONAL SEMICONDUCTOR CONFERENCE (CAS), 40TH EDITION, 87-90; 2017

6. **Liviu C. Tănase, Laura E. Abramiuc, Cristian M. Teodorescu**
Photoelectron spectroscopic and microspectroscopic probes of ferroelectrics
AIP Conference Proceedings, 1916, 030001, 2017

7. **M. Burdusel, A. M. Ionescu, M. Grigoroscuta,** D. Batalu**, M. Enculescu, S. Popa, V. Mihalache, G. Aldica And P. Badica**
Powder-in-tube tapes of MgB_2 In Fe-sheath processed by ex-situ Spark Plasma Sintering
U.P.B. Scientific Bulletin, Series B 79 2, 155-172, 2017.

8. T. Klein, R. Rohlsberger, E. Burkel, **O. Crisan**
New concept for information storage in magnetic films exchange-coupled through non-magnetic layer
Proceedings of 2017 IEEE 12th International Conference on Nano/Micro Engineered and Molecular Systems, **NEMS 2017**, Article number 8017113, Pages 682-686, 2017.

9. M. Sorescu, **F. Tolea, M. Valeanu, M. Sofronie**
Structure, Magnetic Properties and Hyperfine Parameters of Nd-Substituted Ni-Fe-Ga Heusler Alloys
MRS ADVANCES, Volume: 2 Issue: 25 Pages: 1341-1346, 2017.

10. Ionescu, GC; Nae, I; Ripeanu, RG; Dinita, A; **Stan, GE**;
Studies on Tribological Behavior of Aluminum Nitride-Coated Steel
13TH INTERNATIONAL CONFERENCE ON TRIBOLOGY, (ROTRIB'16) Volume: 174, 2017.

11. Chirla, R; Horea, CD; Costea, TO; **Dragomir, R**; Manolescu, A; Moca, CP;
Shiba States Coupled to a Resonant Cavity
TIM15-16 PHYSICS CONFERENCE, Volume: 1796, 2017.

12. Boyadjiev, SI; Stefan, N; Szilagyi, IM; Mihailescu, N; Visan, A; Mihailescu, IN; **Stan, GE; Besleaga, C**; Iliev, MT; Gesheva, KA;
Characterization of MAPLE deposited WO_3 thin films for electrochromic applications
INERA WORKSHOP 2016: MEMBRANE AND LIQUID CRYSTAL NANOSTRUCTURES (MELINA 2016), Volume: 780, 2017.

CONTRIBUTED PRESENTATIONS

01. **Besleaga C, Stan GE**, Raevschi S, **Trinca L, Galca AC, Dumitru V, Radu R, Pintilie I**
AlN as gate dielectric in thin film transistors
9th International Conference on Advanced Materials, ROCAM 2017, Bucharest, Romania
11-14.07.2017 - **Poster**

02. **Besleaga C, Stan G.E., Dumitru V, Radu R, Trinca LM, Galca AC**
Annealing influence on amorphous IGZO based TFTs
4th Central and Eastern European Conference on Thermal Analysis and Calorimetry (CEEC-TAC4), Chisinau, Moldova
28-31.08.2017 - **Poster**

03. **Besleaga C, Stan G.E., Dumitru V, Botea M, Radu R, Trinca LM, Galca AC**
Aluminum nitride based micro-electronics for harsh environments
4th Central and Eastern European Conference on Thermal Analysis and Calorimetry (CEEC-TAC4), Chisinau, Moldova
28-31.08.2017 - **Poster**

04. Craciun D, Dorcioman G, Fufa O, Socol G, **Galca AC**, Swart HC, Erasmus LJB, Kroon RE, Martin C, Craciun V
Radiation effects in amorphous optical films
7th South African Conference on Photonic Materials, Amanzi, South Africa
27-31.03.2017 - **Talk**

05. Craciun D, Fufa O, **Galca AC, Trinca LM**, Pantelica D, Ionescu P, and Craciun V
Optical properties of amorphous IGZO grown by pulsed laser deposition
EMRS spring meeting, Strasbourg, France
22–26.05.2017 - **Poster**

06. Craciun D, Socol G, Fufa O, Cristea D, Pantelica D, Ionescu P, Trusca R, Lambers E, **Galca AC**, Craciun V
Lateral variation of properties in PLD grown films
EMRS spring meeting, Strasbourg, France
22–26.05.2017 - **Talk**

07. **Dogaru D, Besleaga C, Galca AC**, Nistor M, Ion L
TiO2 thin films deposited by rf-magnetron sputtering for optoelectronic applications
17th International Conference on Plasma Physics and Applications (CPPA), Magurele, Romania
15-20.06.2017 - **Poster**

08. Fufa O, Craciun D, **Galca AC**, Swart HC, Erasmus LJB, Kroon RE, Craciun V
Radiation effects in amorphous transparent oxide films
EMRS spring meeting, Strasbourg, France
22–26.05.2017 - **Poster**

09. **Galca AC**, Fufa O, Craciun D, **Besleaga C**, Craciun V
Spectroscopic ellipsometry studies on amorphous oxide semiconductors
9th International Conference on Advanced Materials, ROCAM 2017, Bucharest, Romania
11-14.07.2017 - **Talk**

10. **Galca AC**, Socol G, **Velea A**
Spectroscopic ellipsometry, a useful tool to investigate phase transitions in thin films: case study on phase change materials
4th Central and Eastern European Conference on Thermal Analysis and Calorimetry (CEEC-TAC4), Chisinau, Moldova
28-31.08.2017 - **Talk**

11. Gherendi F, Craciun V, Fufa O, Craciun D, **Galca AC**
IGZO thin film transistors fabricated with shadow masks at room temperature
EMRS spring meeting, Strasbourg, France
22–26.05.2017 - **Poster**

12. Oumezzine Ma, **Galca AC, Pasuk I, Chirila CF, Leca A, Kuncser V, Tanase LC, Kuncser A, Ghica C**, Oumezzine Mo
Epitaxial $La_{0.67}Ba_{0.33}Ti_{0.02}Mn_{0.98}O_3$ oxide thin films
9th International Conference on Advanced Materials, ROCAM 2017, Bucharest, Romania
11-14.07.2017 - **Poster**

13. Oumezzine Ma, **Galca AC, Pasuk I, Chirila CF, Leca A, Kuncser V, Tanase LC, Kuncser A, Ghica C**, Oumezzine Mo
Epitaxial $La_{0.67}Ba_{0.33}Ti_{0.02}Mn_{0.98}O_3$ oxide thin films
24th Congress and General Assembly of the International Union of Crystallography, Hyderabad, India
21-28.08.2017 - **Poster**

14. **Trinca LM, Besleaga C, Galca AC, Radu R, Stancu V, Iuga A, Dumitru V, Pintilie L**
On the memory functionality of PZT/aIGZO based heterostructures
9th International Conference on Advanced Materials, ROCAM 2017, Bucharest, Romania
11-14.07.2017 - **Poster**

15. **Florica C., Costas A., Kuncser A., Diculescu V., Preda N., Enculescu I.**
Electrical properties of single core-shell metal oxide nanowires,
20th Int. conference on Advanced Nanotechnology,
September 11-12, 2017, Amsterdam, Netherlands - **Talk**

16. **Florica C., Costas A., Kuncser A., Diculescu V., Preda N., Enculescu I.**
Core-shell nanowires based on CuO and ZnO,
13th Nanoscience & Nanotechnology Conf.,
Oct. 22-25, 2017, Antalya, Turkey - **Talk**

17. **Costas A., Florica C., Kuncser A., Matei E., Preda N., Enculescu I.**
Electrical properties of single ZnO nanowires prepared by wet and dry methods,
20th International conference on Advanced Nanotechnology,
September 11-12, 2017, Amsterdam, Netherlands - **Talk**

18. **Costas A., Florica C., Negrea R., Boni A., Pintilie L.**, Ion L., **Preda N., Enculescu I.**
Optoelectronic devices based on single CuO nanowires
13th Nanoscience & Nanotechnology Conference,
October 22-25, 2017, Antalya, Turkey - **Poster**

19. **Costas A., Matei E., Enculescu M., Schinteie G., Stavarache I.**, M. E. Toimil-Molares, **V. Kuncser, I. Enculescu**
Magnetic anisotropy in electrodeposited metallic nanowires
The 9th Int. Conf. on Advanced Materials, ROCAM
11-14 July 2017, Bucharest, Romania - **Talk**

20. **Beregoi M., Evanghelidis A., Diculescu V., Matei E., Enculescu I.**
Conducting polymers coated electrospun structures based microactuators
12 Nanoscience and Nanotechnology Conference – NanoTR 2017, Antalya, Turcia,
22-25th of October 2017 - **Poster**

21. **M. Beregoi, A. Evanghelidis, E. Matei, I. Enculescu M**, Actuators based on polyaniline coated electrospun fibers nets,**7th International Conference onElectromechanically Active Polymer (EAP) transducers & artificial muscles – EuroEAP 2017, Cartagena, Spania**, 06-07 June 2017 - **Poster+pitch.**

22. **Evanghelidis A., Beregoi M., Diculescu V., Enculescu I.**
Polypyrrole distributed actuators based on electrospun microribbons
7th International Conference on Electromechanically Active Polymer (EAP) transducers & artificial muscles – EuroEAP 2017, Cartagena, Spania, 06-07 Iunie 2017 - **Poster+pitch**.

23. **Diculescu V. C., Apostol N. G., Teodorescu C. M.**
Fabrication of Hydrogel Embedded Wearable Sensors for Sweat Analysis
XXIV International Symposium on Bioelectrochemistry and Bioenergetics, Lyon, Franta
3-7 Iulie 2017 - **Poster**

24. **Diculescu V. C.**
Nanostructured Electrochemical Biosensors; Basic Concept and Applications
9th International Conference on Advanced Materials: ROCAM 2017
10-14th of July 2017, Bucharest, Romania - **Talk**

25. **Diculescu V. C.**
Electrochemical Biosensors. From Fundamental Applications To Wearable Devices
Second Workshop of Bioelectrochemistry "Bioelectrochemistry and its Applications in life sciences"
19-20th of September 2017 University of Medicine and Pharmacy, Iuliu Hatieganu, Cluj-Napoca - **Talk**

26. **Diculescu V. C., Beregoi M., Evanghelidis A., Enculescu I.**
Fabrication of flexible nanostructured electrodes for wearable sensors development
8TH International Workshop on Biosensors for food safety and environmental monitoring
11-15th of October 2017, Rabat, Maroc - **Talk**

27. **Enache T. A**., Chiorcea-Paquim A. M., **Barsan M., Diculescu V.C.**, Oliveira-Brett A.M.
Structural modification and voltammetric characterization of amyloid beta peptide
The 9th International Conference On Advanced Materials: ROCAM 2017,
July 10 – 14, 2017 (Bucharest-Romania) - **Talk**

28. **Enache T. A., Diculescu V. C.**
Formaldehyde sensor based on Nafion®-modified electrodes
The 8th Workshop on Biosensors for Food Safety and Environmental Monitoring,
October 12-14, 2017 Rabat-Morocco) - **Poster**

29. **Barsan M. M., Enache T. A., Preda N., Diculescu V. C**
Nickel Nanoparticles as a New Tool in the Sensitive Sensing of Biomolecules of Interest
24th International Symposium on Bioelectrochemistry and Bioenergetics (BES),
3-7 July 2017, Lyon, France - **Poster**

30. **Barsan M. M.**
Nanostructured Biosensors for the determination of key analytes in food
The 16th International Symposium Prospects for the 3rd Millenium Agriculture,
28-30 September, Cluj-Napoca, Romania

31. **Barsan M. M., Enache T. A., Diculescu V. C.**
Application of nanostructured materials in (bio)sensing
The 9th International Conference on Advanced Materials, ROCAM 2017, 10-14 July 2017, Bucharest, Romania - **Talk**

32. **Barsan M. M.**
Biosensors based on graphene, carbon nanotubes and magnetic nanoparticles
The second workshop on bioelectrochemistry Bioelectrochemistry and its applications in life sciences, Cluj Napoca, Romania, 19-20th of September 2017

33. **Barsan M. M.**
Nanostructured enzymatic biosensors for food analysis
POC-G 54 MATI2IT project workshop,
25-26th of September 2017, NIMP, Magurele, Romania

34. **Trupina L, Nedelcu L, Radu R, Pasuk I, Banciu MG**, Dumas-Bouchiat F, Constantinescu C, Marchet P, Champeaux C, Huitema L, Ghalem A, Rammal M, Cruntenau A, Madrangeas V, Passerieux D, Cros D, and Monediere T
Ferroelectric varactors based on heteroepitaxialy grown (Ba,Sr)TiO3 thin films
9th International Conference on Advanced Materials, ROCAM 2017, Bucharest, Romania
11-14.07.2017 - **Poster**

35. Rammal M, Ghalem A, Huitema L, Crunteanu A, **Trupina L, Nedelcu L, Banciu MG**, Dutheil P, Constantinescu C, Marchet P, Dumas-Bouchiat F, Champeaux C
Antenne fente reconfigurable en fréquence intégrant un condensateur ferroélectrique type MFM
XXèmes Journées Nationales Microondes– Saint-Malo
16-19.05.2017 - **Talk**

36. **Stancu V, Cernea M, Mihalache V, Nedelcu L, Trupina L, Banciu MG**, Huitema L, Ghalem A, Crunteanu A, Rammal M, Passerieux D, Cros D, Monediere T, Madrangeas V, Constatinescu C, Dumas-Bouchiat F, Marchet P, Champeaux C
Microwave dielectric properties of (1-x)Bi0.5Na0.5TiO3 - xBaTiO3 thin film
9th International Conference on Advanced Materials, ROCAM 2017, Bucharest, Romania
11-14.07.2017 - **Poster**

37. Ghalem A, Huitema L, Crunteanu A, Rammal M, Passerieux D, Cros D, Monediere T, Madrangeas V, Goldner-Constatinescu C, Champeaux C, Dumas-Bouchiat F, Marchet P, **Nedelcu L, Trupina L, Banciu G**
High-frequency characterisation of ferroelectric thin film capacitors and their integration for frequency tunable antennas
9th International Conference on Advanced Materials, ROCAM 2017, Bucharest, Romania
11-14.07.2017 - **Talk**

38. Goldner-Constantinescu CD, Ghalem A, Rammal M, Marchet P, Huitema L, Crunteanu A, **Nedelcu L, Trupina L, Banciu G,** Dumas-Bouchiat, C. Champeaux
Pulsed Laser Deposition of Thin Film Capacitors in Different Configurations with Applications in Highly Tunable Digital and Analog Microwave Devices
9th International Conference on Advanced Materials, ROCAM 2017, Bucharest, Romania
11-14.07.2017 - **Talk**

39. **Geambasu DC, Banciu MG, Nedelcu L, Trupina L**
Novel Microwave antennas using resonators of advanced dielectric materials
9th International Conference on Advanced Materials, ROCAM 2017, Bucharest, Romania
11-14.07.2017 - **Poster**

40. Constantinescu C, Ghalem A, Rammal M, Huitema L, Crunteanu A, **Nedelcu L, Trupina L, Banciu G**, Marchet P, Dumas-Bouchiat F, Champeaux C
Para-/ferro-electric thin films grown by pulsed laser deposition for various configurations of high-frequency tunable microcapacitors,
International Conference on Laser Ablation, COLA2017, Marseille, France
3-8.09.2017 - **Talk**

41. Ghalem A, Rammal M, Huitema L, Crunteanu A, **Trupina L, Nedelcu L, Banciu MG**, Dutheil P, Constantinescu C, Marchet P, Dumas-Bouchiat F, Champeaux C
Capacités ferroélectriques accordables pour la réalisation de dispositifs hyperfréquences reconfigurables,
XXèmes Journées Nationales Microondes, Saint-Malo, France
16-19 mai 2017 - **Talk**

42. **Banciu MG**, Militaru N, Martian A, Nicolaescu I, Tuta L, **Geambasu DC, Nedelcu L, Trupina L**, Ramer R
Microwave antenna array using new dielectric resonator antenna elements
International semiconductor conference CAS 2017, Proceedings pg. 129-132, Sinaia, Romania
11-14.10.2017 - **Talk**

43. **Florea M, Neațu F, Neațu S**, Somacescu S
Synthesis of mesoporous ZrO_2 doped materials as anode for PEMFCs
9th International Conference on Advanced Materials, ROCAM 2017, Bucharest, Romania
11-14.07.2017 - **Talk**

44. Petrea N, Nicolae, Trandafir M, Somacescu S, **Neațu S, Neațu F**, Somoghi V, **Florea M**
Synthesis and characterization of nickel supported on mesoporous tin oxide as anode for PEMFC
XIII European Congress on Catalysis (EUROPACAT 2017), Florenta, Italia
26-31.08.2017 - **Poster**

45. Navarrete L, **Florea M**, Serra JM, Somăcescu S
Mesoporous anodes based on rare earths doped ceria for fuel cells applications
XIII European Congress on Catalysis (EUROPACAT 2017), Florenta, Italia
26-31.08.2017 - **Poster**

46. **Florea M, Neaţu F**, Nicolae S, Culică G, Pârvulescu VI, Cavani F
An unprecedented synthesis of terephthalic acid by p-cymene oxidation
XIII European Congress on Catalysis (EUROPACAT 2017), Florenta, Italia
26-31.08.2017 - **Talk**

47. **Leonat L, Stancu V, Tomulescu AG, Beşleagă C, Enculescu M, Pintilie I**
One Step Toward Large Scale Production of Perovskite Solar Cells
9th International Conference on Advanced Materials, ROCAM 2017, Bucharest, Romania
11-14.07.2017 - **Talk**

48. **Tomulescu AG, Stancu V, Beşleagă C, Leonat L, Trincă L, Pintilie L, Enculescu M, Pintilie I**
Industrial friendly method for titanium oxide layers deposition used in perovskite solar cells
9th International Conference on Advanced Materials, ROCAM 2017, Bucharest, Romania
11-14.07.2017 - **Talk**

49. Boyadjiev SI, Stefan N, **Stan GE**, Arvizu M, Szilágyi IM, Visan A, Mihailescu N, Mihailescu IN, **Besleaga C**, Österlund L, Gesheva KA
Study of the electrochromic properties of MAPLE and PLD deposited WO3 thin films
21st International Conference on Solid State Ionics, Padua, Italy
18-23.06.2017 - **Poster**

50. **Stan GE, Popescu AC**, Florian PE, Popescu-Pelin G, Achim A, **Enculescu M, Zgura I,** Oktar FN, Roseanu A, Duta L
Simple and reinforced biological-derived hydroxyapatite coatings for metallic implants
15th Conference & Exhibition of the European Ceramic Society (ECerS2017), Budapest, Hungary
9-13.07.2017 - **Poster**

51. **Popa AC, Stan GE, Besleaga C**, Necsulescu M, Fernandes HR, Ferreira, JMF
Antibacterial efficiency of alkali-free biocompatible glasses additivated with ZnO and/or SrO active agents
15th Conference & Exhibition of the European Ceramic Society (ECerS2017), Budapest, Hungary
9-13.07.2017 - **Poster**

52. **Trinca L, Besleaga C, Galca A, Radu R, Stancu V, Iuga A, Dumitru V, Pintilie L**
Temperature influence on the memory functionality of PZT/aIGZO based heterostructures
4th Central and Eastern European Conference on Thermal Analysis and Calorimetry (CEEC-TAC4), Chisinau, Moldova
28-31.08.2017 - **Poster**

53. **D. Predoi, S.L. Iconaru** , A.M. Prodan, **C.S. Ciobanu**, M. Beuran, C.S. Turculet, **C.C. Negrila, R.V. Ghita**, M.Soare.
In Vivo Toxicity Of Glycerol Coated Iron Oxide Nanoparticles
19th INTERNATIONAL SOL-GEL CONFERENCE,
SEPTEMBER 3-8, LIEGE, BELGIUM - **Poster**

54. **D. Predoi, S.L. Iconaru, C.S. Ciobanu**, M. Beuran, C.S. Turculet, **C.C. Negrila, R.V. Ghita**, A. Iosif, A.M. Prodan
Antimicrobial evaluation of Silver Doped Hydroxyapatite Layers obtained by Sol-Gel Method
19th INTERNATIONAL SOL-GEL CONFERENCE,
SEPTEMBER 3-8, LIEGE, BELGIUM - **Poster**

55. **D. Predoi**, M.V. Predoi, **S.L. Iconaru, C.S. Ciobanu**, N. Buton, C.C. Petre, A.M. Prodan
Physico-chemical characteristics and antimicrobial studies of silver doped hydroxyapatite
THE 7th INTERNATIONAL CONFERENCE ON STRUCTURAL ANALYSIS OF ADVANCED MATERIALS, BUCHAREST, ROMANIA,
19-22 SEPTEMBER 2017 - **Poster**

56. **S.L. Iconaru**, M. Beuran, C.S. Turculet, I. Negoi, G. Teleanu, A.M. Prodan, M. Motelica-Heino, R. Guégan, **C.S. Ciobanu**, G. Jiga, **Daniela Predoi**.,
Application Of Biocompatible Magnetite Nanoparticles For The Removal Of As And Cu From Water
THE 7th INTERNATIONAL CONFERENCE ON STRUCTURAL ANALYSIS OF ADVANCED MATERIALS, BUCHAREST, ROMANIA,
19-22 SEPTEMBER 2017 - **Poster**

57. **S.L. Iconaru**, S.A. Predoi, M. Beuran, **C.S. Ciobanu**, R. Trusca, **R. Ghita**, I. Negoi, G. Teleanu, S.C. Turculet, M. Matei, Monica Badea, A.M. Prodan.
Fabrication and Characterization of Iron Oxide Dextran Composite Layers
THE 7th INTERNATIONAL CONFERENCE ON STRUCTURAL ANALYSIS OF ADVANCED MATERIALS, BUCHAREST, ROMANIA,
19-22 SEPTEMBER 2017 - **Poster**

58. **R.V. Ghita, C.C. Negrila, D. Predoi**, R.Trusca
Analysis Of PdGe-Based Contact On N-GaSb
THE 7th INTERNATIONAL CONFERENCE ON STRUCTURAL ANALYSIS OF ADVANCED MATERIALS, BUCHAREST, ROMANIA,
19-22 SEPTEMBER 2017 - **Talk**

59. **I. Pintilie, V. Stancu, A. Tomulescu, R. Radu, C. Besleaga, L. Trinca, L. Pintilie**
PbTiO3 ferroelectric films with potential application in solar cells,
The 9th International Conference on Advanced Materials, ROCAM 2017
11-14.07.2017, Bucharest, Romania - **Talk**

60. **Luminita M. Hrib, Marius A. Husanu, Lucian Pintilie**, Marin Alexe
Magnetocapacitance effect in La0.7Sr0.3MnO3/Pb(Zr0.2Ti0.8)O3/La0.7Sr0.3MnO3 multiferroic heterostructures,
3rd Functional Oxide Thin Films for Advanced Energy and Information Technology Conference,
05.07.2017-08.07.2017, Rome, Italy - **Poster**

61. **M.Botea, G.E.Stan, I.Pintilie, G.A.Boni, V.Stancu, A.Iuga, L.Pintilie**
Pyroelectricity in polar materials,
The 9th International Conference on Advanced Materials, ROCAM 2017
11-14.07.2017, Bucharest, Romania - **Talk**

62. **M.Botea**, G.Le Rhun, **A.G.Boni, L.Hrib, C.Chirila, I.Pintilie, L. Pintilie**
Pyroelectric properties in ferroelectric thin films and multilayers
The 9th International Conference on Advanced Materials, ROCAM 2017
11-14.07.2017, Bucharest, Romania - **Poster**

63. **G. A. Boni, L. Filip, C. Chirila, I. Pasuk, R. Negrea, I. Pintilie, L. Pintilie**
Ferroelectric memory with non-destructive read-out operation
The 9th International Conference on Advanced Materials, ROCAM 2017,
11-14.07.2017, Bucharest, Romania - **Talk**

64. **C Chirila, A. Boni, M. Botea, L. Hrib, L. Trupina, I. Pasuk, R Negrea, I. Pintilie, L. Pintilie**
Pulsed laser deposition of epitaxial ferroelectric thin films and their potential applications
The 9th International Conference on Advanced Materials, ROCAM 2017,
11-14.07.2017, Bucharest, Romania - **Talk**

65. **C. Chirila**, G.Le Rhun, **M.Botea, L. Hrib, A. Boni, A.Iuga, I. Pintilie, L. Pintilie**
PZT thin films on Si for pyroelectric applications
EMRS Spring Meeting 2017,
21-26.05.2017, Strasbourg Franta - Talk

66. **C.F. Chirila, G. A. Boni, L. Hrib**, S. B. Porter, G. Atcheson, **I. Pintilie**, K. Rode, **L. Pintilie**
Electrical properties of NiFe2O4 epitaxial ultra-thin films
EMRS Spring Meeting 2017,
21-26.05.2017, Strasbourg Franta - **Poster**

67. **L. Filip, N. Plugaru**
Optimization of Berry phase polarization of Berry phase polarization calculations
The 9th International Conference on Advanced Materials, ROCAM 2017,
11-14.07.2017, Bucharest, Romania - **Talk**

68. **L.C. Tănase, N.G. Apostol, L. Hrib, L. Pintilie, and C.M. Teodorescu**
Combined LEED and XPS characterization of ferroelectric surfaces: ferroelectric dead layers,
9th International Conference on Advanced Materials: ROCAM, Bucharest, Romania,
July 10th–14th, 2017 - **Talk**.

69. **I. C. Bucur, L. C. Tănase, C. M. Teodorescu, A. G. Lungu, L. E. Abramiuc, and C. A.Tache**
Multiferroic Mn:Pb(Zr,Ti)O3,
9th International Conference on Advanced Materials: ROCAM, Bucharest, Romania,
July 10th–14th, 2017 - **Talk**.

70. **A. E. Bocîrnea, L. C. Tănase, R. M. Costescu, N. G. Apostol, and C. M. Teodorescu**
Band bending at magnetic Ni/Ge(001) interface investigated by X-ray photoelectron spectroscopy,
9th International Conference of Advanced Materials ROCAM, Bucharest, Romania,
July 10th–14th, 2017 - **Talk**.

71. **B. Borca**, T. Michnowicz, V. Schendel, R. Pétuya, I. Pentegov, U. Kraft, H. Klauk, A. Arnau, P. Wahl, U. Schlickum, and K. Kern
Electric-Field-Driven Chemical Reaction of Single Molecules,
9th International Conference on Advanced Materials: ROCAM, Bucharest, Romania,
July 10th–14th, 2017 - **Talk**.

72. **L.C. Tănase, N.G. Apostol, L. Hrib, L. Pintilie, and C.M. Teodorescu**
Low energy electron diffraction on ferroelectrics: near-surface charge accumulation and dead layers,
2nd International Workshop on Materials Physics: Materials Science using Synchrotron Radiation, National Institute of Materials Physics, Măgurele, Romania,
May 16th–17th, 2017 - **Talk**

73. **M. A. Husanu, D. G. Popescu, C. M. Teodorescu, L. Hrib, L. Pintilie**, and V. N. Strocov
Mass renormalization and orbital polarization at a ferroelectric/ferromagnetic interface,
9th International Conference on Advanced Materials: ROCAM, Bucharest, Romania,
July 10th–14th, 2017 - **Talk**.

74. **B. Borca**, V. Schendel, R. Pétuya, I. Pentegov, T. Michnowicz, U. Kraft, H. Klauk, A. Arnau, P. Wahl, U. Schlickum, and K. Kern
Strong anchoring between molecular endgroups and metal surface electrode by a locally triggered chemical reaction,
Workshop MOLSPIN, COST meeting – Quantum Spin Science and Technologies,
August 31th – September 1st, 2017, Bucharest, Romania - **Talk**.

75. **N.G. Apostol, L.C. Tănase, L.E. Abramiuc, L. Hrib, L. Trupină, L. Pintilie, and C.M. Teodorescu**
Carbon monoxide adsorbtion on Lead Zirco Titanate PZT (001) surfaces,
17th International Balkan Workshop on Applied Physics and Materials Science, Constanța, Romania, July 11th–14th, 2017 - **Talk**.

76. **L.C. Tănase, N.G. Apostol, L. Hrib, L. Pintilie, and C.M. Teodorescu**
Low energy electron diffraction on ferroelectrics: near-surface charge accumulation and dead layers,
17th International Balkan Workshop on Applied Physics and Materials Science, Constanța, Romania, July 11th–14th, 2017 - **Talk**

77. **S. Neațu, F. Neațu, M. Florea, L. E. Abramiuc, and C. M. Teodorescu**
Three-component photocatalytic systems as new approach for water splitting reaction,
9th International Conference of Advanced Materials ROCAM, Bucharest, Romania,
July 10th–14th, 2017 - **Talk**.

78. **S. Neațu, F. Neațu, M Florea, L. E. Abramiuc, and C. M. Teodorescu**
NiO-ZnO/TiO2 composites in the photocatalytic water splitting reaction,
Europacat2017, Florence, Italy,
August 27th–31st, 2017 - **Talk**

79. **M. Florea, F. Neațu**, S. Nicolae, G. Culica, V. I. Parvulescu, and F. Cavani
An unprecedented synthesis of terephthalic acid by p-cymene oxidation,
Europacat2017, Florence, Italy,
August 27th–31st, 2017 - **Talk**

80. **M. A. Husanu, D. G. Popescu**, F. Bisti, **C. M. Teodorescu, L. Hrib, C. Chirila, I. Pasuk, V. Kuncser, R. Negrea, L. Pintilie**, and V. N. Strocov
Interface effects in a ferromagnetic hole-doped manganite buried under ferroelectric layer revealed in soft X-ray ARPES,
2nd International Workshop on Materials Physics: Materials Science using Synchrotron Radiation, National Institute of Materials Physics Măgurele, Romania, May 16th–17th, 2017 - **Talk**.

81. **M. A. Husanu, D. G. Popescu, L. Tanase, C. M. Teodorescu, L. Hrib, C. Chirila, L. Pintilie**, D. Sostina, and V. N. Strocov
Field-dependent electronic properties of a multiferroic interface obtained during in-operando angle resolved photoelectron spectroscopy measurements,
EMRS Spring Meeting 2017, Strasbourg, France,
May 21st–26th, 2017 - **Talk**.

82. **F. Neațu, S. Neațu and M. Florea**
Selective oxidation of alkyl-substituted benzene in the presence of heterogeneous Mn-Co catalysts,
9th International Conference of Advanced Materials ROCAM, Bucharest, Romania,
July 10th–14th, 2017 - **Poster**.

83. **M. A. Husanu, D. G. Popescu, C. M. Teodorescu, L. Hrib, C. Chirila, V. Kuncser, L. Pintilie**,
and V. N. Strocov
Modified magnetism of a multiferroic interface due to orbital ordering triggered by ferroelectric field effect,
International Conference on Strongly Correlated Electron Systems, SCES 2017, Prague, Czech Republic,
July 16th–22nd, 2017 - **Poster**.

84. **B. Borca**, V. Schendel, R. Pétuya, I. Pentegov, T. Michnowicz, U. Kraft, H. Klauk, A. Arnau, P. Wahl, U. Schlickum, and K. Kern
Reversible isomer selective single molecular switches activated locally or remotely by Scanning Tunneling Microscopy,
6th European Conference on Molecular Magnetism,
August 27th–31st, 2017, Bucharest, Romania - **Poster**.

85. **R. M. Costescu, A. E. Bocîrnea, L. C. Tănase, I. Pasuk, B. Borca, and Cristian M. Teodorescu**
Growth mechanisms of silver on Si(111) investigated by XPS and LEED,
9th International Conference of Advanced Materials ROCAM, Bucharest, Romania,
July 10th–14th, 2017 - **Poster**

86. **M. A. Husanu, D. G. Popescu, C. M. Teodorescu, L. Hrib, C. Chirila, V. Kuncser, L. Pintilie**, and V. N. Strocov
Preferential orbital occupation and the effect on electron mobility at ferroelectric/ferromagnetic interface,
3rd Functional Oxide Thin Films for Advanced Energy and Information Technology, Rome, Italy,
July 4th–8th, 2017 - **Poster**

87. **C. Logofatu, R. Ghita, C. Cotirlan, C. Negrila**, M. I. Rusu, and C. Palade
Characterization of thermally grown oxide layers on n-GaSb (100),
9th International Conference on Advanced Materials: ROCAM, Bucharest, Romania,
July 10th–14th, 2017 - **Poster**

88. **C. Cotirlan-Simioniuc, C. Logofatu, C. C. Negrila, and A. S. Manea**
Characterization of plasmonic metasurfaces for optical components able to manipulate the light beyond the fundamental diffraction limit,
17th International Balkan Workshop on Applied Physics and Materials Science, Constanța, Romania,
July 11th–14th, 2017 - **Poster**

89. **C. Cotirlan-Simioniuc, C. C. Negrila, A. S. Manea**, A. Rizea, and C. Marin
Reconfigurable plasmonic metasurfaces provide great flexibility in the design of photonic devices,
17th International Balkan Workshop on Applied Physics and Materials Science, Constanța, Romania,
July 11th–14th, 2017 - **Poster**.

90. **R. Ghita**, D. Pantelica, **C. Logofatu, C. Negrila**, P. Cristea, and L. Fara,
Features of Si+ implanted n-GaSb(100) photosensitive structure,
33rd European Photovoltaic Solar Energy Conference and Exhibition, EU PVSEC 2017, Amsterdam, The Netherlands, September 25th–29th, 2017 - **Poster**.

91. Ø. Nordseth, I. Chilibon, B. G. Svensson, R. Kumar, S. E. Foss, C. Vasiliu, R. Iordanescu, L. Baschir, D. Savastru, L. Fara, and **R. Ghita**,
Characterization of copper oxide photosensitive thin films,
9th International Conference on Advanced Materials: ROCAM, Bucharest, Romania,
July 10th–14th, 2017 - **Poster**.

92. **I. Stavarache, A. Slav**, M. Braic, **V. S. Teodorescu**, P. Prepelita, **C. Palade, A.-M. Lepadatu, S. Lazanu, M. L. Ciurea**, D. Stange, D. Buca, **T. Stoica**
Nanocrystals of GeSn alloys in oxide matrix for optoelectronic applications,
Applied Nanotechnology and Nanoscience International Conference – ANNIC2017,
October 18-20, Rome, Italy - **Talk**

93. **A. Slav, C. Palade, I. Stavarache, V.S. Teodorescu, M.L. Ciurea**, R. Müller, A. Dinescu, M.T. Sultan, A. Manolescu, J.T. Gudmundsson, H.G. Svavarsson
nfluence of preparation conditions on structure and photosensing properties of GeSi/TiO2 multilayers,
IEEE International Semiconductor Conference - CAS 2017,
October 11-14, Sinaia, Romania - **Talk**

94. **C. Palade, I. Dascalescu, A. Slav, A.M. Lepadatu, S. Lazanu, T. Stoica, V.S. Teodorescu, M.L. Ciurea**, F. Comanescu, R. Müller, A. Dinescu, A. Enuica
Photosensitive GeSi/TiO2 multilayers in VIS-NIR,
CAS 2017, October 11-14, Sinaia, Romania - **Talk**

95. **C. Palade, A. Slav, A.M. Lepadatu, S. Lazanu, M.L. Ciurea, T. Stoica**
Light illumination effects on floating gate memory with Ge nanocrystals in HfO2,
CAS 2017, October 11-14, Sinaia, Romania - **Talk**

96. **C. Palade, A. Slav, A.-M. Lepadatu, A.V. Maraloiu, S. Lazanu, C. Logofatu, T. Stoica, V.S. Teodorescu, M.L. Ciurea**
Ge nanocrystals in oxides with memory and photoelectrical properties,
The 9th International Conference on Advanced Materials - ROCAM 2017,
July 11-14, Bucharest, Romania - **Talk**

97. **A.V. Maraloiu, C. Ghica, M.L. Ciurea, A.M. Lepadatu, A. Slav, C. Palade, I. Stavarache, S. Lazanu, V.S. Teodorescu**
XTEM study of Ge based multilayer structures,
ROCAM 2017, July 11-14, Bucharest, Romania - **Poster**

98. **C. Logofatu, R.V. Ghita, C. Cotirlan, C.C. Negrila,** M. Rusu, C. Palade
Characterization of thermally grown oxide layers on n-GaSb (100),
ROCAM 2017, July 11-14, Bucharest, Romania - **Poster**

99. **A.M. Lepadatu, C. Palade, A. Slav, A.V. Maraloiu, C. Logofatu,S. Lazanu, T. Stoica, V.S. Teodorescu, M.L. Ciurea**
Ge Nanocrystals as charge storage nodes in nano-floating gate capacitor memories with crystalline HfO2,
I**BWAP 2017,** July 11-14, Constanta, Romania - **Talk**

100. **A. Slav, C. Palade, A.M. Lepadatu, A.V. Maraloiu, C. Logofatu, S. Lazanu, T. Stoica, V.S. Teodorescu, M.L. Ciurea**
Active materials based on Ge nanocrystals in oxides for trilayer memory capacitors and photosensitive structures,
IBWAP 2017, July 11-14, Constanta, Romania - **Poster**

101. M.T. Sultan, J.T. Gudmundsson, **M.L. Ciurea**, H.G. Svavarsson
Photoconductive TiO2 films functionalized with Si(1-x)Gex nanoparticles,
DINAMO 2017 in ICELAND,
May 14-19, Siglufjordur, Iceland - **Poster**

102. **V.S. Teodorescu, A.V. Maraloiu, C. Ghica, M.L. Ciurea, A.M. Lepadatu, A. Slav, C. Palade, I. Stavarache, S. Lazanu**
XTEM study of Ge based multilayer structures,
2nd "Conference of the Romanian Electron Microscopy Society - C.R.E.M.S.",
May 16-18, Sinaia, Romania - **Talk**

103. **A.-C. Gâlcă**, G. Socol, **A. Velea**
Spectroscopic ellipsometry, a useful tool to investigate phase transitions in thin films: case study on phase change materials
4th Central and Eastern European Conference on Thermal Analysis and Calorimetry,
August 28 – 31, 2017, Chișinău, Republic of Moldova - **Talk**

104. **A. Velea**, G. Socol, C. Mihai, **A. Lőrinczi, I. D. Simandan, G. Schinteie, F. Sava**
Thermal stability of heterojunction interfaces in GaSb/GeTe, GaSb/SnSe and SnSe/GeTe bilayers revealed by X-ray reflectometry
8th International Conference on Amorphous and Nanostructured Chalcogenides - Fundamentals and Applications,
July 2 – 5, 2017, Sinaia, Romania - **Poster**

105. **P. Ganea**, G. Socol, S. Zamfira, **F. Sava, A. Velea, D. Şimăndan**, C. Creţu, **M. Popescu, A. Lőrinczi**
Dielectric spectroscopy measurements on Cu-As2S3-Cu thin film heterostructures
8th International Conference on Amorphous and Nanostructured Chalcogenides - Fundamentals and Applications,
July 2 – 5, 2017, Sinaia, Romania - **Poster**

106. Doina Manaila-Maximean, Viorel Cîrcu, **Paul Ganea**, Laura F. Chiriac
Luminescent and dielectric properties of a series of lanthanide-containing liquid crystals
The 14th European Conference on Liquid Crystals (ECLC 2017),
June 25 – 30, 2017, Moscow, Russia - **Poster**

107. Doina Manaila Maximean, Octavian Danila, Pedro L. Almeida, **Paul Ganea**
Electric and electro-optic characterization of new cellulose electrospun polymer dispersed liquid crystal
The 14th European Conference on Liquid Crystals (ECLC 2017),
June 25 – 30, 2017, Moscow, Russia - **Talk**

108. G. Popescu-Pelin, R. C. Popescu, **M. Socol,** O. Fufa, A. M. Holban, **C. Florica, I. Zgura**, M. Patachia, G. Socol
PANI-Fe3O4 based coatings deposited by MAPLE for biomedical applications.
EMRS Spring meeting, Strasbourg, France,
May 22 – 26, 2017 - **Poster**

109. L. Duta, **G.E. Stan**, A.C. Popescu, G. Popescu-Pelin, A. Achim, **M. Enculescu, I. Zgura**, P.E. Florian, A. Roseanu, F.N Oktar,
Physical, chemical and in vitro assessment of biological-derived HA thin films for a new generation of metallic implants.
EMRS Spring meeting, Strasbourg, France,
May 22 – 26, 2017 - **Poster**

110. G. Popescu-Pelin, O. Fufa, R. C. Popescu, **M. Socol**, A. M. Holban, **C. Florica, I. Zgura**, G. Socol
FE3O4–embedded PANI–based coatings for biomedical applications
The 9th International Conference on Advanced Materials: ROCAM 2017,
July 11-14, 2017, Bucharest, Romania - **Poster**

111. G. Popescu-Pelin, E. Axente, I. Iordache, C. Nita, A. Visan, **I. Zgura, O.L. Rasoaga, C.S. Breazu, A. Stanculescu**, S. Banita,G. Socol
Coatings based on PCL/PLGA synthetized by maple and dip-coating techniques: a comparative study
The 9th International Conference on Advanced Materials: ROCAM 2017,
July 11-14, 2017, Bucharest, Romania - **Poster**

112. O. Fufă, G. Popescu-Pelin, R. Trușcă, B.Ș. Vasile, **M. Socol, I. Zgură**, R.C. Popescu, A.M. Holban, A.M. Grumezescu, E. Andronescu, G. Socol, V. Crăciun
Bionanostructured CaPs/AgNPs coatings for titanium-based materials
The 9th International Conference on Advanced Materials: ROCAM 2017,
July 11-14, 2017, Bucharest, Romania - **Poster**

113. **M. Socol, N. Preda, C. Breazu, A. Stanculescu, A. Costas**, F. Stanculescu, M. Girtan, F. Gherendi, G. Popescu-Pelin, G. Socol
Functionalized organic heterostructures deposited by MAPLE on flexible substrate,
ROCAM 2017, 11-14 July, Bucharest Romania - **Poster**

114. **Carmen Breazu**, Florin Stanculescu, Gabriel Socol, Loredana Vacareanu, Mircea Grigoras, **Marcela Socol**, **Nicoleta Preda**, Mihaela Girtan, **Anca Stanculescu**
Optical and electrical properties of arylenevinylene based flexible heterostructures withA:ZnO transparent conductor electrode,
ROCAM 2017, 11-14 July, Bucharest Romania - **Poster**

115. **M. Socol, N. Preda, C. Breazu, A. Stanculescu, A. Costas**, F. Stanculescu, G. Popescu-Pelin, F. Gherendi, G. Socol, L. Vacareanu
Organic heterostructures deposited by MAPLE on patterned AZO electrode,
ROCAM 2017, July 11-14, Bucharest Romania - **Poster**

116. F. Stanculescu, **M. Socol**, M. Girtan, **O. Rasoga, C. Breazu, A. Stanculescu**
Electrical Properties of Nucleic Acids Bases Molecular Wide Band Gap Heterostructures,
ROCAM 2017, July 11-14, Bucharest Romania - **Poster**

117. **C. Breazu**, G. Socol, A. M. Catargiu, M. Grigoras, **O. Rasoga, A. Stanculescu, M.**, F. Stanculescu, **N.**, M. Girtan
Effect of 2d electrode patterning on the properties of arylenevinilene based polymer mixed layers,
ROCAM 2017, July 11-14, Bucharest Romania - **Poster**

118. O. Fufă, G. Popescu-Pelin, **M. Socol**, L. Mogoantă, R.C. Popescu, A.M. Holban, G. Socol, V. Crăciun, A.M. Grumezescu, E. Andronescu,
HAp/AgNPs coatings for titanium-based implants,
ROCAM 2017, July 11-14, Bucharest Romania - **Talk**

119. A. Vișan, O. Fufă, **M. Socol**, G. Popescu-Pelin, R.C. Popescu, D. Savu, A.M. Holban, R. Cristescu, M. Pațachia, G. Socol
Antimicrobial composite coatings based on polyaniline grafted lignin loaded with gentamicin functionalized magnetic nanoparticles for medical applications,
ROCAM 2017, July 11-14, Bucharest Romania - **Talk**

120. G. Popescu-Pelin, O. Fufa, R. C. Popescu, **M. Socol**, A. M. Holban, **C. Florica, I. Zgura**, G. Socol
Fe3O4–embedded PANI–based coatings for biomedical applications,
ROCAM 2017, July 11-14, Bucharest Romania - **Poster**

121. A. Mihailescu, G. Popescu-Pelin, **M. Socol**, S. Banita, G. Socol,
SnO2-ZnO Thin Films for CO Gas Sensing Applications,
ROCAM 2017, July 11-14, Bucharest Romania - **Poster**

122. A. Visan, O. Fufa, C. Matei, **M. Socol**, G.Popescu-Pelin, R.C.Popescu, D. Savu, R. Cristescu, D. Craciun, G. Socol
Antimicrobial composite coatings based on gentamicin loaded magnetic nanoparticles for medical applications,
ROCAM 2017, July 11-14, Bucharest Romania - **Poster**

123. F. M. Miroiu, N. Stefan, A. I. Visan, V. Grumezescu, C. Radu, **M. Socol**, R. C. Popescu, D. Savu, M. Temelie, G. Socol,
Deposition of complex hybrid Fe3O4- PEDOT:PSS-PLGA-CYPRESS essential oil coatings by matrix assisted pulsed laser evaporation,
ROCAM 2017, July 11-14, Bucharest Romania - **Poster**

124. **A. Stanculescu, C. Breazu, M. Socol** , A.-M.Catargiu, L.Vacareanu, M. Grigoras, F. Stanculescu , G. Socol, M. Girtan,
Preparation and characterization of organic heterostructures based on arylenevinylene polymer: perylene diimide blends,
EMRS, 2017, May 22-26, Strasbourg, France - **Poster**

125. L. Hrostea, A.Aukštuolis, M. Boclinca, **M. Socol**, L. Leontie, **A. Stanculescu**, M. Girtan
New oxide/metal/oxide electrodes for solar cell applications,
EMRS, 2017, May 22-26, Strasbourg, France - **Poster**

126. A. Visan, O.Fufa, C. Matei, **M. Socol**, G. Popescu-Pelin, R. C. Popescu, D. Savu, R. Cristescu, D.Craciun, G. Socol,
MAPLE Composite coatings enriched with gentamicin loaded magnetic nanoparticles for prevention of bone tissue infections,
EMRS, 2017, May 22-26, Strasbourg, France - **Poster**

127. C.A. Stanciu, A.C. Ianculescu, **L.Trupina, M. Cernea**, R. Trusca, B. S.Vasile, **L. Pintilie**
Doped BaTiO3 1D-nanostructures prepared by colloidal chemistry. Poster number: EMA-WWP-005-2017.
Electronic Materials and Applications 2017 conference (EMA 2017),
January 18 - 20, 2017 at the Orlando, Florida, 'SYMPOSIUM 1: Advanced Electronic Materials: Processing, Structures, Properties and Applications - **Poster**

128. **D. Ghica, M. Stefan, C. Ghica, G. E. Stan**
Correlative TEM and EPR studies of nanostructured ZnO films,
Conference of the Romanian Microscopy Society CREMS 2017,
16-18.05.2017, Sinaia, Romania – **Poster**

129. **A.V. Maraloiu, D. Ghica, M. Stefan, S.V. Nistor**, R. Plugaru
Mn2+ ions distribution in doped sol–gel deposited ZnO films ,
Romanian Electronic Microscopy Society Conference CREMS 2017,
16-18.05.2017, Sinaia, Romania – **Poster**

130. **S. Bulat, D. Zernescu, R. F. Negrea, C. Ghica**
Pumping station for TEM portmans
Romanian Electronic Microscopy Society Conference CREMS 2017,
16-18.05.2017, Sinaia, Romania – **Poster and prototype**

131. **I. D. Vlaicu, R. F. Negrea, V. A. Maraloiu, I. F. Mercioniu**
Microstructural characterization of BaTiO3 nanoparticles using TEM techniques: the effects of post-synthesis treatments,
Romanian Electronic Microscopy Society Conference CREMS 2017,
16-18.05.2017, Sinaia, Romania - **Poster**

132. B.S. Vasile, **M. Cernea**, R. Trusca,
Electron microscopy investigations on ferroelectric domains in multiferroic (Pb1–3x/2Ndx)(Ti0.98–yFeyMn0.02)O3 ceramics,
Romanian Electronic Microscopy Society Conference CREMS 2017,
16-18.05. 2017, Sinaia, Romania - **Poster**

133. **C. Ghica, R. F. Negrea, V. S. Teodorescu, C. F. Chirila**, N. D. Scarisoreanu
HRTEM mapping of residual strain in epitaxial layers, Romanian Electronic Microscopy Society Conference, **CREMS 2017**, 16-18.05.2017, Sinaia, Romania - **Talk**

134. A. Ion, **C. Ghica**
Tehnici de preparare a probelor TEM in stiinta materialelor,
Romanian Electronic Microscopy Society Conference, CREMS 2017,
16-18.05.2017, Sinaia, Romania - **Poster**

135. **A. M. Vlaicu, I. Mercioniu, C. Ghica , V. Manoliu**, A. Mihailescu, Gh. Ionescu
Oxidation processes in NiCoCrAlY bond layers for Thermal Barrier Coatings investigated by XRD and SEM,
Romanian Electronic Microscopy Society Conference, CREMS 2017,
16-18.05.2017, Sinaia, Romania - **Talk**

136. **F. Mercioniu , A.M. Vlaicu, C. Ghica, V. Manoliu**, A. Mihailescu, Gh. Ionescu
TEM observation of oxidations processes in NiCoCrAlY bond layers for Thermal Barrier Coatings,
CREMS 2017, 16-18.05.2017, Sinaia, Romania - **Talk**

137. **A. Kuncser**, I. Solodkyi, I. Bogomol, P. Loboda, **P. Badica**,
Crystal orientation and phase mapping in TEM,
CREMS 2017, 16-18.05.2017, Sinaia, Romania - **Talk**

138. C. I. Nica, M. S. Stan, I. Dumitrescu, **L. Diamandescu**, C. Chifiriuc, A. Dinischiotu
Development and biocompatibility evaluation of photocatalytic graphene oxide/TiO2-based nanoparticles co-doped with iron and nitrogen designed for self-cleaning purposes.
Abstract Book of the 8th European Conference on Nanotechnology (EuroNanoForum 2017),
June 21-23, 2017, Valletta, Malta.http://euronanoforum2017.eu/poster-abstracts/ . **Poster**

139. **I.D. Vlaicu, M. Stefan, D. Ghica, L.C. Nistor, S.V. Nistor, A.V. Maraloiu, A.C. Joita**,
Manganese ions role in redirecting zinc hydroxide synthesis towards zinc oxide: responsibility or complicity?,
9th International Conference on Advanced Materials , ROCAM 2017,
11-14 July 2017, Bucharest, Romania – **Poster**

140. **D. Ghica, I.D. Vlaicu, M. Stefan, L.C. Nistor, S.V. Nistor**,
The curious effect of the Mn ions on the doped Zn(OH)2 synthesis,
9th International Conference on Advanced Materials, ROCAM 2017,
July 11-14, 2017, Bucharest, Romania – **Talk**

141. **M. Stefan, D. Ghica, S. V. Nistor**, S. Bellei, A. Nevin,
CERIC project at the EPR facility from NIMP: EPR investigation of historical pigments,
9th International Conference on Advanced Materials, ROCAM 2017,
July 11-14, 2017, Bucharest, Romania – **Talk**

142. **A.C. Joita, S.V.Nistor, R. Radu, I. Pintilie**
ESR of irradiation point defects in pure and 17O doped Si-FZ single crystals at high doses of 3.5MeV electrons,
9th International Conference on Advanced Materials, ROCAM 2017,
July 11-14, 2017, Bucharest, Romania – **Talk**

143. **V. Stancu, M. Cernea, V. Mihalache, L. Nedelcu**, Mohamad Rammal,
Microwave dielectric properties of (1-x)Bi0.5Na0.5TiO3-xBaTiO3 thin film,
9th International Conference on Advanced Materials, ROCAM 2017, Bucharest, Romania,
July 11-14, 2017 - **Poster**

144. **O.G. Florea**, C.F. Ciobota, R.M. Piticescu, **A. Stanoiu, C.E. Simion**,
Gas sensing performances towards H2S detection with thin and thick Cu doped BaSrTiO3 layers,
9th International Conference on Advanced Materials, ROCAM 2017, Bucharest, Romania,
11-14.07.2017 - **Poster**

145. **A. Kuncser, V. Kuncser**, S. Antohe,
A micromagnetic analysis of domain wall dynamics in high aspect ratio cylindrical Fe-Cu nanowires,
9th International Conference on Advanced Materials, ROCAM 2017, Bucharest, Romania,
11-14.07.2017 - **Poster**

146. A. Dinischiotu, I. C. Nica, M. Stan, I. Dumitrescu, **L. Diamandescu**,
The biocompatibility of new developed TiO2-based photocatalytic nanoparticles on human skin and lung fibroblasts.
Abstract Book of the 3rd International Conference on Advances in Functional Materials (AFM 2017), p. 532.
14-17 August 2017, Los Angeles, USA. http://afm2017.functionalmaterials.org/wp-content/uploads/Consolidated-Abstract-Book-2017.pdf - **Poster**

147. R. Trusca, **L. Diamandescu**, V.A. Surdu,
Structural and morphological evolution with temperature of zinc oxide doped with iron and neodymium,
20th Romanian International Conference on Chemistry and Chemical Engineering (RICCCE 2017),
6-9 September 2017, Poiana Brasov, Romania - **Poster**

148. F. Cordero, F. Craciun, **M. Cernea**, V. Fruth, I. Atkinson, N. Stanica, B. S. Vasile, **L. C. Tanase, L. Diamandescu**, C. Galassi,
Anelastic and dielectric characterization of the multiferroic perovskite (Pb1-3x/2Ndx)(Ti0.98-yFeyMn0.02)O3,
18th. International Conference on Internal Friction and Mechanical Spectroscopy (ICIFMS-18),
September 12-15, 2017. Foz do Iguaçu, Brazil - **Poster**

149. **A. Stanoiu**, S. Somacescu, **C.E. Simion**, Jose Maria Calderon-Moreno, **O.G. Florea**
Gas sensing properties of NiO/mesoporous SnO2,
International Semiconductor Conference CAS 2017 Sinaia, Romania,
October 11-14. 2017 - **Talk**

150. **C.E. Simion, O.G. Florea, A. Stanoiu**,
Gas sensing mechanism involved in H2S detection with NiO loaded SnO2 gas sensors,
International Semiconductor Conference CAS 2017 Sinaia, Romania,
October 11-14, 2017 - **Talk**

151. **D. Ghica, M. Stefan, I. D. Vlaicu, L. C. Nistor, S. V. Nistor, A. C. Joita,**
Challenges in doping nanocrystals: the case of Mn doped nano-ZnO,
9th International Conference on Nanomaterials - Research & Application NANOCON 2017, Brno, Cehia,
October 18 – 20, 2017 – **Poster**

152. **M. Stefan, I.D. Vlaicu, L.C. Nistor, D. Ghica, S.V. Nisto**r
On the origin and chemical composition of the amorphous material from the intergrain region of nanostructured semiconductors,
9th International Conference on Nanomaterials - Research & Application NANOCON 2017, Brno, Cehia,
October 18-20, 2017 – **Talk**

153. **I.D. Vlaicu**, M. M. Kržmanc, D. Suvorov, **A.V. Maraloiu, I.F. Mercioniu, R. F. Negrea, A.C. Kuncser, D. Ghica, M. Stefan, M.A. Vlaicu**
Influence of Calcium Content on Morpho-structural Properties of the Perovskite-type Structure Ba1-xCaxTiO3,
9th International Conference on Nanomaterials - Research & Application NANOCON 2017, Brno, Cehia, October 18-20, 2017 - **Poster**

154. **V.A. Maraloiu, C. Ghica**, D. Zappa, E. Comini,
Microstructural and analytical investigations of SnO2 nanowires for gas sensing applications,
9th International Conference on Nanomaterials - Research & Application NANOCON 2017,
18-20 Octombrie 2017, Brno, Czech Republic – **Poster**

155. **C. Ghica, R. F. Negrea**, M. Karlušić, Z. Siketić, M. Jakšić, M. Schleberger, S. Fazinić,
Analytical TEM/STEM investigations of ion tracks in CaF2: facts and doubts ,
9th International Conference on Nanomaterials - Research & Application NANOCON 2017, Brno, Czech Republic,
October 18-20, 2017 - **Talk**

156. **C.M. Istrate, R.F. Negrea**
Microstructural characterization of BNT-BT ferroelectric thin film by advanced TEM techniques,
9th International Conference on Nanomaterials - Research & Application NANOCON 2017, Brno, Czech Republic,
18-20th of October 2017 - **Poster**

157. **I. Mercioniu, A.M. Vlaicu, R. F. Negrea, C. Ghica**
Study concerning oxidation processes of NiCoCrAlY bond layers for thermal barrier coatings,
9th International Conference on Nanomaterials - Research & Application NANOCON 2017, Brno, Czech Republic,
18-20th of October 2017 - **Poster**

158. **A.C. Kuncser, A. Stanciu, A. Catrina, G. Schinteie ,V. Kuncser**
Micromagnetic analysis on lamellar vs. disperse structures of Fe nanoparticles in Au thin films,
9th International Conference on Nanomaterials - Research & Application NANOCON 2017, Brno, Czech Republic,
October 18-20, 2017 – **Talk**

159. I.Dumitrescu, O.G. Iordache, C.E. Mitran, E. Varzaru, A. Chivu, L.C. Dinca, Arcadii Sobetkii, L. Diamandescu
Attempts to improve the self-cleaning effect of the textile materials
8TH TEXTEH INTERNATIONAL CONFERENCE, Bucharest, Romania,
October 19-20, 2017 – **Poster**

160. **A. Birsan, V. Kuncser**
Magnetic properties in spin gapless semiconductors,
The 9th International Conference on Advanced Materials, ROCAM, Bucharest, Romania,
July 11-14,, 2017 – **Talk**

161. **A. Birsan, V. Kuncser**,
Completely compensated ferrimagnetism in spin gapless semiconductors,
The 9th International Conference on Advanced Materials, ROCAM, Bucharest, Romania,
July 11-14, 2017 – **Poster**

162. **M. Burdusel, G. V. Aldica, P. Badica**,
Processing method and superconducting tape in MgB2 core metal sheath,
The "Designed in Romania" Research Salon, Bucharest, Romania
October 25-27, 2017 (Patent request OSIM nr. A 00150/2016) – **Poster and prototype**

163. **M. Burdusel, G. V. Aldica, P. Badica**
Processing method and superconducting tape in MgB2 core metal sheath,
European Exhibition of Creativity and Innovation, EUROINVENT, Iasi, Romania,
May 25 – 27, 2017 – **Poster and prototype**

164. **A.Crisan, I.Ivan, L. Miu**
Critical current and pinning potential in nanostructured YBa2Cu3O7 superconducting films grown by PLD,
European-Materials Research Society Spring Meeting (E-MRS2017) Strasburg,
21-26 Mai 2017 – **Talk**

165. **A. Crisan**,
Non-centrosymmetric vortices in multi-component superconductors, Quantum physics in Complex Matter,
Superconductivity, Magnetism and Ferroelectricity (Superstripes 2017), Ischia, Italy,
June 3-11 2017 – **Talk**

166. **A. Crisan, I. Ivan, L. Miu,**
Improved critical current and pinning potential in YBa2Cu3Ox superconducting films with nanoengineered pinning centres with various architectures,
The 28-th Low Temperature Physics Conference,
August 8-16, Goteborg, Suedia – **Poster**

167. **A. Crisan, I. Ivan, L. Miu**,
Nanotechnology of Pinning Centres in Superconducting Films for Clean Energy-saving Power Applications,
NANOTECH ME 2017, Dubai, EAU,
3-7 December 2017 – **Talk**

168. **O. Crisan, F. Vasiliu, A.D. Crisan, I. Mercioniu, A. Crisan, A. Leca**,
FeCoPtB as an innovative nanocomposite magnet for next generation renewable energy application,
4th International Conference on Next Generation Computing and Communication Technologies ICNGCCT 2017, Dubai, E.A.U – **Talk**

169. **O. Crisan, A.D. Crisan, I. Mercioniu, F. Vasiliu, A. Leca**,
Hard Magnetic Properties and Interlayer Exchange Coupling in Rare Earth – free FePtMn Layered Nanomagnets,
16th International Materials Research Congress IMRC2017, Cancun, Mexic – **Talk**

170. **O. Crisan**, T. Klein, R. Rohlsberger, E. Burkel,
New concept for information storage in magnetic films exchange-coupled through non-magnetic layer,
IEEE 12th International Conference on Nano/Micro Engineered and Molecular Systems, NEMS 2017, Los Angeles, SUA – **Talk**

171. **A.D. Crisan, O. Crisan**
Alternative solutions for data storage using magnetic films exchange-coupled through non-magnetic layer,
4th International Conference on Next Generation Computing and Communication Technologies ICNGCCT 2017, Dubai, E.A.U – **Poster**

172. **M. Galatanu, M Enculescu, G. Ruiu**, C. Stancu, G. Dinescu, **A. Galatanu**,
Functional interfaces in W-Ti and W-V laminates,
17th International Balkan Workshop on Applied Physics and Materials Science – IBWAP 2017, Constanta, Romania,
July 11-14, 2017 – **Poster**

173. **M. Galatanu, M. Enculescu, G. Ruiu, A. Galatanu**,
High temperature thermo-physical properties of Cu-based thermal barrier composites,
17th International Balkan Workshop on Applied Physics and Materials Science – IBWAP 2017, Constanta, Romania,
July 11-14, 2017 – **Poster**

174. **M. Galatanu, M. Enculescu, G. Ruiu, A. Galatanu,**
Thermophysical properties of W based plasma facing materials for fusion reactors,
17th Conference on Plasma Physics and Applications, Magurele, Romania,
June 15-20, 2017 – **Poster**

175. **M. Galatanu, G. Ruiu, M. Enculescu, A. Galatanu**,
FAST brazing technology for multi-layered composite materials processing,
NUCLEAR 2017 -The 10th Annual International Conference on Sustainable Development through Nuclear Research and Education, Pitești, România,
May 24-26, 2017 – **Talk**

176. **M. Galatanu, M. Enculescu, G. Ruiu, B. Popescu, A. Galatanu**,
Thermal barriers for DEMO W-monoblock divertor,
16th International Conference on Plasma-Facing Materials and Fusion Applications, Duesseldorf/Neuss, Germany,
May 15-19, 2017 – **Poster**

177. **S.G. Greculeasa, G. Schinteie, L. Hrib, I. Pasuk, V. Kuncser**,
Exchange bias effects in BFO/Fe type heterostructures, Magnetism 2017,
University of York, UK,
3-4 April 2017 – **Poster**

178. **M. Grigoroscuta, A.M. Ionescu, M. Burdusel, G. Aldica, P. Badica,**
Pinning force related parameters of the SPS Y2O3 doped MgB2,
ESAS Summer School on Superconductivity, Grenoble-Lans en Vercours, Franta,
24 iunie – 1 iulie 2017 – **Poster**

179. **A.M. Ionescu**, D. Miu, **A. Crisan, L. Miu**,
Origin of the second magnetization peak in iron-based superconductors,
ESAS Summer School on Superconductivity, Grenoble-Lans en Vercours, Franta,
24 iunie – 1 iulie 2017 – **Poster**

180. **A.M. Ionescu, V. Sandu**, L. Craciun, **G. Aldica, L. Miu, A. Kuncser**,
Magnetic properties of proton irradiated MgB2,
Int. Conf. Of Physics Students, Torino,
7-14 august 2017 – **Poster**

181. **V. Kuncser, G. Schinteie, F. Tolea, A. Kuncser, C. Ghica, L. Nistor, S. Nistor, N. Grecu**,
New insights on magnetic interactions and related effects in diluted magnetic systems,
The 9th International Conference on Advanced Materials, ROCAM, Bucharest, Romania,
11-14th of July, 2017 – **Talk**

182. **N. Plugaru**, G.A. Nemnes, **L.D. Filip, I. Pintilie, L. Pintilie**, K.T. Butler, and A. Manolescu
First Principles Study of CH3NH3PbI3-xClx – PbTiO3 Heterostructures,
Workshop "Spin-orbit effects in molecules and solids: diversity of properties and computational precision" and the Tutorial "hands-on-FPLO", Dresden, Germany,
November 13-17, 2017 – **Talk**

183. **A.E. Stanciu, A. Kuncser, A. Catrina, G. Schinteie, V. Kuncser**
Self-organized magnetic clusters in Fe-Au granular thin films. Magneto-structural correlations and perspective for investigations with synchrotron radiation,
International Workshop on Materials Physics, second edition, Magurele, Romania,
16-17 Mai, 2017 – **Talk**

184. **A.E. Stanciu, A. Kuncser, A. Catrina, A. Leca, N. Iacob, O. Crisan, G. Schinteie, V. Kuncser**
Non-collinear spin configurations and related magneto-transport effects in amorphous Fe-Gd thin films,
The European Conference Physics of Magnetism, Poznan, Polonia,
26-30th of June, 2017 – **Poster**

185. **A.E. Stanciu, A. Kuncser, A. Catrina, A. Leca, N. Iacob, O. Crisan, G. Schinteie, V. Kuncser**
Magnetic and magnetoresistive properties of Fe-Au granular thin films in connection with self-organization phenomena,
The 9th International Conference on Advanced Materials, ROCAM, Bucharest, Romania,
11-14th of July 2017 – **Talk**

186. A. Scurtu, N. Udrea, C. Luculescu, **M. Galaţanu, A. Galaţanu**, D. Ticoş, C.M. Ticoş,
Cracks and Nanodroplets Produced on Tungsten Surface by Dense Plasma Jets,
17th Conference on Plasma Physics and Applications, Magurele, Romania,
June 15-20, 2017 – **Talk**

187. A. Scurtu, N. Udrea, C. Luculescu, M. **Galaţanu, A**. Galaţanu, D. Ticoş and C.M. Ticoş,
Impact of Dense Plasma Jets on Tungsten Surfaces,
IONS Balvanyos 2017, International OSA Network of Students, Balvanyos, Romania,
25-28 July 2017 – **Talk**

188. C.M. Ticoş, **M. Galaţanu, A. Galaţanu**, C. Luculescu, A. Scurtu, N. Udrea, D. Ticoş,
Cracks and Nanodroplets Produced on Tungsten Surface by Dense Plasma Jets,
17th International Balkan Workshop on Applied Physics and Materials Science – IBWAP 2017, Constanta, Romania, 11-14, July, 2017 – **Talk**

189. I. Tiseanu, **A. Galatanu**, T. Craciunescu, C. Dobrea, M. Lungu and A. Sima,
Advanced X-ray imaging methods for characterization of plasma facing components structural integrity and operation,
EUROMAT 2017, Thessaloniki, Greece, September
17-22, 2017 – **Talk**

INVITED LECTURES

01. **Ciobotaru C. C., Ciobotaru I. C., Schinteie G., Polosan S.**
Enhancement of the electroluminescence of organic light emitting devices based on ir(ppy)3 by doping with metalic and magnetic nanoparticles,
IBWAP 2017, Constanta
11-14th of July – **Invited**

02. **Stan GE, Popa AC,** Fernandes HR, Ferreira, JMF
The prospects for bio-glass implant coatings
15th Conference & Exhibition of the European Ceramic Society (ECerS2017), Budapest, Hungary
9-13.07.2017 – **Invited**

03. **R. Ghita, C. Logofatu, C. Negrila,** and P. Cristea
Aspects of GaSb active devices technology
9th International Conference on Advanced Materials: ROCAM, Bucharest, Romania
July 10th–14th, 2017 – **Invited**

04. **L. E. Abramiuc, L. C. Tănase, D. G. Popescu, M. A. Huşanu, N. G. Apostol, C. A. Tache, C. Chirilă, L. Pintilie, C. M. Teodorescu,** S. Lizzit, P. Lacovig, and A. Barinov
Photoelectron spectromicroscopy of ferroelectrics
17th International Balkan Workshop on Applied Physics and Materials Science, Constanța, Romania
July 10th–14th, 2017 – **Invited**

05. **N. G. Apostol, L. E. Abramiuc, L. C. Tănase, D. G. Popescu, M. A. Huşanu, G. A. Lungu, I. C. Bucur, R. M. Costescu, A. E. Bocîrnea, C. A. Tache, C. Chirilă, L. Hrib, L. Trupină, L. Pintilie, C. M. Teodorescu,** S. Lizzit, P. Lacovig, and A. Barinov
Photoelectron spectroscopic and microspectroscopic probes of ferroelectrics
TIM 17 Physics Conference, West University, Timişoara, Romania
May 25th–27th, 2017 – **Invited**

06. **C. M. Teodorescu, N. G. Apostol, L. E. Abramiuc, L. C. Tănase, D. G. Popescu, M. A. Huşanu, G. A. Lungu, I. C. Bucur, R. M. Costescu, A. E. Bocîrnea, C. A. Tache, C. Chirilă, L. Hrib, L. Trupină, L. Pintilie,** S. Lizzit, P. Lacovig, and A. Barinov
In situ chemistry at ferroelectric surfaces
2nd International Workshop on Materials Physics: Materials Science using Synchrotron Radiation, National Institute of Materials Physics Măgurele, Romania
May 16th–17th, 2017 – **Invited**

07. **N. G. Apostol, G. A. Lungu, I. C. Bucur, C. A. Tache, L. Hrib, L. Pintilie, and C. M. Teodorescu**
Graphene layers grown on lead zirconium titanate
"Nanostructured materials and their role in the pharmaceutical and medical field" Workshop NIMP Măgurele, Romania
29.09.2017 – **Invited**

08. **T. Stoica, I. Stavarache, A. Slav, A.-M. Lepadatu, M. Stoica,** D. Buca
Two-dimensional MoS_2: growth control of large area and heterostructures,
B. Kardynal, ROCAM 2017, Bucharest, Romania
11-14th of July 2017 – **Invited**

09. **A. Velea**
Chalcogenide materials for selectors and phase change memories.
8th International Conference on Amorphous and Nanostructured Chalcogenides - Fundamentals and Applications
July 2 – 5, 2017, Sinaia, Romania – **Invited**

10. **C. Ghica**
Introduction to Electron Microscopy, CERIC Satellite
Event at the NESY Winterschool 2017, Altaussee, Austria
06.03.2017 – **Invited**

11. **C. Ghica**
Atomic scale resolved processes in strained epitaxial layers
4th User Meeting of ARM Owner Group, Rouen, Franta
20-21.06.2017 – **Invited**

12. **C. Ghica**
Advanced electron microscopy for advanced materials,
9th International Conference on Advanced Materials, ROCAM 2017, Bucharest, Romania
11-14.07.2017 – **Invited**

13. **A. Crisan**
Vortex Matter in the Isovalent Optimally Doped Pnictide Superconductor BaFe2(As0.68P0.32)2
13th Workshop on Magnetism and Superconductivity at nanoscale, Spania, Coma-Ruga
1-7th of July 2017 – **Invited**

14. **A.Crisan, I. Ivan, L. Miu**
Pinning potential in YBa2Cu3O7 superconducting films with correlated and synergetic pinning centres
10-th Int. Conf. (Jub.) Vortex Matter in Nanostructured Superconductors, Kalithea, Rodos, Greece
9-15th of September 2017 – **Invited**

15. **V. Kuncser, A.E. Stanciu, A. Kuncser, A. Catrina, A. Leca and G. Schinteie**
Tuning magnetism and magneto-transport by cluster organization in Fe based nano-globular thin filmsSeminar at
MECAME 2017 Ierusalim
June 2017 – **Invited**

16. **V. Kuncser, G.Schinteie, F.Tolea, A. Kuncser, N.Grecu**, S.Constantinescu, **S.Nistor, L.Nistor**
Mössbauer Spectroscopy and New Magnetic Aspects Revealed in Diluted Magnetic Systems
ICAME 2017 Saint Petersburg
September 2017 – **Invited**

APPLIED RESEARCH

SELECTED RESULTS

Study of the growth mechanism of Ni thin films on Ge(001)

A.E. Bocirnea, R.M. Costescu, L.C. Tănase, I. Pasuk, G.A. Lungu, N.G. Apostol, C.M. Teodorescu
National Institute of Materials Physics

Among metal-semiconductor interfaces, Ni-Ge has been one of the more intensely studied, as nickel (a natural ferromagnet with great potential for spintronics applications) and germanium, a cheaper semiconductor with a direct band gap and better charge mobility than silicon, form compounds with interesting electrical properties for microelectronics applications such as high velocity electron injection MOSFETs [1-5]. Further, Ni-Ge contacts can be useful for applications such as Schottky source/drain transistors (SSDT) [5] and thin film transistors (TFTs). In spite of the extensive existing work on Ni-Ge compounds, however, the growth mechanism of Ni on Ge and the formation of the different compounds based on given conditions remains controversial. At the same time, the magnetic properties of this system have been little investigated so far, and the only compounds determined to be ferromagnetic are Ni_3Ge at RT [6] and Ni_5Ge_3 and NiGe ocurring together for a 100 °C growth followed by 150-190 °C treatments, with Ni_5Ge_3 determined to be ferromagnetic but no conclusions about the magnetic character of NiGe. [7]

In the work presented here we investigated low temperature Ni-Ge compounds in Ni grown by molecular beam epitaxy (MBE) on Ge(001) substrates heated to different temperatures up to 400 °C, as well as the study of the interface and bandbending effects in Ge for Ni thin films grown on the substrate sequentially at RT, taking advantage of X-ray photoelectron spectroscopy (XPS) as a very sensitive ultrahigh vacuum technique to characterize the interface and study interface phenomena [8, 9]. All the samples were characterized by using XPS and magneto-optic Kerr effect (MOKE), as well as low energy electron diffraction(LEED).

Difraction patterns characteristic to Ge(001) show in LEED images even after the deposition of Ni on 300 and 400 °C substrates, showing that the Ge matrix is almost intact after the deposition at higher temperatures [8]. On the other hand, XPS results show Ge signal is still strong for all the samples after the deposition of Ni layers with nominal thicknesses of 20 nm, while Ge binding energies (BE) do not change significantly for Ge in the Ni/Ge samples compared to the clean Ge substrate (Table 1). Thus, both XPS and LEED show us that the diffusion in the Ge lattice is strong, and for the deposition Ni on heated Ge(001).

	Clean Ge	Ni/Ge(001) at RT	Ni/Ge(001) at 100 °C	Ni/Ge(001) at 200 °C	Ni/Ge(001) at 300 °C	Ni/Ge(001) at 400 °C
Ni BE (eV)	-	852.7	853.1	853.8	853.6	853.5
Ge BE (eV)	1216.9	-	1217.5	1217.6	1217.7	1217.5
Ni (%)	-	100%	55.2%	39.7%	22.8%	30.5%

Table. 1 XPS results for the binding energies of Ge and Ni main components, as well as the concentration of Ni in XPS. The binding energies and the concentrations of Ni are obtained from deconvolutions of the XPS spectra [10].

Further, we characterized the composition of the samples with XRD (X-ray diffraction) and XRR (X-ray reflectometry) for information on the evolution of intermetallic compounds and the interface between the substrate and nickel. Figure 1 shows the samples obtained on 100 and 200 °C substrates contain orthorombic NiGe, while for higher temperatures, the compound coexists with Ni-rich orthorombic Ni_2Ge and hexagonal Ni_5Ge_2.

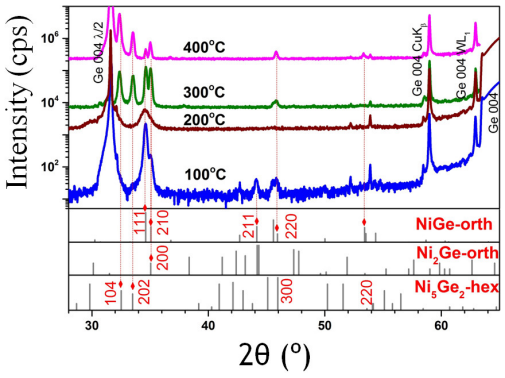

Fig. 1 The XRD diagrams of the samples in log scale. Adapted from [8].

The composition of the samples on higher temperature substrates differs quantitatively: in the 400°C sample Ni5Ge2 is dominant, while the 300°C sample contains equal quantities of all compounds. Because the 400°C sample opens a hysteresis loop, while the other ones do not present magnetic behavior, we can attribute the room temperature ferromagnetism to Ni5Ge2, and we can conclude that neither orthorhombic NiGe nor orthorhombic Ni2Ge show any magnetic behavior at RT [8].

The Schottky barrier height (SBH) at the interface between Ni and Ge has only been studied by using electric measurements [11–13], and the results are similar for Ni/Ge and NiGe/Ge interfaces. By investigating the interface using XPS, we demonstrate the NiGe compound instantenously forms at the interface [9].

Figure 2 is the direct representation of the interface: by gradually depositing Ni over the RT substrate, and acquiring XPS measurements of the core level electrons, we can determine the band bending at the interface.

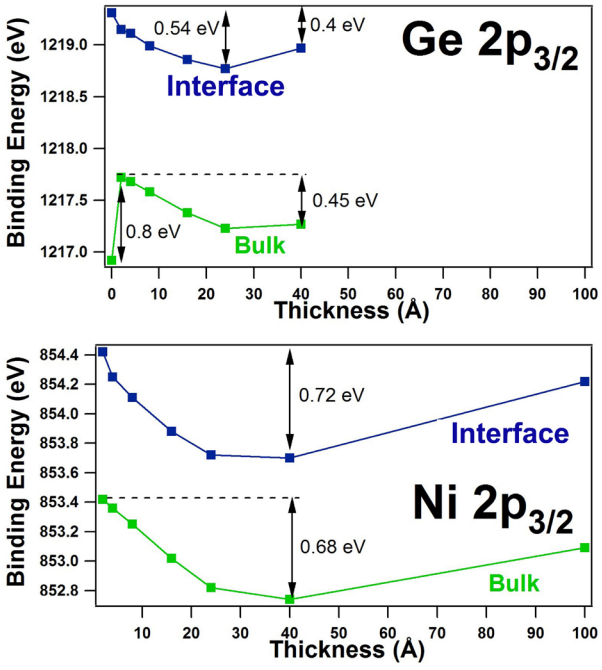

Fig. 2 Evolution of the Ni and Ge 2p binding energies as a function Ni thin layer thickness. Adapted from [9].

As seen in the above figure, Ni electrons are also affected by the deposition, leading us to the conclusion that an interface compound is formed at the interface starting with the very first Ni monolayer.

The 1217.7 eV energy of the Ge 2p electrons after the deposition of the first Ni layer is consistent with the energy determined for the sample on the 100 °C substrate, which only consists of NiGe/Ge (Figure 1). We can conclude that NiGe forms instantaneously at the interface, even for RT depositions.

This work was funded by the Romanian Ministry of Research and Innovation through Core Programme 2016-2017 Contract No. PN16-480101 and CNCS – UEFISCDI Project PN-II-RU-TE-2014-4-1384.

References

1. A. Nash, P. Nash, Bull. Alloy Phase Diag. 8, 255-264 (1987).

2. M. Koike, Y. Kamimuta, T. Tezuka, Appl. Phys. Lett. 102, 032108 (1-4) (2013).

3. Y. Deng, O. Nakatsuka, J. Yokoi, N. Taoka, S. Zaima, Thin Solid Films 557, 84–89 (2014).

4.S. M. Sze, Physics of Semiconductor Devices, 2nd ed., Wiley-Interscience, New York (1981).

5.C.M. Ransom, T.N. Jackson, J.F. DeGelormo, IEEE Trans. Electron Devices 38, 2695 (1991).

6.I.S. Edelman, D.A. Velikanov, A.V. Chernichenko, D.A. Marushchenko, E.V. Eremin, I.A. Turpanov, G.V. Bondarenko, Yu.E. Greben'kova, G.S. Patrin, Physica E 42, 2301–2306 (2010).

7. I.S. Edelman, G.S. Patrin, D.A. Velikanov, A.V. Chernichenko, I.A. Turpanov, G.V. Bondarenko, JETP Lett. 87, 262–265 (2008).

8. A.E. Bocirnea, R.M. Costescu, I. Pasuk, G.A. Lungu, C.M. Teodorescu, Applied Surface Science 424, 337-344 (2017).

9. A.E. Bocîrnea, L.C. Tănase, R.M. Costescu, N.G. Apostol, C.M. Teodorescu, Applied Surface Science 424, 269-274 (2017).

10.C.M. Teodorescu, J.M. Esteva, R.C. Karnatac, A. El Afif, Nucl. Instrum. Methods Phys. Res., Sect. A 345, 141-147 (1994).

11. A. Chawanda, C. Nyamhere, F. D. Auret,W. Mtangi, M. Diale, J. M. Nel,J. Alloys Compd. 492, 649–655 (2010).

12. X. V. Li, M. K. Husain, M. Kiziroglou, C. H. de Groot, Microelectron. Eng. 86, 1599–1602 (2009).

13. M. K. Husain, X. V. Li, C. H. de Groot, Mater. Sci. Semicond. Process. 11, 305–309 (2008).

Ferroelectric multi-layers for multiple states non-volatile memories

A.G Boni, L. D. Filip, C. Chirila, I. Pasuk, R. Negrea, I. Pintilie and L. Pintilie

National Institute of Materials Physics

Nowadays, large amounts of data are being produced and analysed at any given moment, which means that the storage capacity is **the** most important objective for the IT industry. The present trend for higher capacity storage solutions is increasing the density of memory cells which can be done by extreme miniaturization. However, this route presents an important issue for ferroelectric memories due to depolarization effects. A solution to this problem is to increase the number of available memory states.

The objective of the present study was to obtain successive polarization switching in multi-layered structures.

In Fig. 1 the hysteresis loops measured on a tri-layer structure based on PZT/CFO/PZT are presented. For the structure deposited on a SRO bottom electrode a typical hysteresis is obtained for a low amplitude of voltage pulse, however, the remnant polarization is lower than for a typical PZT thin layer of the same composition. By increasing the voltage pulse amplitude to 15 V the saturated polarization loop is obtained, having a remnant polarization around 90 C/cm^2 as for a simple PZT thin film capacitor. The main difference between typical hysteresis and the one for this PZT/CFO/PZT structure deposited on SRO bottom electrode is the step-like switching of polarization for positive voltages which is accompanied by a two switching peak in current-voltage loop. These results suggest a gradual switching of polarization for positive voltages which means that there are 3 stable polarization states in one ferroelectric-based capacitor. This result leads to a 50% increase in the storage capacity.

For the same type of structure but deposited on LSMO bottom electrode, the behaviour disappears at room temperature. These results are attributed to different structural qualities induced by changing the bottom electrode. It was shown in a detailed study [1] that a significant stress gradient for the structure deposited on SRO bottom electrode, can determine a flexoelectric field inside the structure that favours the polarization oriented towards the top electrode and a step-like switching when positive voltage is applied on the top electrode.

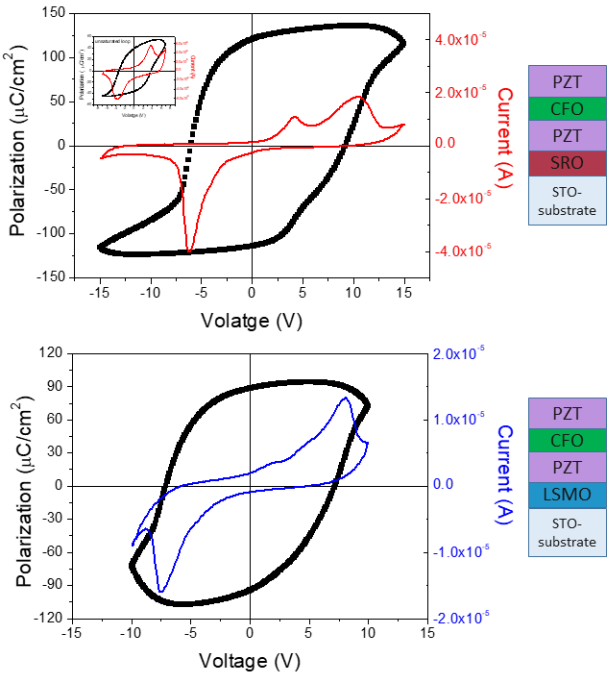

Fig. 1 The high frequency hysteresis loops obtained for PZT/CFO/PZT deposited on a) SRO bottom electrode and b) LSMO bottom electrode. The inset figure represents the unsaturated hysteresis loop for SRO bottom electrode.

In Fig. 2 are represented the hysteresis measurements for a structure of two PZT layers separated by a STO thin interlayer and the hysteresis measurements for a structure of three PZT layers separated by 2 STO interlayers. Four switching peaks can be readily observed for the PZT/STO/PZT structure in the current-voltage loop together with the corresponding step-like increasing of polarization for positive and negative voltages, respectively. This result proves that the memory density can be doubled for a ferroelectric memory cell by constructing symmetrical ferroelectric-insulator-ferroelectric multi-layered structures, in which the polarization has a gradual switching in each ferroelectric layer when the external field is applied. Further, we can

consider that we can obtained 2^n stable states in a similar type of structure, where **n** is the number of ferroelectric layers separated by **n-1** insulating layers. In order to prove this concept, we show the case for a capacitor based on 3 PZT layers separated by 2 STO interlayers. The hysteresis measurement obtained for this structure is presented in Fig.2b). The current-voltage loop shows 6 different switching peaks corresponding to stable polarization states. The remaining two predicted states are accessed by applying a special sequence of voltages as it was evidenced in Ref. [2]. The stability of the different polarization states was also investigated [2].

Using a theoretical model based on the Landau–Ginzburg–Devonshire theory, the existence of 4 different polarization states was demonstrated for the PZT-STO-PZT structure (see Fig. 3). It is also shown how the polarization progresses from one state to the other when an external electric field is applied on the structure [2].

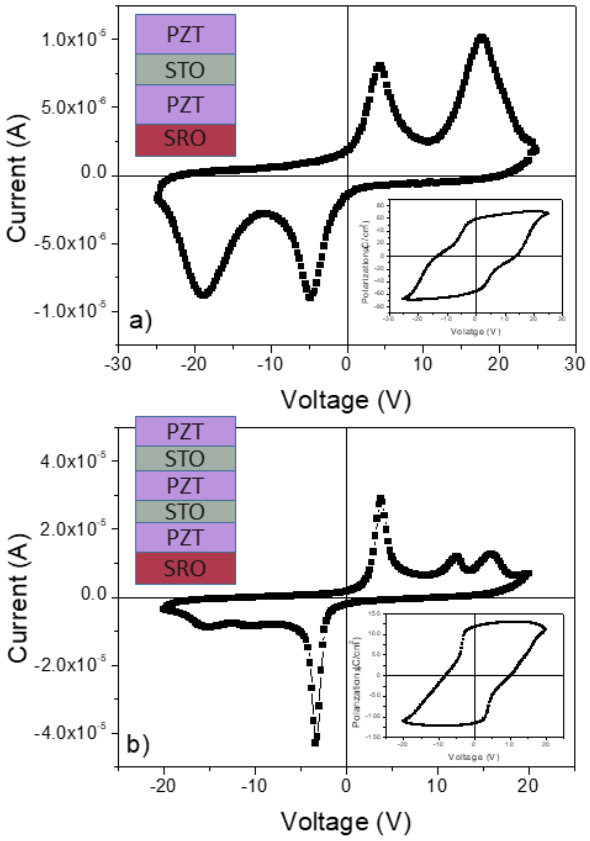

Fig. 2 The current hysteresis loop obtained for a) PZT/STO/PZT and for b) PZT/STO/PZT/STO/PZT. The inset figures presents the polarization loop.

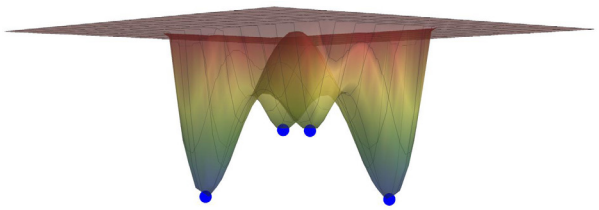

Fig. 3 Prediction of the 4 polarization states deduced using a theoretical model based on the Landau-Ginzburg-Devonshire theory.

The authors acknowledge the Romanian Ministry of Research and Innovation (Core project PNIII-16-48-01).

References

[1] Andra Georgia Boni, Cristina Chirila, Iuliana Pasuk, Raluca Negrea, Ioana Pintilie, and Lucian Pintilie, PHYSICAL REVIEW APPLIED 8, 034035 (2017), DOI: 10.1103/PhysRevApplied.8.034035

[2] Georgia A. Boni, Lucian D. Filip, Cristina Chirila, Iuliana Pasuk, Raluca Negrea, Ioana Pintilie and Lucian Pintilie, Nanoscale 9, 19271–19278 (2017), DOI: 10.1039/c7nr06354g

Transition temperature and giant room temperature magnetoresistance of unrelaxed $La_{.67}Ba_{.33}Ti_{.02}Mn_{.98}O_3$ epilayers grown on 001-oriented $SrTiO_3$

A.C. Galca, A. Leca, C.F. Chirila, I. Pasuk, A. Kuncser, C. Ghica, V. Kuncser
National Institute of Materials Physics
in collaboration with Ma. Oumezzine, Mo. Oumezzine (University of Monastir, Tunisia)

There has been an extensive search for oxide materials exhibiting giant magnetoresistance (GMR). Regarding the mixed-valence manganites $La_{1-x}A_xMnO_3$ (A=Ca, Sr or Ba), with x = 0.3, the both magnetic and electrical transitions from a ferromagnetic metallic state to a paramagnetic state occur around Curie temperature (T_C).

Several manganites possess large room temperature magnetoresistance and considering that the highest GMR occurs at T_C, and correlated with potential room temperature applications, manganites with T_C as close as to room temperature should be envisaged and engineered. $La_{.67}Ba_{0.33}MnO_3$ (LBMO) has a T_C~343K, while the partial substitution of Mn with the not-carrying magnetic moment Ti decreases the transition temperature. One should note that the structural properties of the epilayers are subjected to strain due to lattice mismatch between the 2 materials (substrate and thin film), this aspect contributing also to a variation of T_C.

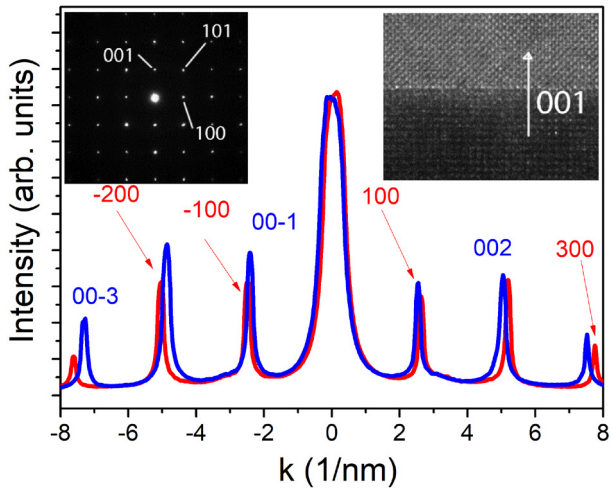

Fig. 1 The line profiles along [100] and [001] of the selected area electron diffraction picture (shown in inset) acquired on LBTMO film. The high resolution transmission electron micrograph of the LBTMO/STO interface is presented in the inset.

The pseudocubic lattice constant of the $La_{.67}Ba_{.33}MnO_3$) is 3.908 Å, mostly being grown epitaxial on the $SrTiO_3$ (STO) 100 surface, due to extremely low lattice mismatch (a_{STO} = 3.905 Å), Doping with Ti doping (2%), the lattice constant of $La_{.67}Ba_{.33}Ti_{.02}Mn_{.98}O_3$ (LBTMO) nanocrystals becomes longer than the one of parent compound. By considering the value of Ti doped sample, 3.912 Å, and the one of STO, the calculated critical thickness (the thickness up to which relaxation does not occur) is above 200 nm.

The films with thicknesses of approximately 100 nm are obtained by ablating a $La_{0.67}Ba_{0.33}Ti_{0.02}Mn_{0.98}O_3$ ceramic target onto STO 100 terraced surface.

There is a structural transformation from the rhombohedral lattice of the target to the cubic/tetragonal one of the film due to the characteristics of the monocrystalline substrate, the out-of-plane lattice parameter (3.928 Å) of the epilayer being larger than the pseudo-cubic one of the material in the powder form, while the in-plane lattice parameter is the same as the one of STO.

The tetragonality of the crystalline structure is sustained by the selected area electron diffraction (SAED) profiles along [100] and [001] directions [Fig. 1], obtained by using a JEM-ARM200F apparatus (the SAED picture being presented in inset of the figure). The other inset is a transmission electron micrograph of a LBTMO/STO area, which confirms the epitaxial growth of the LBTMO film and the smoothness of corresponding interface.

The LBTMO epilayers grown on the STO 100 surface exhibit a relatively sharp para-to ferromagnetic (PM-FM) phase transition [Fig. 2(a)]. The Curie temperature can be estimated as the intersection point of the two tangents to the isofield curve that bounds the transition temperature (T^t_C~295K) [Fig. 2(a)], or as the extreme value found

by representing the temperature dependence of the magnetization derivative (T^d_C~286K) [Fig. 2(b)]. The T_C value is slightly smaller than the 309K one estimated from magnetization of the powdered sample, most probably due to strain effects.

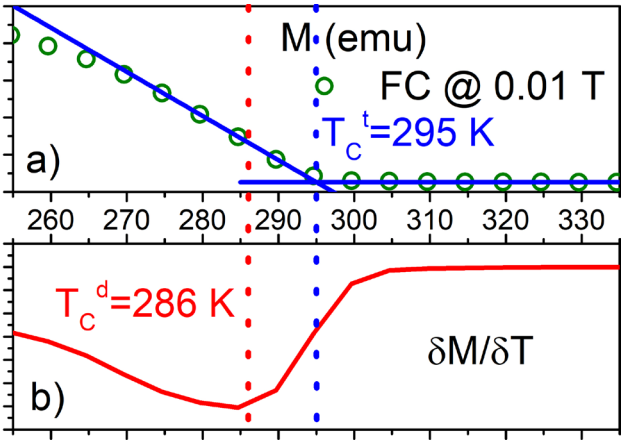

Fig. 2 (a) Magnetization as function of temperature along the in-plane [100] direction (0.01 Tesla field cooling) of the sample. The corresponding T^t_C is marked as the intercept of the straight line with the x-axis and also indicated with a dotted line. (b) The differential magnetization δM/δT representation, where the minimum value is commonly assigned to the Curie temperature, here denoted as T^d_C and marked with a dotted line.

The temperature dependencies of the film resistivity in zero and 5 Tesla external magnetic fields were measured by using a linear geometry, the experimental results being presented in Fig. 3, while the magnetic field is perpendicular to the **ab** plane of the film and consequently to the current direction.

In the external magnetic field, the conductivity increases significantly in the vicinity of T_C, thus the metallic-like character is kept up to the highest achievable temperatures. The external magnetic field assists the hopping of e_g electrons between neighbour Mn ions (from occupied to non-occupied lowest energy states), while a higher temperature increases the relative number of occupied e_g states of lowest energy.

Giant magnetoresistance as high as 60% at room temperature (using the resistance values in a field of 5 Tesla) was recorded for the highly epitaxial $La_{.67}Ba_{.33}Ti_{.02}Mn_{.98}O_3$ thin films grown on the terraced 001 surface of a $SrTiO_3$ monocrystal, being the highest one reported until now on such oxides (extensive care was done for getting the corresponding GMR values at 300K temperature and 5 Tesla magnetic field; and also considering the same equation for deriving the magnetoresistance).

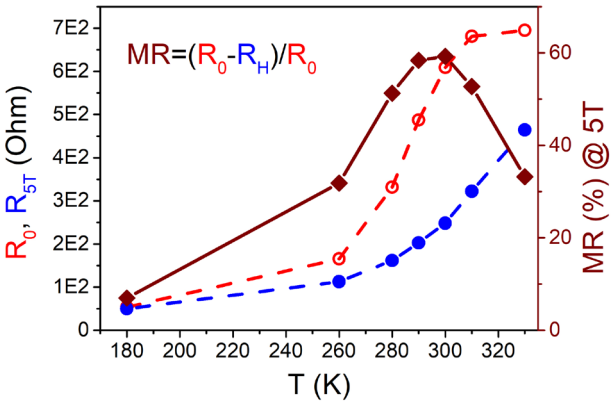

Fig. 3 Recorded resistance at different temperatures under magnetic fields of 0 and 5 T and the calculated magnetoresistance of the 100nm LBTMO thin film.

The authors acknowledge the Romanian Ministry of Research and Innovation (Core project PNIII-16-48-02) and the Tunisian Ministry of Higher Education and Scientific Research for the financial support.

References

[1] Aurelian Catalin Galca, Marwène Oumezzine, Aurel Leca, Cristina Florentina Chirila, Victor Kuncser, Andrei Kuncser, Corneliu Ghica, Iuliana Pasuk, and Mohamed Oumezzine, Applied Physics Letters 111, 182409 (2017), https://doi.org/10.1063/1.4998011

Materials for organic photonics and photovoltaics

A. Stanculescu, O. Rasoga, C. Breazu, E. Matei, N. Preda, C. Florica

National Institute of Materials Physics

in cooperation with
F. Stanculescu, S. Iftimie
University of Bucharest, Faculty of Physics, Magurele, Romania
M. Grigoras, L. Vacareanu
"P. Poni" Institute of Macromolecular Chemistry, Iasi, Romania
G. Socol, G. Popescu-Pelin
National Institute for Laser, Plasma and Radiation Physics, Magurele, Romania
M. Girtan
University of Angers, LPHIA, Angers, France

The great attention paid lately to both thin films and bulk organic materials in order to replace the inorganic ones for photovoltaic (PV) and photonic applications is derived from their properties such as: transparency, compatibility with plastic substrates, high absorption and nonlinear coefficients, cheap technologies, etc. Nonlinear optical (NLO) phenomena in organic molecular crystals, like second harmonic generation (SHG) and two-photon absorption fluorescence emission (TPF), are associated to the extended p-conjugated electronic structures and charge transfer properties. The interest in studying the effect of radiation on the properties of organic crystals is justified by their potential use in detection systems working in hazardous environments. Benzil is specifically attractive because of its behavior similar to the inorganic wide-gap semiconductors and its isomorphism with a-quartz. The effect of irradiation with Ni ions of 11.4 MeV/u at different fluences [1×10^{10} (P1), 5×10^{10} (P2), 10×10^{10} (P3) ions/cm^2] of thick slices (Fig.1) cut from benzil ingot, grown from melt in a modified Bridgman-Stockbarger configuration, has been investigated [1]. We evidenced an increased degree of disorder correlated with an increase in the Urbach energy, when the fluence increases. Small changes appeared in the chemical composition along the track of the Ni ions determined by the disappearance of some deformation vibrations as consequence of the radiation thermal effect or by the synthesis of new species with a triple carbon bond [1]. The morphology (Fig.2a, b) indicated an increase in the roughness and a decrease in the size of the grains by irradiation [1]. Photoluminescence (PL) and non linear optical properties, SHG and TPF, (Fig.2c) are preserved after irradiation [1], this crystal being recommended for space technology photonics.

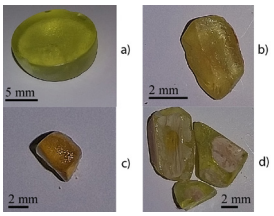

Fig. 1 Typical pictures of: benzil non-irradiated slices (P0) (a); fragments from irradiated benzil: (P1) (b), (P2) (c); (P3) (d) [1].

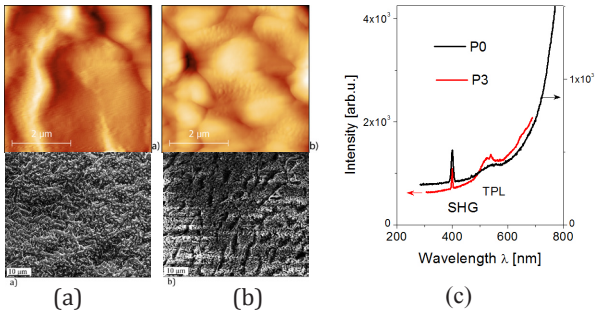

Fig. 2 AFM and SEM images of P0 (a) and P3 (b). SHG/TPF phenomena in P0 and P3 (c) [1].

A way to obtain a good cost/performance ratio for organic solar cell (OSC) can be the identification of new materials for active layer(s) and transparent conductor electrodes (TCE) [2-4]. An improved charge transport, surpassing the effect of the limited donor:acceptor contact, is assured by a mixt active layer. Considering the criterion of a good light absorption, we have selected azomethine oligomers N,N'-bis[(N-hexyl 3-carbazolyl) benzylidene] 2,5-diamino-3,4-dicyanothiophene (LV4/E_g=2.58 eV) and N,N'-bis[(4-diphenylamino) benzylidene] 2,5-diamino-3,4-dicyanothiophene (LV5/E_g= 2.24 eV) characterized by properties similar to vinylene compounds as donor and, a

fullerene derivative [C60]PCB-C4 (C61) with high electron affinity and mobility as acceptor [2]. The effect of donor:acceptor ratio (1:1, 1:2) and solvent (dimethylsulphoxide/DMSO, chloroform/Ch) on the properties of the heterostructures with mixed layers prepared by Matrix Assisted Pulsed Laser Evaporation (MAPLE) at low fluence has been investigated. The layers deposited from Ch are more adequate for PV applications because of the strong emission's quenching at UV-Vis excitation (Fig.3). Its uniform morphology and higher roughness favor an efficient charge carrier generation, transport, collection and the appearance of the photovoltaic effect [2].

The best parameters (FF=0.33; V_{OC}=0.27 (V) [2]) have been shown by the heterostructure glass/ITO/LV5:C61 (1:1) (Fig. 4a).

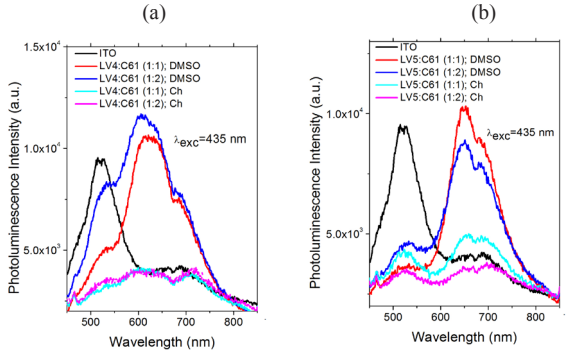

Fig. 3 Mixed layers PL at λ_{exc}=435 nm [2]

We also investigated the effect of (TCE) on the properties of the heterostructures realized in stacked layers or mixed layer configuration [3,4]. Inexpensive and non-toxic (TCE) of ZnO doped with Al (AZO) [3] and In_2O_3 (IZO) [4] have been deposited by Pulsed Laser Deposition on glass or flexible substrate polyethylene terephthalate (PET). The heterostructures realized by MAPLE on glass/AZO with a mixed layer of P3HT:C60 presented photovoltaic properties, the best parameters (V_{OC}=0.72 V, FF=0.32 [3]) being shown by the heterostructure with the largest amount of C60 (Fig.4b) and the best dark current ($5.5x10^{-8}$ A at 1 V) by the heterostructure with a blend ratio of (1:1). The effect of thermal treatment (TA)/oxygen plasma etching (OP) of the IZO layer on the properties of the stacked layers small molecule organic (CuPc/cooper phthalocyanine, PTCDA/3,4,9,10-perylenetetracarboxylic) heterostructures (UN) was also analysed [4].

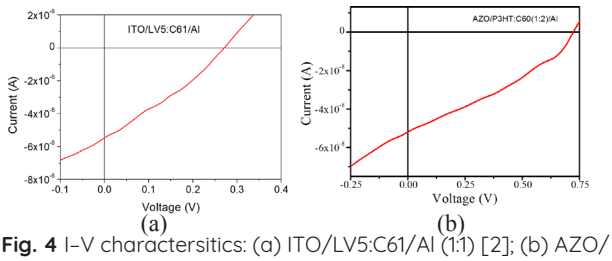

Fig. 4 I–V charactersitics: (a) ITO/LV5:C61/Al (1:1) [2]; (b) AZO/P3HT:C60 (1:2)/Al [3].

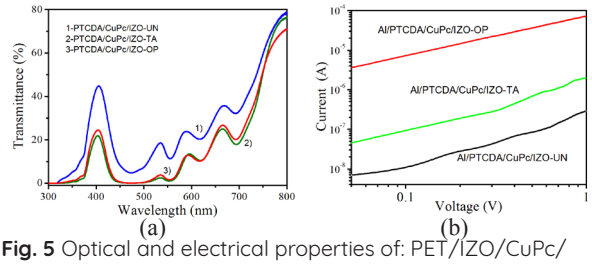

Fig. 5 Optical and electrical properties of: PET/IZO/CuPc/PTCDA [4].

The UV–Vis spectra of the heterostructures obtained by vacuum evaporation on IZO shows many absorption peaks in the visible part of the solar spectrum (Fig.5a). An improvement with more than one order of magnitude in current was evidenced in the heterostructure deposited on PET/IZO treated in oxygen plasma (Fig.5b) [4].

Funding from National Core Founding Program, Contract No: 45N/2009, CEX-05-D11-63, Bilateral cooperation Romania-France project 783/2014, PN-II-PT-PCCA-2013-4-1439, UEFISCDI contracts no 649/2009 and 148/2011, ANCS STARROSA 65/2013.

References

[1] F. Stanculescu, M. Socol, E. Matei, A. Stanculescu, Cryst. Res. Technol. 52, 8, art. no. 1700047 (2017).

[2] A. Stanculescu, O. Rasoga, M. Socol, L. Vacareanu, M. Grigoras, G. Socol, F. Stanculescu, C. Breazu, E. Matei, N. Preda, Appl. Surf. Sci. 417, 183-195 (2017).

[3] M. Socol, N.Preda A. Stanculescu, C. Breazu, C. Florica, F. Stanculescu, S. Iftimie, M. Girtan, G. Popescu-Pelin, G. Socol, Appl. Surf. Sci. 417, 196-203 (2017).

[4] M. Socol, N. Preda, A. Stanculescu, C. Breazu, C. Florica, O. Rasoga, F. Stanculescu, G. Socol, Appl. Phys. A, 123, 5, art. No. 371 (2017).

Sensors based on mesoporous SnO_2-$CuWO_4$ with high selective sensitivity to H_2S at low operating temperature

A. Stănoiu, C.E. Simion, V.S. Teodorescu, M. Florea

National Institute of Materials Physics

in cooperation with

S. Somacescu[1], J.M. Calderon-Moreno[1], P. Osiceanu[1]

[1]"Ilie Murgulescu" Institute of Physical Chemistry, Romanian Academy, Bucharest, Romania

In this report, thick films of mesoporous SnO_2-$CuWO_4$ have been prepared via direct synthesis using tripropylamine (TPA) as template and polyvinylpyrrolidone (PVP) as stabilizer agent [1]. Prior to sensor's fabrication, the obtained powders have been thermally treated at 600 °C (SnWCu600) and 800 °C (SnWCu800) in air for 8h. Further on, the materials were deposited onto Al_2O_3 substrates provided with interdigitated Pt electrodes and heater, via screen-printing technique. The gas sensing performances were acquired through electrical resistance measurements. The measured surface area for SnWCu600 was 5 m^2/g with the average pore diameter of 21.5 nm, whereas SnWCu800 exhibiting a surface area of 4 m^2/g with pore sizes of 27.3 nm due to the structural reorganization and porous structure restructuring. The morphological insights (size and shape) have been highlighted through Scanning Electron Microscopy – SEM (Figure 1).

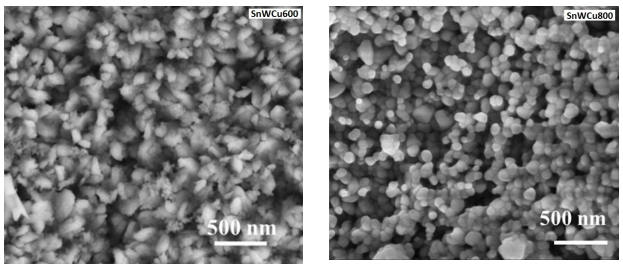

Fig. 1 SEM images of SnO_2-CuWO4 thermally threated at 600 and 800 °C.

and Transmission Electron Microscopy – TEM (Figure 2).

Thus, the SEM measurements revealed the formation of porous 2D flakes. The thermal treatment performed at 800 °C induces a subsequent growth in the crystallite size from 60 to 90 nm.

From the TEM investigation one can see that the sample SnWCu800 shows a degree of agglomeration lower than SnWCu600, effect induced by the calcination temperature.

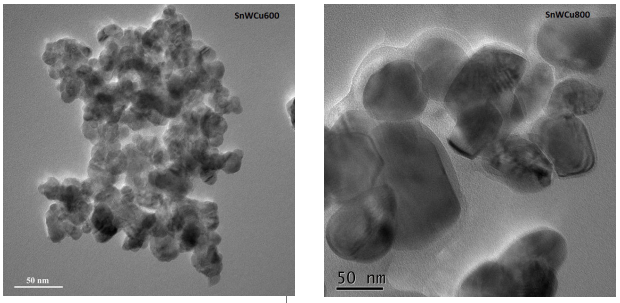

Fig. 2 TEM images of SnO_2-$CuWO_4$ thermally threated at 600 and 800 °C.

From the XPS investigations of the O1s deconvoluted spectra (Figure 3) one can notice a slight decrease in the amount of OH groups and H_2O adsorbed on the surface with increasing temperature.

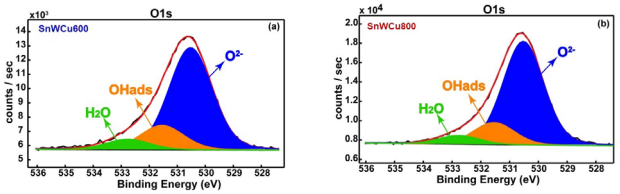

Fig. 3 O1s deconvoluted spectra for SnWCu600 (a) and SnWCu800 (b).

In the case of SnWCu800 can be observed that the amount of the OH adsorbed on the surface decreases from 17.8% to 15.9%, with respect to the operating temperature. Moreover, the adsorbed water on the surface drop from 7.6% in the case of SnWCu600 to 6% for the SnWCu800 sample. The first aim in exploiting the gas sensing performance was oriented towards finding the optimum operating temperature where the maximum sensitivity to H_2S is attained. Therefore, both SnWCu600 and SnWCu800 have been exposed to 20 ppm H_2S in dry air (Figure 4) through a specific

range of temperatures 23÷350 °C and the sensor signal was calculated as: $S=R_{air}/R_{H2S}$.

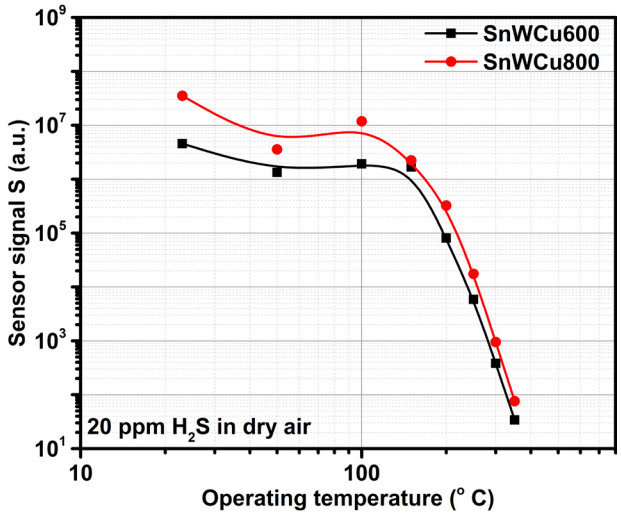

Fig. 4 Sensor signal dependence with respect to the operating temperature in double log. plot.

As can be seen, there is an inflection in the sensor signal response at 150 °C highlighting the existence of different reaction mechanisms with respect to the operating temperature. Accordingly, the following drawings (Figure 5) explain the possible gas interactions at low temperature 23÷150 °C and high temperature 150÷350 °C.

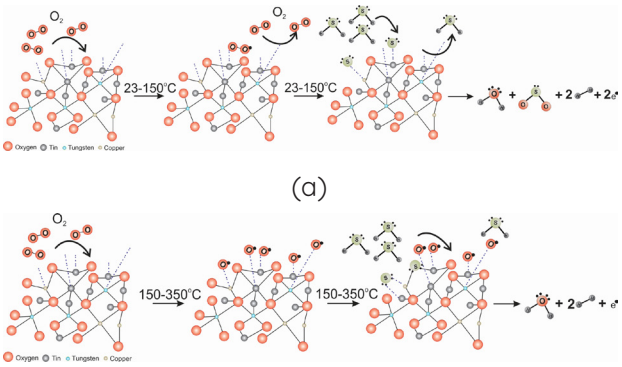

Fig. 5 Representative cartoon of SnWCu materials in interaction with O_2 and H_2S at low (a) and high (b) operating temperatures.

The electrical resistance behaviour of the SnWCu sensitive materials when exposed to different H_2S concentrations at fixed operating temperature of 100 °C were evaluated.

In Figure 6. can be seen the resistance evolution after each gas exposure using a synchronized temperature boost triggering of 500 °C meant to ensure a complete recovery to the base line resistance. The temperature boost is related to a surface cleaning due to the fact that H_2S interaction induced the presence of CuS [2].

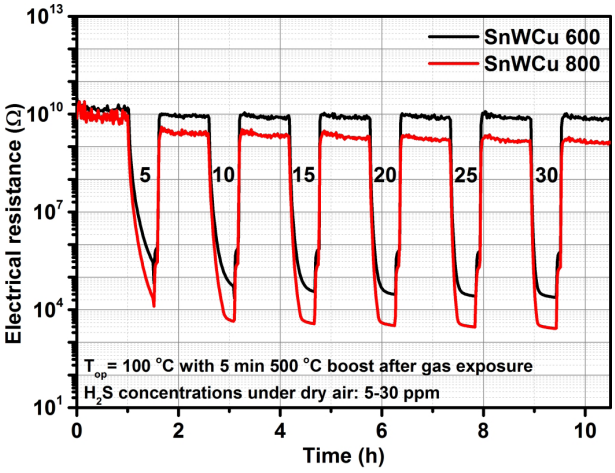

Fig. 6 Dynamic response of the electrical resistance towards different H_2S concentrations.

The average response and recovery times for SnWCu600 are t_{res} = 2.5 min, t_{rec} = 7.3 min and for SnWCu800 are t_{res} = 2.7 min, t_{rec} = 8.3 min. In terms of selectivity, Figure 7 presents the high sensing potential for H_2S compared with different gases.

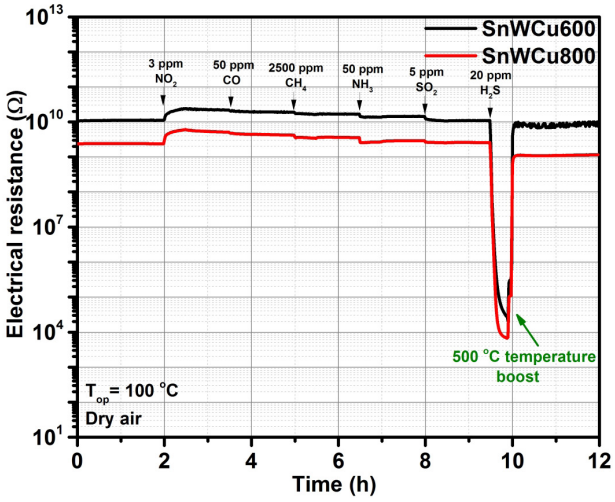

Fig. 7 Dynamic response of the electrical resistance towards different test gases.

We could demonstrate the high selective-sensitivity potential of SnWCu materials towards H_2S detection and the associated gas sensing mechanism.

Funding through the Core Program PN16480102/2016 and PN16480102/2017.

References

[1] A. Stanoiu, C.E. Simion, J.M. Calderon-Moreno, P. Osiceanu, M. Florea, V.S. Teodorescu, S. Somacescu, Journal of Hazardous Materials, 331, 150-160, (2017).

[2] V. Kumar, S. Sen, K. Muthe, N. Gaur, S. Gupta, J. Yakhmi, Sens. Actuators B Chem. 138 (2009) 587-590.

Te-based chalcogenide materials for selector applications

A. Velea

National Institute of Materials Physics

in collaboration with K. Opsomer, W. Devulder, J. Fan, M. Jurczak, B. Govoreanu Imec, Kapeldreef 75, 3001 Heverlee, Belgium

J. Dumortier, C. Detavernier Ghent University, dept. Solid State Sciences, Krijgslaan 281 (S1), 9000 Ghent, Belgium

Emerging resistive switching (RS) non-volatile memory (NVM) technologies, such as resistive random access memory (RRAM) or phase change memory (PCM), are promising candidates for the next generation of advanced data storage applications. Memory devices have to be packed densely in vast cross-bar memory arrays to enable the storage of many terabytes of data. A major bottleneck in the achievement of high density RRAM/PCM arrays is the lack of a high performing selector device, in series with each memory element, that allows for accurate information storage and retrieval by suppressing parasitic currents.

Possible selector implementation are ovonic threshold switches (OTS). OTS is a volatile non-linear electrical characteristic of a two-terminal switching device in amorphous chalcogenide materials. The device can rapidly swap from a high resistive state (HRS) to a low resistive state (LRS) by applying a voltage that exceeds the threshold voltage. This state is maintained as long as a minimum holding voltage is applied to the device, otherwise it switches in HRS. This unique property makes chalcogenide materials convenient for selector applications. An important engineering requirement is that the selector should be able to withstand 400°C for up to 2h, in order to account for the processing needs. In consequence, materials with high crystallization temperatures are necessary.

The goal of this study is to build a map for OTS compounds, test its validity and use the map to predict new materials exhibiting OTS and reliably estimate their thermal stability.

In order to understand the relationship between stoichiometry, structure and physical properties in OTS materials, we compute two bond orbital coordinates, namely hybridization and ionicity for all Te-based OTS compositions that we could find reported in literature (Fig. 1). Additionally, we extend the map with the average number of **p**-electrons (N_p). Surprisingly, OTS materials are clustered in a small area defined by lower ionicity and higher hybridization compared to phase change materials, indicating that they are likely to form more directed covalent bonds that lead to a slower crystallization. The rigidity of the structures is explained by the slight increase in the average number of **p**-electrons, since bonding is primarily promoted by **p**-electrons.

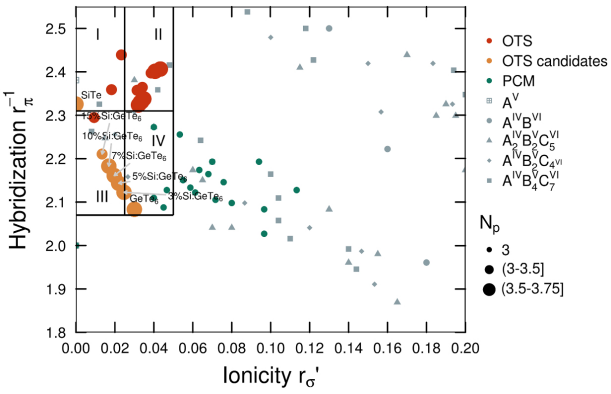

Fig. 1 A map for OTS materials. Areas highlighted in the plot, denoted as I, II, III and IV, are zones with high probability of finding OTS materials.

We subsequently sample several compositions from different zones on the map for OTS materials and test their suitability for selector applications. One example is $GeTe_6$, an eutectic point in the Ge-Te phase diagram reported as a good glass former. Fig. 2 shows a characteristic OTS behaviour, averaged over 100 alternating positive and negative polarity DC sweeps. The maximum current density exceeds 3.3 MA/cm^2 for devices of 55 nm size and the half bias nonlinearity is about 3×10^3. Almost three orders of magnitude contrast between LRS and HRS for a reading voltage 1.4 V, is observed. We have a symmetric behaviour with

similar median values of the threshold voltage for both positive and negative polarities.

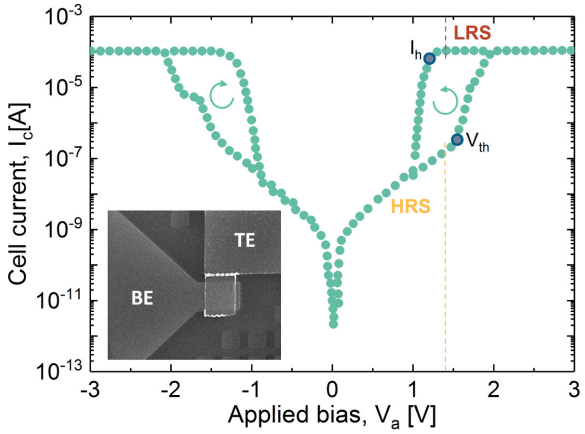

Fig. 2 $GeTe_6$ switching characteristics for a 135 nm device. Average of 100 DC alternate polarity cycles. The inset shows a typical cross-bar device.

To study the thermal stability of $GeTe_6$ we used in-situ X-ray diffraction (IS-XRD) with temperature (Fig. 3). We start with an amorphous film. Te crystallizes first above 200°C, confirmed by the appearance of hexagonal Te (101) and (110) diffraction peaks. It is followed by rhombohedral GeTe crystallization at 300°C ((024) and (220) peaks). A large quantity of Te and GeTe melts just below 400°C as suggested by the disappearance of Te and GeTe crystalline peaks.

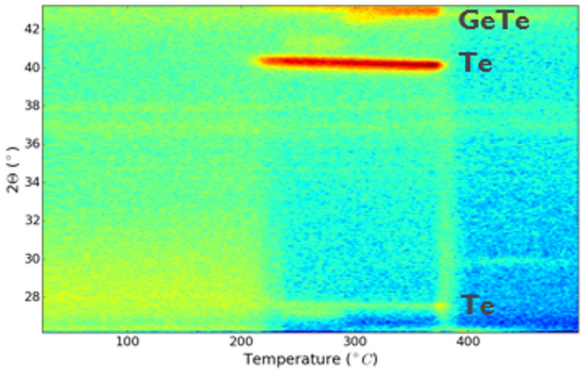

Fig. 3 IS-XRD analysis for $GeTe_6$. Te and GeTe crystalline peaks are observed in red color.

It is difficult to find a binary Te-based chalcogenide material to have the required thermal stability, which could be limited to only several compositions. Therefore, we need to find a way to estimate the thermal stability, especially in ternary compounds. For this, we developed a model which computes the glass transition temperature (T_g) that can be used as the lower limit for crystallization. We compute the thermal stability for possible combinations of $A_xB_{1-x}Te_y$ (Fig. 4). Te concentration was varied between 40 and 85, since no OTS material with less than 40% Te or more than 85% was reported in the literature. **A** and **B** are any of the following elements: Cu, Ag, Au, Zn, B, Al, In, C, Si, Ge, Sn, N, P, As and Sb. In addition to the thermal stability, the bond-orbital coordinates and the average number of **p** electrons are also computed. Only the compositions which are located in the area for OTS materials defined in Fig. 1 and with T_g higher that 400°C are kept. Eye-opening is the fact that materials compositions with a higher thermal stability have a maximum N_p of 3.15. It seems that there is a trade-off between electrical performance and thermal stability.

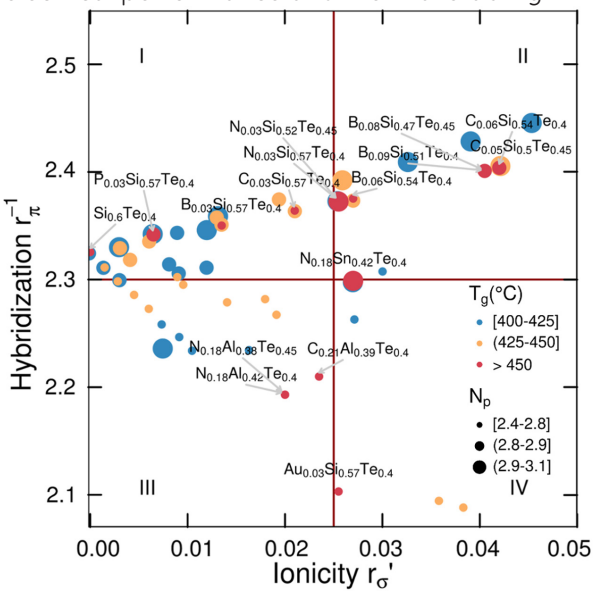

Fig.4 Computed thermal stability of predicted materials exhibiting OTS. Labels are added to the compositions with T_g > 450°C. Point's size is proportional with N_p.

To summarize, we propose a new pathway for OTS materials design and discovery that brings a more systematic search approach based on materials properties. We highlighted promising candidates for thermally stable ternary OTS materials.

Funding from TE 74/2015 (PN-II-RU-TE-2014-4-0498) and imec Core CMOS program on emerging memories.

References

[1] A. Velea, K. Opsomer, W. Devulder, J. Dumortier, J. Fan, C. Detavernier, M. Jurczak, B. Govoreanu „Te-based chalcogenide materials for selector applications", Sci. Rep. 7, 8103 (2017).

Aluminum nitride thin films: assessments on their potential for biomedical application

C. Besleaga, V. Dumitru, L.M. Trinca, A.C. Popa, C.C. Negrila, G.E. Stan
National Institute of Materials Physics
in cooperation with
Łukasz Kołodziejczyk
Institute of Materials Science and Engineering, Lodz University of Technology, 90–924 Lodz, Poland
C.R. Luculescu
National Institute for Lasers, Plasma and Radiation Physics, RO–077125 Magurele, Romania
G.C. Ionescu, R.G. Ripeanu
Petroleum-Gas University of Ploiesti, RO–100680 Ploiesti, Romania
and
A. Vladescu
National Institute for Optoelectronics, RO–077125 Magurele, Romania

The recent advancements in biosensors urges for the entwining of nano- or micro-electronics and biomedicine research fields. Aluminium Nitride (AlN), due to its piezoelectricity, is one of the materials envisaged to serve as multi-functional sensing platform.

But, are the AlN films synthesized by reactive radio-frequency magnetron sputtering (RF-MS) truly compatible with the biosensors market?

RF-MS is a deposition method of choice for many industrial applications dues to its capacity to produce high quality dense, adherent and uniform films on large area substrates. Moreover, using reactive RF-MS technology, one can obtain AlN thin films from a cheap Al target (to the difference of expensive AlN targets), at quite high deposition rates (i.e. ~14 nm/min), which further increases its appeal from economical point of view.

Nonetheless, the ability of reactive RF-MS to produce AlN films at low process temperature (present case ~50 °C), makes it compatible with (flexible) polymeric substrates which typically have softening points situated below 100 °C.

However, reactive RF-MS demands a low base pressure to be achieved in the reaction chamber, which is time consuming, and thus, cost-challenging. Thereby, one way to reduce the fabrication cost of AlN layers would be to use higher base pressures. But, how will this impact the functionality of the AlN films from biomedical point of view? This study aimed to deliver the answers by a thorough scrutinize of four types of AlN sample batches synthesized starting from base pressure levels of ~ 6 x 10^{-3} (S1), ~ 2 x 10^{-3} (S2), ~ 8 x 10^{-4} (S3) and ~ 6 x 10^{-5} (S4). To date, there are only scarce and incomplete assessments of the mechanical, corrosion and cytocompatibility of AlN sputtered thin films. Therefore, a comprehensive evaluation of the physical-chemical and functional (with emphasis on the mechanical, corrosion resistance and cytocompatibility properties) performance of RF-MS AlN films was performed [1], in view of probing their potential suitability for the realization of various type of bio-electronic devices (implantable sensors, included).

Crystalline structure

The rocking curve (RC) is a measure of texturing degree which directly affects the electric properties of AlN layers. Lower RC@002 values (higher crystalline **c**-axis texturing) consequents in superior piezoelectric/pyroelectric properties. Continuous increase of crystallite size/decrease of RC FWHM was recorded with the decrease of base pressure (Fig. 1).

Biocompatibility

At 24h after seeding, for all studied cases (Fig. 2a–c), the fibroblast (Hs27) cells were well-spread, eliciting a normal fusiform polygonal-like aspect, having nuclei without pathological chromatin condensations. Thus, the cell morphology

advocate for the biocompatibility of all AlN films synthesized by reactive RF-MS.

The cell proliferation (MTS–Fig. 2d) and cytotoxicity (LDH–Fig. 2e) assays indicated as well the excellent cytocompatibility of AlN films. In all studied cases (including controls), the number of dead cells was similar (with no significant differences), with the overall cellular mortality situated under 2%.

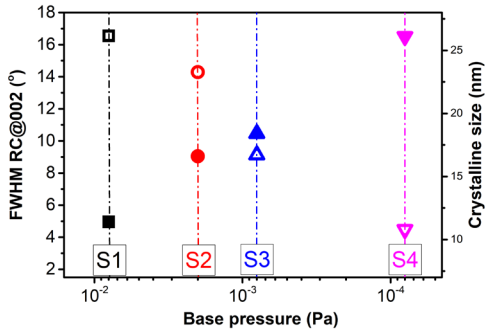

Fig. 1 Evolution of FWHM of RCs (open symbols) crystallite size (solid symbols) determined for the 002 AlN reflections.

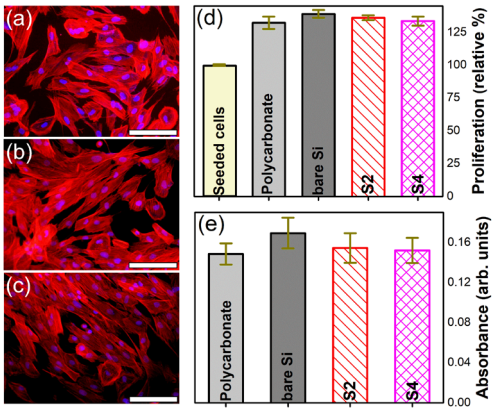

Fig. 2 Epi-fluorescence microscopy images revealing the morphology of Hs27 fibroblast cells grown on: (a) bare Si substrate and (b) S2 and (c) S4 type films. Magnification bar: 50 m. Histograms displaying (d) the cell proliferation results as obtained by the MTS assay and (e) cytotoxicity results as revealed by LDH assay, after 24h of culturing.

Mechanical properties

The pull-out (Fig. 3a) and wear (Fig. 3b) tests revealed remarkable adherence and wear rate values for all AlN films, regardless of texturing degree. Hardness and elastic modulus improved with films crystalline quality [1] up to 26.4±0.8 GPa and 342.3±16.9 GPa, respectively.

Corrosion performance

The corrosion performance of the AlN layers was evaluated according to ISO 16429:2004(E) standard. This type of test is highly relevant in view of developing in vivo sustainable devices. Two testing mediums were used: (i) an isotonic aqueous 0.9% (mass fraction) sodium chloride (NaCl) solution (thus a purely inorganic solution), as recommended by the ISO standard and a (ii) Dulbecco's Modified Eagle's Medium with 10% fetal bovine serum (DMEM-FBS), which better simulates the complex organic-inorganic composition of true intercellular fluid.

The corrosion rate (C_{rr}) results (Table 1) emphasized the superior performance of the well-crystallized and highly c-axis textured AlN films (i.e. 0.13 m/year).

Consequently, although the corrosion products of AlN seem to not deter cytocompatibility, the long-time functionality of implantable AlN-based electronic devices should be questioned. The continuous surface modification of AlN films due to corrosion could negatively influence performance of the device. Thereby, mitigation solutions need to be identified such as to put to good use the noteworthy potential of AlN films to be integrated into implantable devices.

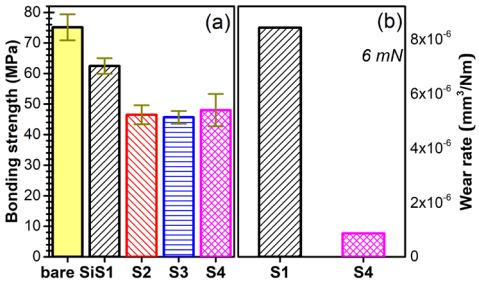

Fig. 3 (a) Pull-out bonding strength values for AlN films with various degree of c-axis texturing. (b) Graphical representation of the wear rate of S1 and S4 films obtained by reciprocal sliding tests carried out at force of 6 mN for 400 cycles.

Table 1. Electrochemical parameters extracted by the corrosion tests.

Sample type	R_P (kΩ)	E_{corr} (mV)	I_{corr} (μA)	C_{rr} (μm/year)
NaCl testing solution				
S2	160.06	-118.70	0.9428	12.93
S4	304.18	-38.60	0.0993	1.36
DMEM-FBS testing solution				
S2	474.08	-34.90	0.4631	6.35
S4	350.06	-110.10	0.0094	0.13

Funding was received from CNCS-UEFISCDI PN-II-RU-TE-2014-4-1122 and PN15/2014.

References

[1] C. Besleaga, et al.; Nanomaterials 7 (2017) 394.

Ceramic composites for biomedical applications

D. Predoi, S. L. Iconaru,
National Institute of Materials Physics
in collaboration with
M.V. Predoi (University Politehnica Bucharest, Romania)
N. Buton (Horiba Jobin Ynove SAS, Paris, France)
A.M. Prodan (Emergency Hospital Floreasca Bucharest, Bucharest, Romania)
A. Deniaud, M. Chevallet and I. Michaud-Soret (CEA, Grenoble, France)
M.E.C. El Kettani and D. Leduc (Université du Havre, Le Havre France)

Lately, it was observed that the incidence of infections associated with prosthetic joints and implant surgeries are increasing. In this context, the development of a new biomaterial with improved antimicrobial activity is an important issue. The most studied materials in the area of biomaterials are the ceramic phosphate ones, mainly hydroxyapatite (HAp). Synthetic HAp is already used on a large scale in bone graft surgeries. Moreover, HAp is frequently used as a coating material for metallic implants due to its remarkable biocompatibility and osteoconductivity. In recent studies, researchers tried to find a solution for enhancing the antimicrobial properties of HAp by incorporating trace elements, such as Zn, Ag, Au, Cu, Ti or Cu into the hydroxyapatite structure. In this context, our studies were focused on the synthesis, characterization and biological properties of hydroxyapatite doped with silver and zinc ions. Furthermore, our research was also focused on obtaining and characterization of biocompatible and antimicrobial coatings of zinc doped hydroxyapatite [1-4]. The zinc and silver doped hydroxyapatite powders (AgHAp and ZnHAp) were synthetized by a modified co-precipitation method. The silver doped hydroxyapatite powders reported in [4] are also prepared in a collagen matrix with different concentrations (AgHApC1 and AgHApC2). The XRD patterns of the Zn:HAp powders with x_{Zn} = 0.01, x_{Zn} = 0.03 and x_{Zn} = 0.05 and the XRD patterns of AgHAp, AgHApC1, and AgHApC2 with x_{Ag}=0.1 are shown in Figure 1. X-ray diffraction results of all Zn:HAp samples (x_{Zn} = 0.01, x_{Zn} = 0.03 and x_{Zn} = 0.05) show only the peaks assigned to the hexagonal $Ca_{10}(PO_4)_{6(}OH)_2$ in $P6_{3/m}$ space group, according to the standard ICDD-PDF No. 9-432 [1, 4].

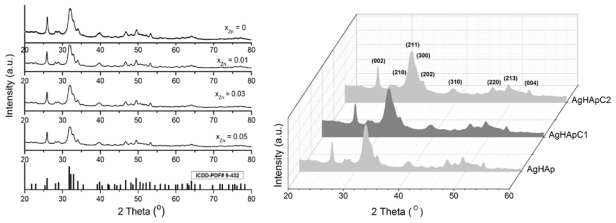

Fig. 1 XRD (X-ray diffraction) patterns of HAp and Zn:HAp, $Ca_{10-x}Zn_x(PO_4)_6(OH)_2$ samples with $0 \le x_{Zn} \le 0.05$ [1] and XRD patterns of the AgHAp, AgHApC1, and AgHApC2 samples [4].

The major characteristic peaks of (002), (210), (211), (300), (202), (310), (222), (213), and (004) were evidenced. As it can be seen, these characteristic peaks occur in all the analysed samples in agreement with the crystalline hydroxyapatite [1,4]. The effect of the synthesized Zn:HAp, $Ca_{10-x}Zn_x(PO_4)_6(OH)_2$ with $0.01 \le x_{Zn} \le 0.05$ against **S. aureus** cell growth at various concentrations from 1.95 to 1000 g/mL are presented in Figure 2 left-A. **S. aureus** cell growth was diminished at concentrations greater than 125 g/mL for the three Zn:HAp tested (Figure 2 left-A). Zn:HAp showed an effect on **Escherichia coli** cell growth only at the very high concentrations (1000 and 500 g/mL). Morphological changes in HepG2 cells after 24h treatment with 62.5, 125 and 500 g/mL Zn:HAp (x_{Zn} = 0.01, x_{Zn} = 0.03 and x_{Zn} = 0.05) are presented in Figure 2-right. The HepG2 cells treated with 62.5 g/mL Zn:HAp (x_{Zn} = 0.01, x_{Zn} = 0.03 and x_{Zn} = 0.05) for 24 h did not show morphological changes.

The texture of Zn:HAp coatings deposited on pure Si and Ti substrate was obtained by performing a 3D surface plot of their SEM images using Image J software. The surface morphologies of the Zn:HAp coatings deposited on a pure Si and Ti substrate were compared by SEM analysis.

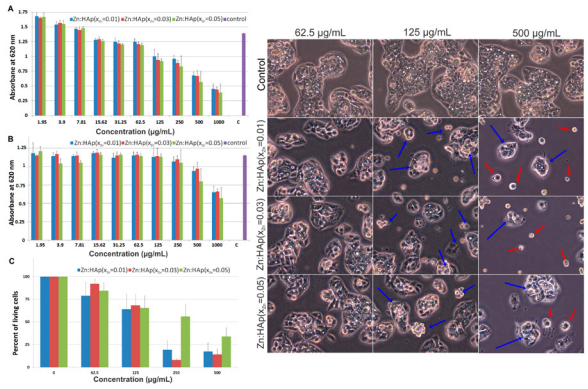

Fig.2 (left) Cell viability assays: (A) S. aureus cell growth (B) E. coli cell (C) HepG2 viability after a 24 h incubation with Zn:Hap; (right) Inverted phase contrast microscopy of HepG2 cells cultivated in the presence of Zn:HAp with xZn = 0.01, xZn = 0.03 and xZn = 0.05 at three different concentrations (62.5, 125 and 500 g/mL) compared to control[2].

A difference in the morphology of the Zn:HAp_Si and Zn:HAp_Ti coatings can be noted (Figure 3), although a dense layer with a homogeneous structure was obtained in both cases. Zn:HAp layer covering the pure Si substrate is uniform while the Zn:HAp layer covering the Ti substrate shows a rougher surface. Bright regions corresponding to the surface of Si or Ti were not observed.

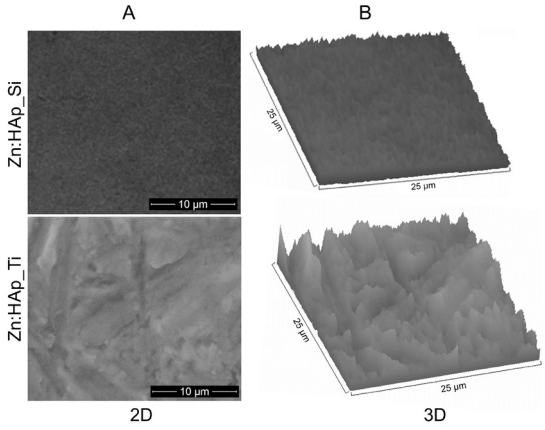

Fig.3 Surface micrographs (A) and 3D surface plots (B) of Zn:HAp_Si and Zn:HAp_Ti coatings [3].

The antifungal activity of new Zn:HAp coatings on substrates of Ti and Si against **C. albicans** was evaluated in different conditions Figure 4 (right). The 3D composite images analysed using Image J software presented in Figure 4 displays the structure and spatial distribution of **C. albicans** surviving cells on different surfaces (HAp_Ti, Zn:HAp_Ti, HAp_Si, Zn:HAp_Si, Ti and Si) kept in the dark and after exposure to day light and UV light. The images exhibited in Figure 4 left reveal the spatial distribution of **C. albicans** surviving cells (red color) along horizontal (coverage) and the vertical (thickness) distributions on Ti, PDMS, HAp-PDMS, Zn:HAp-PDMS and Ag:HAp-PDMS surfaces. The CLSM images presented in Figure 4 demonstrated that the survival of **C. albicans** cells have been significantly reduced in the presence of Zn:HAp_Ti layers (Figure 4 left-I,O) depending on the light. A decrease of **C. albicans** surviving

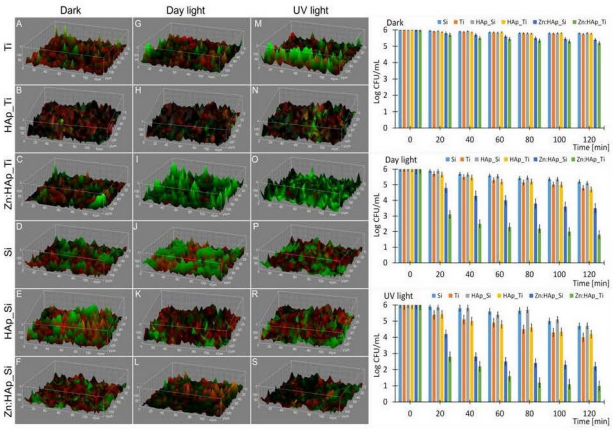

cells depending on the light exposure was also observed in the presence of Zn:HAp_Si layers (Figure 4-left-L,S).

Fig.4 (left) 3D composite images of survival of C. albicans cells on Ti (A, G, M), HAp_Ti (B, H, N) Zn:HAp_Ti (C, I, O), Si (D, J, P), HAp_Si(E, K, R), and Zn:HAp_Si (F, L, S) after exposure to day light, UV light and kept in the dark. Surviving cells appear red; (right) Survival curves of C. albicans on Ti, HAp_Ti, Zn:HAp_Ti, Si, HAp_Si, and Zn:HAp_Si substrate in the dark (A), exposed to day light (B) and UV light (C) [3].

The results of our studies bring new contributions on the biological properties such as antimicrobial activity and cell viability of Zn:HAp an AgHAp biocomposites.

The authors acknowledge the Romanian Ministry of Research and Innovation through the following projects:PN II 259/2014, PN II 131/2014 and PN16480103.

References

[1]. Predoi, D; Iconaru, SL; Deniaud, A; Chevallet, M; Michaud-Soret, I; Buton, N; Prodan, AM. Materials, 10, 229,2017.

[2]. Predoi, D; Predoi, MV; Iconaru, SL; El Kettani, MEC; Leduc, D; Prodan, AM. Materials, 10,681,2017

[3]. Iconaru, SL; Prodan, AM; Buton, N; Predoi, D. Molecules, 22, 604, 2017.

[4]. Predoi, D; Iconaru, SL; Albu, M; Petre, CC; Jiga, G; Polymer Engineering And Science, 57, pp.537-545,2017.

Comparative in vitro behavior of bioglass coatings in simulated body media with improved biomimicry: Challenging a paradigm

A.C. Popa, G.E. Stan, M.A. Husanu, I. Mercioniu

National Institute of Materials Physics

in cooperation with

L.F. Santos

Centro de Química Estrutural, Instituto Superior Técnico (CQE-IST), University of Lisbon, Lisbon, Portugal

and

H.R. Fernandes, J.M.F. Ferreira

Department of Materials and Ceramics Engineering, Centre for Research in Ceramics and Composite Materials (CICECO), University of Aveiro, Aveiro, Portugal

In biomaterials science, the bioactivity concept refers to the capacity of a material to generate the formation of calcium phosphate deposits on its surface in contact with intercellular fluids, as a precursor step towards its osteointegration [1].

In 1990, Tadeshi Kokubo and his collaborators [1] defined a synthetic solution which (fairly) reproduced only the inorganic composition of physiological media (**i.e.**, blood plasma), designated "simulated body fluid" (SBF). Due to the noteworthy simplicity of both the chemical preparation method of SBF and of the **in vitro** testing protocol itself, they were rapidly adopted by the biomaterials scientific community, and thus, used on a wide scale.

However, one should wonder: can the ability of a material to induce the formation on its surface of calcium phosphate-like phases in the Kokubo's SBF solution be regarded as (**i**) a prognosticator of bioactivity, and even more, as (**ii**) a crucial parameter towards defining one material capacity to induce bone-bonding and tissular rehabilitation? This cryptic vision seemed now to have exceeded the status of a blindly accepted paradigm, as criticized by Bohner and Lemaitre [2], and became almost a scientific dogma.

It should be considered that the internal medium itself has a composition radically different from the SBF solution (which is merely a collection of electrolytes). The internal medium contains besides electrolytes, a series of organic moieties: glucose, amino acids, oligopeptides, proteins, vitamins, lactic acids, urea creatinin, metabolic products, lipids, hormones, etc. Moreover, at the implantation site take place complex processes (i.e., bleeding/clotting, inflammation, and tissue repair), and thus one should question: can the intricate and dynamic interaction between tissue, internal medium, and implant be approximated with the simple interaction of a small volume of purely inorganic solution (as SBF) with the implant surface? On the other hand, the internal medium has a steady pH of 7.35 – 7.40, with a partial pressure of CO_2 dissolved in the intercellular medium of ~5 kPa. Nevertheless, the SBF test is performed in most cases in a normal atmosphere. The pH of SBF is known to rise during incubation to values as high as ~9 – 9.5, which uncharacteristically accelerates the nucleation of calcium phosphate layers [2]. It should be stressed that such extreme alkalinization is not naturally achievable in the human body. If the pH rises to such a value in the internal medium, the ionization of the proteins could change along with their functions and cell necrosis could also occur.

These selected criticisms are sufficient to shake the foundations of this cemented way of testing bioactivity (i.e. by the immersion of materials in SBF). However, an uncomplicated, low-cost, yet scientifically more truthful **in vitro** bioactivity assay is still undoubtfully necessary, and would be valuable for the scientific community. The use of synthetic body solution with improved biomimicry would permit not only to infer with a higher degree of certainty the behaviour of a material in a living organism, but also to serve as a dependable selection method for materials, prior to the expensive in vitro tests in cell culture and/or the in vivo tests on an animal model.

With this purpose in our crosshairs, we have comparatively assessed the behavior of bioglass (BG) – the material with the highest bioactive index known today – sputtered films in both SBF (following the Kokubo's protocol), and organic-inorganic solutions (with and without proteins) which mimic the human physiological intercellular medium more closely. The internal medium is best simulated by the complex organic-inorganic solutions (e.g. Dulbecco's Modified Eagle Medium, DMEM) used for the in vitro culturing of cells. DMEM mimics quasi-perfectly the composition of the intercellular fluid, and when completed with the proteins found in human plasma, it allows the harmonious in vitro growth of cells. Thereby, DMEM medium was considered the appropriate choice for simulating in vivo conditions.

The morphological (SEM), compositional (EDS) and structural (FTIR, Raman and GIXRD) investigation, presented in Ref. [3] indicated altogether that the presence of amino acids and/or proteins in the in vitro testing media consequents in a latency of the biomineralization processes. After the 28 days of immersion the calcium phosphate deposits are in an incipient structuring stage only. Conversely, in the case of the SBF tests, the same incubation period allowed for the growth of a thick, rough, and fairly crystallized hydroxyapatite layer [3].

A first explanation lies in the lower pH values attained by the DMEM solutions with respect to the SBF. In the case of SBF tests performed in normal atmosphere, the solution reached pH values of 9 – 9.5. A pH in the range of 8 – 10 is known to be favorable for the nucleation of hydroxyapatite [1,2]. Nevertheless, such high pH values are harmful for the biological equilibrium. Thereby, assessing the biological potential of a material by immersing it in SBF in normal atmosphere is not a reliable test, because it is not replicating faithfully the in vivo conditions. The simple cell culturing medium performed comparable to SBF in a normal atmosphere, slowly turning to an alkaline-like environment after 28 days, with a pH value of ~9. The supplemented cell culturing medium kept in the incubator in homeostatic conditions maintained throughout the assay a constant pH value of ~7.3, similar to the physiological one.

Secondly, the presence of amino acids and other serum proteins could induce the formation of a protective layer by adsorption processes of such organic moieties on the BG surface. Such a shielding layer could play an important role on the hindrance of the bioactivity processes, by halting an earlier dissolution of the BG into the testing medium, and thus consequently partially or even totally impede the ion exchange processes that govern the biomineralization mechanism. The formation of organic protective layers by adsorption processes of amino acids and/or serum proteins on the BG films surface was confirmed by XPS and surface-enhanced laser desorption/ionization time-of-flight mass spectroscopy analyses (see Ref. [3]).

Our results [3] suggest that for a more suitable and truthful in vitro assessment of the biomineralization capacity of given bioactive material, DMEM-like media supplemental with proteins under correct homeostatic conditions should be used. The classical bioactivity tests in SBF, can often force the biomineralization sequence by abnormally increasing the pH value. Furthermore, as the SBF solution is already supersaturated with respect to the components of hydroxyapatite, even a feeble variation of the Ca^{2+} and $(PO_4)^{3-}$ concentration in the solution could determine spontaneous precipitations of calcium phosphates on the surface of the tested samples.

In our opinion, there is an acute need for the scientific community to acknowledge that SBF testing has limitations and advance an improved protocol for bioactivity investigation, after rigorous and extensive research/consensus. Performing the bioactivity tests in biomimetic media could constitute one solution to eradicate false positive events, thus allow to screen with a higher degree of certainty for the bioactive the materials capable to impact positively the biomedicine realm.

References

[1] T. Kokubo, et al.; J Biomed Mater Res. 24 (1990) 721–734.

[2] M. Bohner, J. Lemaitre; Biomaterials 30 (2009) 2175–2179.

[3] A.C. Popa, G.E. Stan, et al.; Int. J. Nanomed. 12 (2017) 683–707.

Wool fabrics covered with semiconductor oxide nanoparticles: Wettability behavior and Photocatalytic activity

L. Frunza, I. Zgura, C.P. Ganea, S. Frunza, M. Birzu, V. F. Cotorobai, M. Enculescu, N. Preda, L. Diamandescu, C. Negrila
National Institute of Materials Physics

Wool is known as a natural fiber that is used largely for clothing but also at home. Among the natural textile fibers, wool has a complicated structure. On the outside of the wool fiber there is a layer called cuticle, where the cells overlap as the plates on the roof. The scales have a waxy coating which stops the penetration of water [1], in this way wool is waterproof in its original form. The inner filaments are surrounded by a protein matrix with high sulfur content, making wool absorbents (for water and dyes). The semiconductor oxide deposition improves the features of the textile and one might find different applications (for example the combination of ZnO and textile can be used effectively for energy harvesting applications [2]) and the use of textile fabric can pave the way for cheap, foldable, wearable, washable and environment friendly nanodevices. Zinc oxide (ZnO) is a known semiconductor which is widely used as a thin or bulk layer due to its remarkable properties, such as high electron mobility, wide band gap, and high luminescence at room temperature but also as photocatalyst. Titanium dioxide (TiO_2) is another widely recognized semiconductor in terms of fundamental research and technological applications based on its UV blocking, antibacterial and photocatalytic activity. TiO_2 or ZnO nanoparticles have been successfully attached to wool [3, 4] in order to obtain hydrophilic properties.

The wetting properties [5] and the photocatalytic activity [6] of knitted Merinos (labeled L1, L18, L19) and indigenous (Țigaie, labeled LVs) wool samples were investigated either in the raw form or after the applied treatments. The samples were initially pretreated by oxygen plasma and then functionalized by deposition with TiO_2 (by sol-gel – SG) or ZnO (by electroless – E or sputtering – SP) nanoparticles. Contact angle values were obtained by sessile drop method using a DSA100 Drop Shape Analysis System from Kruss, at room temperature, Fig. 1. All the samples exhibit hydrophobic properties and even superhydrophobic (water-repelling) ones.

The growth of ZnO or TiO_2 particles takes place on scattered sites as nanoparticles inside the voids of the fabric yarns. The fibers are joined into a structure with a micro- and nano-roughness. In addition, fabrics contain capillaries between, and in, the yarns. Therefore, the surface of the investigated fabrics is far for being flat, really smooth and homogeneous. In this way, the experimentally measured contact angle is in fact an apparent one and can differ considerably from the true (Young) value. The apparent CA values of some raw (original) and deposited samples are given in Table 1.

Table 1 The apparent contact angle (degree)

Sample	Raw	Deposited ZnO(E)	Deposited ZnO(SP)	Deposited TiO_2(SG)
L1	149.3	150.3	151.6	164.8
L18	152.0	137.5	140.7	161.5
L19	149.9	145.3	165.8	147.7
LVs	141.2	137.9	151.6	-

After these treatments, the wetting properties of the analyzed samples were modified, due to additional (hierarchical) roughness introduced by oxide deposition and due to the higher heterogeneity on the fiber surface. CA depends on the size of the mesh fabric/knit, on the considered face and on the finishing treatments applied to the constituent fibers. In the case of textile fibers with small diameter, the surface fiber can dominate most of the interactions.

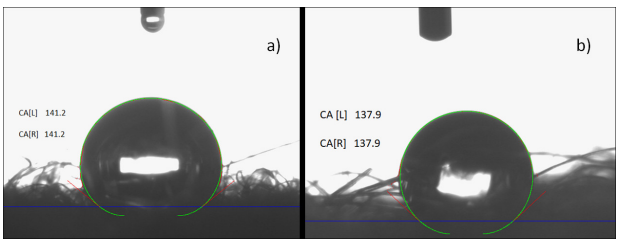

Fig. 1 Contact angle evaluated by sessile drop method on a) LVs; b) ZnO(E)/ LVs [5].

Thus the CA measurements can be used to assess changes in the morphology of the coating, depending on the desired final effect.

The photocatalytic activity of the sample was investigated further [6]. We have found that the photocatalytic activity of the studied fabric-semiconductor oxide systems could be increased as comparing with the activity of the original fabric. We supposed that the increase of this photocatalytic activity can be attributed to the charge transfer from fabric to TiO_2 and to the efficient separation of electron-hole pairs at the fabric-oxide nanoparticle interface. TiO_2 or ZnO nanoparticles deposited upon the fabrics acted as photocatalysts under UV and Vis light to decolorize methylene blue (MB). The time dependence of the MB degradation under irradiation is illustrated in Fig. 2.

To compare the samples behaviour, the efficiency η of the degradation reaction was evaluated with the equation $\eta=C/C_0$, where C_0 is the initial MB concentration and **C** is the concentration of MB at the moment **t**.

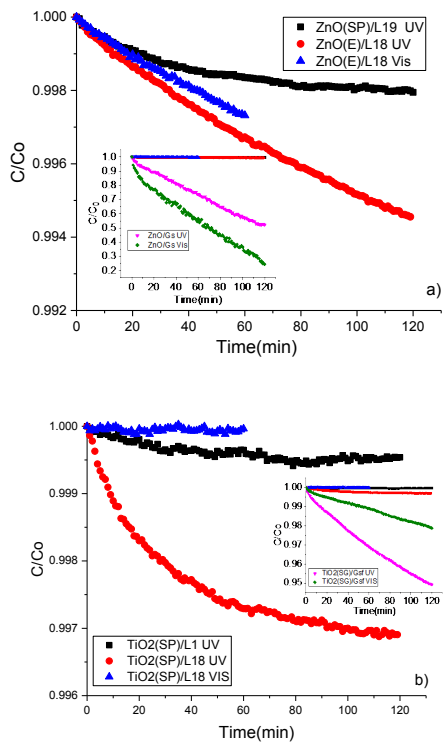

Fig. 2. Efficiency of MB degradation into different samples containing (a) TiO_2 and (b) ZnO catalyst [6].

On a reference glass plate covered with photocatalyst particles, all MB molecules seen by the probe are bonded to the photocatalyst layer so that the time dependence of the MB degradation can be evaluated (see the insertion in fig. 2). On the wool deposited fabric samples, the MB molecules are adsorbed upon the semiconductor oxide particles and upon the uncoated wool surface as well. For our wool samples, the efficiency value is close to 1, indicating that in the cases of less covered wool surface, the most part of MB molecules are bonded to the wool substrate and less to the catalyst nanoparticles. Further, a higher efficiency value means a lesser amount of catalyst particles covering the wool fabric. The values obtained by us (wool samples deposited by TiO2 or ZnO) are smaller than those corresponding to the same oxides as powders or as deposited thick layers.

The MB degradation is increased in the case of the coated fabrics in comparison with the original materials.

The authors thank the Romanian National Research Council for the financial support under the Project ID281.

References

[1] M.T. Huson, D.Evans, J. Church, S. Hutchinson, J. Maxwell, G. Corino, New insights into the nature of the wool fibre surface, J. Struct. Biology, 163 (2008) 127.

[2] A. Khan, M. Hussain, O. Nur, M. Willander Fabrication of zinc oxide nanoneedles on conductive textile for harvesting piezoelectric potential, Chem. Phys. Lett. 612 (2014) 62–67.

[3] E. Pakdel, W.A. Daoud, X. Wang, Self-cleaning and superhydrophilic wool by TiO2/SiO2 nanocompos, Appl. Surf. Sci. 275 (2013) 397.

[4] M. Montazer, M. M. Amiri, R. M. A. Malek, In Situ Synthesis and Characterization of Nano ZnO on Wool: Influence of Nano Photo Reactor on Wool Properties, Photochem. Photobiol. 89 (2013) 1057–1063.

[5] M. Birzu, L. Frunza, I. Zgura, V. F. Cotorobai, C. P. Ganea, N. Preda, M. Enculescu, Wettability by water contact angle upon the surface of wool fabrics covered with oxide nanoparticles, DJNB, 12 (2017) 921 – 931

[6] L Frunza, L Diamandescu, I. Zgura, S. Frunza, CP Ganea, C Negrila, M. Enculescu, M. Birzu, Photocatalytic activity of wool fabrics deposited at low temperature with ZnO or TiO2 nanoparticles: Methylene blue degradation as a test reaction, Catalysis Today, doi:10.1016/j.cattod.2017.02.044, (2017).

Magneto-capacitance in LSMO/PZT/LSMO structures

LM. Hrib, L. Pintilie
National Institute of Materials Physics
in collaboration with
M. Alexe (University of Warwick, Department of Physics, CV4 7AL Coventry, UK)

The magnetocapacitance (MC) effect is the variation of the electrical capacitance in magnetic field. The MC was observed in many compounds and can have different origins such as Maxwell-Wagner effect, magnetoresistance effect [1], [2] or the interaction of the magnetic field with the free charges located at the interfaces (grain boundaries or p-n junctions) [3]. Usually, the measurements are done by sweeping the magnetic field while the electrical capacitance is measured at constant DC and AC voltage. During the last years, this method has been used to study the magnetoelectric coupling (ME) in ferroelectric-ferromagnetic (FE-FM) systems [4] in which the ferroelectric polarization can be controlled via magnetic field and, vice-versa, the spins via electric field. Although the MC method is simple, interpretation of these results as an indication of the presence of ME coupling in the FE-FM structures should be done carefully because they may be affected by artefacts.

In [5] it was studied the MC effect for the $La_{0,7}Sr_{0,3}MnO_3/Pb(Zr_{0,2}Ti_{0,8})O_3/La_{0,7}Sr_{0,3}MnO_3$

(LSMO/PZT/LSMO) heterostructure grown on (100) $SrTiO_3$ monocrystals. The measurements were made by measuring the capacitance-voltage (C-V) curves while applying a DC magnetic field perpendicular to the sample. In this system PZT is the ferroelectric material and LSMO is the ferromagnet which also has metallic conduction and colossal magnetoresistance.

To understand the origin of the observed MC and to rule out the possible contributions from the Maxwell-Wagner and magnetoresistance effects a model was developed. The LSMO/PZT/LSMO structure was modelled as two back-to-back Schottky diodes.

The equivalent circuit (Fig.1(c)) is comprised from a resistance (R_L) corresponding to the LSMO electrodes (which depends on the magnetic field) and two parallel RC circuits: one associated to the interfaces with the electrodes (C_i and R_i) and the other one to the PZT volume (C_p and R_p).

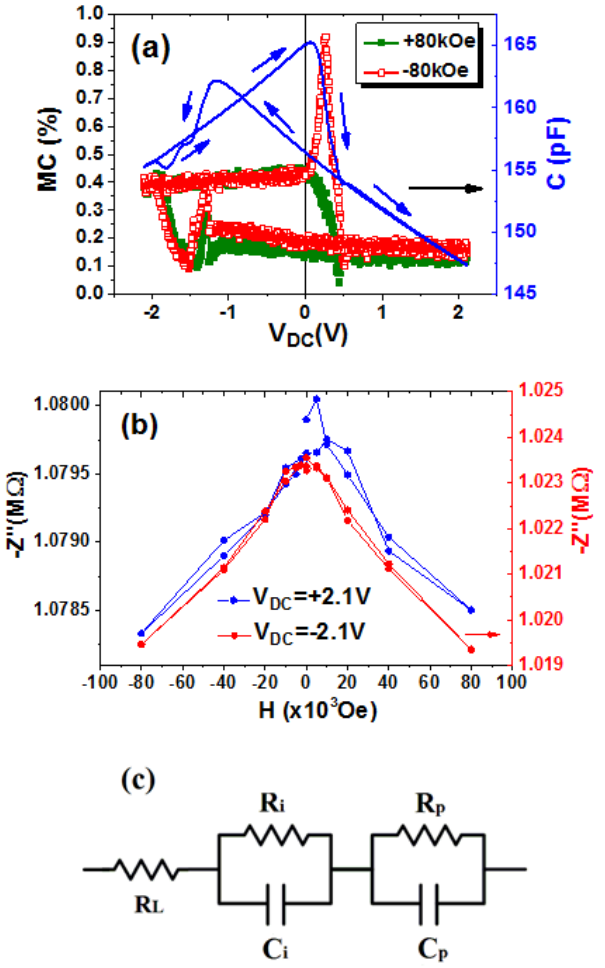

Fig. 1 (a) Magnetocapacitance (MC) as function of the bias voltage. The acquired original data is superimposed (blue line). The blue arrows indicate how the DC voltage is applied; (b) Magnetic field dependence of Z″ at large applied DC voltages; (c) The equivalent circuit used for the simulation of the experimental data.

According to this model, the MC is due only to LSMO magnetoresistance. In this case, only the real part of the dielectric impedance (Z′) would be magnetic field dependent. However experimentally it is observed that both Z′ and Z″ values depend on the magnetic field. This suggests that the LSMO

magnetoresistance has a small contribution to the observed MC and that it is also affected by other phenomena.

Analysing in more detail Z″ it can be observed that at 1kHz, this can be written as:

$$Z'' = \frac{1}{\omega}\left(\frac{1}{C_i} + \frac{1}{C_P}\right)$$

From this formula it results that the only reasonable explanation for the magnetic field dependence of Z″ is the variation with the magnetic field of the interface capacitance C_i.

The specific capacitance of the metal-ferroelectric Schottky barrier is:

$$C = \sqrt{\frac{q\varepsilon_o\varepsilon_{st}n}{2(V + V_{bi}')}}$$

With V_{bi}' being the apparent potential barrier:

$$V_{bi}' = V_{bi} \pm \frac{P}{\varepsilon_o\varepsilon_{st}}\delta$$

From the slope of the $1/C^2$ vs V_{DC} plots represented for different magnetic fields it was determined the magnetic field dependence of density of free charge (**n**) and of the V_{bi}'. From Fig.2(b) it is observed that V_{bi}' values depend on ferroelectric polarization orientation and magnetic field contrary to **n** values.

By calculating MC using **n**, V_{bi}' and the equation for **C** for different magnetic field values it can be observed from Fig.2(a) that a good agreement between the calculated and experimental data was obtained.

This result is an indication of the presence of a genuine ME coupling that is located at the LSMO-PZT interface. This ME coupling is the result of the magnetic field dependence of the apparent built-in potential developed between PZT and LSMO.

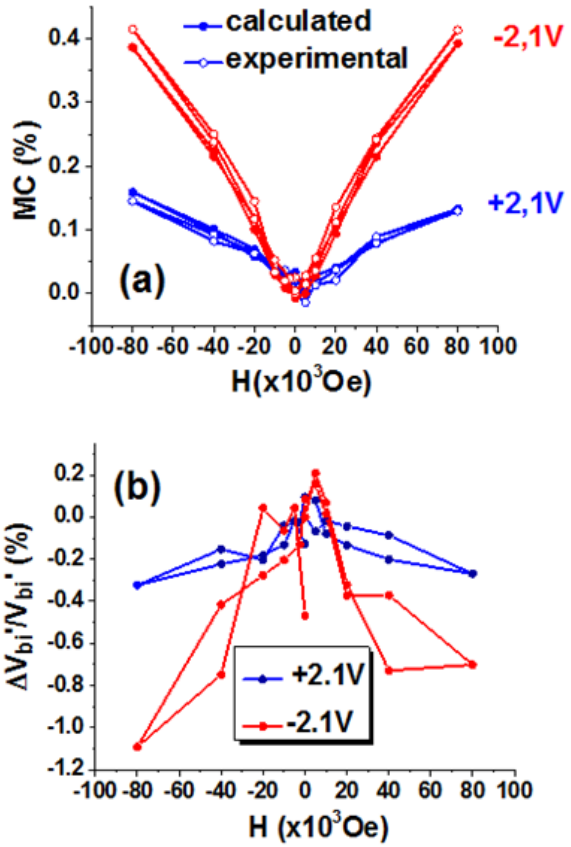

Fig. 2 (a) Comparison between the experimental and calculated MC values; (b) Magnetic field dependence of V_{bi}'.

LMH acknowledges the financial support of STSM Grant from the COST Action MP0904. MA acknowledges the support of Royal Society through Wolfson research Merit Award and EPSRC through grant no. EP/M022706/1. This work was also supported by the Core Program of NIMP (PN09-450102). The authors acknowledge Dr. Daniele Preziosi for performing the magnetoresistance measurements and for valuable discussion.

References

[1] P. Ren, Z. Yang, W. G. Zhu, C. H. A. Huan, L. Wang, J. Appl. Phys. 109, 074109 (2011).

[2] Z. X. Cheng, H. Shen, J. Y. Xu, P. Liu, S. J. Zhang, J. L. Wang, X. L. Wang, S. X. Dou, J. Appl. Phys. 111, 034103 (2012).

[3] M. Maglione, J. Phys.: Condens. Matter 20, 322202, (2008).

[4] T. Kimura, S. Kawamoto, Y. Yamada, M. Azuma, M. Takano, Y. Tokura, Phys Rev B, 67,180401(R) (2003).

[5] L. M. Hrib, L. Pintilie, M. Alexe, Sci Rep-UK, 7, 6563 (2017).

Pyroelectric properties of materials and related phenomena

L.M. Trinca, M. Botea, A.G. Boni, A.C. Galca, I. Pasuk, L. Trupina, I. Pintilie, L. Pintilie
National Institute of Materials Physics

Pyroelectrics are a class of materials with wide applications nowadays, including infrared detectors, thermal imaging or energy harvesting fields. Their operation is based on the pyroelectric effect which implies the temperature variation of the spontaneous polarization. Ferroelectrics have the best performances in terms of pyroelectric response, but there are also other polar non-ferroelectric materials that exhibit such effect.

Zinc oxide (ZnO) display a classic example for a pyroelectric, but non-ferroelectric material. Under certain conditions (doping with lithium, thermal annealing), ZnO might exhibit ferroelectric properties, enhancing the pyroelectric response [1]. In order to analyze the correlation between the potential ferroelectric feature of lithium doped zinc oxide (LZO) and its pyroelectric properties, several ZnO and LZO symmetric capacitors with top and bottom platinum electrodes were fabricated on silicon substrates. In most of the applications, the active element in a pyroelectric device has a capacitor geometry.

The introduction of lithium increases the resistivity of ZnO layers and generates a butterfly shaped capacitance-voltage (C-V) characteristic, indicating ferroelectricity. Surprisingly, undoped zinc oxide also presents butterfly C-V, but it disappears when the measurements are performed with long delay time, thus eliminating the assumption of ferroelectricity in intrinsic ZnO.

Pyroelectric signal was recorded on annealed structures (Fig.1). The pyroelectric measurements were performed with an infrared source (λ=800 nm) coupled with a mechanical chopper having a variable frequency and a lock-in amplifier. The response of the LZO capacitors is with one order of magnitude higher than that of ZnO structures. The frequency dependence of the pyroelectric signal on the two types of structures is also different: quasi-constant in the case of ZnO samples, indicating short values for the electric time constants, and smooth decreasing conduct (vs. increasing modular frequency, ω) in the case of Li doped structures, pointing out large values of the electric time constants. These findings envisage the low resistivity of intrinsic ZnO and increasingly resistivity of LZO with ω. In both cases, the thermal time constant is larger due to the silicon substrate that controls the temperature variation under infrared illumination. At high modulation angular frequency, the pyroelectric response for both type of capacitors is almost comparable, due to fact that the radiation is only absorbed by a very thin layer below the top electrode, whereas the rest of structures remains inactive from pyroelectric point of view.

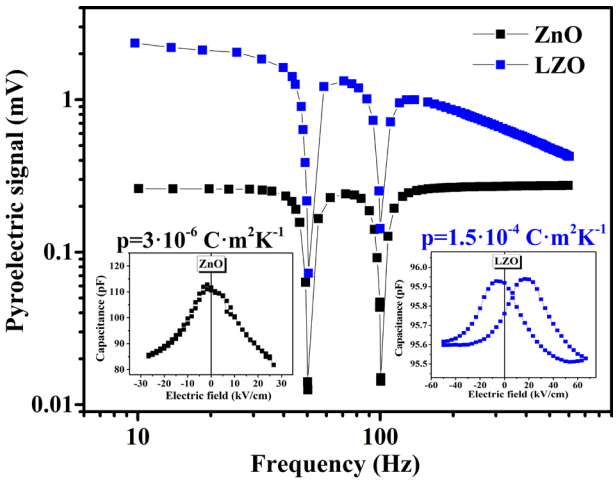

Fig.1 Frequency dependence of pyroelectric signal generated by annealed capacitors based on ZnO and LZO layers. The insets show C-V characteristics of ZnO (left) and LZO (right) based structures, registered after annealing.

The pyroelectric coefficients were estimated from the log – log representations of the pyroelectric signal measured in voltage mode vs. modular frequency of incident radiation (Fig.1), using the procedure presented in [2], for both undoped and Li-doped zinc oxide thin films. The extracted values are ~$3 \cdot 10^{-6}$ $C \cdot m^{-2} \cdot K^{-1}$ in the case of ZnO and ~$1.5 \cdot 10^{-4}$ $C \cdot m^{-2} \cdot K^{-1}$ for LZO. The lithium doping increases the pyroelectric coefficient with almost two orders of magnitude compared to intrinsic material, placing LZO next to classical ferroelectrics. The enhancement of

the pyroelectric response, corroborated with butterfly C-V characteristic, show a behavior resembling ferroelectrics, but it also can only be a pseudo-ferroelectricity explained in the frame of Landau-theory [3]. Regardless the nature of pyroelectricity enhancement, Li-doped ZnO is a performant material that can be easily integrated in pyroelectric detector as active element.

Some of the best alternatives for pyroelectric components are lead zirconate titanate (PZT) solid solutions. Their response in terms of pyroelectric properties depends on a lot of factors: the thickness and thermal properties of the films, the thermal properties of the substrate, domain structure of the layer, orientation of the polarization, the difference between the expansion coefficients of the film and the substrate, etc. By depositing epitaxial PZT films, one can increase the material response.

The evolution of the domain structure was investigated (hence, the pyroelectric performance) when the mechanical constraints are the same, but the resistivity of the substrate differs. In this respect, identical PZT films were epitaxially deposited on 001 $SrTiO_3$ (STO) single crystal buffered with a thin layer of conductive $SrRuO_3$ (SRO), respectively on conductive 001 oriented 0.5% Nb doped $SrTiO_3$ (STON) single crystal. It was found that the domain structure changes when the resistivity of the substrate is different. Also, the self – poling effect occurs disparately.

The pyroelectric response of the PZT/SRO/STO and PZT/STON structures (with different top electrodes – Pt, respectively Au) was assessed in respect with the modular frequency (Fig. 2). The magnitude of the signal is higher for the PZT layer deposited on SRO/STO substrate. The pyroelectric coefficients of both structures were obtained by using the same procedure aforementioned [2]. The determined values are ~$11{\cdot}10^{-4}$ $C{\cdot}m^{-2}{\cdot}K^{-1}$ in the case of PZT grown on SRO/STO and ~$0.09{\cdot}10^{-4}$ $C{\cdot}m^{-2}{\cdot}K^{-1}$ in the case of PZT/STON [4]. The discrepancy is surprising, and it can only be explained by different conditions of compensation for the depolarization fields, taking into account that the substrates have different resistivities. The compensation might be more effective for PZT grown on SRO/STO and only partial in the case of PZT deposited on STON, which leads to a depolarization field inside the ferroelectric layer. This induces different domain structures, as it was determined by PFM, TEM and XRD measurements. The PZT layer grown on SRO/STO show fine grid of 90° domains (**a** domains) and upward oriented spontaneous polarization, whilst PZT on STON show 180° domains (**c** domains) with both upward and downward polarizations. Hence, the substrate resistivity and its ability to compensate the depolarization field seems to be responsible for such a discrepancy of pyroelectric response.

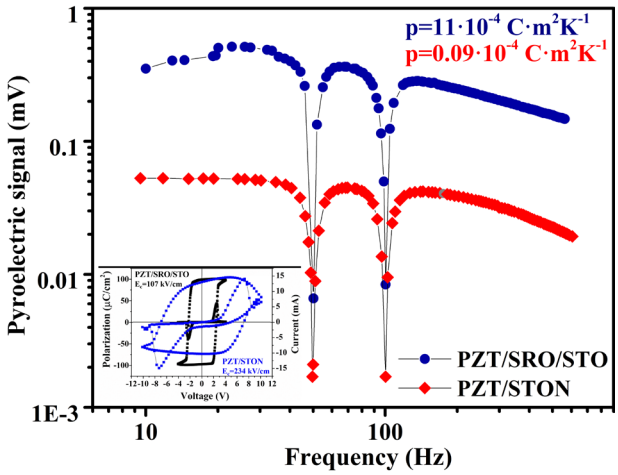

Fig.2 Frequency dependence of pyroelectric signal generated by PZT layers deposited on similar substrates with different resistivity. The inset shows ferroelectric response of both samples, through hysteresis loops.

The authors acknowledge the Romanian Ministry of Research and Innovation (CORE Program project PN16-480102, M-ERA NET project NOPYDET, Partnership project OPTIPYROGRAD).

References

[1] L.M. Trinca, A.C. Galca, A.G. Boni, M. Botea, L. Pintilie, Appl. Surf. Sci. 427, 29–37 (2018).

[2] M.Botea, A.Iuga, L.Pintilie, Appl. Phys.Lett. 103, 232902 (2013).

[3] A.K. Tagantsev, Appl. Phys.Lett. 93, 202905 (2008)

[4] I. Pintilie, L. Trinca, L. Trupina, I. Pasuk, L. Pintilie, Mater. Res. Bull. 93, 201–207 (2017).

High responsive polypyrrole coated microribbons actuator

M. Beregoi, A. Evanghelidis, V.C. Diculescu, I. Enculescu

National Institute of Materials Physics

The development of actuators which could be used in various applications such as artificial muscles, manipulators for micro-objects or cells, and which could also sense the modification of different external stimuli is a challenging task. In this context, polypyrrole (PPy) is an electroactive polymer very used for fabricating soft actuators providing a low operating voltage, fast response time, high displacement etc. As well, electrospinning is a technique suitable to produce reproducible polymer fibers or ribbons (when a precursor polymer solution with a high concentration and a volatile solvent is used).

In this context, PPy coated microribbon nets were fabricated and tested as actuators, following three straightforward steps: electrospinning of a poly(hexamethylene adipamide) (nylon 6,6) solution in preset conditions, the coverage of the polymer networks collected on copper frames with a thin gold layer by sputtering and the electrochemical deposition of PPy from a solution containing pyrrole and $LiClO_4$.

The SEM images of the prepared microribbons taken after successive deposition of gold and PPy are depicted in **Fig. 1a** and **b**, respectively. It can be noticed that the microribbons are partially aligned, and uniformly covered with gold and subsequently with PPy.

The PPy film thickness is about 80 nm, with a smooth surface and continuous along the ribbons. Likewise, the chosen deposition time was short enough to have PPy only on the microstructures (not also between them).

The actuator based on PPy coated microribbons presents good actuation properties in terms of displacement, response time and applied potential when is in contact with an ions source like 1 M NaCl or phosphate buffer saline (PBS) having various pH values or temperatures.

The functionality of such an actuator was demonstrated in two potential applications using 1 M NaCl as electrolyte. In the first case, the actuator can hold a piece of cooper wire (**Fig. 1a**) by keeping the potential at -0.6 V. When the potential is switched to +0.6 V, the actuator releases the object (**Fig. 1b**) due to the deprotonation/protonation processes of PPy which causes the contraction of the system.

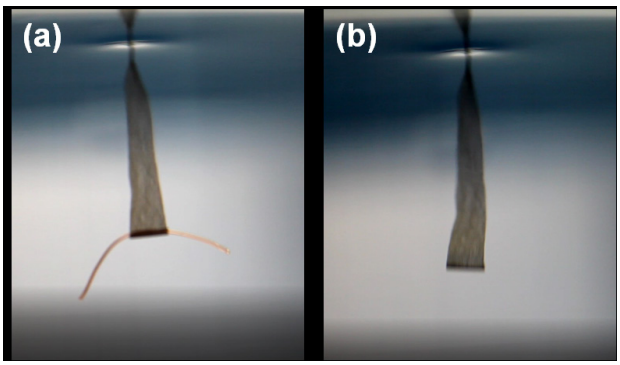

Fig. 2. Snapshots taken when the actuator (a) held a piece of cooper wire maintaining the potential at -0.6 V and (b) released the object by switching the potential at +0.6 V.

In the second case, the actuator can collect polystyrene (PS) microspheres placed on the bottom of the electrochemical cell using a bioadhesive, when the potential is switched between -0.6 and +0.6 V.

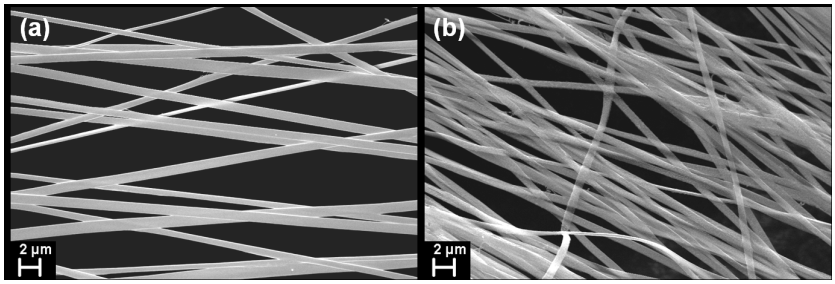

Fig. 1 SEM images of (a) as spun gold covered nylon 6,6 and (b) PPy coated metalized microribbons.

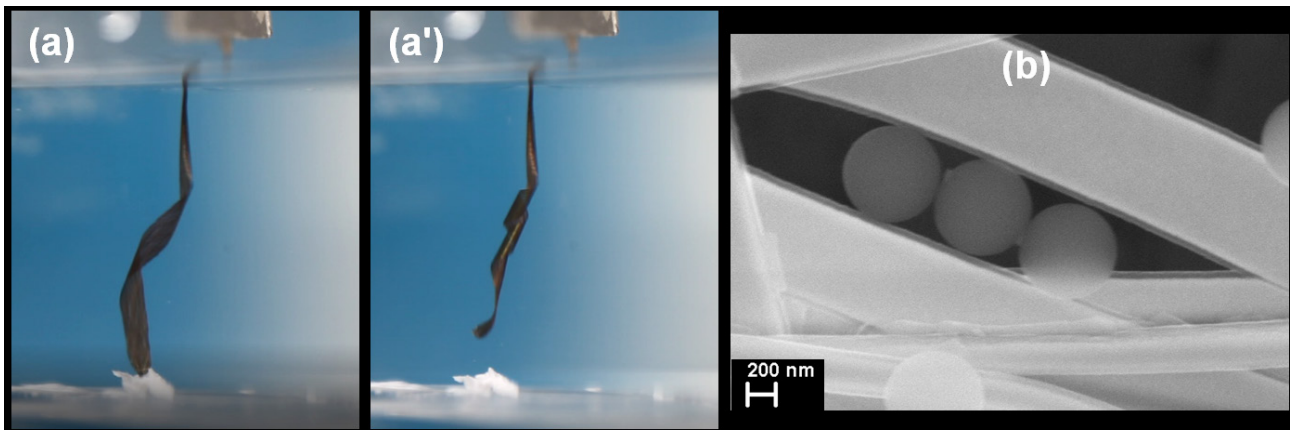

Fig. 3. (a, a') Snapshots taken during collecting PS microspheres placed on the bottom of the electrochemical cell by switching the potential between +0.6 and -0.6 V, in 1 M NaCl; (b) SEM image of the microribbons after collecting process.

Thus, this kind of actuator configuration could be used as a micromanipulator in biomedical applications for harvesting cells of handle low tools.

The research was financially supported by the Core Founding Programs, Romanian Ministry of Research and Innovation, contract no. PN16-480102 and project PED 128/2017.

References

[1] M. Beregoi, A. Evanghelidis, V.C. Diculescu, H. Iovu, I. Enculescu, "Polypyrrole Actuator Based on Electrospun Microribbons", ACS Applied Materials & Interfaces, Vol. 9, 2017, pp. 38068-38075.

Electrochemomechanical artificial muscles based on polyaniline coated microtubes

M. Beregoi, A. Evanghelidis, E. Matei, I. Enculescu

National Institute of Materials Physics

Soft actuators, artificial muscles in particular, represent an important pillar in the tissue engineering field, being used as substitutes when the recovery of injured organ/muscle is impossible to achieve. Thus, conducting polymers (CP) are suitable materials, successfully utilized for developing such devices due to their enhanced actuation properties in terms of applied voltage, response time, displacement, etc. when are compared with other materials types. Polyaniline (PANI) is a well-studied CP, the movement of PANI based structures being initiated by the swelling/shrinking processes as a results of insertion/expulsion of ions into the polymer chains. The electrospinning technique allows the preparation of fibers with similar sizes as muscles fibers, in this way the final devices having a close configuration to natural muscles.

In this context, PANI coated fibers were prepared using three main steps. Firstly, the poly(methyl methacrylate) (PMMA) fibers were prepared by electrospinning a precursor solution, the fiber networks being collected on cooper frames. After that, to have a conductive surface, the fibers were sputter covered with a thin gold layer. In the end, the metalized nets were electrochemically coated with PANI using an aniline and sulfuric acid aqueous solution. The microtubes were obtained by dissolving the PMMA core with a solvent that does not alter the PANI structure. The last step improves the actuation performances of the final device, the fiber templates being removed in order to increase the active surface of the obtained materials for facilitating the ion diffusion.

SEM images of PANI microtubes after PMMA dissolution are presented in **Fig. 1**. It can be noticed that PANI is uniformly deposited on the partially aligned microtubes, the structures being hollow and well separated.

Regarding the actuation properties, a PANI microtubes based actuator was tested using a biocompatible electrolyte, namely simulated gastric fluid (SGF). When the applied potential was -0.2 V, the actuator shrinks due to the expulsion of ions from PANI film, and by switching the potential at +1 V, the actuator returns to the initial position (**Fig. 2**). The stability during many actuation cycles was also analyzed in SGF, by applying -0.2 and +1 V. The actuator is stable over 200 cycles, so it can be noticed from **Fig. 3** that the current presents a slow decrease, followed by a stabilization.

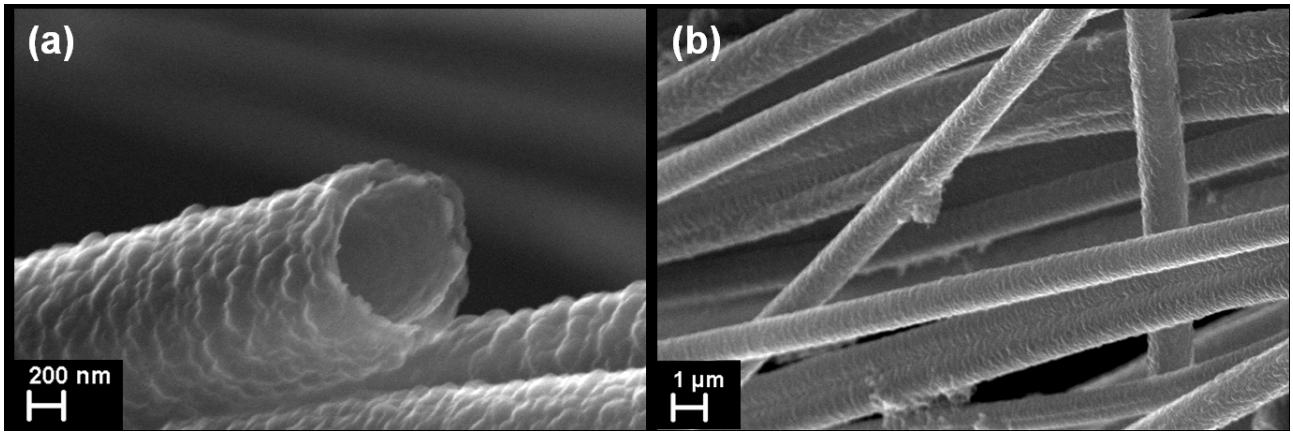

Fig. 1 SEM images of PANI coated microtubes.

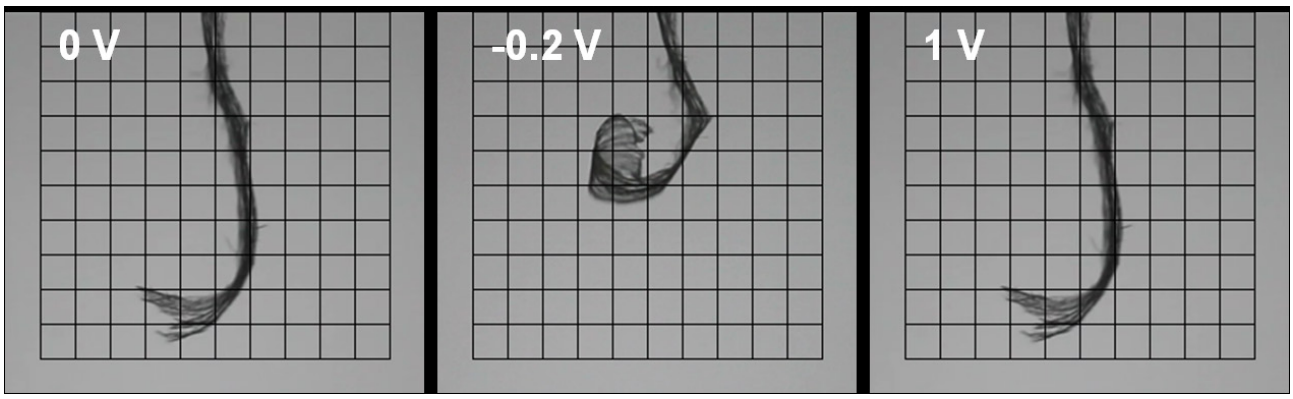

Fig. 2 Snapshots taken during the movement of PANI coated microtubes in SGF when the potential was switched between -0.2 and +1 V.

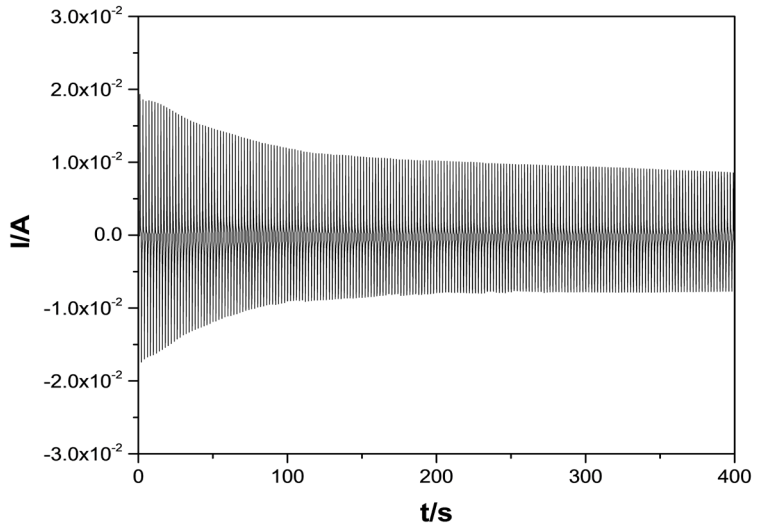

Fig. 3 Pulse program registered for 200 cycles of actuator movement.

The use of such actuators in the artificial tissue engineering domain presents many advantages considering low operation voltages, great displacement and fast response time, stability, etc.

The research was financially supported by the Romanian Ministry of Education and Research through the Core Program and by the Executive financing unit through Grant 159/2012 Heffes.

References

[1] M. Beregoi, A. Evanghelidis, E. Matei, I. Enculescu, "Polyaniline based microtubes as building-blocks for artificial muscles applications", Sensors and Actuators B: Chemical, Vol. 253, 2017, pp. 576-583.

Ferromagnetic and photoluminescence properties of Fe-doped ZnO, prepared by hydrothermal method

M. Cernea, L. Diamandescu, V. Mihalache, E. C. Secu, and I. Pasuk

National Institute of Materials Physics

in collaboration with

R. Trusca,

University POLITEHNICA of Bucharest, 060042, Romania

V. Bercu,

University of Bucharest, Romania

Zinc oxide (ZnO) is intensively studied due to its semiconducting, piezoelectric and electro-optic properties and to its large range of applications [1]. ZnO has been doped with different transition elements in order to improve their electronic and optical properties [2]. Doping ZnO with iron can influence the properties of ZnO, such as: photocatalytic and optical properties. Moreover, ZnO doped with Fe shows interesting magnetic properties.

We studied the influence of Fe^{3+} dopant concentration on the change of the undoped ZnO powder morphology, prepared by hydrothermal method, as the main cause of the variation of its photocatalytic, photoluminescence and ferromagnetic properties. $Zn_{1-x}Fe_xO$, with x = 0, 0.01, 0.03 powders were synthesized by hydrothermal method at 200 °C, 2 h and pH=9. All the samples shown a single phase: ZnO hexagonal wurtzite.

The magnetic properties of the $Zn_{1-x}Fe_xO$ powders were investigated using a SQUID magnetometer (Fig.1).

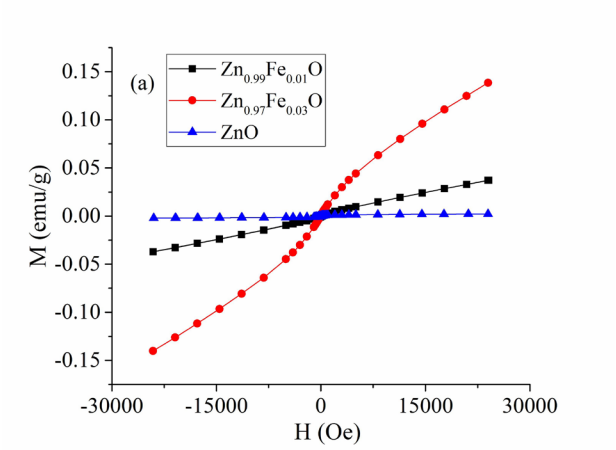

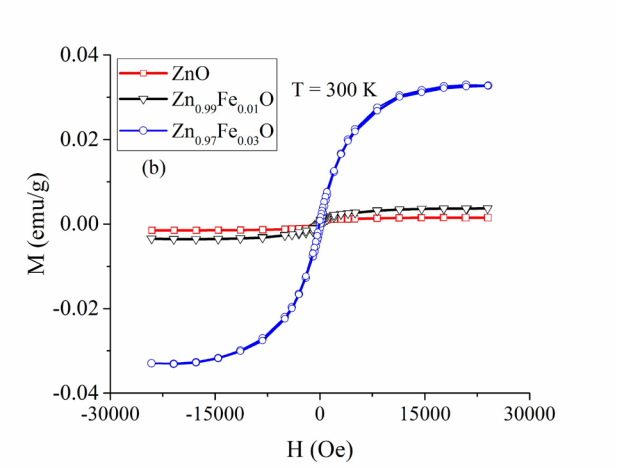

Fig. 1. **M** vs. **H** curves measured at 300 K for $Zn_{0.97}Fe_{0.03}O$, $Zn_{0.99}Fe_{0.01}O$ and undoped ZnO powders.

As indicated in Fig.1, no tendency toward saturation can be seen at high applied fields which suggests that Fe doping also give a paramagnetic contribution. More precisely, the isolated Fe^{3+} ions are not participating in the magnetic ordering or ferromagnetic coupling. The magnetizations $\mathbf{M}_s$ and $\mathbf{M}_r$ of Fe doped powders as compared to the undoped ZnO powder show values increasing for x = 0.01, then decreasing values for x = 0.03, while $\mathbf{H}_c$ has a reverse variation of the magnetization [3]. Undoped ZnO display weak room temperatures ferromagnetism, with high coercivity ($\mathbf{H}_c$ = 107 Oe) and saturation magnetization $\mathbf{M}_s$ of 1.5×10^{-3} emu/g. ZnO samples containing 1% and 3 at.% Fe prove a significant increase of the magnetization in comparison with the undoped sample. In the case of ZnO sample with 3% at. Fe, $\mathbf{M}_s = 32.5\times10^{-3}$ emu/g and $\mathbf{M}_{rem} = 0.78\times10^{-3}$ emu/g.

The electron paramagnetic resonance (EPR) signal obtained for undoped and Fe doped ZnO samples (Fig.2), indicated different defects present in the ZnO nanocrystals and the presence of Fe^{3+}

state ($^6S_{5/2}$, S = 5/2) in ZnO nanocrystals [4].

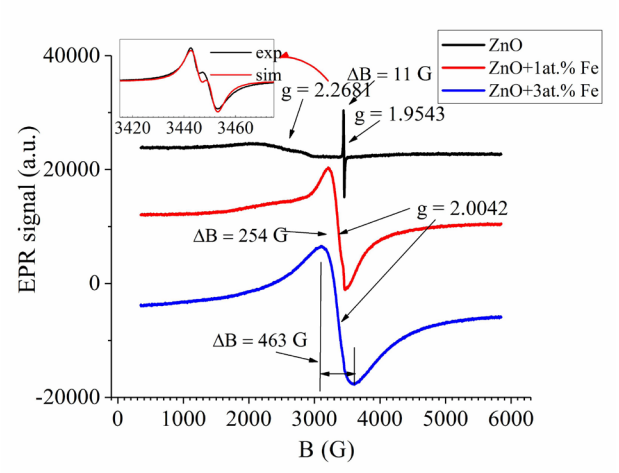

Fig. 2. EPR spectra recorded for undoped and Fe doped ZnO samples; the inset shows in detail the analysis of the narrow EPR signal.

The EPR measurements of Fe doped ZnO have shown a superposition between the electron paramagnetic resonance signal of the Fe^{3+} ions and the signal of the paramagnetic defects observed for undoped ZnO sample.

All the samples exhibit a sharp UV luminescence peak at about 390 nm accompanied by a broad green-yellow band ranging in the whole visible region (Fig.3).

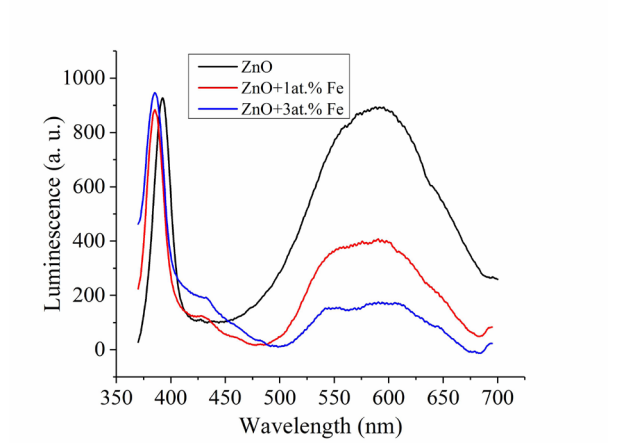

Fig. 3. Photoluminescence spectra of undoped (A_0 (a)) and Fe-doped ZnO (A_1 (b) and A_3 (c)) powder samples at excitation wavelength of 325 nm.

The UV peak was assigned to the excitonic recombination corresponding to near-band-edge emission of ZnO, while the broad visible emission was assigned to the recombination of electrons trapped in singly ionized oxygen vacancies with holes and the interstitial oxygen ions.

The intensity of the ZnO characteristic green-yellow photoluminescence band at about 550-600 nm diminishes with the Fe concentration because the number of oxygen vacancies and interstitial oxygen ions also decreases.

In summary, Fe doped-ZnO, prepared by hydrothermal route shown magnetic and photoluminescence properties that depend on the Fe concentration.

Funding from the Partnership Project no 94/2014.

References

[1] S. K. Gupta et al., J. Chem. Sci. 122, 57–62 (2010). Vasundhara et al., J. Appl. Phys. 113, 194101 (2013).

[2] Y. Wang et al., J. Phys. Chem. B, 110, 21413-21415 (2006).

[3] V. Mihalache, M. Cernea, I. Pasuk, Curr. Appl. Phys. 17, 1127-1135 (2017).

[4] M. Cernea, V. Mihalache, E. C. Secu, R. Trusca, V. Bercu, L. Diamandescu, Superlattices Microstruct. 104, 362-373 (2017).

Advanced materials for catalytic applications

M. Florea, Ş. Neaţu, and C. Bucur

National Institute of Materials Physics

in collaboration with C. Rizescu,[a] I. Podolean,[a] V.I. Pârvulescu,[a] S.M. Coman,[a] B. Cojocaru,[a] F. Neaţu,[a] M.M. Trandafir,[a] R. Zăvoianu,[a] O.D. Pavel,[a] A. Cruceanu,[a] M. Puche,[b] J. Alberto,[b] H. Garcia,[b] D. Avram,[c] I. Porosnicu,[c] R. Bîrjega,[c] I. Tiseanu,[c] C. Tiseanu,[c] M. Marcu,[d] L. Preda,[d] J.M. Calderon-Moreno,[d] and S. Şomăcescu[d]

[a]University of Bucharest, Faculty of Chemistry, Bucharest, Romania

[b]Instituto Universitario de Tecnología Química CSIC-UPV, Valencia, Spain

[c]National Institute for Laser, Plasma and Radiation Physics, Bucharest-Magurele, Romania

[d]"Ilie Murgulescu" Institute of Physical Chemistry, Romanian Academy, Bucharest, Romania

At the National Institute of Materials Physics, a top priority topic is represented by the extensive studies of advanced materials for catalytic applications, among which we are mentioning: i) selective oxidation reactions, ii) electrocatalysis, and iii) down/up-conversion emission studies. Exhaustive characterisation of such materials can reveal important features which renders advanced knowledge in the foresight of their catalytic behaviour.

i) In the chemical industry, one of the key biomass transformations is related to the conversion of glucose into succinic acid (SA), by wet oxidation (WO). This process can be improved using a metal-free catalyst. Defective graphenes (Gs) act as oxidation catalysts and one topic to be investigated is how the presence of Gs can alter the product distribution in the catalytic WO. N-doped Gs prepared by two methods: simultaneous amination and reduction of graphene oxide and by pyrolysis of chitosan under inert atmosphere are effective in SA synthesis [1].

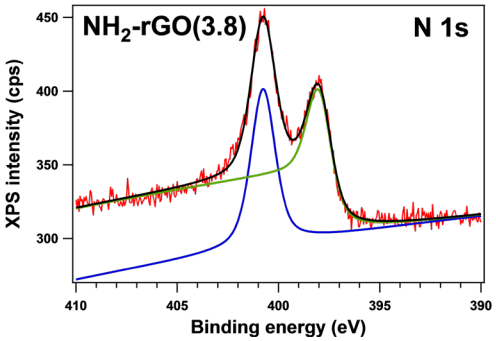

Fig. 1 N1s core level for the sample with the highest selectivity. Adapted from ref. [1]

The nature of grafenic N-atoms (pyridinic or quaternary) evidenced by XPS corelated with TPD-CO_2 analyses, have been demonstrated to be mainly responsible for the notable selectivity to SA (over 60%),

ii) Electrocatalysis stands as a catalytic application where advanced materials could be successfully implemented. Regarding this aspect, one of our collaboration was focused on the direct synthesis of Ni and Co doped ZrO_2 through a self-assembling method, which uses Triton X100 as template [2]. The main purpose, for which this template method was chosen, was to obtain a porous structure with small particle sizes to allow the improvement of the electrocatalytic performances of the final material. The thermal treatment ensures the removal of both hydrophilic polyethylene oxide chains and hydrophobic groups present in the template and thus the creation of a proper porosity that can facilitate oxygen transport through the layers of the material.

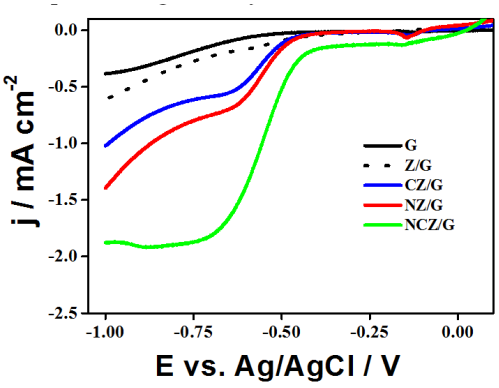

Fig. 2 Linear sweep voltammetry curves for ORR in 0.1 M KOH solution recorded at 20 mV s^{-1}. Adapted from ref. [2]

The incorporation of Ni and Co into ZrO_2 lattice induces structural, textural and surface modifications that allow the improvement of the electroactivity toward oxygen reduction reaction

(ORR), as described in Fig. 2.

These results indicate that self-assembling procedure allows the tuning of key parameters during the synthesis process in order to perform crystalline structures with thermal stability showing a good porosity. Thus, this synthesis process might represent an essential first step in the improvement of the electrocatalytic performance of future advanced materials.

iii) Down- and up-conversion (UPC) emission studies on different materials represents a topic of great interest due to their potential applications in bioimaging, theranostics and photonics. The emission enhancement can be achieved by doping and increasing the number of oxygen vacancies induced by charge compensation, tailoring the crystal-field via lowering of the local symmetry or/ and improved crystallization, but also by changing the preparation method and therefore, among others, the reduction of surface OH defects can occur. In this particular case, Li doped Y_2O_3 materials were studied, since Li addition has been established as an effective method for the enhancement of UPC emission, without any direct evidence that supports tailoring the local crystal field [3]. We found that the role of Li addition is to reduce the surface OH groups and does not manipulate the local structure by changing the local symmetry around Ln sites or modify their relative occupancy. Moreover, the effect of Li addition was found to be assimilated to an improved crystallization and similar with the increases of the calcination temperature, from 800°C to 1000°C. Additionally, very interesting results were obtained on the down- and up-conversion processes in Er doped and Er, Yb co-doped CeO_2 nanoparticles by use of time-gated luminescence spectroscopy under optical down/up-conversion and X- ray excitation [4]. The samples were synthesized by a cost efficient and environmentally friendly citrate method and the structural properties were intensively characterized by X-ray diffraction, Raman, Diffuse Reflectance UV/ Vis and Diffuse Reflectance Fourier Transform Infrared spectroscopies. The up-conversion mechanisms responsible for populating the emitted levels were characterized under excitation at 650, 790, 977 and 1470 nm for Er-CeO_2, and 971 nm excitation in the Yb absorption band for 1Er20Yb-CeO_2. The competitive contribution of ground state absorption/excited state absorption versus energy transfer up-conversion mechanisms were explained in terms of the up-conversion excitation spectra, emission decays (down- and up-conversion excitation) and the evolution of red to green emission ratio. The shortening of the emission lifetime for 3Er-CeO_2 can be attributed to 4I11/2 - 4F9/2 4 4F7/2 - 4F9/2 cross relaxation effect, given by the increase of Er concentration (Scheme 1).

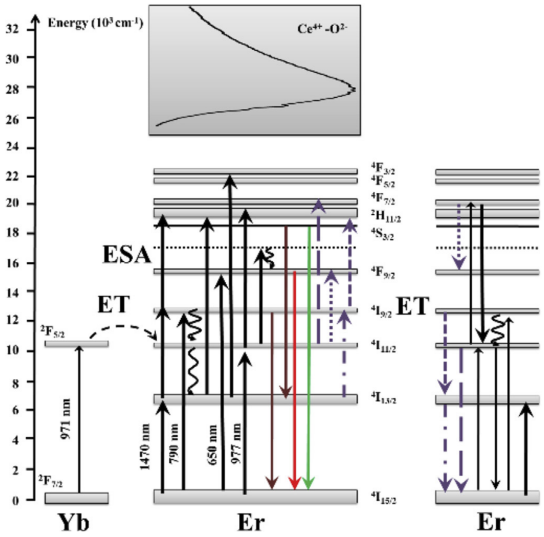

Scheme 1. Simplified energy-level scheme of Er-CeO_2 and Er,Yb-CeO_2 indicating major up - conversion emission processes. Adapted from ref. [4]

The obtained results show that all studied materials: Er-CeO_2, Er,Yb-CeO_2 and Li,Er–Y_2O_3 are promising candidates for photovoltaics, photocatalysis, (bio)photonics applications, including probes in the second/third biological windows and therapy applications.

Further research will explore other isostructural Y_2O_3 or CeO_2 hosts for Er activator in combination with Li- and non-Li-based chemical preparation strategies.

References

[1] C. Rizescu, I. Podolean, J. Alberto, V.I. Parvulescu, S.M. Coman, C. Bucur, M. Puche, H. Garcia, Green Chem. 19, 1999-2005 (2017)

[2] F. Neatu, M. M. Trandafir, M. Marcu, L. Preda , J. M. Calderon-Moreno, S. Neatu, S. Somacescu, M. Florea, Catal. Commun. 93 37-42 (2017)

[3] D. Avram, B. Cojocaru, I. Tiseanu, M. Florea, C. Tiseanu, J. Phys. Chem. C 121, 14274-14284 (2017)

[4] I. Porosnicu, D. Avram, B. Cojocaru, M. Florea, C. Tiseanu, J. Alloys Compd. 711, 627–636 (2017)

Up-conversion luminescence of RE^{3+} - doped nanostructured phosphors

M. Secu, C.E. Secu, C. Bartha, E. Matei and I.Pasuk
National Institute of Materials Physics

Rare-earth doped phosphors showing efficient up-conversion (UC) effects (i.e. near-infrared (NIR) conversion into the visible spectral range) are of keen interest to scientists due to their high potential for applications in various fields (photovoltaic, optical amplifiers, optical waveguides, OLEDs, etc.) or life sciences [1].

The crystallization mechanism of sol-gel derived $NaYF_4$:(Yb,Er) up-converting phosphor has been studied by using complex thermal analysis [2,3]. The process has been described by an autocatalytic type one where the amorphous xerogel exhibits a fast self-accelerated crystallization due to the simultaneous presence of both $NaYF_4$ hexagonal and cubic phases resulted from the trifluoracetates thermolysis above 300 °C (Figures 1-2).

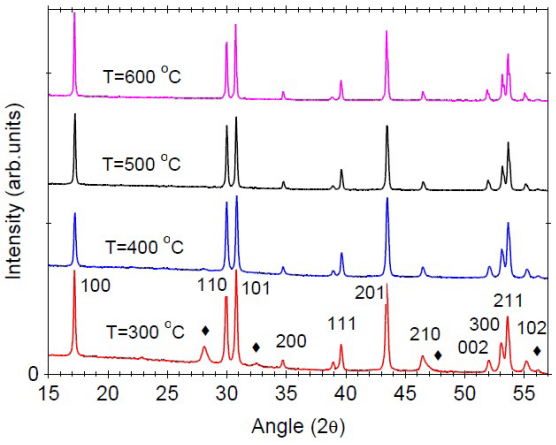

Figure 1. Normalized XRD patterns of the $NaYF_4$:(Yb,Er) xerogel after annealing

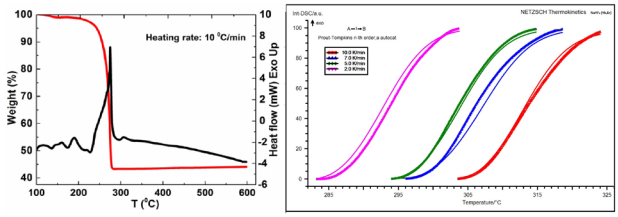

Figure 2. TG-DSC curves of the xerogel recorded for 10 °C/min (left) and the crystallization curves obtained within the Prout-Tompkins model (Bna) (right).

The $NaYF_4$ cubic phase played a catalytic role by reducing the energy barrier against the crystallization of the hexagonal phase and caused its fast self-accelerated crystallization. The analysis within the Prout-Tompkins autocatalytic model (Bna) (Figure 2) has indicated that initial microcrystalline particles are disintegrated generating a higher number branching nuclei and the process continues on larger surfaces.

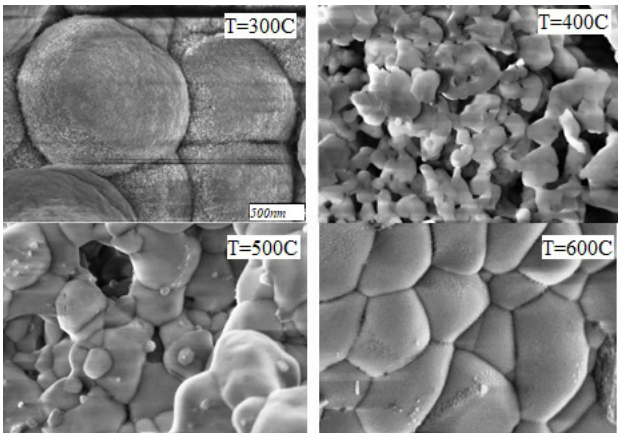

Figure 3. SEM images of the $NaYF_4$:(Yb,Er) xerogel after annealing.

The energy resulted from the disintegration process contributed to the growth and agglomeration of the nuclei and at the end, the nanoparticles collapsed and their size increases with the temperature (Figure 3).

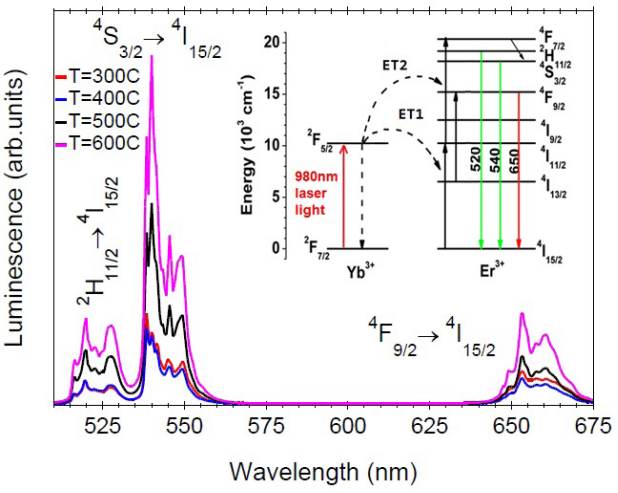

Figure 4. Up-conversion spectra of the $NaYF_4$:(Yb,Er) xerogel after annealing

The UC spectra showed Er^{3+} ions luminescence bands and increase due to the hexagonal phase crystallinity improvement and dehydratation process (Figure 4).

A comparative study of the up-conversion properties of Yb^{3+}/Er^{3+} co-doped $LiYF_4$ thin films obtained by pulsed laser deposition (PLD) and matrix-assisted pulsed evaporation (MAPLE) growth techniques has been perfomed [4].The samples surface morphology is typical for laser processed thin films with roughness values of the order of hundreds of nanometers (Figure 5).

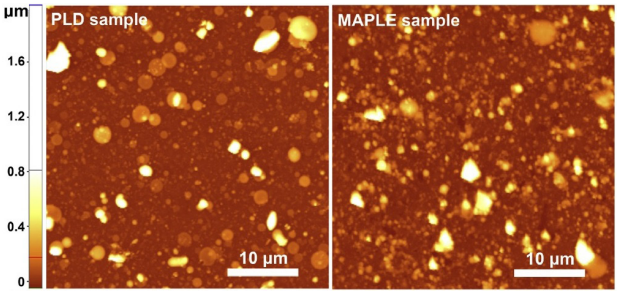

Figure 5. AFM images of the $LiYF_4$:**(Yb^{3+}/Er^{3+})** thin films surfaces.

Up-conversion spectra showed green (($^2H_{11/2}$, $^4S_{3/2}$) → $^4I_{15/2}$) and red ($^4F_{9/2}$ → $^4I_{15/2}$) luminescence bands of the Er^{3+} ions; the UC mechanism involves a two-photon process as in the pellet sample (Figure 6). The UC properties are preserved during transfer from the pellet target by either PLD or MAPLE techniques.

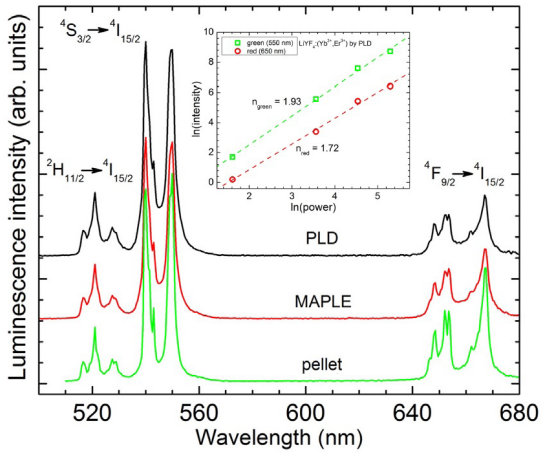

Figure 6. Up-conversion luminescence spectra shown by **Yb^{3+}/Er^{3+} co-doped $LiYF_4$ thin films** grown by PLD and MAPLE, by comparison to the pellet target.

For biological related applications there are issues related to long-term stability and toxicity due to exposure to the body. One of the simplest and most popular strategy is the coating of the RE-doped nanocrystals with a silica shell which is highly biocompatible. BaFBr:Er^{3+}@SiO_2 core-shell heterostructures have been prepared by a two-step process from BaFBr:Er^{3+} crystalline ore grains with square sheets shape synthesized by co-precipitation method, followed by coating with a silica shell [5] (Figure 7).

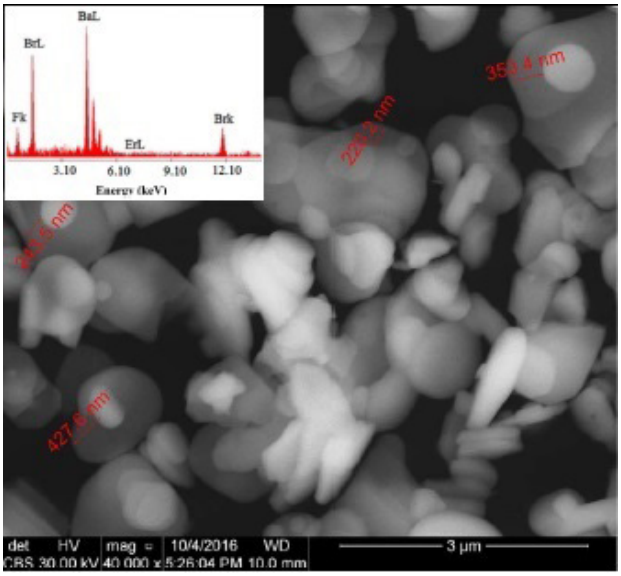

Figure 7. SEM image of the BaFBr:Er^{3+}@SiO_2 heterostructure and the EDX spectrum.

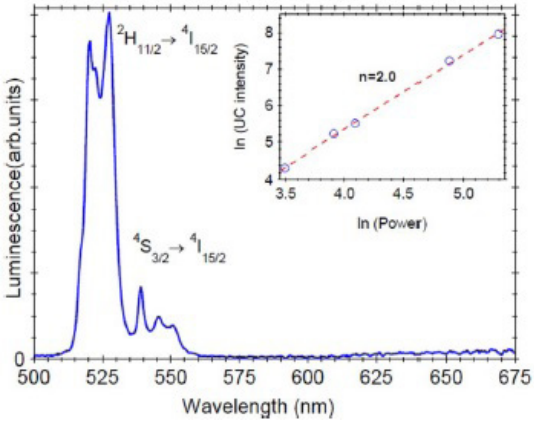

Figure 8. Up-conversion luminescence of the BaFBr:Er^{3+}@ SiO_2 heterostructure.

Up-conversion spectrum showed green luminescence of the Er^{3+} ions ascribed to a two-photon processes (Figure 8).

References

[1] M. Haase, H. Schäfer, Angew. Chem. Int. Ed. 50, 2011, pp. 5808 – 5829.

[2] C. Bartha, C.E. Secu, E. Matei, M. Secu CrystEngComm vol 19 (34), p.4992 (2017)

[3] C. Bartha, C.E. Secu, M. Secu Ceramics International 42 (2016) 18732–18736

[4] C.E. Secu, M. Secu, F. Stokker-Cheregi, V. Ion, S. Brajnicov, M. Dinescu Thin Solid Films 625 (2017) 6–10

[5] C.E. Secu, M. Secu, M. Cernea Journal of Luminescence188, pp. 96-100 (2017)

Photoanodes for solar water oxidation based on hematite films

M. Sima, C. Logofatu, Ma. Sima

National Institute of Materials Physics

in cooperation with

Eugeniu Vasile- University "Politehnica"of Bucharest

The intermittency of the energy available from sunlight determined the search for efficient technologies for solar energy storage in the form of chemical fuel. One method to store solar energy is the formation of hydrogen, which is a clean energy carrier, through photo-electrochemical (PEC) water splitting. The oxygen evolution reaction is the kinetic barrier in PEC water splitting in hydrogen and oxygen. Hematite (α-Fe_2O_3), a n-type semiconductor seems to be a promising candidate due to its excellent chemical stability in water and electrolyte, its nontoxicity and abundance, composition of low-cost, and especially due to its optical band gap of 2.1-2.2 eV which permits absorption of a large portion of solar irradiation spectrum (λ<620 nm) and has the valence band edge position suitable for water oxidation. However, hematite suffers from a slow kinetics for hole transfer to water, possesses a relatively poor absorptivity of photons near its band-edge due to an indirect band gap and shows poor electronic properties. As a result, much of photogenerated holes in hematite photoanode will be lost by recombination before carrying out the chemical reactions at the interface electrode/electrolyte. Another drawback of hematite is the inadequate position of its conduction band for water reduction process, and an external bias is necessary for PEC hydrogen generation at the cathode. In order to improve the electrical properties of hematite there have been used some methods like the doping for improving of electrical conducting properties, the nanostructuring to increase the photoanode surface or the modification of photoanode surface with a co-catalyst to facilitate oxygen evolution reaction. High-valent ions like Sn^{4+} and Ti^{4+} are the most used dopants to enhance electrical conductivity of hematite photoanode. We used agarose gel as a non-traditional template for electrochemical synthesis of porous hematite films. The photoelectrochemical performance of these photoanodes both as Sn doped hematite and hematite decorated with NiO was evaluated.

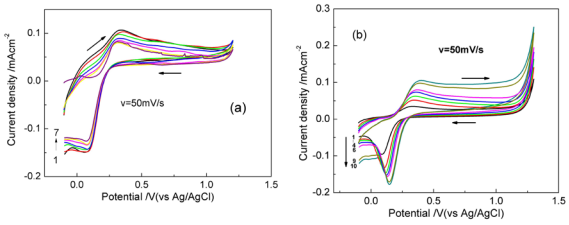

Fig. 1 Cyclic voltammograms for (a) FTO electrode and (b) FTO covered with an agarose gel in contact with 0.1 M iron sulfate solution (pH 6) at 60^{0}C.

In the Fig.1 are presented cyclic voltammograms recorded for the bare FTO electrode and FTO covered with an agarose gel film, in aqueous solution containing 0.1 M iron sulfate (pH~6) at 60^{0}C. The anodic process involves electrochemical oxidation of Fe^{2+} to Fe^{3+} and precipitation of Fe^{3+} as iron oxyhydroxide (FeOOH) film in aqueous media with pH values between 3 and 7:

$$Fe^{2+} \rightarrow Fe^{3+} + e^-$$

$$Fe^{3+} + 2H_2O \rightarrow FeOOH + 3H^+$$

The gradual decreasing of the current during repeated potential sweeping between -0.1 and 1.3 V can be seen. This indicates a progressive covering of FTO electrode with a less electroconductive FeOOH film. In comparison, the anodic deposition of FeOOH at FTO electrode covered with a film of agarose gel takes place with current increase after each scan of the potential between -0.1 and 1.3 V (Fig.1b). In this case, the reactive chemicals can be reserved within the agarose hydrogel and gradually delivered to the electroactive surface of FeOOH nanostructure surrounded by gel.

FeOOH films were prepared on FTO substrate, without or in the presence of agarose gel film by electrodeposition at 1.2 V vs Ag-AgCl in 0.1 M $FeSO_4$ solution at 60^{0}C. The hematite film was prepared as a result of FeOOH film annealing at 525^{0}C. In

order to remove all hydroxyls from hematite it was necessary annealing at 800^{0}C. SEM images from Fig.2 show the morphology both of the porous and compact hematite samples prepared into agarose gel film and directly on the FTO substrate, respectively.

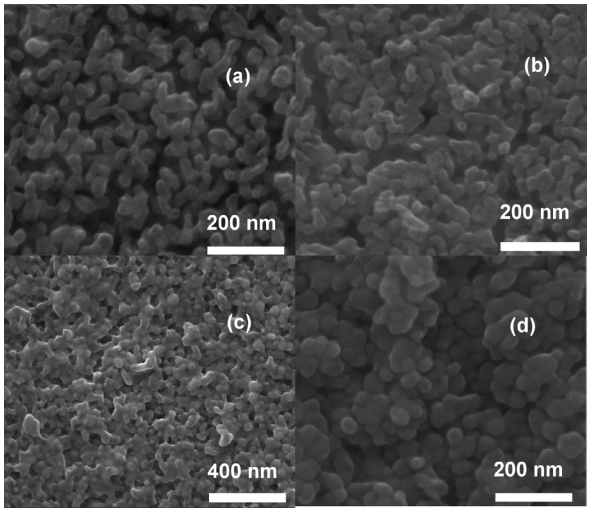

Fig.2. SEM images of porous hematite samples: (a) pristine, (b) Sn doped, (c) decorated with NiO; (d) SEM image of compact hematite film.

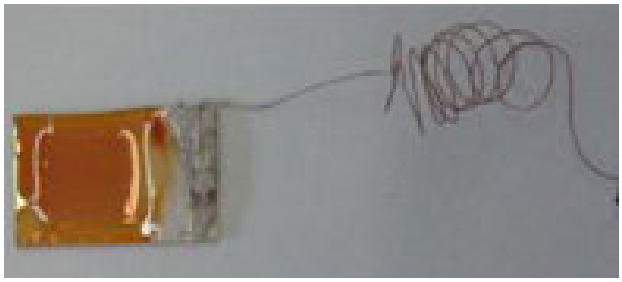

Fig.3. The hematite photoanode with connecting cable

The performance of the prepared hematite photoanodes (Fig.3) was evaluated from J-V curves and electrochemical impedance spectroscopy (EIS) measurements under simulated solar illumination (100 mWcm^{-2}) conditions. The oxygen evolution reaction takes place on the hematite surface via trapping of holes at Fe species, which are often referred to as surface states, followed by the transport of these holes to the electrolyte. Moreover, it was considered that these surface states display an ambivalent nature, also acting as recombination centers.

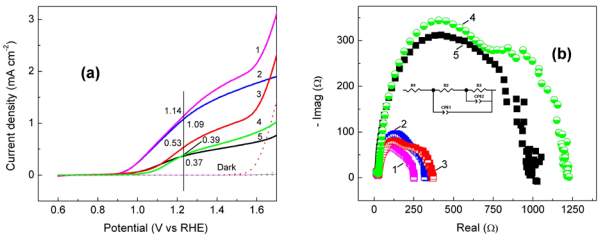

Fig.4. (a) J-V characteristics and EIS obtained under simulated solar illumination in 1M NaOH solution, pH 13.6 for porous hematite samples (1)Sn doped and decorated with NiO, (2)Sn doped, (3)decorated with NiO, (4)pristine; (5)compact hematite film.

The largest value of the photocurrent density (0.39 mAcm^{-2}) at 1.23 V vs reversible hydrogen electrode (RHE) was obtained for the thinnest (215 nm) porous hematite film (Fig.4). Both doping with Sn and slight modification with thin and discontinuous NiO film of the hematite surface improved the performance of the hematite photoanode. A synergistic improvement of photocurrent density (1.14 mAcm^{-2}) was observed, induced by Sn-doping and modification of hematite surface with thin NiO film. The modification of hematite surface with thin and discontinuous NiO film determined only a slight cathodic shift for photooxidation of water, but instead there is an increase in photocurrent. From EIS measurements resulted that samples doped with Sn show the lowest charge transfer resistance at electrode/electrolyte interface. On the other hand, the presence of NiO film on the hematite surface facilitates hole trapping process in surface states.

References

[1] M. Sima, E. Vasile, A. Sima, C. Logofatu, Electrochimica Acta 258 (2017) 1453-1462.

[2] M. Sima, E. Vasile, Ma. Sima, Digest Journal of Nanomaterials and Biostructures 12 (2017) 751-758.

Relationships between additives and properties in spark plasma sintered MgB_2 superconductor

P. Badica*, G. Aldica, S. Popa, M. Burdusel, A.M. Ionescu,

National Institute of Materials Physics

in collaboration with University 'Politehnica' of Bucharest, University of Bucharest, Tohoku University, Karadeniz Technical University, Recep Tayyip Erdogan University, Sinop University and University of Warwick

MgB_2 is a light-weight superconductor, with a relatively high critical temperature T_c of about 39 K. It has a relatively large coherence length ξ (10-30 nm). The last observation has few convenient consequences:

(i) supercurrent can 'flow' over the grain boundaries since their thickness is comparable with ξ and also due to this feature, the grain boundaries can be effective pinning centers;

(ii) point (i) indicates that nano impurity phases introduced e.g. with the help of additives can play the role of pinning centers;

(iii) point (i) also enables the idea of less sophisticated technologies for fabrication of the material than for high temperature superconductors for which single crystal-like materials (low angle boundaries) are required.

However, for maximization of the functional characteristics such as the critical current density J_c and the irreversibility field B_{irr} towards different applications of MgB_2, strong flux pinning is necessary. Control of the additives and of the processing procedures leading to specific composite microstructures and chemical doping effects promote formation of effective flux pinning centers. At present, criteria for selection of an effective additive vs. processing technology is not established. Relationships between additives and properties are weakly understood and our work is devoted to this problem. In our studies samples of MgB_2 are produced by Spark Plasma Sintering (SPS)

Additives introduced into MgB_2 were classified into 4 groups [1]:

T1. **Additives (almost) not reacting with MgB_2** such as c-BN, h-BN, and graphene (G)

T2. **Additives reacting with MgB_2 and formation of impurity boride RE_aB_b phases**, where RE is (usually) a RE element. We used RE-oxide additives (RE=Ho, La, Eu) forming HoB_4, LaB_6 and EuB_6.

T3. **Additives reacting with MgB_2 and formation of Mg_uM_v (M=metal) impurity phases**: Sb, Sb_2O_3, Sb_2O_5, Bi, Bi_2O_3, Te, TeO_2, Ge and GeO_2. The newly induced impurity phases were Mg_3Sb_2, Mg_3Bi_2, MgTe and Mg_2Ge.

T4. **Additives which are source of carbon substituting for boron in the crystal lattice of MgB_2**: fullerene (F), F + c-BN, SiC + Te, $Ge_2H_{10}C_6O_7$ (GEP), and B_4C **(**BC**)**. Apart from the 'substitution' effects, the 'composite' effects as for the groups 1-3 are also active. We can consider that additive F is of purely type 4, (F + c-BN) of type 4+1, (Te + SiC) and GEP of type 4+3, while B_4C is approximately of type 4+1 or 4+3. Impurity phases for the (Te + SiC) co-added samples were MgTe and Mg_2Si.

Scaling of the reduced pinning force $f=F_p/F_{p,max}$ ($F_p = J_c \cdot H$) vs. reduced field $h=B/B_{irr}$ with the universal law $f_p = Ah^p(1-h)^q$ [2] was undertaken. Pinning force parameters **p**, **q** and $h_0=h(F_{p,max})$ were represented as a function of carbon amount **x** ($Mg(B_{1-x}C_x)_2$) [1] substituting for boron in the crystal structure of MgB_2. The carbon amount was calculated based on the variation of the **a**-lattice parameter of MgB_2. One observes (Fig. 1) that **x**-carbon has a strong influence and additives inducing composite effects are effective for **x**<0.018.

In three other studies Ag [3], $C_6H_{10}Ge_2O_7$ [4] and Sb_2O_5 [5] were added to MgB_2. In the first case, the additive was introduced to control the levitation force, while in the other two, processing processes were investigated in detail. Comparative analysis between Sb_2O_5, Sb_2O_3 and Sb suggested that to obtain improved pinning properties, a higher

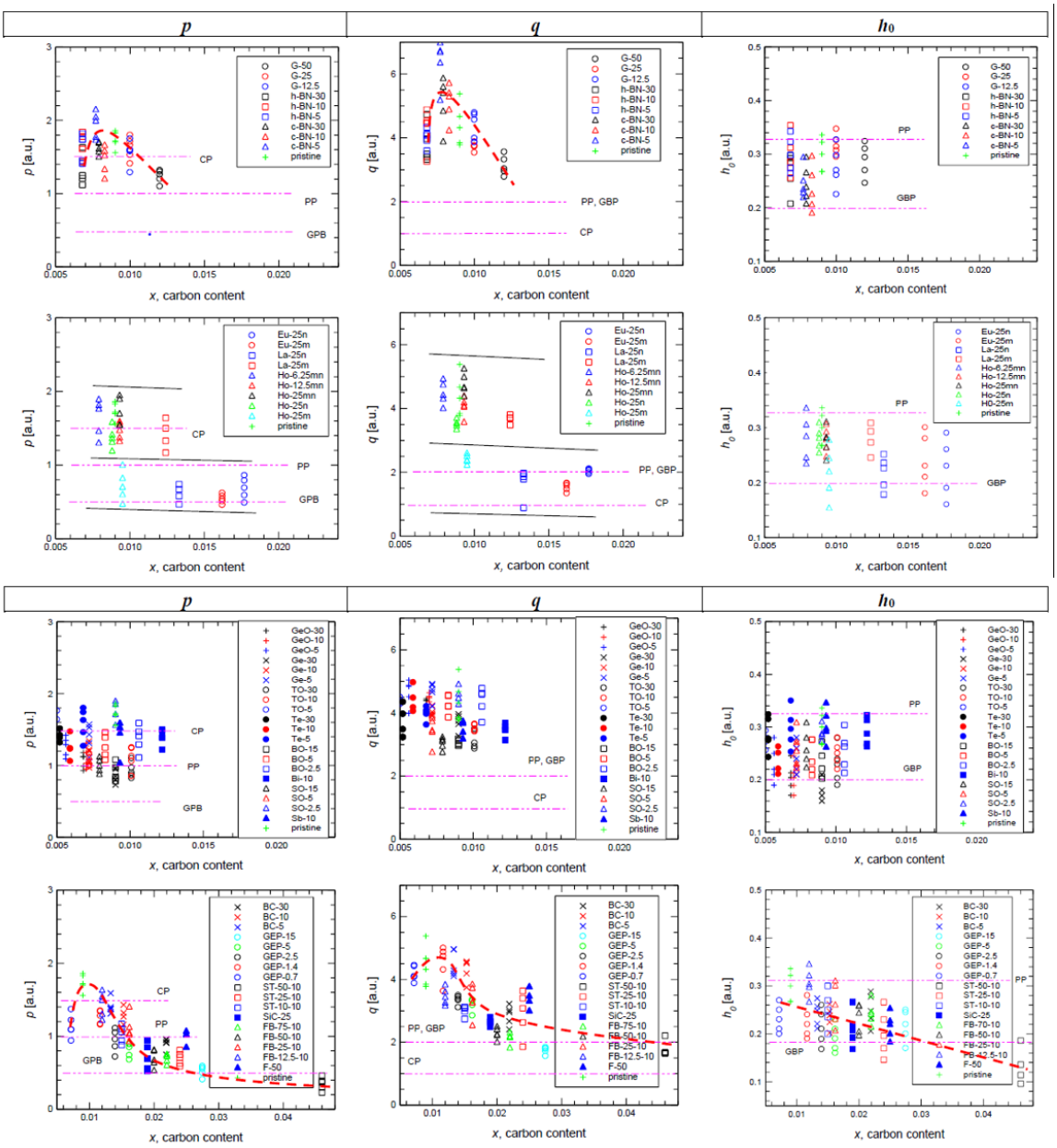

Fig. 1 Parameters **p(T)**, **q(T)** and h_0**(T)** as a function of **x** – carbon for samples with different additives of T1-4 type (top raw is for T1). Theoretical values are shown for PP=point pinning, GBP=grain boundary pinning and CP=special core pinning [2]. For each sample, data are for **T** = 10, 15, 20, 25 and 30 K. Dashed thick lines are quide for eyes.

decomposition temperature of the additive is recommended. When adding $C_6H_{10}Ge_2O_7$, carbon substitutes boron at temperatures above 590 °C.

References

1. P. Badica, G. Aldica, A.M. Ionescu, M. Burdusel, D. Batalu, The influence of different additives on MgB_2 superconductor obtained by ex-situ spark plasma sintering: pinning force aspects, Ch. 4 in Correlated Functional Oxides: Composites and Heterostructures, Springer (2017) 75-116.

2. D. Dew-Hughes, Flux pinning mechanisms in type II superconductors, The Philos. Mag.: A Journal of Theoretical Experimental and Applied Physics 3 (1974) 293-305.

3. K. Ozturk, C.E.J Dancer, B Savaskan, C. Aksoy, B. Guner, P. Badica, G. Aldica, S. Celik, The investigation on the regional nanoparticle Ag doping into MgTi0.06B2 bulk for improvement of magnetic levitation force and bulk critical current, J. Alloys Comp. 724 (2017) 427-434.

4. G. Aldica, C. Matei, A. Paun, D. Batalu, M. Ferbinteanu, P. Badica, Thermal analysis on $C_6H_{10}Ge_2O_7$-doped MgB_2, J. Therm. Anal. Calorim. 127 (2017) 173-179.

5. P. Badica, M. Burdusel; S. Popa, Yuichiro Hayasaka, M. A. Ionescu, G. Aldica, Addition of Sb_2O_5 into MgB_2 Superconductor Obtained by Spark Plasma Sintering, J. Supercond. Nov. Magn. 30 (2017) 2073–2080.

*Contact: badica2003@yahoo.com (P. Badica)

Efficiency enhancement of iridium-based Organometallic Light Emitting Diodes

I.C. Ciobotaru, C.C. Ciobotaru, S. Polosan
National Institute of Materials Physics
in collaboration with
T. Tsuboi
Kyoto Sangyo University, Kamigamo, Kita-ku, Kyoto 603-8555, Japan

Typically, an Organic Light Emitting Diode (OLED) is composed by a sandwich structure with different thin layers that include the active layer, formed by an organometallic compound dispersed in transparent and conductive polymer layer between other two functional layers commonly employed to assist charge injection, transport and blocking for improved device performance. The whole structure is capped by two electrodes which ensure the charge injection in these structures.

The efficiency of these sandwich structures is given either from the internal quantum efficiency of the organometallic compound or by the improvements of the charge transport across OLED. The whole efficiency of OLED is called external quantum efficiency.

In the last decade, many efforts have been devoted to finding efficient organometallic emitters not only for a single color like in the case of classical green emitter $Ir(ppy)_3$ but also to cover the main fundamental colors: red, green and blue color. In order to obtain the white light phosphorescent emission, a combination of these three colors is required which can be given either by using three organometallic compounds simultaneously for each color or by using the same organometallic compound with different ligands. In the first case, an aggregation process occurs leading to the separation of colors.

The crystallization behaviors can be seen in the luminance spectra which gives a direct measure of the internal quantum efficiency of the two concentrations of $IrQ(ppy)_2$ in CBP (figure 1). Depending on the doping level, the luminance is balanced between red and green emission. CIE measurements suggest a shift of the all over emission color from yellow to red with the concentration going from 8%wt to 15%wt [1] (figure 2).

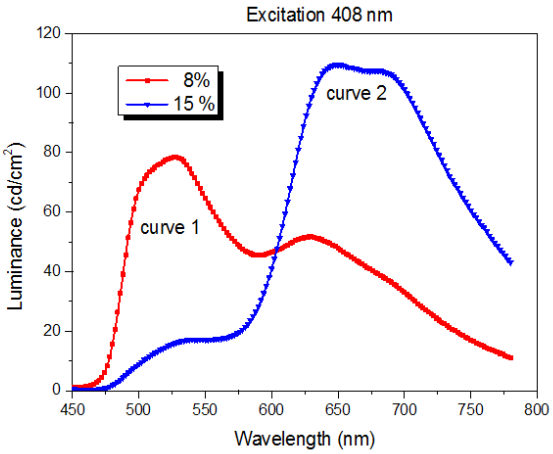

Fig. 1 Luminance of $IrQ(ppy)_2$:CBP films.

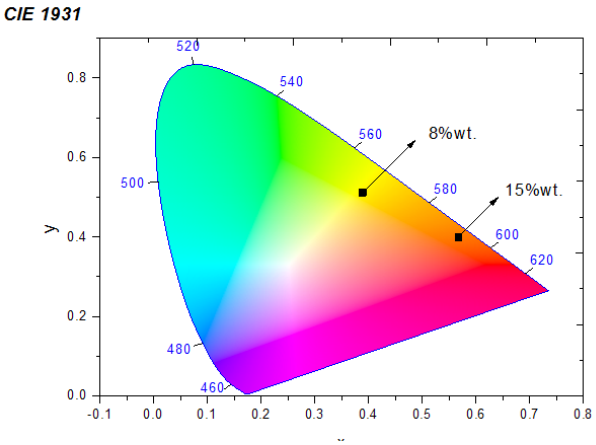

Fig. 2 CIE measurements on $IrQ(ppy)_2$:CBP films.

Coming back to the internal quantum efficiency, this is an intrinsic property of the organometallic compound and can be described by the following relation:

$$\eta = \gamma * r_s * q$$

where γ represents the ratio between the total number of excitons formed during the charge injection and the total carriers, r_s is the fraction of singlets among excitons while **q** is the decay efficiency of these singlet excitons. An increase of γ and r_s reveals a superior internal quantum efficiency by using spin-polarized charge transfer

processes in those structures [2] (figure 3).

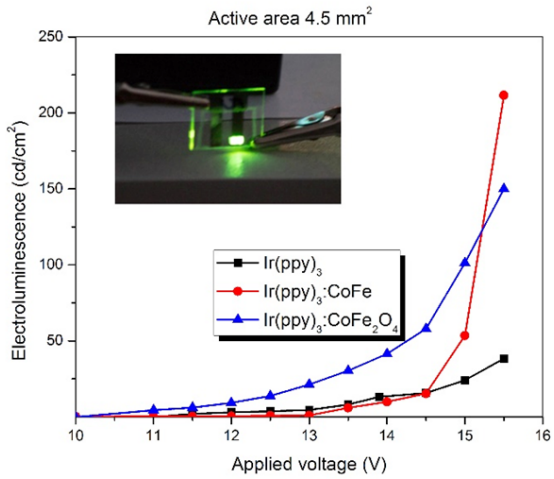

Fig. 3 Electroluminescence of OLED with magnetic nanoparticles and current voltage characteristics

The low mobility of the holes compared with the electron one may be influenced by metallic nanoparticles added in the transparent and conductive polymer, in our case in CBP. In the ITO/PEDOT:PSS/$Ir(ppy)_3$:CBP:$CoFe_2$/Al structure, the $CoFe_2$ metallic nanoparticles may influence the hole injection given by the reduction of the threshold voltage shown in the electroluminescence and current-voltage characteristics [2]. The strong magnetism of the $CoFe_2$ nanoparticles induces a spin polarization for the holes injected from the anode, which interact with the non-polarized electrons leading to an increase of the electroluminescence with about 8%.

$CoFe_2O_4$ magnetic nanoparticles embedded in CBP may act as electron traps, which balances also the charge injection in the OLED structures leading to a significant increase of the electroluminescence efficiency, especially at higher voltages, as a consequence of the balancing of the charge carriers in the OLED structures.

The authors acknowledge the Romanian Ministry of Research and Innovation (Core project PNIII-16-48-02) and the grant of the Romanian National Authority for Scientific Research, CNCS-UEFISCDI, project number PN-II-ID-PCE-2011-3-0620.

References

[1] Polosan, S; Ciobotaru, CC; Ciobotaru, IC; Tsuboi, T, “Crystallization properties of IrQ(ppy)2 organometallic complex films”, J. of Mater. Res., 32,1735-1740, (2017).

[2] Ciobotaru, CC; Ciobotaru, IC; Schinteie, G; Negrea, R; Polosan, S; “Enhancement of the electroluminescence of organic light emitting devices based on Ir(ppy)(3) by doping with metallic and magnetic nanoparticles”, Mater. Sci. Semicond. Proc., 72, 78-84, (2017).

Magnetic properties of glass-ceramics with magnetite nanoinclusions

V. Sandu, S. Greculeasa, A. Kuncser, V. Kuncser
National Institute of Materials Physics
in collaboration with Mirela Nicolescu, Elena Cimpoiasu

Magnetic glass-ceramics are a class of materials consisting of a glassy matrix in which a magnetic phase crystallizes. They are obtained by controlled crystallization of a glass parent which contains magnetic ions and a number of nucleating agents. Complex systems are formed of a crystalline ferrimagnetic phase (in the present case, magnetite) embedded in a paramagnetic glass matrix generated by the Fe ions which were left in the glassy network. These materials inherit the great flexibility characteristic to glasses which practically admit an unlimited range of compositions.

The nucleators have considerable influence on the inner structure of the glasses, as also revealed by Mössbauer spectroscopy. The presence of magnetite was evidenced in the Mössbauer spectra (see **Fig. 1**) [1], based on the Verwey model which, at high temperatures, considers a delocalization of the electrons in the octahedral (B) sites, so that the average valence of Fe ions is +2.5. Consequently, only two magnetic sublattices (sextets) are necessary above T_V. The ratio of the two spectral areas R is proportional to the ratio of occupation of the octahedral and tetrahedral sites. For ideal magnetite, R_{id}=2. Two additional paramagnetic sublattices (doublets) are necessary to depict both the paramagnetic response of the Fe^{2+} and Fe^{3+} ions which are still involved in the glassy matrix and the superparamagnetic response of the tiny nanoparticles. Below T_V, where the electron is considered localized, four magnetic sublattices are necessary to depict the distinct Fe^{2+} and Fe^{3+} ions in the octahedral sites as well as the Fe^{3+} ions in tetrahedral sites. It is also worthwhile to mention that Mössbauer data provide the most reliable way to discriminate between Verwey transition and superparamagnetic unblocking. The sample with Cr_2O_3 (BSFC) has stoichiometric magnetite, while for Al_2O_3+Cr_2O_3 (BSFCA) and P_2O_5 (BSFP) nuclear agents, there is an important fraction of unoccupied B sites. The outer spins are less coupled with the core spins. These outer spins can be easily oriented by the magnetic moment of the large particles which remain blocked at the experimental temperatures.

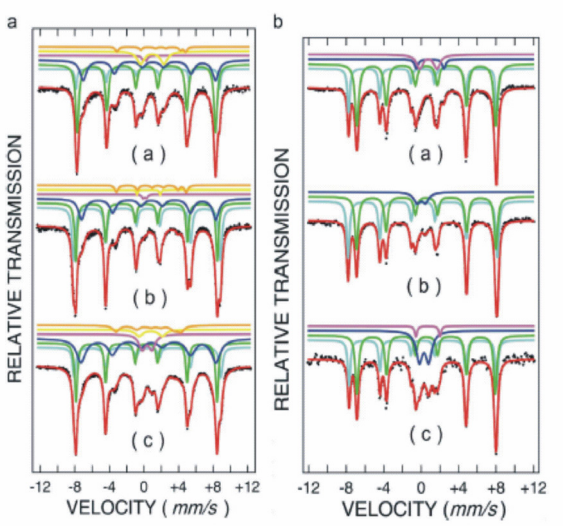

Fig. 1 Mössbauer spectra of the samples BSFC(a), BSFCA (b), and BSFP (c) collected at 4.5 K (left) and 300 K (right).

Opposingly, the sample with P_2O_5 as nucleating agent shows a deficit of Fe^{3+} ions in the B sublattice, i.e., those ions that antiferromagnetically couple to the A sublattice. Consequently, the outer spins can couple antiferromagnetically to the core spins, hence, they are less affected by the external field. Also, there is an increase of the relative area of the paramagnetic central doublets, assigned to Fe^{3+} ions in octahedral and tetrahedral coordination, as well as to Fe^{2+} ions in octahedral coordination, with increasing temperature. We attribute that increase to the gradual unblocking of the tiny magnetite crystallites/clusters as the temperature increases.

The dynamic magnetic properties of the magnetite-based glass-ceramics obtained from borosilicate parent glasses with high content of Fe are strongly dependent on the internal structure which in turn is also dependent on the nucleating agents (see **Fig.2**) [2,3].

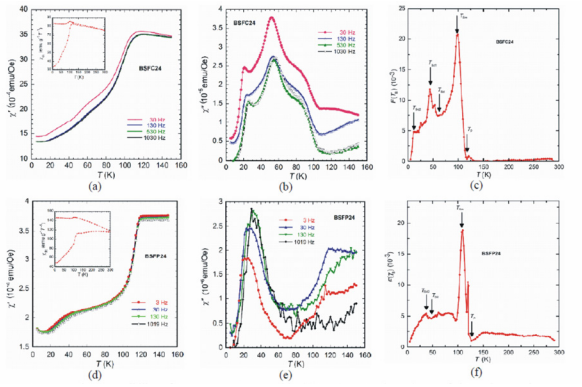

Fig. 2 AC magnetic susceptibility of BSFC (upper panels): (a) temperature dependence of the real part χ'. Inset: DC susceptibility. (b) Temperature dependence of the imaginary part χ". (c) Temperature dependence of the distribution function $F(T_B)$. And BSFP samples (lower panels), as measured at different frequencies. (d) Temperature dependence of the real part χ'. Inset: Temperature dependence of DC susceptibility. (e) Temperature dependence of the imaginary part χ". (f) Temperature dependence of the distribution function $F(T_B)$.

The rich content of iron of the parent glass leads to the growth of a series of submicron crystallite magnetite and to a large amount of nanoparticles with a bimodal size distribution. Consequently, the blocking temperatures show also a multimodal distribution and the AC-magnetic susceptibility data confirm this bimodalism. The analysis of the distribution of the blocking temperatures (T_B) suggests the existence of a mixture of collective and single spin behavior. Specifically, the larger nanoparticles with higher T_B have a predominantly collective behavior, similar to a superspin-glass but an important fraction of nanoparticles, the "fast superspins", still display characteristics of free superspins, typical for a superparamagnetic system with dipolar interaction. The contribution of these spins is more important at low temperatures where the higher spins are practically frozen. The nucleating agents have influence on both freezing temperature T_G and the interparticle interaction. Particularly, after using Cr_2O_3 as nucleating agent, large submicron particles (with typical magnetite behaviour) are immersed in a dense, uniformly distributed collection of tiny nanoparticles (particular superparamagnetic response). Negative and positive relaxation rates are observed, in different temperature ranges which roughly correlate with the main features of the distribution function of the blocking temperatures $f(T_B)$. This behaviour is attributed to a field stimulated interaction between the ferrimagnetic core of the small nanoparticle (clusters) and the disordered, spin-glass like shell. The interaction is enhanced by the existence of structural deficiencies of magnetite which were revealed by Mössbauer spectroscopy. The details of this dependence are the result of the interplay between the relaxation times related to the Néel superspin reversal and the relaxation of the field driven core-shell interacting spins in different temperature ranges. The sample with P_2O_5 as nucleating agent, which is much closer to the canonic glass, shows only positive relaxation rate but the temperature derivative of the relaxation rate is negative in the temperature range where the first percolation transition of the spin glass occurs.

References

[1] V.Sandu, E.Cimpoiasu, S.Greculeasa, A.Kuncser, M.Nicolescu, V.Kuncser, Ceram Internat 43 (2017) 3405.

[2] V.Sandu, S.Greculeasa, A.Kuncser, M.Nicolescu, V.Kuncser, J Europ Ceram Soc 37 (2017) 3089.

[3] V.Sandu, E.Cimpoiasu, A.Kuncser, M.Nicolescu, J Adv Ceram 6 (2017) 251.

BASIC RESEARCH

SELECTED RESULTS

Time and temperature dependent evolutions of magnetization. Theoretical approaches and magnetic implications

A. Kuncser, V.Kuncser

National Institute of Materials Physics

in cooperation with

S. Antohe[1] and V. Barsan[2]

[1]Faculty of Physics, University of Bucharest

[2]Horia Hulubei National Institute for R&D in Physics and Nuclear Engineering (IFIN-HH), Magurele

The time and temperature dependent evolutions of magnetization may have significant implications in the functionality of various devices. On the other hand, depending on the approach used in their treatment, the experimentally obtained dependencies may provide a range of magnetic parameters of real interest.

Increasing the density of information stored in magnetic recording media or decreasing the size of spintronics devices involve smaller and smaller sizes of magnetic entities down to nanoscopic levels. At this scale, a peculiar behavior of the magnetic structure under applied magnetic fields/ electric currents may appear in time or versus a temperature and a fully understanding of the magnetization dynamics is essential for future development of magnetic recording or sensor applications. 1D structures such as magnetic nanowires (NWs) are extensively investigated due to potential applications [1] in the above mentioned fields but also from a fundamental point of view, given the geometrical simplicity of the system. So far, this peculiarity recommends NWs as excellent physical supports for studying various aspects regarding their magnetic behavior in various combinations of well controlled sizes, magnetic parameters and external excitations. Both NW's sizes and chemical compositions (of influence on associated magnetic parameters) can be experimentally controlled by the well known template method of preparation.

Magnetization reversal as well as the dynamics of magnetic structure under applied external fields has been investigated by micromagnetic simulations on a cylindrical 1:10 aspect ratio Ni0.92Cu0.08 nanowire. As the magnetization reversal mechanism is shown to be complex and diameter-dependent in long 1D cylindrical structures, a 40 nm diameter (assumed to be consistent with the formation of domain walls in Ni wires) and a 400 nm long nanowire was considered.

Simulations have been performed using OOMMF (Object Oriented Micromagnetic Framework) public domain software, developed by the Applied and Computational Mathematics Division of NIST. The 40x400 nm cylinder was defined using 3x3x3 nm rectangular cells. Magnetic parameters have been chosen according to [2] and swept on a certain interval as follows: spontaneous magnetization Ms from 3e5 A/m to 6e5 A/m with a 4e5 A/m reference and stiffness constant A from 7e-12 to 1000e-12 J/m with 7e-12 J/m as reference. Although a cubic magneto-crystalline anisotropy was defined it can be neglected due to the prevalence of shape anisotropy.

Time independent micromagnetic simulations performed with reference magnetic parameters and field applied along (parallel geometry) and orthogonal (perpendicular geometry) to the nanowires axis suggested a magnetization reversal mechanism involving the formation of domain walls, due to major discrepancies between the required fields for bringing the system to saturation in perpendicular geometry vs. parallel geometry [3]. By sweeping the magnetic parameters it was shown that magnetization reversal is sensitive to both Ms and A and for a very large A (1000e-12 J/m) the system has a Stoner-Wohlfarth like behavior, suggesting a coherent-like rotation of the spins in perpendicular and a step-like jump in parallel geometry.

Formation and evolution of domain walls has been followed by time-dependent simulations

[3]. In Fig 1a. and Fig1b, it is shown the evolution in time of the magnetic structure through a section of the nanowire (median (a) and transversal, (b)), under an applied field ΔB=9mT higher than the field at which magnetic switching occurs in static simulation case, in parallel geometry. In Fig1c the time evolution through a median longitudinal section shows a coherent spin-like rotation under an applied field equal to the saturation magnetic field from the static case, specific to a perpendicular geometry.

As nucleation time is affected by ΔB whereas the velocity of the wall remains constant, the real nucleation time of around 3 ns was obtained by extrapolation to ΔB=0, as in Fig 2a.

In Fig 2b it is shown that the domain wall velocity is dependent on the angle between applied magnetic field and NW axis. Accordingly, a velocity of 150 m/s was evaluated for the transversal walls in longitudinal geometry.

On the other hand, excepting such numerical approaches, analytical tools for solving transcendental Weiss-like equations of ferromagnetism are also of large interest for a proper exploration of the temperature dependence of magnetization.

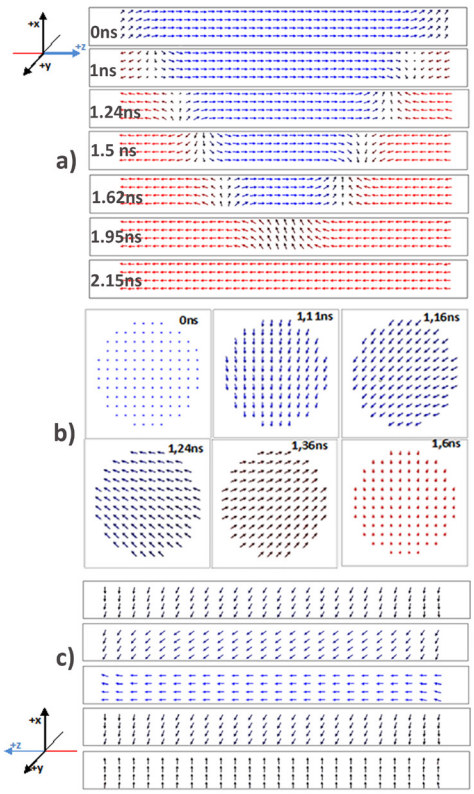

Fig.1. Time evolution of magnetic moments pictured in longitudinal geometry on longitudinal median section (a), cross section at 1/3 of the NW length (b). Median longitudinal section in perpendicular geometry (c)

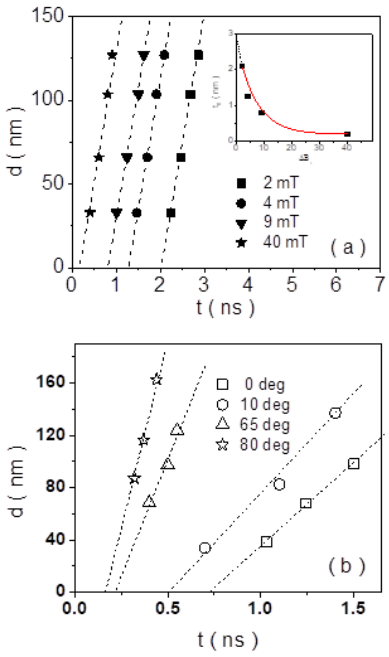

Fig.2. Domain wall displacement in time with respect to the NW end (a), evolution of the nucleation time with ΔB (inset) and domain wall displacement in time with the applied field direction relative to the NW axis.

As a direct application, an analytical solution of the magnetization versus temperature in different applied fields might be used for fitting experimental data in a regime of intermediate temperatures in order to get Curie/Neel temperatures outside the temperature measuring range of sensitive magnetometers. Exact and approximate solutions of the Weiss equation of ferromagnetism have been found and discussed with respect to their practical implications, by starting from the generalized Lambert functions [4].

Funding from PED95/2017 and Core Program PN16-4801.

References

[1] S.S. Parkin, M. Hayashi, L. Thomas, Science, 320(5873), 190-194 (2008)

[2] E. Matei, I. Enculescu, M.E. Toimil Molares, A. Leca, C. Ghica, V. Kuncser, J. Nanopart. Res., 15, 1863 (2013)

[3] A.Kuncser, S.Antohe, V. Kuncser, J. Magn. Magn. Mat., 423, 34 (2017)

[4] V.Barsan, V.Kuncser, . Phil. Mag. Lett. 97(9), 359 (2017)

Exciton-phonon interactions in layered crystals ($Cs_3Bi_2I_9$, BiI_3) and different mixtures of semiconductors (PbI_2/TiO_2, PbI_2/Si and CdS/Si) evidenced by Raman spectroscopy studies

A. Nila, A. Matea, I. Baltog, M. Baibarac, I. Mercioniu

National Institute of Materials Physics

A general feature of polar semiconductors is the enhancement of the Raman emission at low temperatures, when the incident excitation light is close to the fundamental absorption band. In condition of low temperatures and under resonant excitation lights, a strong enhancement of the Raman scattering is observed. This was interpreted as an exciton-phonon interaction that corresponds to a nonlinear optical effect of the Stimulated Raman Scattering (SRS) type. The phenomenon is very well represented for layered crystals of the type $Cs_3Bi_2I_9$ [1] and BiI_3 [2] and this is explained by the adjustment of the incident laser light in order to coincide with the maximum of the photoluminescence band of semiconductors. A schematic diagram of this process is shown in Fig. 1.

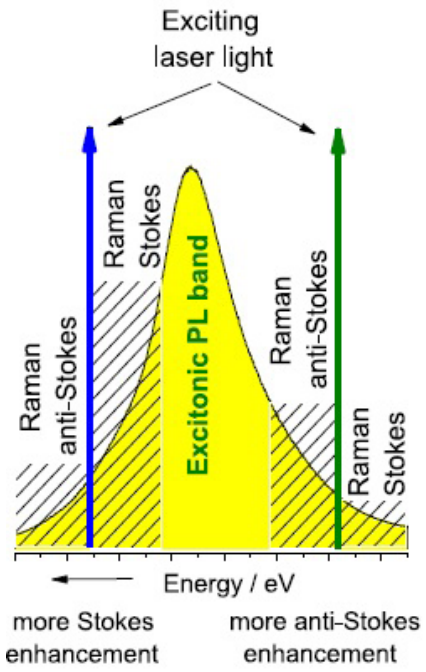

Fig. 1. Different superposition of the incident light over the profile of the PL band that gives unequal enhancement in the Stokes and anti-Stokes branches (hatched area).

According to Fig. 2a, for the particular case of the BiI_3 semiconductor, when the incident wavelength of 647 nm overlaps the states associated with the right side of the maximum PL band, an anti-Stokes Raman enhancement was expected. In the reverse situation, a Raman Stokes enhancement was predicted at 676 nm, while in the case of overlapping the PL band maximum, a strong Raman enhancement was expected (Fig. 2). Therefore, the nonlinear effect implies the coherent coupling of the incident laser light with the quasi-monochromatic PL light shifted Stokes or anti-Stokes.

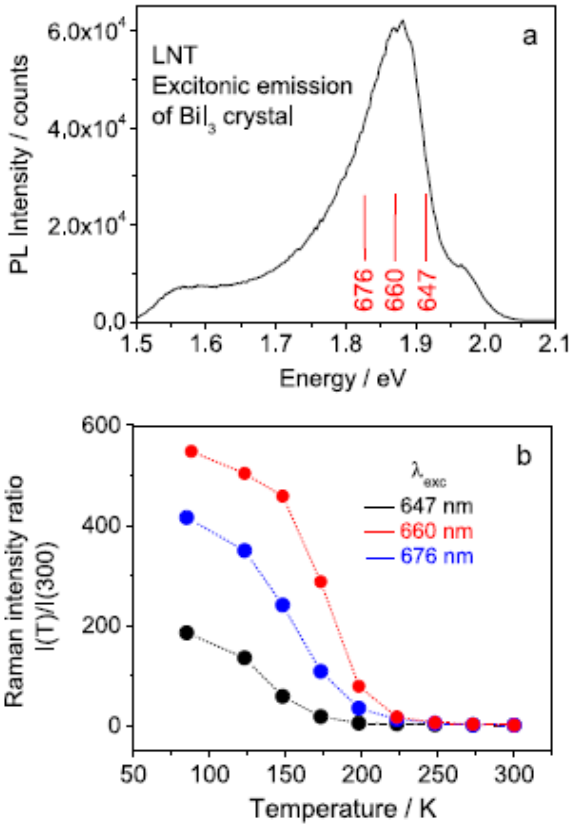

Fig. 2. (a) The PL band of BiI_3 with the superposition of three incident lights (676, 660 and 647 nm); (b) The ratio of the relative intensities of the A_g band, I(T)/I(300K), at a given temperature T and 300 K

The behavior of the Raman effect is highlighted by the ratio between the relative intensities recorded at a low temperature and at 300K,

$I_{(T)}/I_{(300K)}$ (Fig. 2b). The stronger enhancement of the Raman scattering is observed for excitation wavelength of 660 nm, when the maximum number of photons involved in the SRS process will give the strength of the exciton-phonon interaction.

A new interpretation of the exciton–phonon interaction is proposed, in which the nonlinear optical response is manifested simultaneous in mixtures of semiconductors (PbI_2/TiO_2, PbI_2/Si and CdS/Si), where TiO_2 and Si are chosen as potential electron collectors [3]. The super-radiant emission and the short lifetimes of several ns of PbI_2 and CdS semiconductors are correlated with the coherence of light and made them suitable candidates for the coupling of the incident laser light with the quasi-monochromatic PL light to determines a nonlinear optical effect such us SRS process.

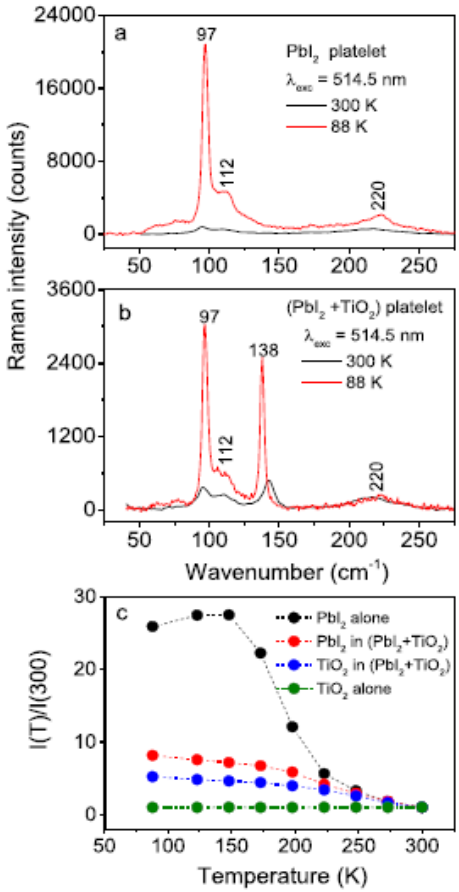

Fig. 3. (a) Raman spectra at 300K (black curves) and 88K (red curves) under excitation light of 514.5 nm in (a) PbI_2 and (b) the PbI_2/TiO_2powders mixture. (c) The ratio I(T)/I(300K) between the relative intensities of the Raman lines peaked at 97cm^{-1} (PbI_2 alone and PbI_2 in PbI_2/TiO_2 mixture) and 138 cm^{-1} (Si alone and Si in PbI_2/TiO_2 mixture), for a T range of 88–300K.

Based on a convenient energy difference between the levels of the conduction (CB) and valence bands (VB), a charge transfer mechanism was predicted, when the electrons migrate from the CB levels of PbI_2 and CdS directly to the CB levels of TiO_2 and/or Si. Therefore, this phenomenon leads to a decrease in the intensities of the Raman lines of the PbI_2 and CdS semiconductors and an increase of the TiO_2 and Si Raman lines intensities. An example is presented in Fig. 3 for PbI_2/TiO_2 mixture.

In condition of resonant excitation wavelength for PbI_2 (514.5 nm), one observed that the intensity of the vibrational mode of PbI_2 in PbI_2/TiO_2 mixtures decreases 7 times compared to the pristine PbI_2 relative intensity (Figs. 3a and 3b). Due to the charge transfer from CB of PbI_2 to the CB of TiO_2, the Raman mode of TiO_2 (blue curve) is enhanced compared with the case when TiO_2 pristine is optically excited (green curve). The behavior is evaluated by the ratio of the relative Raman intensities I(T)/I(300K) recorded at T and 300K (Fig. 3c). Since the excitation wavelength is higher than the electronic band gap of TiO_2 (377 nm), the Raman enhancement for TiO_2 in mixture is associated to a nonlinear optical effect, such as the SRS process, involving two optical fields, i.e. the incident laser light and the excitonic PL light of PbI_2.

References

[1] A. Nila, M. Baibarac, A. Matea, R. Mitran, I. Baltog, Exciton–phonon interactions in the Cs3Bi2I9 crystal structure revealed by Raman spectroscopic studies, 254, 1552805 (2017)

[2] A. Nila, A. Matea, M. Baibarac, I. Baltog, The exciton–phonon interaction as stimulated Raman scattering effect supported by the excitonic photoluminescence in BiI3 layered crystal structure, Journal of Luminescence, 182, 166 (2017)

[3] A. Nila, I. Baltog, D. Dragoman, M. Baibarac, I. Mercioniu, Influence of TiO2 and Si on the exciton-phonon interaction in PbI2 and CdS semiconductors evidenced by Raman spectroscopy, Journal of Physics-Condensed Matter, 29, 365702, 2017.

Intriguing magnetic behaviour of specific nanoparticulate systems

A. Stanciu, G. Schinteie, A. Kuncser, A. Leca, G. Filoti, P. Palade, S. Greculeasa, A. Catrina, C. Plapcianu, I. Mercioniu, C. Comanescu, V. Kuncser

National Institute of Materials Physics

in cooperation with

R. Vidu

University of California, 3123 Bainer Hall, Davis, California 95616, United States

A wide variety of nanoparticulate magnetic systems, as for example diluted magnetic oxides (DMO), iron-based granular thin films, hydrogenated steels and iron nitrides can be used in spintronics, sensoristics, magnetic storage, nuclear fusion technology, as well as for obtaining permanent magnets.

The diluted magnetic oxides chosen for the present study are TiO_2 nanoparticles, un-doped and doped with Fe. The un-doped nanoparticles and their Fe-doped counterparts (up to 12 at. % Fe, resulting in sample S12) were obtained by laser pyrolysis (in collaboration).

In the diluted magnetic oxides case, stable structures of anatase and rutile were evidenced together with either dispersed or agglomerated very fine Fe clusters in Fe doped samples. The simultaneous presence of anti- and ferromagnetic phases both in un-doped and doped TiO_2 nanomaterials pleads for the specific role of morpho-structural aspects influencing the type of magnetic defects and of surface distributed iron entities. ^{57}Fe Mössbauer spectroscopy data, give evidence for a bimodal size distribution of Fe based clusters: very fine ones consisting of single/a few Fe^{3+} ions with paramagnetic behaviour already at 5 K and larger ones with superparamagnetic behaviour above 50 K (Fig.1.). According to the calculated number of effective magnetic moments belonging to Fe^{3+} ions, as resulting from high sensitivity SQUID magnetometry data, the larger clusters consist in a few hundreds of Fe^{3+} ions which are antiferromagnetically coupled. A ferromagnetic phase persisting also above 400 K has been observed in these nanoparticulate systems, as specific to the diluted magnetic oxide case. Moreover, an interfacial coupling between the long range ferromagnetic phase and the antiferromagnetic clusters has been evidenced, giving rise to exchange bias fields and increased coercivity above the blocking temperature of the unidirectional anisotropy. Such interfacial coupling studied for the first time in nanoparticulate DMO systems [1] can be tuned by controlling the density and size of Fe oxide clusters at the surface of larger TiO2 nanoparticles. This feature opens new possibilities for applications, as for example the magnetic actuation of different DMO systems with catalytic activity.

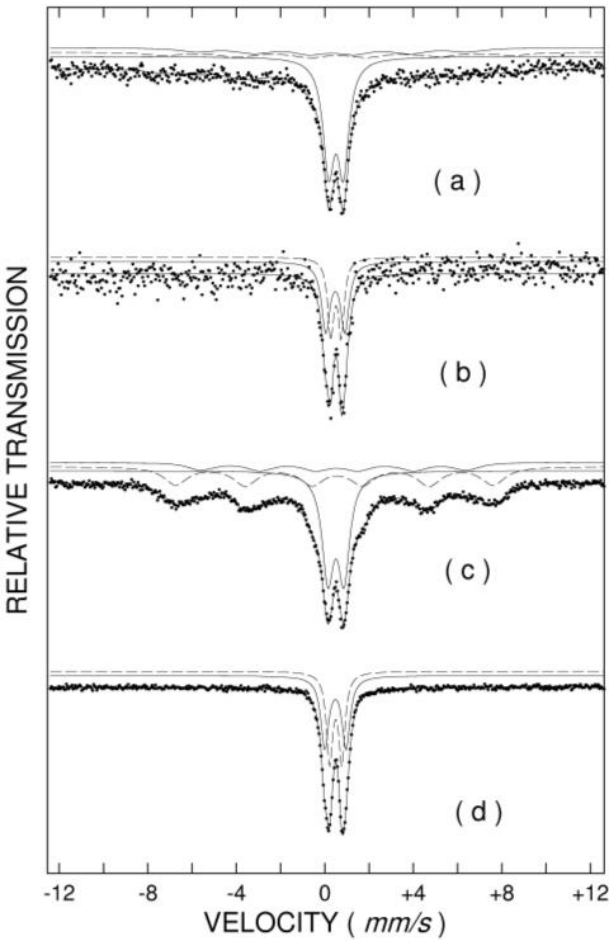

Fig. 1 Mössbauer spectra of iron doped sample: a) S6 at 5 K, b) S6 at 50 K, c) S12 at 5 K, d) S12 at 50 K.

The granular films were prepared by RF sputtering co-deposition from Fe and Au targets in Ar atmosphere (11.2 mbar). In what concerns

such Fe–Au nano-granular thin films [2], we observed different organizations of metallic Fe particles with similar size, depending on the preparation conditions corresponding to different Fe concentrations in the Au metallic matrix. Magnetic measurements revealed a magnetic order with strong texture effects in the sample of higher Fe concentration (30 at.% of Fe) and superparamagnetic behaviour in the case of the sample with lower Fe concentration (15 at.% of Fe). The observed in-plane uniaxial anisotropy in the sample of higher Fe concentration (Fe30) is explained via α-Fe precipitates assembled in lamellar structures as supported by corroborating STEM-DF imaging with MOKE and CEMS result. The superparamagnetic behaviour of the sample with a lower Fe concentration (Fe15) is related to well-dispersed and randomly distributed superparamagnetic α-Fe precipitates. To note that the cluster average size is similar in the two cases, but the ordered structure of the first case impose strong interparticle interactions leading to a blocked magnetic regime. As a result of the different magnetic behaviour of the two samples, also the MR effects observed in different measurement geometries are different, depending on the inter-particle interaction and hence, on the specific organization of the magnetic clusters in the Au matrix [2].

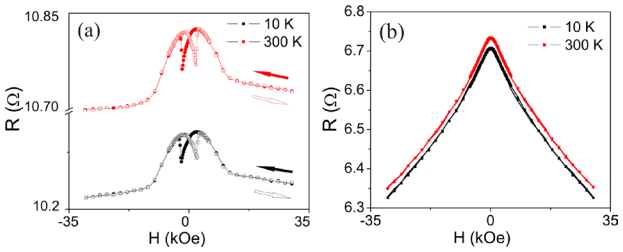

Fig. 2 Magnetic field dependence of resistance at 10 K (black points) and 300 K (red points) in perpendicular geometry for Fe30 (a) and Fe15 (b). In (a), empty symbols are used for increasing fields.

Structural parameters of the as prepared EU sample are close to the **bcc** phase, whereas the EDS data infer an average alloy composition for $Fe_{0.9}Cr_{0.1}$. After the hydrogenation treatments, the degree of oxidation at the Eurofer surface is considerably reduced. A depth dependent composition in the first 100 nm, with Cr content increasing toward the surface, can be considered. The main observations of practical interest is that the hydrogenation treatments reduce the oxidation and increase the expulsion of the Cr atoms toward the surface layer with considerable influence on the local composition and atomic configurations of the steel in the vicinity of the surface. The hydrogenation treatment is therefore proposed as a potential alternative for a convenient engineering of the surface of different Fe-Cr based alloys [3].

Suitable precursors for the synthesis of α"-$Fe_{16}N_2$ were produced using both an inexpensive experimental set-up and environment friendly raw materials. A microwave assisted process of preparing α"-$Fe_{16}N_2$ powders starting from a mixture of iron nitrate and urea solutions was used. Using the amorphous hematite obtained via microwave route, $Fe_{16}N_2$ fine particles were obtained by reducing in 5% H_2/Ar gas flow, followed by long time nitridation in NH_3 flow at temperatures below 200 ^{0}C. Depending on nitridation temperature, at 130 ^{0}C more bcc Fe phase is formed than α"-$Fe_{16}N_2$ and above 150 ^{0}C an increasing amount of Fe_3N and Fe_4N occurs by rising nitridation temperature, with detrimental effect on the magnetic properties. Besides crystalline phases, 10% superparamagnetic iron oxide is observed. After nitridation, the grains remain well separated with sizes in the range of 50÷100 nm. Rietveld refinements of XRD data show that crystallite sizes of α"-$Fe_{16}N_2$ and bcc Fe increase with nitridation temperature, but the lattice parameters do not change significantly. The crystallite sizes of Fe_4N and Fe_3N are much smaller than those of $Fe_{16}N_2$ and bcc Fe. The amount of phases obtained via Rietveld refinements are in good agreement with the Mössbauer spectroscopy results. We estimated that $Fe_{16}N_2$ prepared by this method has a convenient saturation magnetization and coercive field (M_s=222 emu/g at 25 ^{0}C and H_C= 40 kOe), as suitable for permanent magnet behavior [4].

References

[1] V. Kuncser, G.Schinteie, A. Kuncser, A.Leca et al., J.Phys. Chem. C, 121, 9063 (2017)

[2] A. Stanciu, A.Kuncser, G.Schinteie, P.Palade et al., J.Phys. D-Appl. Phys. 50, 275004 (2017)

[3] S.G.Greculeasa, P.Palade, G. Schinteie et al., Appl.Surf. Sci. 402, 114 (2017)

[4] P. Palade, C.Comanescu et al., Ind. and Eng. Chem. Res. 56, 2958 (2017)

New insight about the microstructure and formation mechanism of ion tracks in CaF_2 by conventional and aberration-corrected electron microscopy

C. Ghica, R. F. Negrea

National Institute of Materials Physics

in collaboration with

M. Karlušić, Z. Siketić, M. Jakšić, S. Fazinić

Ruđer Bošković Institute, 10000 Zagreb, Croatia

M. Schleberger,

Universität Duisburg-Essen, D-47048 Duisburg, Germany

The effect of swift heavy ions (SHI) on materials raises an increasing interest in the context of nowadays applications and technological challenges in micro and nanotechnology, fabrication of radiation detectors, hadron therapy or radiation waste storage. In this work, SHI-induced ion tracks in CaF_2 have been investigated by complementary techniques of conventional and aberration-corrected transmission electron microscopy (TEM) in an attempt to explain issues of the formation mechanism, energy threshold and atomic structure within the ion track [1].

SHI irradiations were performed at the Ruđer Bošković Institute (RBI) using a Van de Graaff accelerator. Iodine ions with energies of 10, 15 and 23 MeV were used to irradiate CaF_2 crystal grains previously deposited onto TEM grids.

The SHI irradiation effects could only be revealed for high values of objective lens defocus, either underfocus (df<0) or overfocus (df>0), knowing that for the TEM images obtained in the diffraction contrast mode, the features exhibiting a bright Fresnel fringe correspond to regions in the sample with lower density than the surrounding matrix (e.g. voids), with an opposite behaviour on overfocus. When observing the irradiated crystal grains in no-tilt or slightly tilted orientation, the ion tracks are imaged as doublets of bright dots. The TEM images obtained in underfocus and overfocus conditions after tilting the specimen in the microscope reveal a certain structuring of the irradiation tracks along their trajectory. They show a contrast modulation with 2-4 maxima along their length (Fig. 1).

Even in low-beam conditions, the prolonged observation in the TEM of the SHI irradiated CaF_2 sample leads to the formation of two additional kinds of defects apart from the irradiation tracks: (i) aggregated defects (voids) sometimes organised in periodic arrays and (ii) dislocation loops located in the (111) planes.

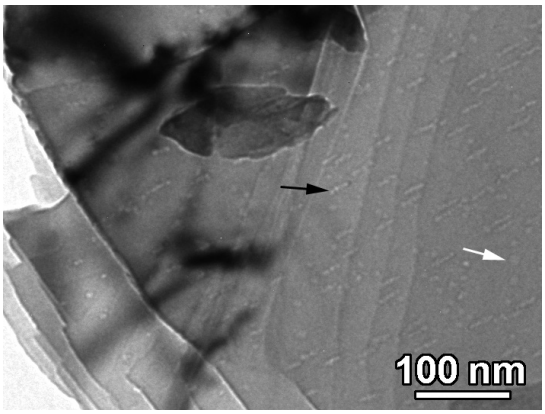

Fig.1. TEM image of a tilted CaF_2 grain containing irradiation tracks (black arrow) and an array of e-beam induced voids (white arrow).

Measuring the ion track size on the basis of conventional TEM images is subjected to at least two sources of error: the value of the objective lens defocus (Fig. 2) and the duration of sample examination under the e-beam. One way of eliminating this uncertainty is working in STEM mode on an aberration-corrected instrument. This insures a reduced e-beam irradiation and a lower impact in terms of sample damage, while improving the precision in measuring the size of nanometric objects by employing a different contrast mechanism.

The STEM measured ion tracks size is in the range of 3-4 nm, as displayed by the intensity profile in Fig.3.

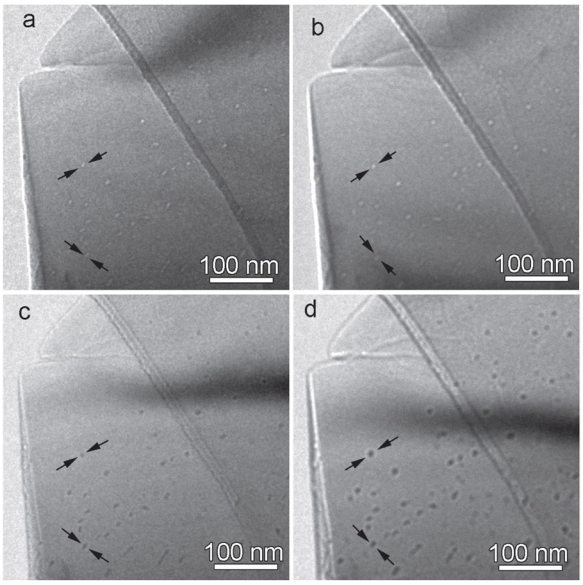

Fig. 2. Through-focus TEM image series provide different results in measuring the size of the same ion tracks: (a) $\Delta f_1<0$; (b) $\Delta f_2<0$, $|\Delta f_1|<|\Delta f_2|$; (c) $\Delta f_3>0$; (d) $\Delta f_4>0$, $\Delta f_4>\Delta f_3$.

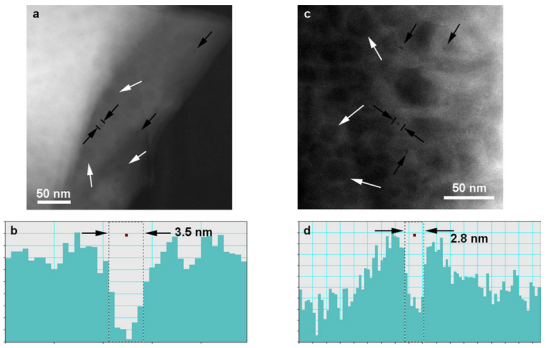

Fig. 3. STEM ADF images (a), (c) of a CaF_2 grain containing irradiation tracks (black arrows) and e-beam induced defects (white arrows). Intensity line profiles across the irradiation tracks (b), (d).

The irradiation effect on the local chemical composition has been evidenced by STEM-EELS spectrum imaging (Fig. 4). By corroborating the information from TEM, STEM and STEM-EELS spectrum imaging we have shown for the first time that:

i. The observed ion irradiation tracks consist of rows of nano-voids (lower Ca signal in the EELS elemental maps) where F may be trapped in gaseous state (higher F signal in the EELS elemental maps).

ii. The e-beam induced defects consist in nanometric volumes where CaF_2 dissociates with the formation of Ca-rich nanometric pockets. The mass density of Ca (1.54 g/cm^3) is lower than the one of CaF_2 (3.18 g/cm^3), which explains the void-like behaviour of the e-beam induced defects.

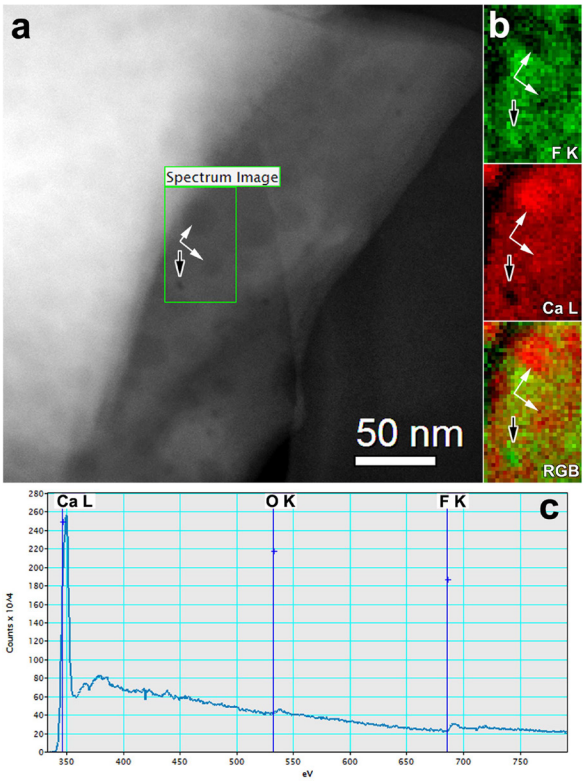

Fig. 4. (a) STEM–ADF image of a CaF_2 grain containing ion tracks and e-beam induced defects. (b) Elemental maps and composed RGB image inside the green rectangle illustrating the local content of F and Ca; (c) EEL spectrum corresponding to the marked area showing the absorption edges of Ca, F and O.

This work has been funded from the Core Project PN16-480102 in the frame of an international collaboration within the CERIC-ERIC consortium.

References

[1] M. Karlušić, C. Ghica, R. F. Negrea, Z. Siketić, M. Jakšić, M. Schleberger and S. Fazinić

New Journal of Physics 19, 023023 (2017)

Specific properties of Ni-Fe-Ga magnetic Heusler alloys

F. Tolea, M. Valeanu, M. Tolea, M. Sofronie, B. Popescu, A. Crisan, A. Leca

National Institute of Materials Physics

The wide scientific interest and promising applicative potential of Heusler type Ferromagnetic Shape Memory Alloys (FSMA) is owed to the fact that such materials feature both a magnetic order-disorder transition and a first order structural one, namely the so called Martensitic Transformation (MT). The MT takes place between a high-temperature, higher-symmetry austenite phase to a low-temperature, lower-symmetry martensite phase by shifting atoms on a small distance compared to the inter-atomic distances. Recent research indicated the off-stoichiometric Ni-Fe-Ga alloys as good candidates to replace the brittle Ni-Mn-Ga due to improved mechanical durability when experiencing a reversible austenite-martensite transformation. In magnetic alloys, the magnetoresistance (MR) reflects the resistivity change due to the reduction in magnetic disorder caused by an applied magnetic field at a given temperature. For a ferromagnetic material, one expects a negative MR having a peak at Tc and going to zero at very low temperatures. Numerous substitutions have been tested on Ni-Fe-Ga alloys in order to increase the Curie temperature, magneto-crystalline anisotropy or the mechanical properties, which motivated our studies**.** The influence of Cu, Co, and Al substitutions on the transport properties, and in particular, the magnetoresistive effect in Ni-Fe-Ga ferromagnetic shape memory alloys (FSMAs) prepared as ribbons by melt spinning method and subjected to different thermal treatments (10 minutes at 400°C (TT1) and 20 minutes at 800°C (TT2) followed by rapid cooling) was investigated. All tested compositions showed reversible thermo-elastic transformations[2]. The nominal composition of alloys are: $Ni_{52}Fe_{20}Co_2Ga_{26}$ and $Ni_{52}Fe_{20}Co_2Ga_{23}Al_3$, $Ni_{52}Fe_{20}Co_3Ga_{23}Al_2$, $Ni_{50}Fe_{22}Ga_{25}Co_3$, $Ni_{50}Fe_{20}Ga_{27}Cu_3$, denoted Co2, Co2Al3, Co3Al2, Ni50Co3 and respectively Ni50Cu3. The segregation and growth of a secondary γ phase contribute essentially to the decrease of the MT temperature. Higher magnetization at lower temperatures and residual magnetization observed at temperatures higher than Tc are also an effect of the γ phase precipitation. The main properties of analyzed samples are shown in Table I.

TABLE I
THE MT CHARACTERISTICS

Sample	T_M//T_A//Tc (K)	Q (J/g)	Max. value of MR% at 50 kOe on
Co2Al3AQ	248//262//350	2.5	Max -4.8 on Tc
Co2Al3TT1	244//259//365	2.74	Max -5.2 on Tc
Co2Al3TT2	160//180//347	0.2	Max -5 on Tc
Co3Al2AQ	335//360//385	2	Max -5.3 on MT and Tc
Co3Al2TT1	326//351//395	2.2	Max -5.5 on Tc
Co3Al2TT2	145//158//365	0.42	Max -4.3 on Tc
Ni50Co3AQ	299//323//>400	3.0	Max -5.5 on Tc
Ni50Co3TT1	283//288//>400	3.4	Probably on Tc
Ni50Co3TT2	215//240//370	2	-
Ni50Cu3AQ	131//147//316	1.6	Max -9 at T_A
Ni50Cu3TT1	146//159//330	1.5	Max -9 at 25K
Ni50Cu3TT2	167//177//320	0.87	-

DSC peak transformation temperatures (T_M and T_A for the direct and reverse MT respectively), the Curie temperature Tc and the average transformation heat Q (calculated as average between the direct and reverse transformation) for studied samples as-quenched (AQ) and thermal treated ribbons (TT1 and TT2). On the last column we give the maximum value of the MR for some compositions, and where they are reached - see discussion in text.

To characterize the magnetoresistance we actually measured the variation of the resistivity in zero and 5T magnetic fields (Fig. 1a) for a large temperature range (100K-400K) for the AQ and annealed ribbons. The temperature dependence of the resistivity curves shows an hysteretic anomaly at MT for Co3Al2 alloy.

Magnetoresistance was calculated using the formula:

$$MR = \frac{\rho(H) - \rho(0)}{\rho(0)},$$

Fig.1 b), c), and d) reveals the behavior of MR

for Co3Al2 ribbons. MR reach a maximum (in module) value for AQ, TT1 and TT2 samples at the Curie temperature, because of the charge carriers scattering by magnetic fluctuations at temperatures close to Tc. Also, temperature dependence of MR shows a hysteresis corresponding to MT.

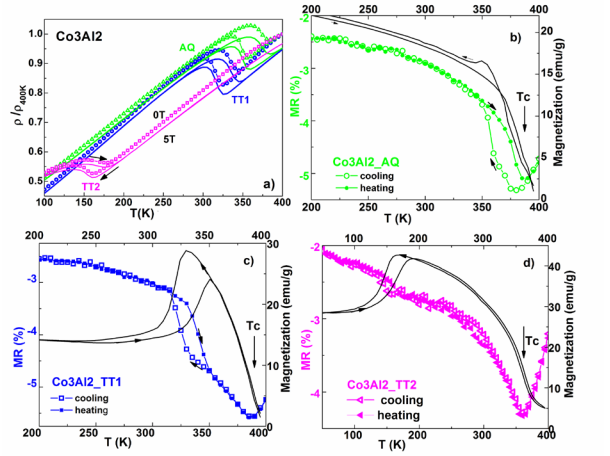

Fig. 1. a) The temperature dependence of resistivity curves. The curve represented with empty symbols corresponds to the resistivity dependence without applied magnetic field; continuous line – under 5T applied field. b) Temperature variation of MR and the MT reflected by the thermo-magnetic scans at 200 Oe applied magnetic fields on Co3Al2 ribbons AQ. c) the same for Co3Al2 ribbons TT1. d)) the same for Co3Al2 ribbons TT2.

The technological processing route - rapid solidification and subsequent thermal annealing - induce structural transitions of the ferromagnetic matrix which modify the local magnetic disorder. The type and degree of local disorder are specific for each alloy and there is not a unique rule regarding the evolution of MR in the different FSMA compounds / phases, but rather a rich spectrum of different behavior :

In the range of the martensitic transformation (MT), different FSMA compositions show a rich spectrum of different behaviors. From the studied compositions, the highest MR found on the MT of -9% for 5 T is for Ni50Fe20Ga27Cu3. As a general trend the MR is negative in the temperature range up to Tc and its value rise with the temperature and has a maximum at Tc.

Shape memory alloys are known to memorize one -or several-temperatures at which the MT transformation was stopped before completion in the past, the memory manifesting as specific dips in subsequent calorimetric scans [2]. Previous studies have shown that this memory can be erased by heating to **higher** temperatures than the ones previously recorded. We have studied a distinct memory fading effect which takes place by heating to a **lower** temperature. This effect is reported, for first time in literature, in NiFeGa as polycrystalline ribbons, the alloy being initially studied as bulk for which the thermal memory effect was not found. If, after an initial incomplete heating up to T_1 one performs a second incomplete heating up to $T_2 < T_1$, a new calorimetric dip appears at T_2, as expected, while less expected was that the dip corresponding to T_1 reduces in amplitude or even vanishes (if the arrest at T_2 is repeated). The memory fading effect is more clear for small differences T-1-T-2 and less obvious or absent for large ones. The second part of [2] employs a statistical 2D model, which supports the memory fading effect.

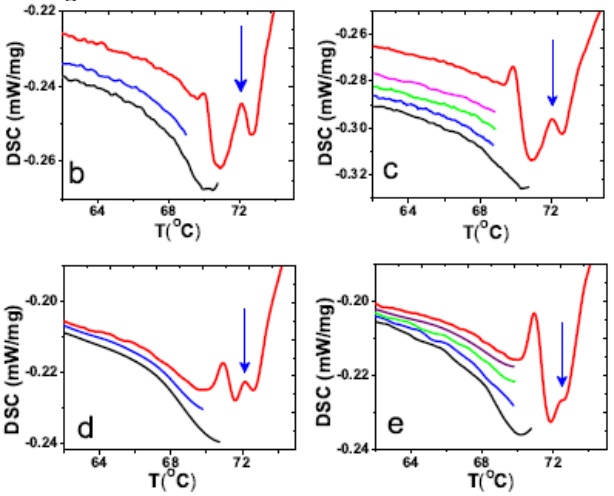

Fig. 2. Complete DSC scans (red curves) corresponding to the martensite-austenite phase transition in NiFeGa ribbons, recorded after one or several incomplete scans (curves with other colors then red): (up left) one arrest at T_1 and one at T_2 = 69°C, (up right) one arrest at T_1 and three at T_2, (down left) one arrest at T_1 and one at T_3 = 70°C, (down right) one arrest at T_1 and three at T_3.The blue arrows indicate the position of the dips associated with T_1.

Authors acknowledge “Core Program”- PN16-480103, 2016-2017.

References

[1] F. Tolea, M. Tolea, M. Sofronie, B. Popescu, A. Crisan, A. Leca, M. Valeanu, IEEE Transac. on Magn., 53, 4400307 (2017)

[2] F. Tolea, M. Tolea, M. Valeanu, Soild State Comm., 257, 36-41, (2017

[3] F. Tolea, M. Tolea, Physica E 85, 169-173 (2017)

Spectro-microscopic follow-up of Auger induced surface dissociation of ferroelectric lead zirco-titanate

L.E. Abramiuc, L.C. Tănase, N.G. Apostol, C. Chirilă, L. Trupină, L. Pintilie, C.M. Teodorescu
National Institute of Materials Physics
in collaboration with
A. Barinov, Elettra Sincrotrone Trieste, S.S. 14 - km 163,5, 34149 Basovizza, Trieste, Italy

The ability of ferroelectric perovskites to be used in photovoltaic applications due to the hypothetical existence of strong internal fields may be hindered by the possible photo-degradation of the material under irradiation. We analysed surface decomposition of a 50 nm thick PZT(001) film by photoelectron spectro-microscopy with sub–mm lateral resolution, using soft X-rays of 74 eV photon energy.

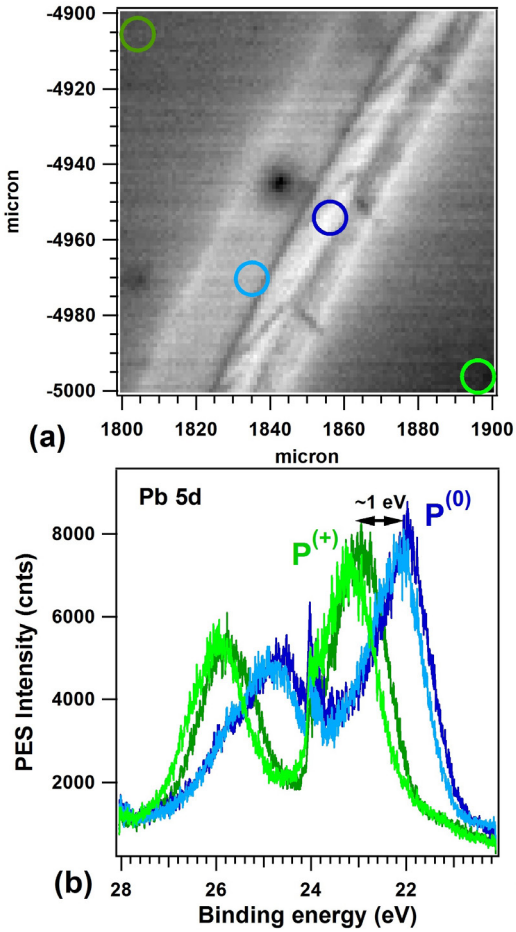

Fig. 1 (a) Total photo-emitted intensity map between 24 and 28 eV binding energy. (b) spectra obtained from "bright" and "dark" areas, (blue and green colours, respectively), corresponding to leading contributions of null out-of-plane polarization $P^{(0)}$ and outwards polarization $P^{(+)}$. Adapted from [3].

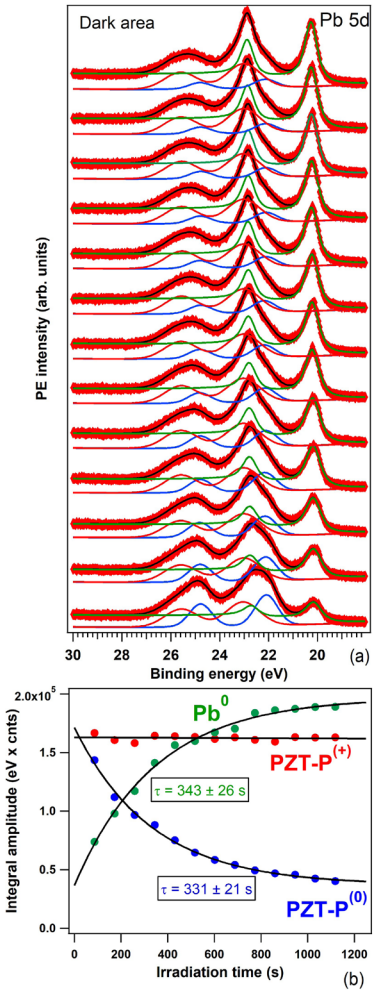

Fig. 2 (a) XPS recorded successively on an area of a 50 nm PZT(001) film presenting initial states with $P^{(+)}$and $P^{(0)}$. (b) Time evolution of components corresponding to different polarization states. Adapted from [3].

The ability of this method to quantify areas with different out-of-plane polarization through binding energy contrast was certified a few years ago [1,2]; an additional proof is given in Fig. 1, where areas with different binding energy corresponding to different polarization states are easily identified.

The time evolution of XPS spectra recorded on different areas revealed surface decomposition, with formation of metal Pb.

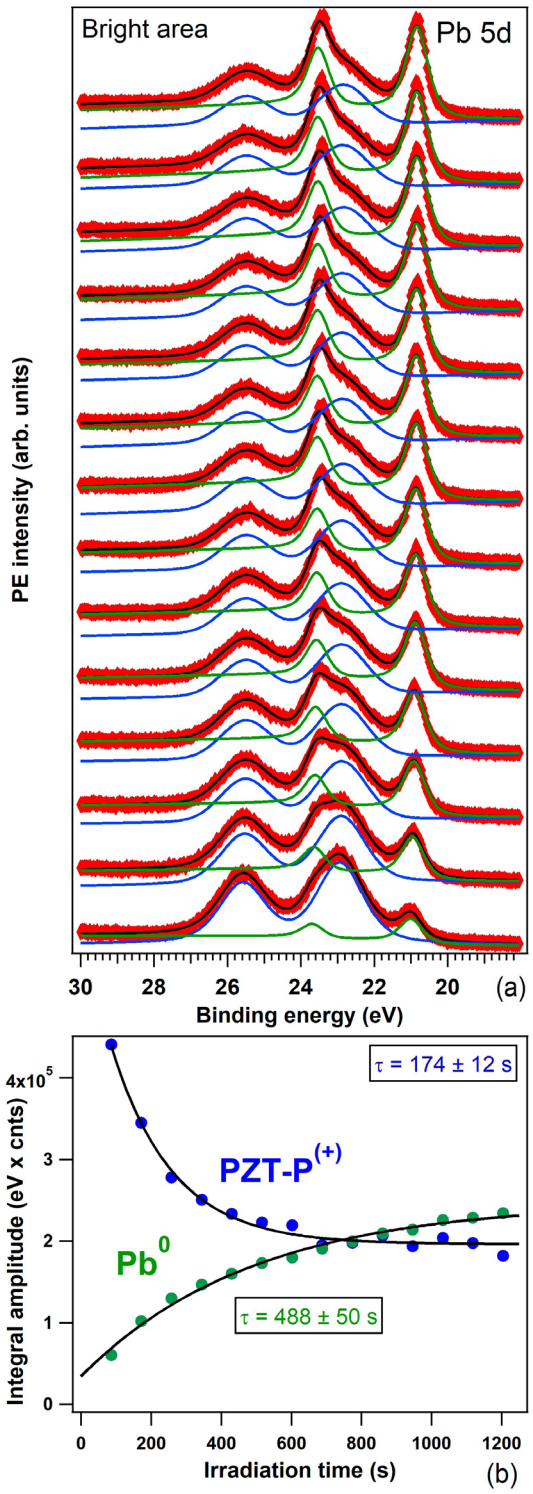

Fig. 3 Same as previous Figure, but for a microscopic area presenting only $P^{(+)}$ initially. Adapted from [3].

When initially $P^{(+)}$ and $P^{(0)}$ states coexisted, metal Pb is created on the expense of areas with $P^{(0)}$ polarization (Fig. 2), whereas when the investigated area is in the $P^{(+)}$ state, metal lead is created on the expense of this state (Fig. 3). Dissociation induced by secondary and Auger electrons for the $P^{(+)}$ state may be written as $e^- + PbO^+ \rightarrow PbO^* \rightarrow Pb + O$, while for the $P^{(0)}$ state it may be written as $e^- + PbO^0 \rightarrow (PbO^-)^* \rightarrow Pb + O^-$. The relative stability of the microscopic $P^{(+)}$ state with respect to the $P^{(0)}$ state is connected to the dissociation energy of PbO^0 (about 4 eV) higher than that of PbO^- (about 3.2 eV) [3]. The first is higher than the electron affinity of PZT, thus secondary electrons which might produce the dissociation leave the material; whereas, in the case of $P^{(0)}$, electrons able to produce the dissociation are able to travel longer inside the material. In the case of absence of neighbouring $P^{(0)}$ areas for a microscopic $P^{(+)}$ area, the potential energy outside the sample acts as an attractive potential for the secondary electrons, therefore they are confined near the surface; thus, these electrons can still induce dissociation. The same effect occurs also in the case of contaminants, where these molecules may scatter emitted electrons and contribute to their confinement near surface.

The mechanisms inferred from this study may be easily extended to the case of photoelectrons produced by absorption in the UV – visible range, thus ellucidating processes of relevance for photocatalytic and photovoltaic applications.

This work was funded by the Romanian Ministry of Research and Innovation through UEFISCDI Contract No. PN-II-RU-TE-2014-4-0456 and through the Core Program, Project No. PN16-480103/2016.

References

[1] D.G. Popescu, M.A. Huşanu, L. Trupină, L. Hrib, L. Pintilie, A. Barinov, S. Lizzit, P. Lacovig, C.M. Teodorescu, Phys. Chem. Chem. Phys. 17, 509-520 (2015).

[2] M.A. Huşanu, D.G. Popescu, C.A. Tache, N.G. Apostol, A. Barinov, S. Lizzit, P. Lacovig, C.M. Teodorescu, Appl. Surf. Sci. 352, 73-81 (2015).

[3] L.E. Abramiuc, L.C. Tănase, A. Barinov, N.G. Apostol, C. Chirilă, L. Trupină, L. Pintilie, C.M. Teodorescu, Nanoscale 9, 11055-11067 (2017).

Interplay between charge accumulation and ferroelectric polarization, determined by photoelectron spectroscopy and low energy electron diffraction

L.C. Tănase, N.G. Apostol, I.C. Bucur, L.E. Abramiuc, R.M. Costescu, G.A. Lungu, L.E. Abramiuc, N.G. Apostol, L. Hrib, C. Chirilă, L. Trupină, A.E. Bocîrnea, R.F. Negrea, L. Pintilie, C.M. Teodorescu

National Institute of Materials Physics

Ferroelectric thin films are nowadays synthesized with high crystallinity and well-defined stoichiometry on different homomorphic substrates. These films were

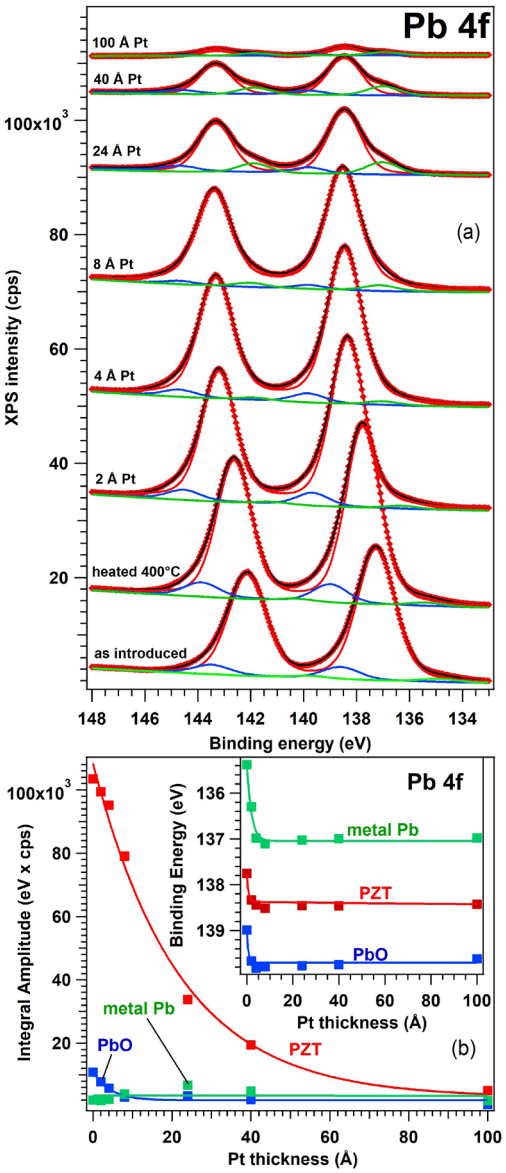

Fig. 1 Pb 4f XPS analysis of Pt/PZT(001): (a) evolution with Pt deposition; (b) derived amplitudes and binding energies (insert) from data analysis by curve fitting.

shown to exhibit, under a critical thickness of about 50 nm, single domain states with well defined out-of-plane polarization.

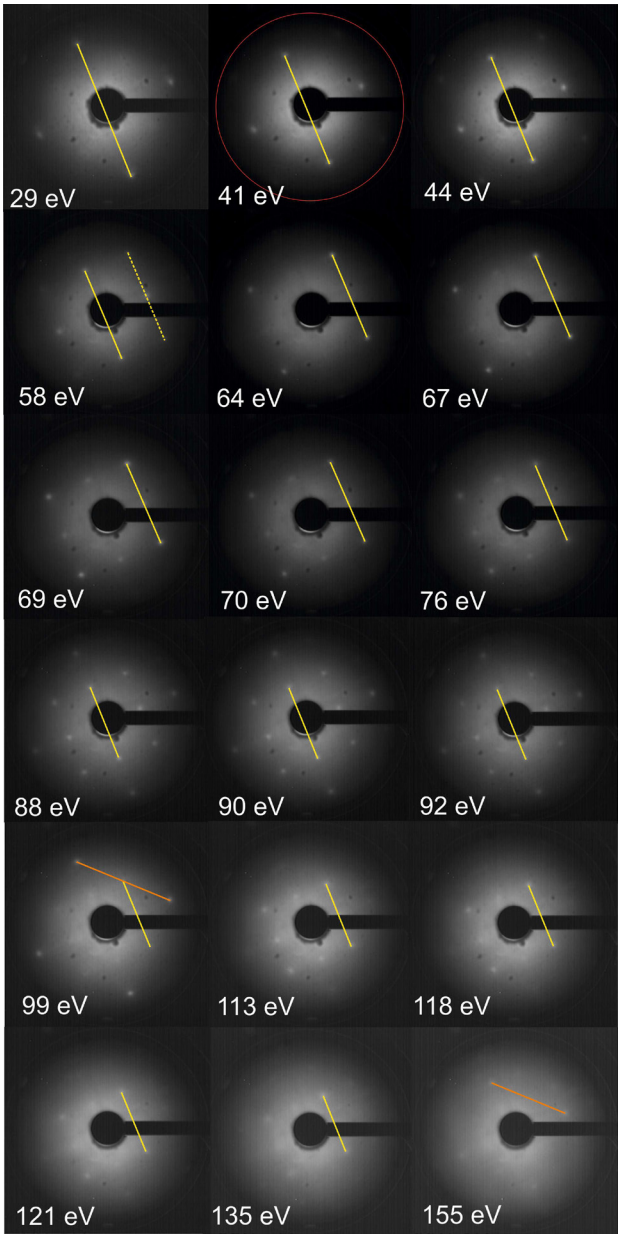

Fig. 2 LEED patterns for a 100 nm thick PZT(001) film grown on LSMO.

X-ray photoelectron spectroscopy (XPS) has shown the polarization orientation of these films. Owing to the combined effect of fixed charges due to the polarization and sheets of compensating charges, the outer layers from these films exhibit a depolarization field and

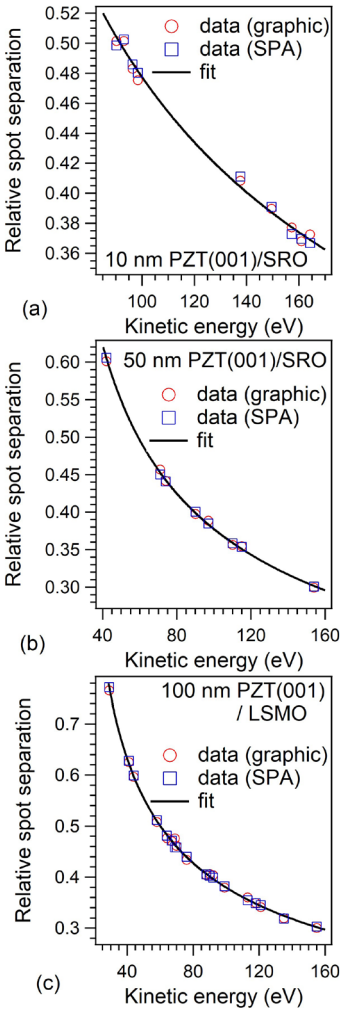

Fig. 3 Analysis of LEED spot positions for several samples vs. the electron kinetic energy. Adapted from [3].

henceforth the core levels from the surface layers are shifted with respect to that of the bulk [1]. As an example, in Fig. 1 we present an XPS investigation of PZT(001) film of relatively large thickness (150 nm), where initially there was no preferred orientation of polarization and it was shown that, by deposition of platinum, the outwards polarization $P^{(+)}$ might be induced, most probably since electrons injected by the metal are able to produce the depolarization charge sheet near surface (Fig. 1).

Another surface science technique which may be used to assess surface polarization is low energy electron diffraction (LEED), if the surface is clean and crystalline enough to provide such patterns. Recently, LEED may be routinely obtained on ferroelectric thin films grown by pulsed laser deposition. In Ref. [3] a formalism was developed to derive the outer surface potential from the position of the LEED spots (e. g. Fig. 2) at different electron kinetic energies. The result of this analysis by fitting with the formulas provided in [3] (Fig. 3) is that the outer surface potential (in the range of 5 to 9 eV) is considerably higher than the inner band bending due to the depolarization field (from 0.6 to 1 eV for PZT). In fact, the ratio between these values should have been considerably higher, of about (half of the dielectric constant of the material). This implies that the outer region of the ferroelectric sample has a considerably lower dielectric constant, in the range of about 30, which is by a factor of 5–6 lower than the material constant derived by macroscopic measurements. This is explained by the formation of a ‚dead layer' near surface in the ferroelectric. The existence of such ‚dead layers' was inferred from several theoretical works in ferroelectrics interfaced with metals, but no such data were reported before our work for free ferroelectric surfaces.

This work was funded by the Romanian Ministry of Research and Innovation through UEFISCDI Contract No. PN-II-RU-TE-2014-4-0456 and through the Core Program, Project No. PN16-480103/2016.

References

[1] L.C. Tănase, N.G. Apostol, L.E. Abramiuc, C.A. Tache, L. Hrib, L. Trupină, L. Pintilie, C.M. Teodorescu, Sci. Rep. 6, 35301 (2016).

[2] C.M. Teodorescu, L. Pintilie, N.G. Apostol, R.M. Costescu, G.A. Lungu, L. Hrib, L. Trupină, L.C. Tănase, I.C. Bucur, A.E. Bocîrnea, Phys. Rev. B 96, 115438 (2017).

[3] I.C. Bucur, L.C. Tănase, L.E. Abramiuc, G.A. Lungu, C. Chirilă, L. Trupină, N.G. Apostol, R.M. Costescu, L. Pintilie, C.M. Teodorescu, Appl. Surf. Sci. 432, 27-33 (2018).

Vibrational and photoluminescence properties of the composites based on macromolecular compounds and carbon nanoparticles of the type single-walled carbon nanotubes and reduced graphene oxide

M. Baibarac, A. Matea, M. Ilie, I. Smaranda, M. Dăescu

National Institute of Materials Physics

in cooperation with

Bernard Humbert, Jean-Yves Mevellec, Sophie Quillard, Serge Lefrant

Institut des Materiaux "Jean Rouxel", 2 rue de la Houssiniere, B. P. 32229, F-44322, Nantes, France

A special interest was given to the composite materials based on carbon nanoparticles for applications in the field of energy storage. In this context, the composite material poly(2,2'-bithiophene-co-pyrene) functiona-lized single-walled carbon nanotubes (SWNTs) was successfully used in the supercapacitory field, when a specific capacitance of 59 F g^{-1}, for a current density of 100 mA g^{-1}, was reported. [1] The developing of other applications in the optoelectronic field has involved a better knowledge of optical properties and in this context it is worth mentioning the recent progress concerning the anti-Stokes photoluminescence (PL) properties of the poly[(2,5-bisoctyloy)-1,4-phenylene viny-lene]/SWNTs composite. [2] In comparison with the above studies reported on composites based on macromolecular compounds and SWNTs as a mixture of semiconducting (33%) and metallic (66%) tubes (M+S-SWNTs), few information were found about the vibrational and PL properties of SWNTs highly separated in metallic (M-SWNTs, 98%) and semiconducting (S-SWNTs, 99%) tubes functionalized with insulating or conducting polymers. Therefore, in 2017, the influence of M-SWNTs and S-SWNTs on the vibrational and PL properties of different macromolecular compounds as poly (vinylidene fluoride) [3] and poly(ortho-phenylenevinylene) (POPV) [4] was studied. Focusing our attention on the POPV/SWNTs composite, we have demonstrated that by the electrochemical polymerization of α,α,α',α'-tetrabromo-o-xylene (TBOX) onto Au electrodes covered with M-SWNTs or S-SWNTs films, composite materials of the POPV type covalently functionalized with S-SWNTs, and POPV non-covalently functionalized with M-SWNTs were synthetized. [4] A POPV PL quenching process in the presence of M+S-SWNTs, M-SWNTs and S-SWNTs was reported to take place in the case of the tubes with chirality (14,7), (12,10) and (11,9), respectively. [4] Another carbon nanoparticle which plays the role of PL quenching of macromolecular compounds is reduced graphene oxide (RGO). Our studies have demonstrated that RGO was able to induce a PL quenching process of poly(para-phenylenevinylene) (PPV), in un-doped and doped state, when the macromolecular compound was prepared by the annealing conversion (AC) method of the PPV precursor solution at 300 ^{0}C and the electroreduction of α,α,α',α'-tetrabromo-p-xylene (TBPX) in the presence of a solution of 0.1 M tetrabuthyl ammonium bromide in DMF:H_2O, respectively. [5] According to Fig.1, the PL spectrum of PPV in un-doped state, obtained by the AC method, was characterized by a complex band at ~2.25 eV. [5] In the case of the samples resulted by the interaction of PPV in doped state with NH_4OH solution, four emission bands peaked at 2.42, 2.25, 2.1, and 1.96 eV were observed according to Fig. 2b. [5] The PL bands at 2.42 and 2.26 eV were assigned to the formation of PPV macromolecular chains (MCs) with lengths of 5 and 7–10 repeating units, respectively.[5 and its references] Similar changes were reported in the case of the PPV-pyrene/RGO composite synthetized by AC method. [6]

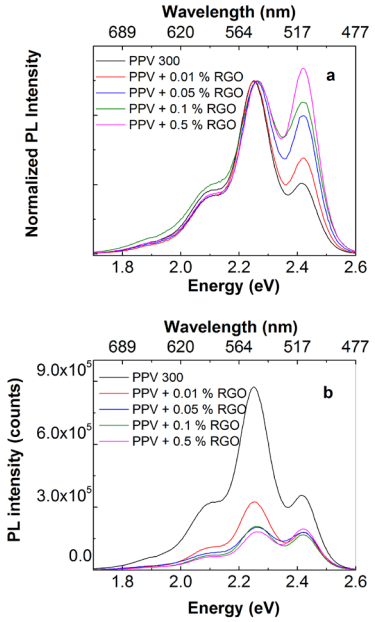

Fig.1 PL spectra in normalized (a) and normal scale (b) of the samples obtained by the AC method of PPV PS with different RGO weight percentage concentration: 0 wt.% (black curve), 0.01 wt.% (red curve), 0.05 wt.% (blue curve), 0.1 wt.% (green curve) and 0.5 wt.% (magenta curve) [5]

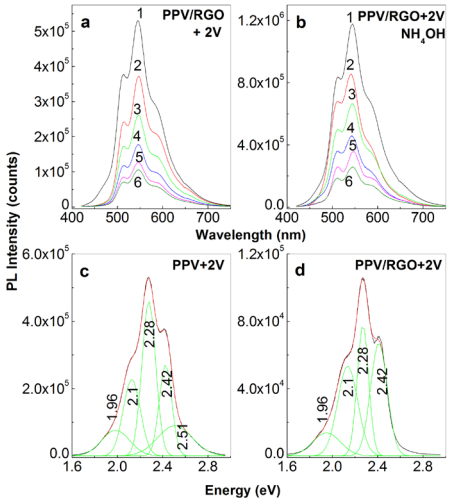

Fig.2 (a) The PL spectra of the PPV films electrochemical synthesized in the absence and the presence of different RGO weight percentage concentrations, i.e. 0.01 wt.% (curve 2), 0.025 wt.% (curve 3), 0.05 wt.% (curve 4), 0.1 wt.% (curve 5), and 0.5 wt.% (curve 6). Fig. (b) shows the PL spectra of above films, chemically interacted with the 1 M NH_4OH solution. [5] Fig. c and d show de-convolution of PL spectra of PPV and the PPV/RGO composite.

An assessment of the wrapping angle of RGO sheets with PPV in un-doped and doped state was performed by the anisotropic PL studies. [5] The wrapping angle of RGO sheets with PPV MCs (q_{PL}), via the p–p* interactions between the phenyl groups of PPV in un-doped state and the RGO sheets, was demonstrated to vary from 12^0 to 31^0 when the RGO weight percentage concentration was changed from 0 to 0.5 wt.%, respectively. [5]

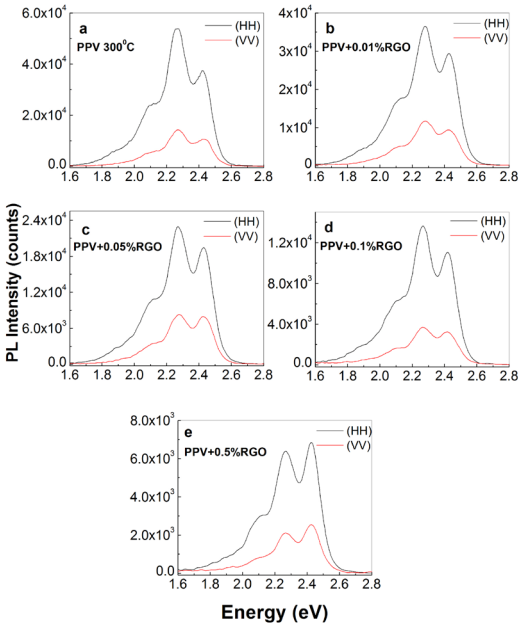

Fig.3 The polarized PL spectra (l_{exc} = 440 nm) of the films deposited on Au supports, resulting from the AC at 300 ^{0}C of the PPV PS with different RGO weight percentage concentrations of: 0 wt.% (a), 0.01 wt.% (b), 0.05 wt.% (c), 0.1 wt.% (d), and 0.5 wt.% (e). [5]

References

[1] M. Baibarac, I. Baltog, M. Dăescu, Int. J. Electrochem. Sci., 12 (3): 2013, (2017)

[2] M. Baibarac, I. Smaranda, I. Baltog, S. Lefrant, J.Y. Mevellec, Opt. Mat., 67: 52, (2017)

[3] A. Matea, M. Baibarac, I. Baltog, J. Mol. Struct., 1130: 38, (2017)

[4] M. Baibarac, A. Nilă, I. Baltog, S. Lefrant, J.Y. Mevellec, S. Quillard, B. Humbert, Eur. Polym. J., 88: 109, (2017)

[5] M. Baibarac, M. Ilie, I. Baltog, S. Lefrant, B. Humbert, RSC Adv. 7: 6931, (2017)

[6] M. Ilie, M. Baibarac, Opt. Mater., 72: 140, (2017)

Hund and anti-Hund rules in circular molecules

M. Nita, M. Tolea, C. Marinescu, A. Manolescu
National Institute of Materials Physics

The aplicability of Hund's first rule in systems beyond atomic physics raised a high interest due to the fundamental implications regarding the mechanisms of spins alignment [1,2,3].

In the present study, published in [4], we study the Hund's rule in circular molecules (see Fig.1, upper part) with an arbitrary number of atoms (N). The single-particle spectrum of such molecules shows a ladder of double degenerated electronic states (see Fig.1, lower part), on which the top-most two electrons can accomodate either as a triplet (Hund rule) or as a singlet (anti-Hund rule). Therefore, the highest quantity of interest is in the difference between the energies of the lowest Singlet (from the subspace with Sz=0) and lowest Triplet (from the subspace with Sz=1):

$$\Delta E = E_0 - E_1 \tag{1}$$

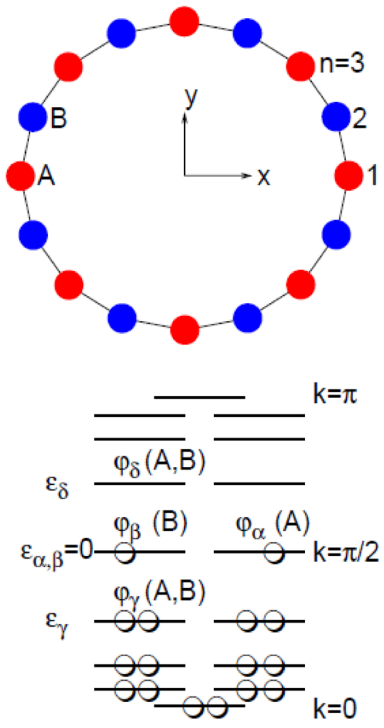

Fig. 1 (up) The circular molecule with Ns = 16. (down) The single particle eigenstates are represented by horizontal lines, while the circles indicate occupied states, in this case half-filling, a particular case for which the Hund rule is not obeyed and our calculations indicate a singlet ground state. For other filling cases, the ground state can be either singlet or triplet, as discussed in text.

In our theoretical description of the molecules, we consider the extended Hubbard model by including also a long-range interaction potential. The interaction term between two electrons located in the sites "n" and "m" is:

$$V_{nm} = \frac{V_L}{|r_n - r_m|}(1 - \delta_{nm}) + U_H \delta_{nm} \tag{2}$$

The first term from the r.h.s. standing for the long range interaction and the second for the short range one (both electrons on the same site). Calculations will be done by considering a perturbative approach in the interaction strength (the starting point being the non-interacting ground state). In the first order of the perturbation theory, the energy difference in Eq.1 is directly given by the so-called exchange energy, and only in the case when this exchange energy vanishes one must proceed to the second order of perturbation.

Our main results can be grouped in 2 categories:

(i) This is actually an "exception", or better said, a particular case, depicted also in Fig.1. For N=4N' (multiple of 4 atoms in molecule), and at precisely half-filling (N electrons), our calculations indicate that the singlet is always the ground state. Thus we have an anti-Hund situation regardless of the interaction strength (provided that the perturbative approach remains valid). The result is obtained in the second order of perturbation, as the exchange interaction vanishes. This cancellation of the exchange interaction, the origin for the Hund rule violation, is owed to the fact that the mid-spectrum states are disjoined (see [4] and also Fig.1: the two mid spectrum eigenstates are located one on the "red" sites and the other one on the "blue" ones). Our formula for ΔE reads (for

symbols definitions see [4]):

$$\Delta E = -\frac{2(V(\pi/2))^2}{|\varepsilon_0|} - \sum_q \frac{(V(q)-V(\pi-q))^2}{|\epsilon_{\frac{\pi}{2}}-q|} \quad (3)$$

(ii) For all the other cases except for the one presented at (i), the exchange energy does not vanish, and its sign directly indicates the singlet or triplet ground state (i.e. anti-Hund or Hund rule); moreover, the exchange energy can be directly expressed in terms of the Fourier transform of the interaction potential (noted by us as the "V" function)[4]:

$$\Delta E = V(2k_0) \quad (4)$$

Furthermore, after some straightforward manipulation, it can be shown that the "V" function can be expressed as:

$$V(k) = \frac{U_H}{N_S} + \frac{V_L}{N_S}\sum_{n=1}^{N_S-1}\frac{\cos kn}{R_n} \quad (5)$$

The full technical details are given in [4], here we only gave the formula to draw attention that, while all constants involved are positive, the second term can have a "-" sign due to the summation over the cosine functions - case in which, depending also on the ratio V_L/U_H, the sign of V(k) can ~~be~~ in principle be negative, meaning the singlet ground state and an anti-Hund rule. For this, is instructive to plot the second term of Eq.5 (see Fig.2).

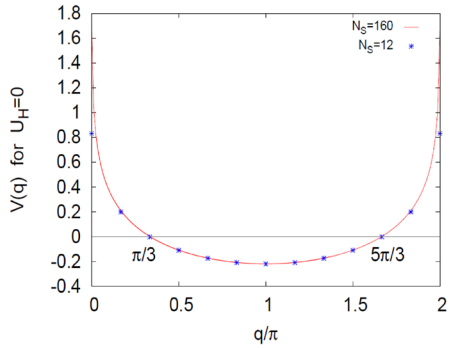

Fig. 2 Long-range part of V(q) (constants disregarded i.e. R=1 and V_L=1) for N_S=12 and N_S=160.

As seen from Fig.2, the highest chance for a negative value of the exchange energy (Eq.5) is met for k=π, and further refining of the formula for this value leads us to the following criterion (we were able to derive a simple analytical formula for large N):

$$V(\pi) \longrightarrow \frac{1}{N_S(U_H - 2ln2\frac{V_L}{\Delta})} \quad (5)$$

,for $N_S \longrightarrow \infty, \Delta = 2\pi R/N_S$.

The above formula brings us to the final result : (a) if $U_H > 2\ln 2\ V_L/\Delta$, the exchange energy is always positive and we have triplet ground state and Hund rule preserved, while (b) if $U_H < 2\ln 2\ V_L/\Delta$, the exchange energy may be negative and for some vales of k we can have singlet ground state and an anti-Hund rule. The highest chances to achieve this is for k values close to π, which means a situation close to half-filling.

Finally, in the below table, we give the exchange energy calculated for some simple cases (R_i stands for the distance between neighbours of order "i"):

System	Electron Configuration		$\Delta E = E_S - E_T$
	t>0 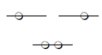	t<0 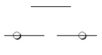	$\Delta E = \frac{1}{3}(U_H - V(R_1))$
	t>0 	t<0 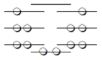	$\Delta E = \frac{1}{8}(U_H + V(R_4)) - \frac{1}{4}V(R_2)$

Table 1. Exchange energy calculated for some simple cases.

Authors acknowledge "Core Program"- PN16-480101, 2016-2017 and National Research Program PN-III-P4-IDPCE-2016-0221.

References

[1] S. Tarucha et al.,Phys. Rev. Lett. 77, 3613 (1996).

[2] S.M. Reimann et al., Rev. Mod. Phys. 74, 1283 (2002).

[3] A.F. Ho, Phys. Rev. A 73, 061601(R) (2006).

[4]M. Nita, M. Tolea, C. Marinescu, A. Manolescu, Phys. Rev. B 96, 235101 (2017).

Origin and chemical composition of the secondary phases in manganese doped nanostructured II-VI semiconductors

M. Stefan, L. C. Nistor, I. D. Vlaicu, D. Ghica, S. V. Nistor, A. V. Maraloiu
National Institute of Materials Physics

Doping II-VI semiconductor nanostructures with transition metal ions (TMIs) is an effective strategy for controlling their remarkable physical properties for a broad range of applications [1]. However, a significant part of the doping TMIs tend to aggregate in the intergrain region, often forming secondary phases. As shown in ref. 2, the low temperature collective magnetism observed in mesoporous cubic ZnS:Mn (cZnS:Mn) nanocrystalline powders prepared by colloidal synthesis, with nominal doping concentrations above 0.2 at.%, is due to the formation of Mn^{2+} clusters with distributed antiferromagnetic coupling localized in an amorphous phase found between the cZnS nanocrystals (NCs) [3].

Considering the importance of such amorphous phases in understanding and controlling the physical properties of the cZnS:Mn nanocrystalline powders, it is important to determine their composition, formation and stability. Therefore we investigated the amorphous phase in a nanocrystalline cZnS:Mn sample doped with 5 at.% nominal concentration of Mn by analytical high resolution (scanning) transmission electron microscopy (analytical HRTEM/STEM), Fourier transform infrared spectroscopy (FTIR) and multifrequency electron paramagnetic resonance (EPR) spectroscopy. The sample was prepared by a surfactant assisted colloidal synthesis from hydrated Zn and Mn acetate precursors, in similar conditions with the samples from refs. 1 and 2. We also monitored the amorphous phase evolution under annealing in air at temperatures up to 270 °C, a temperature which does not affect the mesoporous structure of the cZnS sample [3].

The HRTEM image of the as prepared cZnS:Mn 5% sample from Fig. 1 shows the presence of an amorphous material in the pores (marked by arrows) and on the surface of the cZnS NCs forming the pore walls. The chemical composition analysis by electron energy loss spectrum imaging (EELS-SI) revealed a very large amount of O and significant contents of Mn, Zn and C.

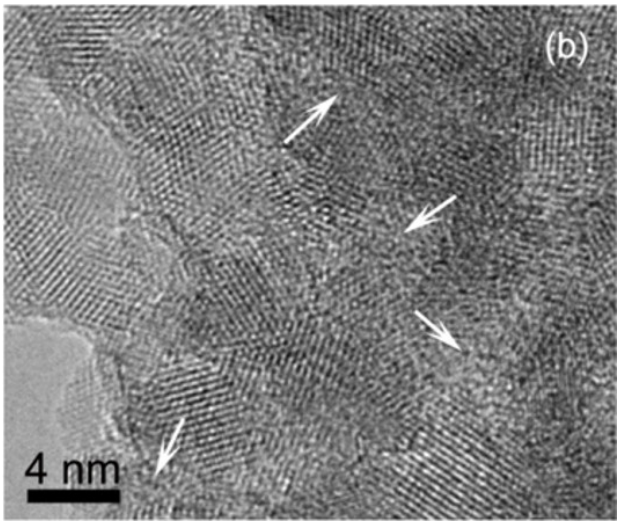

Fig. 1 HRTEM image of mesoporous cZnS:Mn 5%. The arrows mark pores filled with amorphous material [3].

The FTIR spectrum evidenced small amounts of remaining precursor hydrated acetates, especially manganese acetate tetrahydrate [$Mn(Ac)_2$]. Taking into account the EELS-SI results, it is very likely that the amorphous material filling the pores consists mostly of $Mn(Ac)_2$. The analysis of the EPR spectrum of the cZnS:Mn 5% sample (Fig. 2a) revealed the presence of isolated Mn^{2+} ions localized at substitutional Zn^{2+} sites in the core [Mn^{2+}(I) centers] and on the surface of the NCs [Mn^{2+}_{surf}(1) centers], as well as in an aggregated phase [Mn^{2+}_{aggr}(1) centers]. The Mn^{2+}_{surf}(1) centers consist of isolated Mn^{2+} ions in zinc acetate dihydrate [$Zn(Ac)_2$], thus confirming the presence of this precursor on the cZnS NCs surface. The Mn^{2+}_{aggr}(1) centers are very likely Mn^{2+} clusters in the $Mn(Ac)_2$ precursor trapped in the pores.

Further investigations of the sample isochronally annealed in air at selected temperatures up to 270 °C confirmed these results. The chemical composition analysis of the 270 °C annealed sample by EELS-SI showed a significant increase in the C content and a decrease in the O content in the pores, while the FTIR spectrum indicated a conversion of the acetate into carbonate.

The decomposition of the two acetates under annealing was accompanied by progressive mass loss, amounting to a ~7% total mass loss after the last annealing step, and changes in the EPR spectra of all Mn^{2+} centers (Fig. 2b).

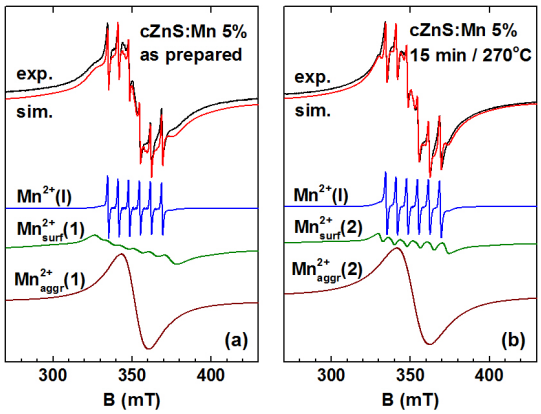

Fig. 2. Deconvolution of the EPR spectra of the (a) as prepared and (b) 270 °C annealed cZnS:Mn 5% sample [3].

The dehydration of $Zn(Ac)_2$ and further decomposition of the resulting anhydrous zinc acetate were reflected in the change in the line separation of the surface Mn^{2+} spectrum from ~9.0 mT to 8.5 mT. This variation was explained by the change in the local coordination of the surface localized Mn^{2+} from sixfold to fourfold. Moreover, the width and intensity of the EPR line from the aggregated Mn^{2+} ions increased under annealing, pointing to a change in the magnetic interactions between the Mn^{2+} ions, associated with the compositional changes induced by the decomposition of the $Mn(Ac)_2$ incorporated in the pores.

Using EPR, we were able to evidence the presence of an amorphous phase rich in dopant ions in a nanostructured sol-gel ZnO film doped with 5 at.% Mn [4], as well. As shown in Fig. 3, only 15% of the Mn^{2+} ions are found as isolated ions, namely 10% in ZnO and 5% segregated in the disordered intergrain region (Mn^{2+}-s centers), while the remaining 85% (Mn^{2+}-a centers) are aggregated in a high concentration phase. The chemical composition analysis by energy dispersive X-ray spectroscopy (EDX) mapping showed a non-uniform, insular-like distribution of the aggregated manganese between the ZnO nanograins, possibly forming a secondary phase composed of Zn, Mn and O. While this phase could be detected by EPR and observed by elemental EDX-STEM mapping, it could not be observed by X-ray diffraction techniques due to both lack of crystallinity and relative low concentration, below the detection limit.

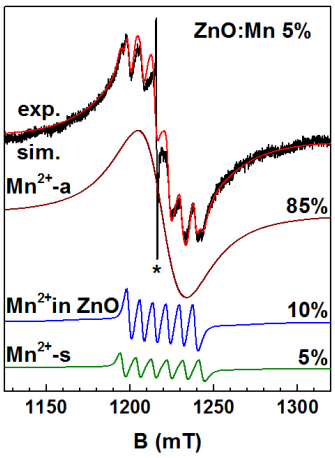

Fig. 3. Deconvolution of the EPR spectrum of a sol-gel ZnO film doped with 5 at.% Mn^{2+}.

*: dangling bonds in the float zone silicon substrate [4].

These results demonstrate that the presence of even small amounts of a secondary, amorphous phase in nanocrystalline semiconductors should be seriously considered. Such phases rich in dopant ions, observed in nanocrystalline powders and films of II-VI semiconductors, can be responsible for collective magnetism and affect the optical and electrical properties as well. Our results also point to an interesting possibility to modulate these properties not only by changing the precursors, solution pH, synthesis temperatures, but also by post-synthesis thermo-chemical treatments.

Funding from PNII-IDEI-74/2011, Nucleus Program PN16-480101, STAR CDI no.94/2013

References

[1] S.V. Nistor, M. Stefan, L.C. Nistor, D. Ghica, I.D. Vlaicu, A.C. Joita, Doping Ultra-small Cubic ZnS Nanocrystals with Mn2+ Ions over a Broad Nominal Concentration Range. J. Phys. Chem. C 119, 23781 (2015).

[2] S.V. Nistor, M. Stefan, L.C. Nistor, V. Kuncser, D. Ghica, I.D. Vlaicu, Aggregates of Mn2+ Ions in Mesoporous Self-Assembled Cubic ZnS:Mn QDs. Composition, Localization, Struc-ture and Magnetic Properties. J. Phys. Chem. C 120, 14454 (2016).

[3] M. Stefan, I.D. Vlaicu, L.C. Nistor, D. Ghica, S.V. Nistor, Origin and chemical composition of the amorphous material from the intergrain pores of self-asembled cubic ZnS:Mn nanocrystals. Appl. Surf. Sci. 426, 342 (2017).

[4] M. Stefan, D. Ghica, S.V. Nistor, A.V. Maraloiu, R. Plugaru, Mn2+ ions distribution in doped sol-gel deposited ZnO films. Appl. Surf. Sci. 396, 1880 (2017).

Ferroelectrics in perovskite solar cells

N. Plugaru, V. Stancu, A. Tomulescu, C. Besleaga Stan, L. Trinca, L. Filip, R. Radu, L. Pintilie and I. Pintilie

National Institute of Materials Physics

in collaboration with

Nemnes, GA (University of Bucharest, Romania); Butler, KT (University of Bath, UK); Manolescu, A. (Reikjiavik University, Iceland)

The substantial increase in the power conversion efficiency of hybrid perovskite solar cells, exceeding values of 20% in laboratory conditions, has strongly motivated research on this class of organic-inorganic materials and related devices, particularly based on $CH_3NH_3PbI_{3-x}X_x/TiO_2$ heterostructures (X = Cl,Br). We have started to investigate the possible integration of perovskite ferroelectrics in perovskite solar cells. The idea that triggered

the study has been to replace the TiO_2 layer with a ferroelectric one, assuming that the internal electric field associated with the presence of the ferroelectric polarization will enhance the charge collection at the electrodes by attracting more electrons towards the FTO transparent contact. Under this assumption, we have considered systems consisting of $CH_3NH_3PbI_{3-x}Cl_x$ halide perovskite (HP) layers deposited on the (001) surfaces of ferroelectric (FE) materials as $PbTiO_3$ (PTO) and $BaTiO_3$ (BTO), with spontaneous polarizations of 78 C/m^2 and 25 C/m^2), respectively. The aim was to unveil the relationship between the FE polarization and the electronic properties of the heterostructures. Taking under consideration that a ferroelectric substrate may act as an efficient electron transporter, positively influencing charge collection across the interface and allowing the tuning of the band alignment at the halide perovskite - ferroelectric junction, we performed extensive density functional theory calculations on $CH_3NH_3PbI_{3-x}X_x/TiO_2$ layers deposited on tetragonal $PbTiO_3$ (PTO) (001) surfaces, to study their structural and electronic properties. The main findings of this study are [1]: (i) A ferroelectric polarization pointing from the PTO/HP interface to the PTO is favorable for the photogenerated electrons transfer across the interface and their transport to the collecting electrode (see Fig.1). (ii) The PTO internal electric field leads to a position dependent energy levels diagram. (iii) The HP gap may be tuned by chlorine concentration at the interface, as well as by the surface terminations of PbTiO3 and hybrid perovskite layers. (iv) The presence of the PTO ferroelectric surface is likely to have just a slight orientational effect on the $(CH3NH3)^+$ dipoles.

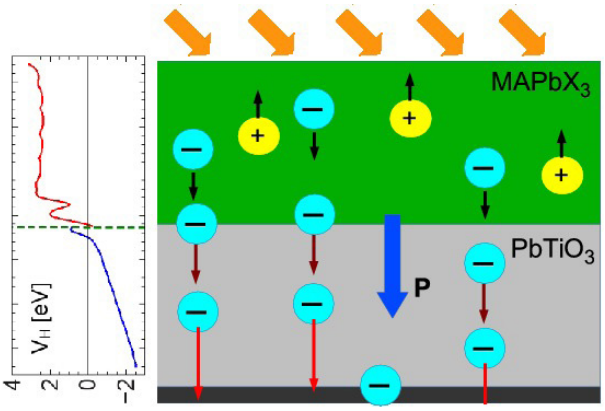

Fig. 1 Macroscopic average (blue for PTO and red for HP) of the Hartree potential, VH, for the depicte direction of polarization (P) in the PTO layer. The green dashed line marks the position of the PTO-HP interface.

Novel test perovskite solar cells were fabricated by replacing the TiO_2 layer with PTO and BTO perovskite ferroelectrics. The test structures were prepared by depositing PTO and BTO ferroelectric thin film on FTO/glass substrates, using sol-gel and PLD methods [2]. The deposition of HP layer ($CH_3NH_3PbI_{2.6}Cl_{0.4}$) is described in Ref. [3]. The first attempts to fabricate solar cells using sol-gel deposited PTO produced no enhancement of PCE, instead they have shown almost total destruction of the signal most probably due to the very large serial resistance introduced by the PTO film. Therefore, the electric properties of sol-gel deposited PTO were investigated and compared with those of TiO_2 layers, both with bottom FTO and top SRO electrodes. PTO shows good ferroelectric properties, while TiO_2 behaves as a semiconductor. It has been found that the PTO

layer has a higher resistivity although the density of the free carriers is similar to the one in the TiO_2 layer. Also, the potential barrier at the FTO/PTO interface is significantly higher than for the FTO/TiO_2 interface, of 0.24 eV and 0.1 eV for FTO/PTO and FTO/TiO_2 interfaces, respectively [2]. In order to lower the resistance of the ferroelectric film the deposition method was changed from sol-gel to PLD. Indeed, the solar cells containing either PTO or BTO layer instead of TiO_2 have shown better results, with PCE values going towards 1% [2]. The experiments performed on structures depicted schematically in Fig.2, have shown some relevant features such as: (a) The open circuit voltage (V_{oc}) is larger for the solar cell with BTO layer, about 0.9 V compared to about 0.75 V for the cell with PTO; (b) V_{oc} is independent of the amplitude of the poling voltage; (c) The short-circuit current is slightly larger for the cell with PTO, which may be a reflection of a higher polarization value in PTO compared to BTO; (d) The ferroelectric layers breakdown at poling voltage of about +4 V for BTO and +3 V for PTO; (e) A significant hysteresis is always present, which can include contributions from both the ferroelectric hysteresis and the low mobility ionic charges present in the structure; (f) The PCE value is apparently larger for BTO, although the polarization value may be lower than in PTO; a possible explanation is the larger value for the open-circuit voltage.

Although the PCE value is still low, the experimental results clearly indicate that the efficiency of charge collection can be enhanced by the ferroelectric layer. This is particularly evident from the fact that the magnitude of the short-circuit current increases as the amplitude of poling voltage applied on the structure, prior the I-V measurement under illumination, increases. In other words, a higher poling voltage leads to a better orientation of the spontaneous polarization, reflected in a higher value of the polarization in the ferroelectric layer. As a consequence, the magnitude of the short-circuit current is enhanced. Notably, the polarization orientation in the ferroelectric film must be from the HP layer towards the FTO collecting electrode in order to enhance the short-circuit current, in agreement with the theoretical findings [1]. Further studies are needed to optimize the electric properties (lower resistance) of the PTO or BTO layers, while preserving the ferroelectricity.

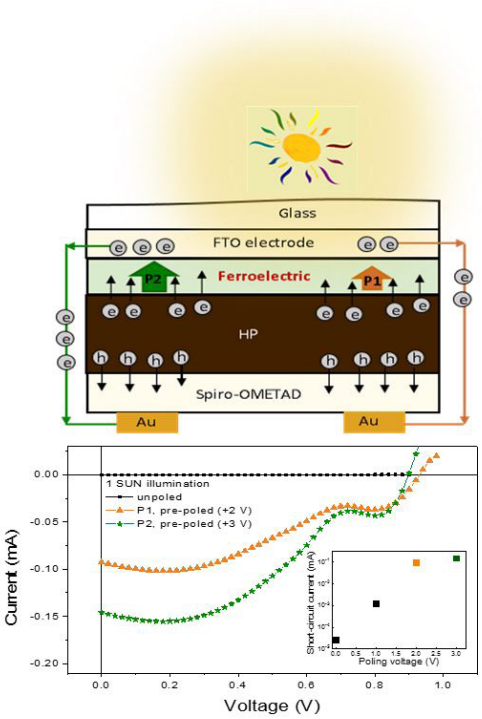

Fig. 2. Schematic representation of the perovskite solar cell in which the TiO_2 electron transporter was replaced with a ferroelectric layer and the measured I-V characteristics for two values of the ferroelectric polarization (P2>P1).

References

[1] N. Plugaru et al, "Atomistic Simulations of Methylammonium Lead Halide Layers on PbTiO3 (001) Surfaces", J. Phys. Chem. C 121, 17, 9096 - 9109 (2017).

[2] I. Pintilie et al, "Properties of perovskite ferroelectrics deposited on F doped SnO2 electrodes and the prospect of their integration into perovskite solar cells", Mater. Des. 135, 112-121 (2017).

[3] C. Besleaga et al. "Iodine Migration and Degradation of Perovskite Solar Cells Enhanced by Metallic Electrodes", J. Phys. Chem. Lett. 7, 5168–5175 (2016).

CONTRIBUTIONS

SELECTED RESULTS

Direct desulfurization reaction induced locally by an electric field

B. Borca

National Institute of Materials Physics

Here I briefly describe the scientific results realised in collaboration with the group of Professor Klaus Kern at the Max Planck Institute for Solid State Research, Stuttgart, Germany.

The investigations were published with the title "**Electric-field-driven direct desulfurization reaction**" in ACS Nano 11 (5), 4703 (2017) by Bogdana Borca[1,2], Tomasz Michnowicz[1], Rémi Pétuya[3], Marcel Pristl[1], Verena Schendel[1], Ivan Pentegov[1], Ulrike Kraft[1], Hagen Klauk[1], Peter Wahl[1,4], Rico Gutzler[1], Andrés Arnau[3,5], Uta Schlickum[1], and Klaus Kern[1,6] with the affiliations:

[1]Max Planck Institute for Solid State Research, 70569 Stuttgart, Germany;

[2]National Institute of Materials Physics, 077125 Măgurele-Ilfov, Romania,

[3]Donostia International Physics Centre, E-20018 Donostia - San Sebastián, Spain,

[4]SUPA, School of Physics and Astronomy, University of St. Andrews, North Haugh, St. Andrews KY16 9SS, United Kingdom,

[5]Departamento de Física de Materiales UPV/EHU and Material Physics Center (MPC), Centro Mixto CSIC-UPV/EHU, E-20018 Donostia - San Sebastián, Spain,

[6]Institut de Physique, École Polytechnique Fédérale de Lausanne (EPFL), CH-1015 Lausanne, Switzerland.

The use of the electric field as a stimulus in chemical reactions has attracted the scientific interest due to the possibility to significantly improve the reaction efficiency [2] or its catalytic activity [3]. Studies at the atomic scale offer the possibility to access such reactions in detail. An ideal tool, which allows investigating and activating chemical reactions at the individual molecular level, is Scanning Tunneling Microscopy (STM). At the tunnelling junction, the adjustable parameters are the tip-sample distance, the applied bias voltage and the flow of current into the junction. Thus, we can control the electric field, the electronic injection and/or the mechanical interactions, which may induce chemical reactions.

The study reported in Ref. [1] is focused on the direct desulfurization process of single tetracenothiophene (TCT) molecules supported on the monocrystalline closed packed copper surface. The experiments were performed **in-situ**, in ultra-high vacuum conditions and at low temperature.

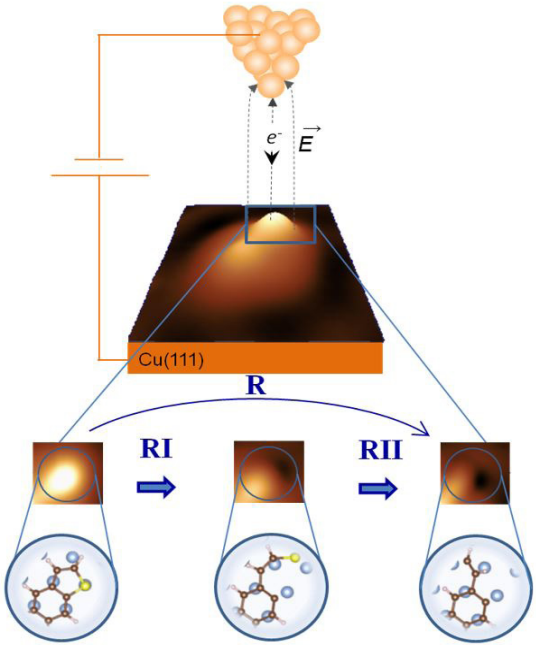

Fig. 1: Schematic representation of a direct desulfurization reaction, induced locally by STM at the single molecular level. The reaction consists of a successive dissociation of C-S bonds of a TCT molecule, illustrated in STM images of the molecular configurations and the corresponding ball-and-stick representations of the thiophene unit obtained by DFT calculations. (Lower panels adapted partially from Ref. [1]).

The reaction is triggered by positioning, with sub-molecular precision, the STM tip apex above the thiophene moiety and applying an electric field confined at the tunneling junction (Figure 1).

Our experimental and theoretical investigations allowed resolving the reaction pathway that consists on a two-step reaction, a successive scission of the two C-S bonds.

First, the thiophene ring is opened to an intermediate configuration by a threshold electric field exceeding 2V/nm, practically in the absence of an effective tunnelling current. Thus, this reaction step R1 occurs by positioning the tip more than 2 nm above the thiophene unit of the TCT molecule and applying a bias voltage higher than 5 V.

For the same threshold field but with a simultaneous injection of electrons, the second C-S bond breaks. The final molecular state corresponds to a stable derivative that is strongly bound to the metallic surface, and the sulfur atom is expelled from the molecular vicinity.

This reaction step R2 is induced by positioning the tip at a defined height above the molecule in its intermediate state and by ramping the bias voltage while recording the tunnelling current with the feedback loop disconnected. A change in the tunnelling current trace occurs at the moment when the reaction is activated. The corresponding threshold voltage varies linearly with the tip-sample distance, characteristic behaviour for an electric field stimulus.

Following the same reaction mechanism, a direct transition from the initial to the final state (reaction R) can be activated but applying the same threshold electric field with a simultaneous injection of electrons into the molecule. In this case the intermediate state is not visualised, the second reaction step occurs instantaneously when the stimuli are applied.

In conclusion, the investigations reveal the reaction mechanism of a direct desulfurization reaction activated locally by an electric field. Such a process shows the high potential of the electric field stimulus to drive single-molecule chemistry. As reported in other works [4], lithium location was indirectly deduced from its derivative effects on the experimental results in correlation with the presence of other co-dopants. Thus, it was assumed that vanadium promotes the B-site, while niobium facilitates the A-site Li substitution in PZT.

References

[1] B. Borca, T. Michnowicz, R. Pétuya, M. Pristl, V. Schendel, I. Pentegov, U. Kraft, H. Klauk, P. Wahl, R. Gutzler, A. Arnau, U. Schlickum, and K. Kern. Electric-Field-Driven Direct Desulfurization Reaction. ACS Nano 11 (5), 4703 (2017)

[2] S. Shaik, D. Mandal, R. Ramanan. Oriented Electric Fields as Future Smart Reagents in Chemistry. Nat. Chem. 8, 1091 (2016)

[3] A.C. Aragonès, N.L. Haworth, N. Darwish, S. Ciampi, N.J. Bloomfield, G.G. Wallace, I. Diez-Perez, M.L. Coote. Electrostatic Catalysis of a Diels–Alder Reaction. Nature 531, 88 (2016)

Sustainable carbon-based materials for applications in sensors and electrochemistry

L.C. Tănase, C.M. Teodorescu

National Institute of Materials Physics

in collaboration with **K. Preuss, M. Qiao, D.-W. Zhang, M.-M. Titirici**
Materials Research Institute, Queen Mary University of London, Mile End Road, E1 4NS London, UK

Carbon-based materials are one of the most studied class of materials nowadays do to their many proposed applications and to wide versatility in the way of production and preparation. Moreover, it seems a very straightforward and sustainable way to use hydrothermal carbonization methods in order to produce nano-carbon based on biowaste, biodegradable agents or inexpensive compounds and primary products that can be extracted from easy to obtain, natural and environmentally friendly precursors.

In this context, the Group of Surfaces and Interfaces has proven its expertise with the X-Ray Photoelectron Spectroscopy (XPS) measurements in collaboration with the group of Prof. M.M. Titirici from Queen Mary University, London, UK, on three different topics related to carbon applications and functionality.

One of the studies concerned the preparation of sustainable metal-free carbogels based on glucose and ovalbumin doped with N in order to explore their tunability in terms of morphology, surface area and pore properties, which are supposed to influence the effect into the electrocatalytic activity for the final application in electrolyte fuel cells. In this case, the samples were produced via hydrothermal carbonisation of D-(+)-Glucose and lyophilised Ovalbumin (OvA) from chicken egg white, using a well-established method, and characterized by physical and electrochemical tests. The experiment followed different aspects, either regarding the influence of the O_2 activation of the active centers in the carbon structure, under different exposure of O_2 gas, or their production under the incorporation of sulphur (S) or boron (B) during the carbonization by adding TCA (2-Thiophenecarboxaldehyde) or BA (Boric acid). The effect of the O_2 dosing and/or of the presence of S or B in the structure was investigated by Scanning Electron Microscopy (SEM), Transmission Electron Microscopy (TEM) and XPS, correlated with the electrocatalytic performance and the surface area. For example, Fig. 1 and Fig. 2 present the N 1s XPS spectra in the samples with N, B and/or S, as well as the electrocatalytic tests.

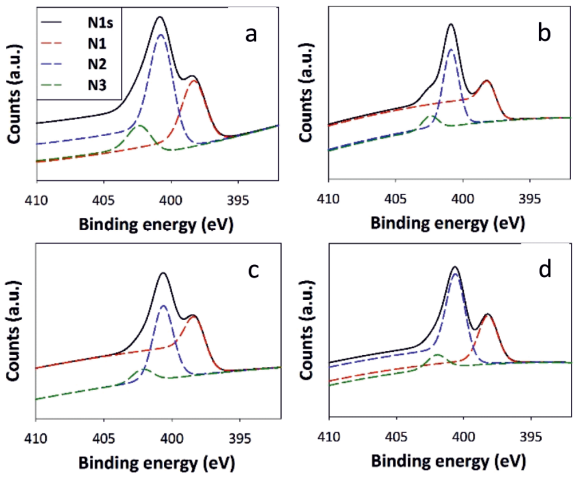

Fig. 1. Deconvoluted N 1s photoelectron spectra with nitrogen species (dashed lines), N1/red = pyridinic N, N2/blue = graphitic N, N3/green = N-oxides. For a) CN, b) CN_S, c) CN_B and d) CN_{SB}. Reproduced from Ref. [1].

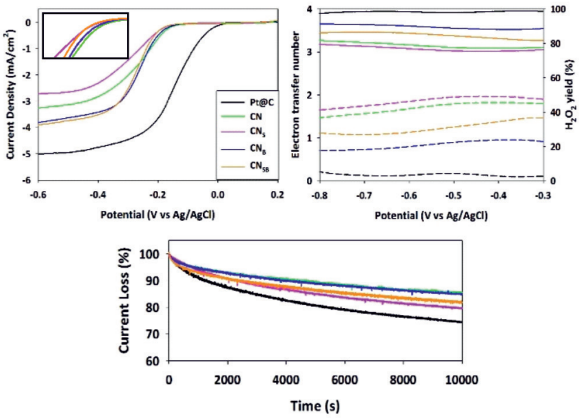

Fig. 2: a) Linear sweep voltammogram recorded in 0.1 M KOH with an RDE setup at 1600 rpm, b) electron transfer number and hydrogen peroxide yield and c) chronoamperometric response at a constant potential of 0.25 V (vs Ag/AgCl) for a commercially available platinum catalyst (60 wt% Pt@C) and nitrogen carbogels, CN, treated at 1000°C doped with sulphur, CN_S, boron, CN_B, or sulphur and boron, CN_{SB}. Reproduced from Ref. [1].

The second study concerned the passivation of the surface of carbon-based Pt-free materials by using oxygenophilic and hydrophobic ionic liquids (ILs) at the triple point between the electrocatalyst–electrolyte–gas interface where the Oxygen Reduction Reaction (ORR) takes place, also for application in the Polymer Electrolyte Membranes (PEMs) and Alkaline Fuel Cells (AFCs). After preparation, the samples have been subjected to physical and electrochemical characterization, before and after the insertion of the ionic liquid, similar to the ones from the previous study. Fig. 3 presents some results regarding the TEM, XPS, water contact angle and N2 sorbtion isotherms on the samples with and without ionic liquid treatment.

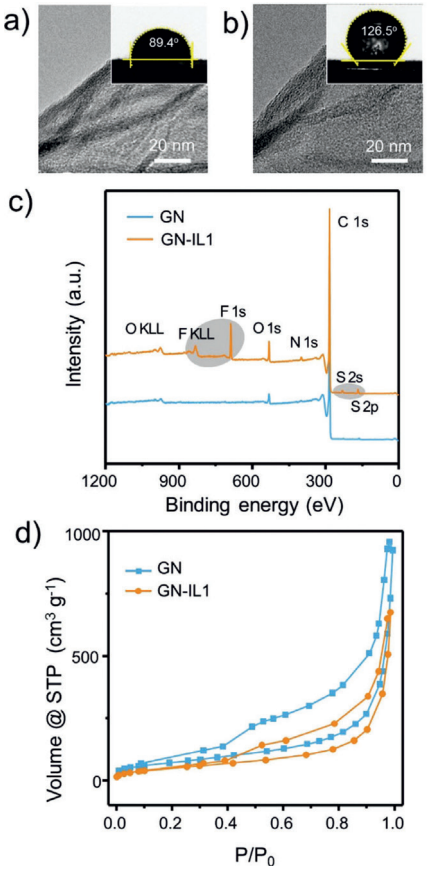

Fig. 3 Characterization of the IL-modified GN catalyst. TEM images of (a) GN and (b) GN-C_4C_1. The inset images show the static water contact angle measurements, respectively. (c) The XPS surveys and (d) N_2 sorption isotherms of GN and GN-C_4C_1. Reproduced from Ref. [2].

The third study concerns the development and photoelectrochemical test of carbon dots (CDs) produced by a one-step solvothermal carbonization of chitosan dispersed in ethanol for the final application as light-addressable electrochemical sensors in bio-analytical and bio-imaging applications. After preparation, the CDs are self-assembled on an ITO-silane surface and subjected to illumination tests. Fig. 4 presents the scheme which describes the way by how CDs got attached to the ITO-silane surface, with proof (provided by XPS) that the CDs are attached to the surface by the presence of nitrogen peak in the survey spectra, as well as the corresponding peak in the C high resolution spectrum (not shown).

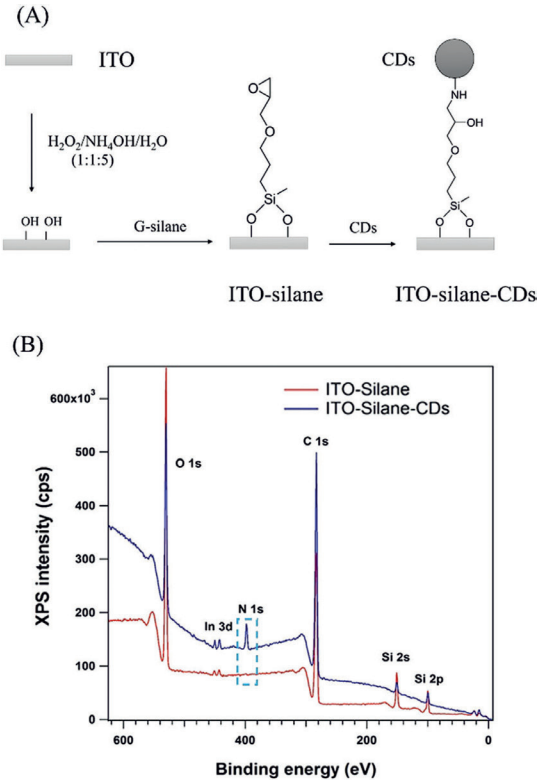

Fig. 4 (A) Scheme of CDs binding onto ITO via a reaction with 3-glycidoxypropyldimethoxymethylsilane; (B) XPS full scan spectrum of the ITO–silane and ITO–silane–CDs. Reproduced from Ref. [3].

Funding from the UEFISCDI Agency through the Project PN-II-RU-TE-2014-4-0456 and by the NIMP Core Project PN16-48012, both projects being granted by the Romanian Ministry of Research and Innovation.

References

[1] K. Preuss, L.C. Tănase, C.M. Teodorescu, I. Abrahams, M.-M. Titirici, J. Mater. Chem. A 5, 16336-16343 (2017).

[2] M. Qiao, C. Tang, L.C. Tanase, C.M. Teodorescu, C.-M. Chen, Q. Zhang, M.-M. Titirici, Mater. Horiz. 4, 895-899 (2017).

[3] D.W. Zhang, N. Papaioannou, N.M. David, H. Luo, H. Gao, L.C. Tanase, T. Degousée, P. Samorì, A. Sapelkin, O. Fenwick, M. Titirici, S. Krause, Mater. Horiz., DOI: 10.1039/c7mh00784a (2018).

Emergent phases in materials featured by strong by spin-orbit coupling

M. A. Husanu

National Institute of Materials Physics

in collaboration with:
V. N. Strocov, J. A. Krieger, D. Sostina, T. Prokshca, A. Suter, Z. Salman, T. Schmitt, Paul Scherrer Institut 5232, Villigen, Switzerland;
V.A. Rogalev, M.R. Scholz, F. Reis, L. Dudy, A. Fleszar, J. Schaefer, R. Claessen, Universitat Wurzburg, 97074 Wurzburg, Germany;
T. Rauch, J. Henk, I. Mertig, Martin Luther University Halle-Wittenberg, 06099 Halle (Saale), Germany;
C.Z. Chang, J.S. Moodera, Massachusetts Institute of Technology, Cambridge, Massachusetts 02139, USA;
A. Ernst, Johannes Kepler Universitat, A 4040 Linz, Austria ;
M.M. Otrokov, Centro de Fısica de Materiales CFM - MPC and Centro Mixto CSIC-UPV/EHU, 20080 San Sebastian/Donostia, Spain;
M.G. Vergniory, E.V. Chulkov, Donostia International Physics Center, P. Manuel de Lardizabal 4, San Sebasti´an, 20018 Basque Country, Spain;
S.Y. Xu, N. Alidoust, I. Belopolski, D.S. Sanchez, H. Zheng, M.Z. Hasan, Department of Physics, Laboratory for Topological Quantum Matter and Spectroscopy (B7), Princeton University, Princeton, NJ 08544, USA;
C.Q. Chang, B. Singh, H. Lin, X. Zhang, S.M. Huang, C.H. Hsu,, National University of Singapore, 6 Science Drive 2, Singapore 117546, Singapore;
H. Lu, G. Bian, International Center for Quantum Materials, School of Physics, Peking University, Beijing, China;
T.R. Chang, H.T. Jeng, National Tsing Hua University, Hsinchu 30013, Taiwan;
A. Bansil, Northeastern University, Boston, MA 02115, USA;
T. Neupert, University of Zurich, Winterthurerstrasse 190, CH-8052, Switzerland;
S.A. Jia, International Center for Quantum Materials, School of Physics, Peking University, Beijing, China;

The broad class of topological systems relying on strong spin-orbit coupling (SOC) is explored using soft X-ray angle-resolved photoelectron spectroscopy (SX-ARPES). Systems featured by quantum states which manifest as topologically protected conducting channels at the edges, surfaces or interfaces of otherwise insulating materials rely on band inversion driven by strong spin-orbit coupling [1,2]. Their most prominent aspects are the linear dispersion of the energy bands near the Fermi level, and spin-momentum locking. For α-Sn, strained compressively on InSb(001) substrates, a new non-trivial topological state is observed for the first time and an orbital mechanism which prevents its hybridization with the trivial surface states is suggested [3].

Films prepared **in-situ** by molecular beam epitaxy with simultaneous Sn deposited on the substrates at room temperature, and Te in order to n-dope the substrate were investigated by angle-resolved photoelectron spectroscopy (ARPES) with high probing depth. The subsurface state results from an „inverted" SOC-induced bandgap. Its topological invariant $\mathbf{Z_2}$ $(\nu_0;\nu_1\nu_2\nu_3)$ **= (1;000)** while the mirror Chern numbers are n_M = -1 thus confirming its non-trivial topology.

Due to the increased $k_\perp$ resolution in SX-ARPES, dispersing bulk bands at varied photon energies around bulk Γ point in Fig. 1a, as well as at different k_y values (Fig. 1c) are revealed.

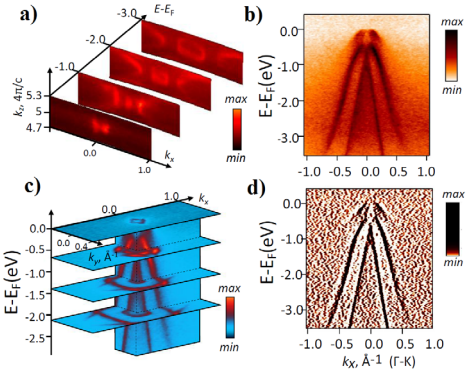

Fig. 1 a) Constant energy maps obtained by varying the photon energy hν=320-400 eV (s-polarized); b) ARPES map $I(E;k_x)$ measured at hν = 350 eV (p-polarized) along ΓK direction for the sample with lowest Te doping; c) ARPES constant energy maps measured at hν = 352 eV acquired by varying k_y through sample tilting; d) second derivative along the momentum direction for data shown in b). Adapted from [3]

ARPES data measured along bulk ΓK direction on the sample with the lowest Te content (Fig. 1b,d) clearly demonstrate the presence of the

topological surface states.

On the other hand, when doped with magnetic impurities, topological insulators (TI) may exhibit quantum anomalous Hall effect, but its observation may be hindered by the additional conduction channels introduced by the impurity band. In this perspective, for V-doped Sb_2Te_3, it is shown [4] that the impurity band originating in V substitution of Bi/Sb lies close to the Fermi energy (E_F). Bulk states at this binding energy are expected to destroy any quantized transport signature but may be essential to mediate the magnetic coupling at higher temperature.

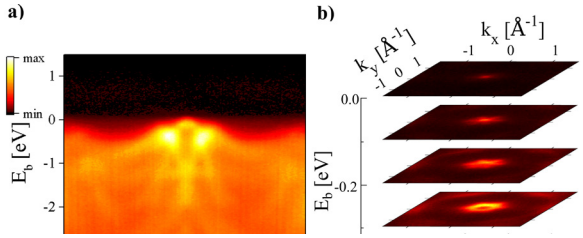

Fig. 2 a) Band structure at 355 eV of the V0:06 sample measured along the ΓM direction. b) Constant energy cut maps measured at hν = 355 eV. Adapted from [4]

As such, low energy muon spin rotation (LE-SR) indicate that mostly the carriers at E_F mediate the magnetic coupling between weakly coupled ferromagnetic islands through a combination of double exchange and RKKY mechanisms.

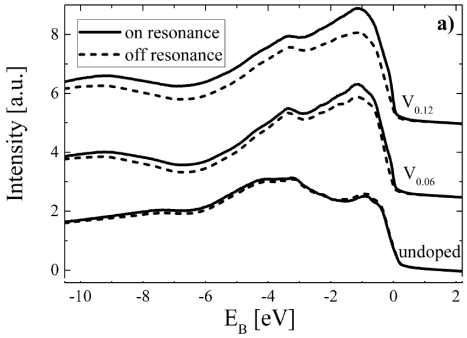

Fig. 3 Angle-integrated resonant ARPES at different V doping levels. Adapted from [4]

Figure 2a) and b) indicate the bandstructure recorded on V:Sb_2Te_3 with the topological surface states crossing the Fermi level. The resonant excitation at the L line of V (516 eV) allows for precise assessement of V contribution in the spectral function (Fig.3).

A newly emerging class of topological systems are the Weyl semimetals (WS). Compared to Dirac semimetals, they have only two bands crossing the Fermi level with a signature of point, thus with 0D Fermi surface acting as topological charge [5].

Type II Weyl fermions are seen in a crystalline solid as electronic excitations near the Fermi level with Weyl quasiparticle breaking the Lorenz symmetry.

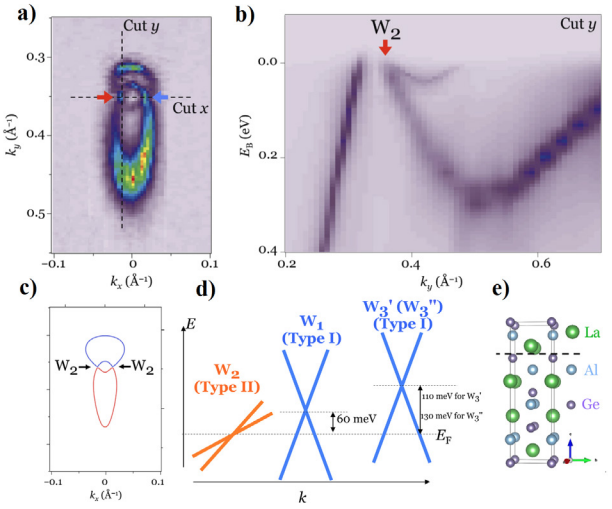

Fig. 4 a) The k_x – k_y Fermi surface map revealing a pair of type II W2 Weyl nodes in the form of touching points between electron and hole pockets; b) Measured E – k_y dispersion map along the cut y direction denoted in a), which clearly resolve the W_2 type II Weyl node at the crossing of two bands with the same sign of Fermi velocity; c) calculated k_x – k_y Fermi surface in the region recorded in a); d) Schematics comparing the three types of Weyl nodes appearing upon the inclusion of SOC. The W2 nodes are type II Weyl nodes, and W1, W3′, and W3″ nodes are type I. W2 Weyl nodes are located almost exactly at the Fermi level, whereas W1, W3′, and W3″ Weyl nodes are about 60, 110, and 130 meV above the Fermi level, respectively; e) Body-centered tetragonal structure of LaAlGe, with space group $I4_1md$ (109). The structure consists of stacks of La, Al, and Ge layers, and along the (001) direction, each layer consists of only one type of element. Adapted from [6]

More clearly, compared to type I Weyl semimetals, the fermion cone arises from the crossing between two bands that have the same sign of velocity along a certain direction. For the first time, their experimental observation in LaAlGe [6] reveals the Fermi surface of a type II Weyl semimetal where bulk electron and hole pockets touch to form the type II Weyl node (Fig. 4).

References

[1] D. Hsieh et al., Nature 452, 7190 (2008)

[2] M. Z. Hasan, C. L. Kane, Rev. Mod. Phys. 82, 3045 (2010)

[3] V.A. Rogalev et al. Phys. Rev. B 95, 161117 (2017)

[4] J.A. Krieger, et al. Phys. Rev. B 96, 184402 (2017)

[5] A. A. Soluyanov et al. Nature 527, 495 (2015)

[6] S.Y. Xu et al. Science Advances 3, e1603266 (2017)

PATENTS AND PATENT REQUESTS

PATENT AWARDED

1. Cotîrlan-Simionuc Costel, Lăzărescu Mihail Florin.
Method and device for measuring the optical properties of thin layers deposited on surfaces or interfaces with total internal reflection
Patent granted by decision no. 6 / 141 / 29.11.2017

2. Slav Adrian, Palade Cătălin, Lepadatu Ana-Maria, Lazanu Sorina, Ciurea Lidia Magdalena, Vasilache Dan, Dragoman Mircea
Capacitive matrix for non-volatile memory, based on germanium nanocrystals immersed in hafnium dioxide and process for achieving it
Patent granted by decision no. 3 / 232/ 29.11.2017

3. Florica Camelia-Florina, Preda Nicoleta-Roxana, Costaș Liliana-Andreea, Evanghelidis Alexandru Ionuț, Oancea Mihaela, Enculescu Maria-Monica, Matei Elena, Enculescu Marius-Ionuț
Process for obtaining one-dimensional zinc oxide nanostructures by in-air thermal oxidation of Zinc foils
Patent granted by decision no 3 / 233 / 29.11.2017

4. Evanghelidis Alexandru Ionuț, Busuioc Cristina, Matei Elena, Enculescu Maria-Monica, Preda Nicoleta-Roxana, Florica Camelia-Florina, Costaș Liliana-Andreea, Oancea Mihaela, Enculescu Marius-Ionuț
Process for obtaining polymeric micro and nanofibers by electrospinning using textiles for obtaining multiple jets
Patent granted by decision no 3 / 194 / 30.10.2017

5. Ciurea Lidia Magdalena, Stavarache Ionel, Teodorescu Valentin Șerban
Capacitor structure for non-volatile memoriy based on Germanium nanocrystals immersed in silicon dioxide
Patent granted by decision no 6 / 135 / 30.10.2017

PATENT REQUESTS

1. Iliescu Mihaiela, Lazăr Marian, Pintilie Ioana, Vlădăreanu Luige, Necșoiu Teodor, Stancu Viorica, Tomulescu Andrei Gabriel, Beșleagă-Stan Cristina, Sima Marian, Leonat Lucia, Stanciu Elena Manuela, Comănescu Brinduș, Enuică Alexandra Valentina
Printer for successive deposition of ultra-thin layers with different physico-chemical properties
A00195 / 2017

2. Cotîrlan-Simionuc Costel, Rizea Adrian, Marin Constantin
Plasma meta-glasses functioning as a polarization state analyzer
A00167 / 2017

3. Stavarache Ionel, Ciurea Lidia Magdalena, Maraloiu Valetin-Adrian, Teodorescu Valentin Șerban
The photosensitive structure based on germanium nanocrystals immersed in silicon dioxide for photodetectors and the process for their realization
A00069/2017

PATENT REQUESTS

4. Boni Georgia Andra, Chirilă Cristina, Hrib Luminița, Pintilie Ioana, Pintilie Lucian
Ferroelectric memory structure with multiple states of memory and method of production
A00109 / 2017

5. Secu Mihail, Secu Elisabeta Corina
Process for preparing the BaCl2:Eu2+ luminophore
A00295 / 2017

6. Comănescu Cezar Cătălin, Palade Petru, Kuncser Andrei Cristian, Plăpcianu Carmen Gabriela
Magnetic material based on iron nitride nanoparticles ordered with martensitic structure and process for its production
A00686 / 2017

7. Ghiță Rodica, Negrilă Constantin-Cătălin, Logofătu Constantin, Mihai Maria-Diana, Predoi Daniela, Stoicu Marius
Realisation of a photoactive structure on n-GaSb
A00685 / 2017

8. Secu Mihail, Secu Elisabeta Corina
Process for separating the LaOCI:RE3+(RE=Ce,Tb,Eu) luminophore
A00623 / 2017

9. Feder Marcel, Diamandescu Lucian Constantin, Cernea Marin, Sterian Gheorghe, Dumitrescu Iuliana
Process for obtaining a titanium dioxide composite material doped with iron and reduced nitrogen/ oxide, with extended photocatalytic activity in the visible field
A00615 / 2017

10. Grigoroșcuță Mihai Alexandru, Burdușel Mihail, Aldica Gheorghe Virgil, Bădică Petre
Processing method and superconductor tape / wire in a light metal sheath with MgB2 core
A00589 / 2017

11. Boni Georgia Andra, Chirilă Cristina, Hrib Luminița, Pintilie Ioana, Pintilie Lucian
Ferroelectric memory with non-destructive reading
A00226 / 2017

12. Pintilie Lucian, Pintilie Ioana, Botea Mihaela, Iuga Alin, Cioca Mihai, Ianculescu Carmen Adelina, Ofrim Dragos Vasile, Ofrim Bogdan Alexandru, Ofrim Dragos Mihai
Pyroelectric ceramic detector with planar concentration gradient and universal pyroelectric signal amplifier for voltage mode
A00697 / 2017

13. Predoi Daniela, Ghiță Rodica, Iconaru Simona-Liliana, Beuran Mircea, Prodan Alina Mihaela, Chifiriuc Mariana Carmen
Bio-doped hydroxyapatite bandage with silver in collagen matrix
A00769 / 2017

PATENT REQUESTS

14. Predoi Daniela, Iconaru Simona-Liliana, Soare Marian, Florea Nănescu, Nicolaescu Dan Adrian, Mocanu Aura-Cătălina, Predoi Mihai Valentin, Beuran Mircea, Prodan Alina Mihaela
Application of ultrasonic spectroscopy in colloidal suspension analysis with emphasis on biocompatible materials
A00768 / 2017

15. Beşleagă-Stan Cristina, Dumitru Viorel-Georgel
Device for breath monitoring
A00851 / 2017

16. Stan George, Popa Adrian-Claudiu, Beşleagă-Stan Cristina, Dumitru Viorel-Georgel, Rădulescu Cătălin
Method for the realization of osteointegrative implants coated with bio-active glass layers synthesized in magnetron plasma
A00909 / 2017

17. Velea Alin, Gâlcă Aurelian-Cătălin, Socol Gabriela, Mihai Claudia
Structure consisting of two overlaid layers of phase shift materials with three logical memory states
A00964 / 2017

EVENTS

2nd International Workshop on Materials Physics

Dates: **May 16-17, 2017**
Venue: **NIMP Conference Hall, 405A Atomistilor Str., Magurele**

Keynote Speakers:

- Lucia Aballe, ALBA Synchrotron Barcelona, Spain
- Francesco d'Acapito, ESRF, Grenoble, France
- Jean Daillant, Soleil Synchrotron, Saint-Aubin, France
- Sarnjeet S. Dhesi, Diamond Light Source, Didcot, U.K.
- Konstantin Klementiev, Max IV, Lund, Sweden
- Axel Knop, Fritz-Haber Institut, Berlin, Germany
- Rosanna Larciprete, Institut for Complex Systems, Rome, Italy
- Silvano Lizzit, Elettra, Trieste, Italy
- Vladimir Matolin, Charles University, Prague, Czech Republic
- Cătălin Miron, ELI – Nuclear Physics, Măgurele, Romania
- Vasile I. Pârvulescu, Chemistry, University of Bucharest, Romania
- Kai Schlage, PETRA, DESY, Hamburg, Germany
- Cristian M. Teodorescu, National Institute of Materials Physics, Măgurele, Romania
- Ion Tiseanu, NI Lasers, Plasma and Radiation Physics, Măgurele, Romania
- Rodica Turcu, NI Isotopic Molecular Technologies, Cluj-Napoca, Romania
- Jens Viefhaus, PETRA, DESY, Hamburg, Germany
- Carlos Vaz, Swiss Light Source, Paul Scherrer Institut, Zürich, Switzerland

PROGRAM

16TH OF MAY	**2017**
09:00 - 09:20	***Introduction, Ionuț Enculescu, NIMP Măgurele***
SESSION I	***CHEMISTRY AND CATALYSIS (I)***
09:20 – 10:00	**Vasile PÂRVULESCU** *University of Bucharest* *"Complementarity between EXAFS and XPS in investigation of nano-catalytic materials"*
10:00 – 10:40	**Vladimir MATOLIN** *Charles University, Prague* *"Synchrotron radiation photoelectron spectroscopy study of nanostructured catalysts"*
10:40 – 11:00	***COFFEE BREAK***
SESSION I	***CHEMISTRY AND CATALYSIS (II)***
11:00 – 11:40	**Axel KNOP** *Fritz-Haber Institute, Berlin* *"The electronic structure of iridium oxide anodes used in the oxygen evolution reaction - An ambient pressure photoelectron spectroscopy study"*
11:40 – 12:20	**Cristian M. TEODORESCU** *NI Materials Physics, Măgurele* *"In situ chemistry at ferroelectric surfaces"*
12:20 – 13:50	***LUNCH***
SESSION II	***BULK MATERIALS (I)***
13:50 – 14:30	**Jean DAILLANT** *Soleil Synchrotron, Saint-Aubin* *"Soleil: a suite of complementary tools for the structural and functional characterization of materials"*
14:30 – 15:10	**Francesco D'ACAPITO** *ESRF, Grenoble* *"Using X-ray absorption spectroscopy in the study of materials for microelectronics"*
15:10 – 15:30	***COFFEE BREAK***
SESSION II	***BULK MATERIALS (II)***
15:30 – 16:10	**Konstantin KLEMENTIEV** *Max IV, Lund* *"X-ray absorption spectroscopy: basics, application examples and recent extensions"*
16:10 – 16:50	**Ion TISEANU** *NI Lasers Plasma and Radiation Physics, Măgurele* *"Comparative study on X-ray tomography/fluorescence by synchrotrons and conventional X-ray sources"*
16:50 – 17:10	***COFFEE BREAK***

SESSION ROMANIAN YOUNG RESEARCHERS (I)	
17:10 – 18:30	***4 TALKS, 20 MINUTES EACH***
18:30	***DEPARTURE FOR DINNER***

17TH OF MAY	**2017**
SESSION III	***SURFACES AND INTERFACES (I)***
09:00 – 9:40	**Rosana LARCIPRETE** *Institute for Complex Systems, Rome* *"Surface reactions on, in and below epitaxial graphene studied by synchrotron radiation photoelectron spectroscopy"*
09:40 – 10:20	**Carlos VAZ** *PSI, Zürich* *"Interface structure of charge modulated systems probed by X-rays"*
10:20 – 10:40	***COFFEE BREAK***
SESSION III	***SURFACES AND INTERFACES (II)***
10:40 – 11:20	**Lucia ABALLE** *ALBA, Barcelona* *"From nano-magnetism to catalysis: selected results from the CIRCE beamline for electron spectroscopy and microscopy at the ALBA Synchrotron"*
11:20 – 12:00	**Silvano LIZZIT** *ELETTRA,TRIESTE* *"2D materials: growth and characterization"*
12:00 - 13:30	***LUNCH***
SESSION IV	***MAGNETISM***
13:30 – 14:10	**Rodica TURCU** *NI Isotopic and Molecular Technologies, Cluj-Napoca* *"Magnetic nanostructures with tailored morphology and surface properties"*
14:10 – 14:50	**Sarnjeet S. DHESI** *Diamond, Didcot* *"Nanomagnetism using polarised soft X-rays"*
14:50 – 15:30	**Kai SCHAGE** *DESY, Hamburg* *"In-situ X-ray studies reveal new ways towards functional magnetic nanostructures"*
15:30 – 15:50	***COFFEE BREAK***
SESSION V	***GAS PHASE, NEW TECHNIQUES, FREE ELECTRON LASERS***
15:50 – 16:30	**Jens VIEFHAUS** *DESY, Hamburg* *"The variable polarization XUV beamline P04 at PETRA III - A unique source of soft X-rays"*

16:30 – 17:10	**Cătălin MIRON** *Extreme Light Infrastructure – Nuclear Physics, Măgurele* *"Short wavelength radiation: a powerful probe of fundamental radiation-matter interactions"*
17:10 – 17:30	***COFFEE BREAK***
SESSION ROMANIAN YOUNG RESEARCHERS (II)	
17:30 – 18:50	***4 TALKS, 20 MINUTES EACH***
18:50 – 19:00	**Discussions, concluding remarks and workshop closure**
19:00	**DEPARTURE FOR DINNER**

THE 9th INTERNATIONAL CONFERENCE ON ADVANCED MATERIALS ROCAM 2017

JOINT EVENT ROCAM & ISyDMA 2017:

THE 9th INTERNATIONAL CONFERENCE ON ADVANCED MATERIALS, ROCAM 2017
&
THE 2nd INTERNATIONAL SYMPOSIUM ON DIELECTRIC MATERIALS AND APPLICATIONS, ISyDMA 2017

11-14 JULY 2017, BUCHAREST, ROMANIA

Parallel Event: International Summer School on Crystal Growth and Advanced Materials for Energy Conversion

Held under the auspices of ACADEMY OF ROMANIAN SCIENTISTS

Abstract submission deadline is extended.

The Conference aims at presenting an overview of the latest developments in some topics on advanced materials theory, modeling, processing, characterization and applications.

Organized every three years, the ROCAM Conference is the place to be for scientists, students and industrialists willing to have a direct access to the community of international experts of advanced materials and applications.

The presentations will cover a broad range of topics from basic to applied science in relationship with major issues such as energy, environment, biotechnologies, electronics and optoelectronics. The conference will also be a unique occasion for students to introduce their work, some of them having the possibility to take part to the student speech contest, and for exhibitors to meet their customers.

Special keywords will be in attention: *single crystals, nanomaterials, multifunctional and photovoltaic materials.*

IMPORTANT DATES:

ORGANIZERS

ROCAM 2017 ORGANIZERS

ROMANIAN MATERIALS SCIENCE - CRYSTAL GROWTH SOCIETY
UNIVERSITY OF BUCHAREST, FACULTY OF PHYSICS, ROMANIA
NATIONAL INSTITUTE OF MATERIALS PHYSICS (NIMP), ROMANIA
NATIONAL INSTITUTE FOR LASER, PLASMA & RADIATION PHYSICS
CULTURE AND PHYSICS AT MAGURELE" FOUNDATION, ROMANIA

ISyDMA 2017 ORGANIZERS

MOROCCAN ASSOCIATION OF ADVANCED MATERIALS (A2MA)
Moroccan Association of Applied Physics (MAPP)

SECTIONS

S1: Crystals: Growth, Characterization, Modeling and Applications

S2: Solar Energy. Advanced Materials and Devices

S3: Thin films and nanostructures of advanced functional materials

S4: Advanced Materials for Energy and Environmental Applications

S5: Electronic materials and devices: from RF to THz

S6: Advanced Biomaterials, Biodevices and Biotechnology

S7: Advances in dielectric, ferroelectric, multiferroic materials

S8: Emerging materials

ORGANIZING COMMITTEE

Chairmen:	Horia Alexandru, University of Bucharest, Romania
	Joseph Greene, University of Illinois, Urbana, Illinois,USA
	Thomas Kuech, University of Wisconsin- Madison , USA
	Stefan Antohe, University of Bucharest, Romania
	Lucian Pintilie, NIMP, Bucharest - Magurele, Romania
Program Chair:	Florin Stanculescu, University of Bucharest, Romania
Treasurer:	Marcela Socol, NIMP, Bucharest, Romania
Secretary:	Anca Dumitru, University of Bucharest, Romania
Members:	Emil Barna, University of Bucharest, Romania
	Daniela Dragoman, University of Bucharest, Romania
	Ionut Marius Enculescu, NIMP, Bucharest - Magurele, Romania
	Lucian Gheorghe, INFLPR, Bucharest - Magurele, Romania
	Sorina Iftimie, University of Bucharest, Romania
	Lucian Ion, University of Bucharest, Romania
	Daniel Munteanu, Transilvania University of Brasov, Romania
	Florin Nastase, National Institute for Research and Development in Microtechnologies, Romania
	Liviu Nedelcu, NIMP, Bucharest - Magurele, Romania
	Mihai Popescu, NIMP, Bucharest - Magurele , Romania
	Marius Volmer, Transilvania University of Brasov, Romania
Technical Committee:	
	Stefania Mazilu, "Carol I" Central University Library, Bucharest, Romania
	Claudia Nastase, University of Bucharest, Romania
	Adrian Radu, University of Bucharest, Romania
	Silviu Vulpe, University of Bucharest, Romania
	Catalin Manu, NIMP, Bucharest - Magurele, Romania
	Carmen Breazu, NIMP, Bucharest - Magurele, Romania
	Oana Fufa, INFLPR, Bucharest - Magurele, Romania
	Marinel Dan, University of Bucharest, Romania
	Luminita Dan, University of Bucharest, Romania

8th International Conference on Amorphous and Nanostructured Chalcogenides - FUNDAMENTALS AND APPLICATIONS - ANC 8 CONFERENCE

Dates: **JULY 02-05, 2017**

Venue: **SINAIA, Romania**

Website: **http://www.infim.ro/anc8_conference/**

8th International Conference on Amorphous and Nanostructured Chalcogenides

Sinaia, Romania, July 2 - 5, 2017

~Final Short Program~

Timetable	Sunday, July 2	Chairs on Monday	Monday, July 3	Chairs on Tuesday	Tuesday, July 4	Chairs on Wednesday	Wednesday, July 5
08:00 - 08:20			Registration				
08:20 - 08:40							
08:40 - 09:00			Opening Ceremony				
09:00 - 09:30		P. Boolchand L. Calvez	M. Wuttig	M. Mitkova A. Piarristeguy	P. Boolchand	S. Kugler J. Teteris	G. A. Kaur
09:30 - 10:00			A. A. Kryuchyn		E. A. Chechetkina		A. Kovalskiy
10:00 - 10:30			A. Velea		S. Hosokawa		M. Popescu
10:30 - 10:50			Coffee Break		Coffee Break		Coffee Break
10:50 - 11:20		S. Hosokawa D. Tsiulyanu	L. Calvez	N. Mousseau J. Singh	M. Mitkova	E. Chechetkina G. A. Kaur	J. Singh
11:20 - 11:50			S. Kugler		A. Piarristeguy		J. Teteris
11:50 - 12:20			N. Mousseau		S. Kökényesi		D. Tsiulyanu
12:20 - 12:40			M. Kristl		V. Komanicky		V. I. Verlan
12:40 - 14:00			Lunch Break		Lunch Break		Lunch Break
14:00 - 14:30		A. Kovalskiy M. Wuttig	J. R. Stellhorn			A. Kryuchyn A. Velea	S. Dyussembaev
14:30 - 15:00			V. Kalugin				G. Osayemwenre
15:00 - 15:20			S. Kozyukhin				D. K. Dwivedi
15:20 - 15:40			Coffee Break				Coffee Break
15:40 - 16:00							Closing Ceremony
16:00 - 16:20					Conference Trip		
16:20 - 16: 50			Poster Session				
16:50 - 17:10	Registration						
17:10 - 17:30							
17:30 - 17:50							
17:50 - 18:00							
18:00 - 19:00							
19:00 - 20:00	Welcome Reception				Conference Dinner		
20:00 - 21:00							
21:00 - 22:00							

Organization & Committee

Organizers :

- National Institute of Materials Physics;
- Virtual Company of Physics;
- Culture and Physics at Magurele Foundation.

Director of the Conference:

- Prof. Dr. Mihai Popescu, National Institute of Materials Physics, Magurele, ROMANIA.

International Advisory Board:

- Dr. Punit Boolchand, University of Cincinnati, Cincinnati, USA;
- Dr. Shinya Hosokawa, Kumamoto University, Kumamoto, JAPAN;
- Dr. Matthieu Micoulaut, Pierre and Marie Curie University, Paris, FRANCE;
- Dr. Andrea Piarristeguy, Montpellier University, Montpellier, FRANCE;
- Dr. Matthias Wuttig, RWTH University, Aachen, GERMANY;
- Dr. Normand Mousseau, Université de Montréal, Montréal, CANADA;
- Dr. Kaikai Xu, University of Electronic Science and Technology of China, Chengdu, CHINA;
- Dr. Elena A. Chechetkina, Russian Academy of Sciences, Sankt Petersburg, RUSSIA;
- Dr. Mihail Iovu, Moldova Academy of Sciences, Chisinau, MOLDOVA;
- Dr. Sandor Kokenyesi, University of Debrecen, Debrecen, HUNGARY;
- Dr. Alexander Kolobov, National Institute of Advanced Industrial Science and Technology, Tsukuba, JAPAN;
- Dr. Diana Nesheva, Bulgarian Academy of Sciences, Sofia, BULGARIA;
- Dr. Janis Teteris, University of Latvia, Riga, LATVIA.

National Organizing Committee:

- Dr. Adam Lorinczi, National Institute of Materials Physics, Magurele, ROMANIA;
- Dr. Florin Sava, National Institute of Materials Physics, Magurele, ROMANIA;
- Dr. Iosif-Daniel Simandan, National Institute of Materials Physics, Magurele, ROMANIA;
- Dr. Alin Velea, National Institute of Materials Physics, Magurele, ROMANIA.
- Dr. Lucian Pintilie, National Institute of Material Physics, M<agurele, ROMANIA
- Jean Narcis Barascu, National Institute of Materials Physics, ROMANIA

INTERNATIONAL COOPERATION

INTERNATIONAL COOPERATION PROJECTS

LARGE COOPERATIONS
CERN RD50 "Radiation hard semiconductor devices for very high luminosity colliders" **Pintilie I** (http://rd50.web.cern.ch/rd50/): 48 research institutions from 27 countries around the world Scientific coordonator of the workpackage "Defect/Material Characterization"
NORWAY FUNDS **Pintilie I** Project funds SEE (EEA Grants) "Perovskites for Photovoltaic Efficient Conversion Technology" (PERPHECT) Partners: NIMP (INCDFM), Physics Faculty U. Bucharest, Optoelectronics 2000 SA (Romania); U. Iceland, U. Reykjavík (Iceland); U. Oslo (Norway) 2014-2017
H2020 and EURATOM **Galatanu A** EUROfusion Consortium, Grant agreement No. 633053 2014-2018 **Galatanu A** EURATOM Enabling Research "Low-activation cemented carbides for high heat flux applications", coord Jožef Stefan Institute (JSI), Slovenia, parteneri INCDFM (Romania), CIEMAT (Spania) si FZJ (Germania). 2017-2018 **Galatanu A** EUROfusion WPMAT, GA633053 "Romanian participation in the EUROfusion WPMAT and complementary research" 2014-2018 **Galatanu A** H2020 "Accelerator Research and Innovation for European Science and Society (ARIES)", GA730871 2017-2021
Cross Border Romania-Bulgaria **Galatanu A** "D-EMERSYS - Rapid intervention force to chemical, biological, radiological and nuclear emergencies on the Danube River" Interregrobg Cod e-MS ROBG - 123 coord INCDFM 2016-2018 **Galatanu A** "JEROME - Capabilities and interoperability for joint RO-BG cross-border first responder intervention to chemical-biological-radiological-nuclear-high yield explosive emergencies", Interregrobg Cod e-MS ROBG - 121 coord INCDFM 2016-2018

COST project
Pintilie L
COST actiunea MP1308 "Towards Oxide-Based Electronics (TO-BE)" (http://www.cost.eu/COST_Actions/mpns/Actions/MP1308) Coordinator: Dr Fabio Miletto Granozio (IT)
2014-2018

COST project
COST action HERALD (MP1402) "Hooking together European research in Atomic Layer Deposition (HERALD)"
(http://www.cost.eu/COST_Actions/mpns/MP1402)
Coordonator: Dr. Simon Elliott, Ireland
2014-2018

COST project
COST CA16218 Nanoscale Coherent Hybrid Devices for Superconducting Technologies (NANOCOHYBRI).
Principal representative of Romania in the Management Committee.
2017-2021

ERA-NET project
Mercioniu IF
Project M-ERA NET 9/2015
Integrated sensors with microfluidic characteristics using the LTCC technology (INTCERSEN)
Coordinator: TU Iasi, Romania
Partners: NIMP, Magurele, Romania; SC INTELECTRO SRL, Iasi, Romania; „J. Stefan" Institute Slovenia; HIPOT Slovenia; Dropsens, Spain; NAMASTE, Slovenia.
2015-2017

ERA-NET project
Trupina L
Integration of new and improved materials for smart millimeter-wave sensors
Project M-ERA.NET
French partner: Universitatea din Limoges, AirMems (SME)
2016 – 2019

ERA-NET project
Ciurea ML
Project M-ERA NET Call 2014
PhotoNanoP (High photoconductive oxide films functionalized with GeSi nanoparticles for environmental applications)
Partners from Romania (IMT, OPTOELECTRONICA- 2001 S.A) and Iceland (Reykjavik University (School of Science and Engineering) - RU-SSE, Pi Technology)
2016-2018

ERA-NET project
Stoica TS
Project M-ERA NET Call 2015
GESNAPHOTO (Nano-structured GeSn coatings for photonics)
Partners from Romania (INOE-2000, OPTOELECTRONICA- 2001 S.A) and Germany (Forschungszentrum Jülich, Peter Grünberg Institute PGI-9, nanoplus Nanosystems and Technologies GmbH)
2016-2019

ERA-NET project
Vlaicu ID
Innovative nano-materials and architectures for integrated piezoelectric energy harvesting applications (HarvEnPiez)
Coordonator: Iosef Stefan Institute from Ljubljana, Slovenia
Partners: Institute of Solid State Physics, University of Latvia (ISSP UL), Latvia; National Institute of Materials Physics (NIMP), Romania; Faculty of Electrical Engineering, Power Engineering and Information Technology, (Intelectro Iasi SRL), Romania; Technical University Iasi (TU Iasi), Romania
2016-2019

COFUND M-ERA.NET II / Contract 74/2017
Badica P
BIOMB, Advanced biodegradable materials based on MgB2 resistant to microbial colonization,
Coordonator: INCDFM, Partners: UPB, UB, U. Torino
2017-2020

C-ERIC
Graphene for Water in Life Science,
CERIC Grant
Coordinator: Elettra Sincrotrone Trieste
Partners: Technical University Graz (Austria), Charles University Prague (Czech Republic), NIMP (Romania)

OTHER INTERNATIONAL PROJECTS

Project PICS
Predoi D
Nanoparticles for remedy of contaminated soils
French partner: Institut des Sciences de la Terre d'Orléans.

Project IFA-CEA
Chirila C
Optimised pyroelectric elements on Si wafers for sensing and energy harvesting
French partner: CEA Grenoble Laboratorul de Componente pentru Micro-Actuatori
2016-2019

Programme Hubert Curien PHC Brancusi
Crisan O
Surface-functionalized nanostructures for applications in photonics and spin manipulation technologies
Partner: Laboratoire Léon Brillouin UMR12 CEA-CNRS, Commissariat à l'Énergie Atomique et aux Énergies Alternatives CEA Saclay, France: Prof. A. Filoramo
2016-2018

BILATERAL COOPERATION PROJECTS (AGREEMENTS)

Banciu MG
Memorandum of Agreement between the National Institute of Materials Physics (INCDFM) and the Research Center for Development of Far-Infrared Region, University of Fukui (FIR-UF)
Signed 2017

Crisan O
Bilateral cooperation project Romania-Franta PN-III-P3-3.1-PM-RO-FR-2016-0043
Director Proiect

Kuncser V
Task Partener of the National Research Council (CNR) Italy, within the project FREECATS financed by European Institute of Technology, RawMaterials,
2017-2018

Badica P
Romania (NIMP+UPB) – Ucraina (National Technical University of Ukraine,"Kiev Politechnical Institute"), Bilateral Cooperation PN3-P3-127.3BM/2016,
2016-2017

Grigoroscuta M
NIMP – NIMS, cooperation through the NIMS "MSc, PhD internships program", "c-axis oriented MgB2 bulks by high magnetic field", Tsukuba, Japonia,
11 Sept-01 Dec. 2017

Badica P
Tohoku University, Japonia
Joints of superconducting tapes: fabrication and characterization
Project: ICC-IMR Visiting Prof. collaboration and exchange of researchers/students INCDFM-HFSLM-Tohoku University

Stan GE
University of Aveiro, Portugal
Development of a new generation of highly biocompatible dental titanium implants functionalized by sputtering techniques with novel bioactive glass materials
2016 – 2020

A. Stanculescu
University of Angers- Photonics Laboratory, France
Accord de coopération scientifique dans le domaine des films minces notamment sur les thématiques suivantes: structures multicouches organiques à basse dimension et composantes or oganiques et hybrides.

A. Stanculescu **University of Western Cape, Departament of Chemistry, SensoLab, Soth Africa** Polymeric single/multylayer heterostructures for photovoltaic and electronic applications; polymeric field effect transistors for sensing applications; organic and hybrid devices (realisation, characterization)
Badica P **Tohoku University, Japonia** Joints of superconducting tapes: fabrication and characterization Proiect: ICC-IMR Visiting Prof. collaboration and exchange of researchers/students INCDFM-HFSLM-Tohoku University
M. Baibarac **Institut des Materiaux Jean Rouxel, Nantes, France** Surface plasmons enhancement of optical properties of SWNTs, highly separated in metallic and semiconducting components, electrochemically functionalized with conjugated polymers.
COOPERATION PROJECTS WITH FOREIGN INSTITUTES AND UNIVERSITIES
Ciurea ML **Department of Physics and Astronomy, University of Catania, CNR-IMM, Catania, Italy** Ge-based nanostructures for applications as photodetectors or transparent electrodes for photovoltaic cells
Ciurea ML, Lepadatu AM **Istituto Nazionale di Fisica Nucleare-Laboratori Nazionali di Frascati, Frascati, Italy** Nanostructures based on Ge nanoparticles immersed in oxidic matrices for optical sensors applications
Ciurea ML **Reykjavik University, School of Science and Engineering, Iceland** GeSi nanocrystals in oxides with targeted photoconductive properties in VIS-NIR
Kuncser V **Laboratory of Applied Materials, Universitatea Portsmouth, UK, Asoc. Prof. Melvin M. Vopson**
Crisan O **Swiss Federal Laboratory for Materials Research & Technology, EMPA, Thun, Switzerland** Prof. Patrik Hoffman
Crisan O **Institut des Materiaux et Molecules du Mans I3M, Fac. Des Sciences, Universite du Maine, Le Mans, France** Prof. N. Randrianantoandro
Crisan O Department of Renewable Energy, University of Sharjah, United Arab Emirates Prof. Hamid al-Naimyi
Miclea CF **Los Alamos National Laboratory, Los Alamos, NM. USA.** Measurements, co-publication, specimen exchange

Miclea CF **Los Alamos National Laboratory, Los Alamos, NM. USA.** Measurements, co-publication, specimen exchange
Miclea CF **Max Planck Institute for Chemical Physics of Solids, Dresden, Germany** Measurements, co-publication, specimen exchange
Nedelcu L **Research Center for Development of Far-Infrared Region, University of Fukui, Japan** Measurements, specimen exchange
Nistor SV **Institute of Physics, Czech Academy, Prague** Investigation by magnetic electronic resonance techniques and optical spectroscopy of the semiconducting II-VI materials optically activated with transitional ions
Nistor SV **Physics Department, Antwerp University, Belgium** Development of new advanced multifunctional materials containing defects
Pintilie L **UMP CNRS-Thales, Palaiseau, France and Université Paris-Sud** Measurements, specimen exchange
Pintilie L, Pintilie I **University of Oulu, Finland** Ferroelectric measurements
Pintilie L **Universitatea Tehnica Darmstadt, Germany** Specimen exchange, co-publication
Pintilie I **Universitatea din Oslo, Norway** Specimen exchange, working stages
Pintilie L **UMP CNRS-Thales, 1 Av. Fresnel, Palaiseau, 91767, France and Université Paris-Sud** Specimen exchange, common measurements
Preda N **Yildiz Technical University, Turkey** Learning Agreement for Traineeships within the ERASMUS Program
Predoi D **Institut de Chimie de la Matière Condensée de Bordeaux CNRS-UPR 9048 France** Elemental analysis, hydrogen storage
Predoi D **Universite Bordeaux, EA 4592 Géoressources&Environnement, ENSEGID, France** Collaboration project IFA CEA C2-06, TEM, environment tests
Predoi D **Marcoule Institute for Separative Chemistry, France**

Predoi D **Technical University Ostrava, Cehia**
Predoi D **Institute of Life Sciences Research and Technologies: Laboratory of Chemistry and Biology of Metals (LCBM) Grenoble, France** Collaboration project IFA CEA C4-05- biological tests
Predoi D **Institut des Sciences de la Terre d'Orléans, France** Raman, ICP, magnetic measurements
Predoi D **Université du Havre, France** Ultrasound studies
Predoi D **Horiba Jobin Yvon S.A., France** Zeta potential, DLS, photoluminescence
Predoi D **University of Dayton, Research Institute, USA** Carbon nanotubes
Stoica T **Peter Grünberg Institute, Forschungszentrum Jülich, Germany** 2D materials based on chalcogenides of transition metals, 2D-TMD
Teodorescu CM **Elettra Trieste (Italia)** CoSMoS -Combined Spectroscopy and Microscopy operating at SuperESCA
Teodorescu CM **IRAMIS CEA Saclay (France)** Chemical switching of ferroelectric surface topology (proiect RO-FR PN-II-ID-JRP-2011-2)

NIMP FUNDING

Core Programme	5,293,194.69 Euro
Ideas	567,649.40 Euro
Partnerships	322,942.12 Euro
International Projects	208,982.26 Euro
Human Ressources	435,315.90 Euro
Competitivness PED, PTE, BG	684,136.57 Euro
ROSA	25,161.38 Euro
M-ERA Net	208,089.07 Euro
Economic Contracts	167,465.18 Euro
Structural funds	716,530.54 Euro
Other national project (IFA, copbil)	328,098.11 Euro
TOTAL	**8,957,565.24 Euro**

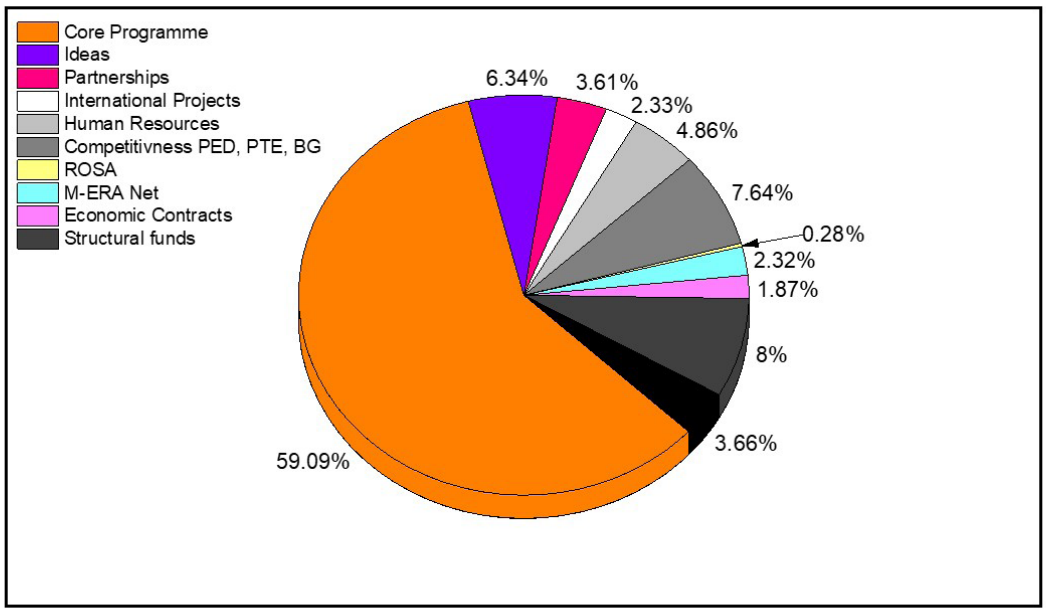

Scan the QR code, for electronic version

National Institute of Materials Physiscs

405A Atomistilor Street, 077125, P. O. Box: MG 7 Magurele, Ilfov, Romania

Phone: +4021 369 01 85, Fax: +4021 369 01 77, e-mail: director@infim.ro, www.infim.ro